



HAL
open science

Contribution of mechanical stress to cell division plane orientation at the shoot apical meristem of *Arabidopsis thaliana*

Marion Louveaux

► **To cite this version:**

Marion Louveaux. Contribution of mechanical stress to cell division plane orientation at the shoot apical meristem of *Arabidopsis thaliana*. Morphogenesis. Ecole normale supérieure de lyon - ENS LYON, 2015. English. NNT : 2015ENSL1019 . tel-01500091

HAL Id: tel-01500091

<https://theses.hal.science/tel-01500091>

Submitted on 2 Apr 2017

HAL is a multi-disciplinary open access archive for the deposit and dissemination of scientific research documents, whether they are published or not. The documents may come from teaching and research institutions in France or abroad, or from public or private research centers.

L'archive ouverte pluridisciplinaire **HAL**, est destinée au dépôt et à la diffusion de documents scientifiques de niveau recherche, publiés ou non, émanant des établissements d'enseignement et de recherche français ou étrangers, des laboratoires publics ou privés.

THÈSE

en vue de l'obtention du grade de

Docteur de l'Université de Lyon, délivré par l'École Normale Supérieure de Lyon

Discipline : Sciences de la Vie

Laboratoire Reproduction et Développement des Plantes, ENS de Lyon

École Doctorale Biologie moléculaire, intégrative et cellulaire (BMIC)

Soutenance prévue le 02 Octobre 2015

par Madame Marion LOUVEAUX

Contribution of mechanical stress to cell division plane orientation at the shoot apical meristem of
Arabidopsis thaliana

Directeur de thèse : M. Olivier HAMANT

Après l'avis de :

Mme Dorota KWIATKOWSKA

M. David BOUCHEZ

Devant le jury composé de :

M. M. David BOUCHEZ, INRA (Versailles), Rapporteur

M. Christophe GODIN, INRIA (Montpellier), Examineur

M. Olivier HAMANT, ENS de Lyon, Directeur de thèse

Mme Dorota KWIATKOWSKA, Université de Silésie (Katowice, Pologne), Rapporteur

M. Patrick LEMAIRE, CRBM (Montpellier), Examineur

M. Stéphane VINCENT, ENS de Lyon, Invité

Funding and L^AT_EX template credits

This PhD thesis was funded by the "ARC3 Environnement", Région Rhône-Alpes, France.

L^AT_EX template was created by Manuel Kuehner
www.bedienhaptik.de/latex-template/

Remerciements

Ces remerciements marquent l'achèvement de mes 3 ans de thèse, un long voyage au cours duquel j'ai partagé ma route avec de nombreuses personnes. Il est temps de se retourner, contempler le chemin parcouru et de saluer tous ceux, qui, de près ou de loin, ont contribué à ce périple. J'espère n'oublier personne.

Je commence par Olivier, mon directeur de thèse, sans qui cette aventure n'aurait jamais eu lieu. Merci pour ton optimisme et ton enthousiasme à toute épreuve, merci pour la confiance que tu as placée en moi et pour la liberté que tu m'as donnée, notamment celle de pouvoir parfois travailler à distance. Ma thèse n'aurait pas eu cette dimension biophysique sans la présence d'Arezki, mon chef d'équipe. Merci pour ta disponibilité, tu as toujours réussi à dégager du temps pour discuter de mon projet, malgré ton emploi du temps incroyablement rempli.

J'ai beaucoup apprécié cette interdisciplinarité qui fait écho à mon parcours d'ingénieur en agronomie. J'ai à mon tour pu engager plusieurs collaborations fructueuses et plusieurs papiers sont en cours. Je remercie JD avec qui je collabore depuis le début de ma thèse sur les règles de division géométriques et mécaniques. Ce travail n'aurait pu se faire également sans l'aide et les précieux conseils de Vincent. Je remercie également Léna, qui m'a formée à l'indentation, et avec qui j'ai mis au point le protocole de compression des méristèmes sur plusieurs heures. Je remercie enfin Olivier Ali avec qui j'ai engagé une collaboration prometteuse sur la fin de ma thèse, qui permettra peut-être d'apporter une nouvelle pierre au travail engagé avec JD.

Je souhaite également remercier mes collaborateurs à l'étranger. Mon travail de thèse n'aurait pas été le même sans le précieux script Matlab développé par Sébastien Besson et Jacques Dumais et qui permet de calculer les prédictions de leur règle de division. Je les remercie aussi pour leurs conseils et remarques éclairantes. Ma thèse a également profité du développement du logiciel de reconstruction 3D et segmentation d'image confocales MorphoGraphX et accompagné son évolution. Je remercie les développeurs principaux de MorphoGraphX, Pierre Barbier de Reuille et Richard Smith, pour leur formation et leurs conseils ainsi que leur réactivité à répondre à mes questions.

Au delà de ces collaborations, je remercie toutes les personnes qui ont apporté un regard extérieur sur mon travail au cours de ma thèse, en particulier Olivier, Arezki, Sébastien, Thomas et Olivier Ali qui ont relu et corrigé ce manuscrit.

Je remercie également les chercheurs extérieurs à mon laboratoire qui m'ont conseillé tout au long de mon parcours et/ou ont corrigé mon travail. Dans l'ordre chronologique, je remercie Didier Gascuel pour m'avoir convaincue d'entrer à l'agro sans pour autant renoncer à faire une thèse. Je remercie également mes responsables de master 2 à AgroParisTech, Jean-Denis Faure et Claire Neema pour m'avoir conseillée et aiguillée vers Olivier pour mon stage de master 2. Je remercie les membres de mon comité de thèse, Jean-Christophe Palauqui et Marie Delattre, pour leurs conseils. Je remercie enfin mon jury de thèse :

Dorota Kwiatkowska et David Bouchez, mes rapporteurs, ainsi que Christophe Godin, Patrick Lemaire et Stéphane Vincent, mes examinateurs.

Je remercie toutes les personnes qui ont assuré un soutien logistique et ainsi contribué au bon déroulement de ma thèse. Je remercie en particulier Alexis, Justin et tous ceux qui ont veillé sur mes plantes. Je remercie aussi Hervé et Isabelle sans qui aucune de mes manip n'aurait été stérile, les informaticiens, Éric, Stéphane et Kevin, et les secrétariats du RDP, du LJC et de BMIC, en particulier Maryline et Roxanne. J'aimerais également remercier les correspondants informatique, Steven et Mohammed, avec qui j'ai passé une année très intéressante à participer à l'évaluation des besoins du RDP en terme de renouvellement du parc informatique. Au delà du RDP et du LJC, je remercie le CBP, et en particulier Emmanuel Quémener, qui a assuré l'installation et le maintien de MorphoGraphX pendant les premiers mois de tests. Je remercie également les membres du Platim, Christophe, Claire et Élodie, pour leurs formations, leurs conseils, leur réactivité et leur zénitude face aux thésards en détresse et aux microscopes récalcitrants. Je remercie également Jan pour m'avoir autorisé à utiliser le LSM700 de l'équipe Méristème, sans lequel je n'aurais pu effectuer le suivi des ablations réalisées au spinning disk du Platim.

Je remercie toutes les personnes qui ont contribué à créer une atmosphère agréable au cours de ma thèse. Je remercie l'ensemble de l'équipe Biophysique et Développement, ses membres passés et présents, en particulier Mathilde, Nelly, Léna, Naomi, Sam, JD, Thomas, Stéphane et Jo. J'ai apprécié les piques-nique d'équipe et les bières du vendredi soir au Ninkasi. Même si la cadence a ralenti ces derniers temps, je retiens qu'en bons scientifiques, nous y seront allés suffisamment de fois pour vérifier la contenance des pichets de 2L.

Je remercie l'ensemble des membres du RDP pour leur accueil, leur disponibilité et leur dynamisme. J'ai apprécié la possibilité de discuter science et autre avec toutes et tous, ainsi que le mélange entre équipes dans les espaces de manips et les bureaux. Je remercie en particulier Philippe, mon voisin de bureau pendant presque toute ma thèse avec qui j'ai discuté science et autre, et Annick qui m'a formée à la culture des calcs. L'équilibre est fragile mais réussi, et il tient entre autre aux occasions de se retrouver ensemble. Je remercie les organisateurs et les participants des Skiminar. Grâce à vous j'ai pu m'éclater en skating mais aussi apprendre le ski alpin. Merci à Marina et Nelly, mes profs de ski. Merci aux habitués du foyer le vendredi soir (et parfois aussi les autres soirs). Je fais une dédicace spéciale à Steven mon partenaire de rock préféré, à Duvelman, et à Stéphane pour sa dextérité à envoyer les capsules de bière (voire la bière) exclusivement sur Mathilde. Je remercie également les filles avec qui j'ai fait du yoga, du pilates et/ou du dessin, les deux Mathilde, Léna, Julie, Marie-France, Annick, Alessia et Marie-Cécile.

Je remercie également le LJC, mon deuxième labo qui, même s'il a été plus discret que le RDP, m'a aussi apporté son soutien et contribué à la réussite de mon projet de thèse. Je remercie en particulier Bertrand Fourcade pour m'avoir accueilli dans son bureau pendant la rédaction de ce manuscrit.

Au-delà de mon projet de recherche, j'ai également eu l'opportunité d'enseigner, d'encadrer et de vulgariser la science. Je remercie Sylvie Baudino, Jean-Claude Caissard, Christine Miège et Sandrine Charles pour m'avoir confié mes premières heures d'enseignement et m'avoir aidée à les préparer. Grâce à vous, j'ai pu découvrir l'enseignement supérieur côté enseignant, découvrir trois structures d'enseignement (l'université de St Étienne, l'université de Lyon et l'ENS de Lyon), trois formats de cours (TP, TD et cours magistraux) et trois niveaux (L1, L2 et L3). Je remercie également mes

étudiants qui ont été les cobayes de ces premières heures d'enseignement. Je remercie Yannick, mon stagiaire de L3 et le premier à expérimenter mes compétences d'encadrement, pour la qualité de son travail. Je remercie au passage Pradeep pour ses précieux conseils pour la dissection et la coloration au FM4-64 des méristèmes. Faire de la science, ce n'est pas uniquement travailler entre spécialistes d'une même thématique. Je suis convaincue de la nécessité de communiquer auprès du grand public et en particulier auprès des jeunes, afin de combattre l'ignorance scientifique (car non *Escherichia Coli* n'est pas une maladie) et donner le goût des sciences. Je remercie Alessia et Aurélie avec qui j'ai participé à un projet de l'ASTEP (Accompagnement en Science et Technologie à l'École Primaire) avec Mme Félix et sa classe de CP de l'école Descartes à Villeurbanne. Je remercie Christèle Izoard-Martin, coordinatrice des ARCs pour la Région Rhône-Alpes, ainsi que les doctorants de l'ARC Environnement avec qui j'ai participé à la Fête de la Science 2013 au lycée de la Mache (Lyon 8ème). Je remercie également l'équipe 'Fête de la Science 2015' du RDP, Antoine, Olivier, Stéphane, Mathilde, Léa, Kateryna, David et Anaïs. Je considère également qu'au-delà de l'interdisciplinarité indispensable entre sciences "dures", il est nécessaire d'échanger avec d'autres disciplines. C'est dans ce cadre que j'ai participé au projet Art'Lab encadré par la Région Rhône-Alpes. Ce projet mêlant art et sciences fut l'occasion de rencontrer une équipe formidable composée d'Elsa (designeuse), Ronan (doctorant en physique), Chloé (étudiante en art), Maïmouna (doctorante en Sciences Politiques) et Anaïs (doctorante en chimie), d'échanger sur nos travaux et de concevoir ensemble, sur deux résidences de 3 jours aux Grands Ateliers intercalées de nombreuses discussions, une installation à mi-chemin en art et sciences, qui fut exposée à la Biennale du Design de St Étienne en 2015.

Parce qu'il y a une vie en dehors de la thèse, je souhaite aussi remercier les amis lyonnais et/ou grenoblois, musiciens ou non, physiciens ou non, Cyril, Chloé, Timothée, Sarah, Pol, Nicolas, Pierre, Franca, Léa, Coralie et Thomas. Merci pour tous ces moments hors thèse, randonnées dans les alpes, concerts en tant que spectateurs à l'auditorium de Lyon, concerts en tant que musiciens à l'ENS ou ailleurs, répétitions de musique, match d'improvisation, soirées jeux et soirées tout court. Cette thèse a aussi été un voyage au sens propre. En 3 ans, j'ai parcouru l'équivalent de plus d'une fois et demi le tour du monde et ai acquis une certaine aisance à travailler quelles que soient les conditions (dans le train, dans l'avion, pendant les préparatifs du mariage d'amis...). Si les derniers 20 000 km sont dus à mon voyage à Nagoya pour la conférence et le workshop organisé par le programme ERATO, le reste est principalement dû à mes aller-retours fréquents sur Paris et encore plus à Brest où j'ai travaillé à distance. Je remercie les brestois qui m'ont accueillie et j'en profite pour démentir un mythe tenace : non, il ne pleut pas tout le temps à Brest. Il fait beau plusieurs fois par jour et parfois, il bruine (surtout quand ce sont les vacances des parisiens). Merci à Jacques, Touria, Mick, Stevonn, Tristan, Jean-Yves et Jacqueline pour leur accueil dans les bureaux de l'équipe Dyneco-AG à IFREMER. Merci aux membres de la Ligue d'Improvisation de Brest et de l'Île D'Ouessant, en particulier Amaury, Tony, Rosie, Sandrine, Kévin et Fanny pour les moments pré et post match partagés, les cabarets, les après-midi jeux, les soirées Mario Kart et les 24h de l'INSA à Lyon. Je remercie aussi ceux qui ont partagé ma route bien avant que je n'entre en thèse, qui ont continué de la croiser malgré la distance et les emplois du temps chargés de chacun et qui m'ont eux aussi soutenue. Je commence par les agros and co, Bertrand, Marleen, Pierre, Natch, Fanf, Marie et Antoine. Je remercie aussi les parisiens : Ju, Mat, Cécile et

Remerciements

Philou. Je vous souhaite le meilleur pour la fin de vos études respectives et en particulier, je croise les doigts pour la 6ème année de médecine de Cécile et Philou.

Je remercie également ma famille qui ne me voit pas souvent et qui ne comprend pas toujours tout à ce que je fais mais qui m'a toujours apporté son soutien. Merci papa pour la biblio. Je remercie également ma belle-famille qui me voit encore moins souvent.

Je finis par un remerciement spécial à Sébastien, ma moitié dans la vie et mon mentor en sciences. Merci de m'avoir poussée à faire ce qui me plaisait et à développer mon projet professionnel. Merci pour ta patience, notamment lorsque tu m'as formée à R. Merci aussi de m'avoir éclairée par ton expérience sur le chemin de la thèse et de m'avoir aidée à maintenir le cap sur mes objectifs dans les moments difficiles.

Abstract

Morphogenesis, the shaping of a new organism along development, is driven by four processes: cell division, growth, migration and apoptosis. In most plants, only two processes remain: cell division and growth. Mechanical stress is one of the coordinating factors that couple these two processes. Growth generates mechanical stress during development and, in turn, mechanical stress can impact cellular events, including cell division, and channel morphogenesis. In animal cells, mechanical stress is known to influence the orientation of division plane (Fink et al. 2011), as well as mitotic progression (Itabashi et al. 2012). In plants, mechanical stress was shown to influence gene expression (Braam 2004) and cytoskeleton organization (Hamant et al. 2008; Uyttewaal et al. 2012; Sampathkumar et al. 2014), but its contribution on division remains to be demonstrated. Here we focused our attention on the potential contribution of mechanical stress on the orientation of cell division plane at the shoot apical meristem of *Arabidopsis thaliana*. At the end of the XIXth century, cell geometry was proposed to play a key role in plant cell division plane orientation and several geometrical division rules were proposed by Hofmeister, Errera and Sachs (Hofmeister 1863; Errera 1888; Sachs 1878). Recently, the rule of Errera was re-examined and generalised into a probabilistic rule: the Besson-Dumais rule. The Besson-Dumais rule has been tested only on tissues with rather isotropic shapes or growth and the exact molecular mechanism controlling division plane orientation is still unknown. A mechanical stress patterns can be derived from the three-dimensional shape of the meristem (Boudaoud 2010), revealing a anisotropic stress in the boundary region separating the outgrowing primordia from the meristem. Moreover, in this region growth is also anisotropic. We performed time-lapse imaging on dissected meristems using a confocal microscope and processed the stacks with MorphoGraphX. We used the script of Sébastien Besson to predict probable planes associated with each cell geometry and compared this output to observed orientations. We found that if a majority (three quarter) of the cells chose the shortest plane, the distribution of planes was spatially biased. The boundary region displayed longer planes than expected. Growing tissue were simulated with two possible division rules: geometrical or mechanical. Tissues simulated with a mechanical division rule displayed an enrichment in long planes, especially when tissue was submitted to an anisotropic stress field comparable to those in the boundary region of the SAM. Mechanical perturbations of local stress pattern, by laser ablations biased cell division plane orientation. We explored other means of perturbing mechanically the tissue and developed a protocol to apply continuous controlled loads with an indenter. We tested our protocol by analysing the microtubule response in two microtubule marker lines, as well as in the *katanin* and *spiral2* mutant backgrounds. We confirmed previous results and proposed different quantitative tool to quantify the response of microtubules to mechanical stress in regard to a quantified load. In parallel, we developed a pipeline based on the statistics and data analysis oriented R-software to synthesize information from confocal microscopy images in a semi-automatic way. Altogether these new tools should help us understand how mechanical stress controls cell division plane orientation and microtubule behaviour.

Contents

Funding and L^AT_EX template credits	i
Remerciements	iii
Abstract	vii
List of Figures	xiii
List of Tables	xv
1 Introduction	1
1.1 Cell division	1
1.1.0.1 Mitosis	2
1.1.0.2 Cytokinesis	3
1.1.1 Temporal control	4
1.1.1.1 The cell cycle, a molecular clock	4
1.1.1.2 Progression through the cell cycle	5
1.1.2 Spatial control	6
1.1.2.1 Molecular actors involved in cell division plane orientation	6
1.1.2.2 Identifying the centre of mass of the cell	7
1.1.2.3 A probabilistic rule for division plane orientation	8
1.1.2.4 The importance of cell division positioning and timing of	
division in development	10
1.1.3 Case study: the shoot apical meristem, a place of divisions	11
1.2 The cytoskeleton	13
1.2.1 Historical and biochemical description of members of the cytoskele-	
ton elements	13
1.2.1.1 Microtubules	13
1.2.1.2 Actin	14
1.2.1.3 Intermediate filaments	14
1.2.2 Regulation of cytoskeleton polymers	15
1.2.2.1 Nucleation	15
1.2.2.2 Polymerization and depolymerization	16
1.2.2.3 Monomers sequestering and modulation of + and - ends . .	17
1.2.2.4 Severing	18
1.2.2.5 Filament stabilisation, bundling and zippering	21
1.2.2.6 Cross-talk between cytoskeletal networks	21
1.2.3 Case study: the importance of cytoskeleton dynamics during plant	
mitosis	22
1.3 Mechanical stress	23
1.3.1 Definitions	23
1.3.2 Evidence of stress within tissues and their origin	25

1.3.3	Quantification of stress	26
1.3.3.1	Mechanical properties of living materials	26
1.3.3.2	Intrinsic mechanical stress	28
1.3.3.3	Range of forces exerted by the cell on its environment	29
1.3.3.4	Range of mechanical stress perception	29
1.3.4	Prediction/Deduction of stress patterns	30
1.3.4.1	Analogies with physical systems	31
1.3.4.2	Numerical mechanical models	31
1.3.5	Exploring the effects of mechanical stress on cells and tissues	32
1.3.6	Case study: mechanical stress within the shoot apical meristem of <i>Arabidopsis thaliana</i>	34
1.4	The mechanics behind cell division	35
1.5	Aims of the PhD thesis	35
2	A mechanics-based rule accounts for the orientation of cell division in the boundary of the shoot apical meristem of <i>Arabidopsis thaliana</i>	39
2.1	Abstract	39
2.2	Introduction	40
2.3	Results	41
2.3.1	A non negligible proportion of cells does not select the shortest plane at the epidermis of the SAM	41
2.3.2	The Besson-Dumais division rule partially accounts for observations, but long planes are over-represented at the SAM	44
2.3.3	The boundary region is enriched in long planes	44
2.3.4	Simulation of a growing boundary suggests a contribution of mechanical stress to the bias in the division plane distribution	45
2.3.5	Mechanical perturbations influence division plane orientation	47
2.3.6	Towards a mechanics-based division rule?	49
2.4	Discussion	49
2.5	Material and Methods	50
2.5.1	Plant material and growth conditions	51
2.5.2	Imaging	51
2.5.3	Ablations	52
2.5.4	Model	52
2.5.4.1	Mechanics	52
2.5.4.2	Tissue growth	53
2.5.4.3	Cellular division	54
2.5.4.4	Properties of the daughter cells	54
2.5.4.5	Implementation	55
2.6	Supplemental Figures	55
3	Mechanical compression leads to microtubule bundling in <i>Arabidopsis</i>: a quantitative approach	59
3.1	Preamble	59
3.2	Abstract	61
3.3	Introduction	61
3.4	Results	62
3.4.1	Applying controlled compression on living plant tissues with a microindenter	62

3.4.2	Compressive stress induces reversible apparent bundling in the <i>GFP-MBD</i> microtubule marker line and depolymerisation of microtubules in the <i>TUA-GFP</i> microtubule marker line	64
3.4.3	The <i>spr2-2</i> mutant has a lower apparent stiffness and lower growth speed compared to wild type microtubule marker lines and <i>bot1-7</i> mutant	66
3.4.4	Compressive stress induces apparent bundling in the <i>spr2-2</i> mutant but not in the <i>bot1-7</i> mutant	67
3.4.5	Quantifying the microtubule response to mechanical perturbations	68
3.5	Discussion	72
3.6	Material and Method	73
3.6.1	Plants material and growth conditions	74
3.6.2	Imaging	74
3.6.3	Indentation	74
3.6.4	Image analysis	75
3.7	Supplemental Figures	76
4	A pipeline for the quantitative analysis of epithelia from cell to tissue scale	77
4.1	Preamble	77
4.2	Abstract	77
4.3	Introduction	78
4.4	The choice of 3D surface	79
4.5	Detailed description of the pipeline	81
4.5.1	Reconstruction of 3D surface and segmentation with MorphoGraphX	81
4.5.2	From MorphoGraphX to R: integration of several snapshots and computation of new variables	83
4.5.3	Combining and synthesizing information	84
4.6	Application: New perspectives for the study of cell division at the shoot apical meristem	85
4.6.1	Spatio-temporal regulation of the division at the SAM	86
4.6.2	Cell shapes characteristics correlating with the absence of division in the short term	87
4.7	Discussion	88
4.8	Material and Methods	89
4.8.1	Plant material and growth conditions	89
4.8.2	Imaging	89
4.8.3	R pipeline	90
5	General discussion	91
5.1	Anisotropic mechanical stress fields contribute to the orientation of division plane at the epidermis of the SAM	91
5.2	Towards an experimental demonstration of the contribution of mechanical stress on division plane orientation	93
5.3	Contribution of mechanical stress to cell cycle	96
5.4	About the complex interplay between cytoskeleton and mechanical stress	97
5.5	Conclusion	102
	Bibliography	103
	A Appendix Chapter	117

List of Figures

1.1	Cell division	2
1.2	The cell cycle and its checkpoints	4
1.3	Positioning the nucleus	8
1.4	The Besson-Dumais rule	9
1.5	The shoot apical meristem of <i>Arabidopsis thaliana</i>	11
1.6	Examples of toxins produced by plants, fungi and sponge, which affect cytoskeletal dynamics	17
1.7	Examples of proteins modifying cytoskeleton dynamics	18
1.8	The katanin, a protein necessary to the establishment and maintenance of microtubule network architecture	19
1.9	Examples of cross-talk between cytoskeletal networks	21
1.10	Cytoskelal structures involved in mitosis	22
1.11	Definitions of Hooke's law, stress and strain	24
1.12	Evidence of forces within tissues and their origin	25
1.13	Range of forces, pressure and stiffness within tissues	26
1.14	Prediction/Deduction of stress patterns	30
2.1	Division planes at the shoot apical meristem of <i>Arabidopsis thaliana</i>	43
2.2	A domain-based comparison between observations at the SAM and predictions of the Besson-Dumais rule	45
2.3	Modeling the contribution of mechanical stress to division plane orientation	47
2.4	Effects of mechanical perturbation on division plane orientation	48
2.5	Comparison between simulated tissues and predictions of the Besson-Dumais rule	49
2.6	Besson script can be applied on 3D surface of the SAM	55
2.7	2D projection of two daughter cells	56
2.8	Examples of computations of the Besson script	57
2.9	Comparison between ranks and pairwise probabilities	58
2.10	Predictions of Besson-Dumais and bootstrap tests on all dividing cells (including the most asymmetric divisions)	58
3.1	Cell wall elongation following an ablation	60
3.2	Preliminary results on abnormal positioning of division plane close to an ablation site	61
3.3	Indentation protocol	63
3.4	Effect of compressions on <i>GFP-MBD</i> at a load value corresponding to different initial displacements	64
3.5	Effects of compression on <i>TUA-GFP</i> compared to <i>GFP-MBD</i>	65
3.6	Apparent stiffness of meristems and tip displacement speed	67
3.7	Effects of compression on <i>spr2-2 GFP-MBD</i> and <i>bot1-7 GFP-MBD</i>	68
3.8	FibrilTool measures of difference of microtubules anisotropy and orientation	69

3.9	Characterization of microtubule networks	70
4.1	Analysis pipelines in 2D and surface 3D	80
4.2	Extraction of 3D surface and cell segmentation with MorphoGraphX	81
4.3	Examples of maps generated by MorphoGraphX	82
4.4	Cellular Mesh	83
4.5	Description of regions	85
4.6	PCA on all SAM cells	86
4.7	Mitotic index	86
4.8	Characteristics of dividing cells	87

List of Tables

1.1	Division rates in the SAM	12
1.2	Young's modulus of some proteinaceous filaments	27
1.3	Examples of exogenous mechanical perturbations	33
3.1	Wilcoxon tests	76

1 Introduction

Morphogenesis, the shaping of a new organism along development, is driven by four processes: cell division, elongation, migration and apoptosis. These four processes are coordinated to form new organs. In plants, apoptosis is limited to very specific types of morphogenesis such as the formation of xylem or during the formation of dissected leaves (for instance, those of *Monstera*) (Doorn and Woltering 2005). Migration is prevented by the cell wall, a polysaccharide matrix gluing the cells together, and the growth or the pollen tube is not a true form of cell migration.

Here we focus on cell division. Cell division is a complex cellular process, controlled both temporally, by the cell cycle, and spatially, by the position of the division plane. The molecular basis of division are now well known and involve in particular cytoskeleton components. However, we do not understand well how cells, and in particular plant cells, position their division plane. Cell shape was proposed as a possible directional cue but do not explain all observed divisions. In a supracellular context, where cells are connected together, internal mechanical stress appears as another major candidate.

In this introduction, we give an overview of the temporal and spatial aspects of cell division and its coupling to growth, and we focus more particularly on a hotspot of division in plants: the shoot apical meristem (SAM) of *Arabidopsis thaliana* (see §1.1). We review the main features of the cytoskeleton and detail its implication during cell division (see §1.2). We highlight the existence of mechanical stress within tissues, and we review different ways of quantifying, perturbing and predicting mechanical stress patterns (see §1.3). We conclude this introduction with a review published in 2013 in *Current Opinion in Plant Biology*, which summarizes our current knowledge of the interplay between mechanical stress and cell division (see §1.4). Another review on mechanical stress and morphogenesis in the shoot apical meristem is added in Appendix §A, as direct contribution of M. Louveaux is limited to the paragraph concerning cell division in the SAM.

1.1 Cell division

Division, also called M phase, is the process by which a (mother) cell is splitted into two (daughter) cells. It is preceded by a phase of duplication of the genome and organelles, during the interphase. The alternation of interphase and M phase constitutes the cell cycle, that will be described later. M phase is divided into 2 parts: mitosis and cytokinesis.

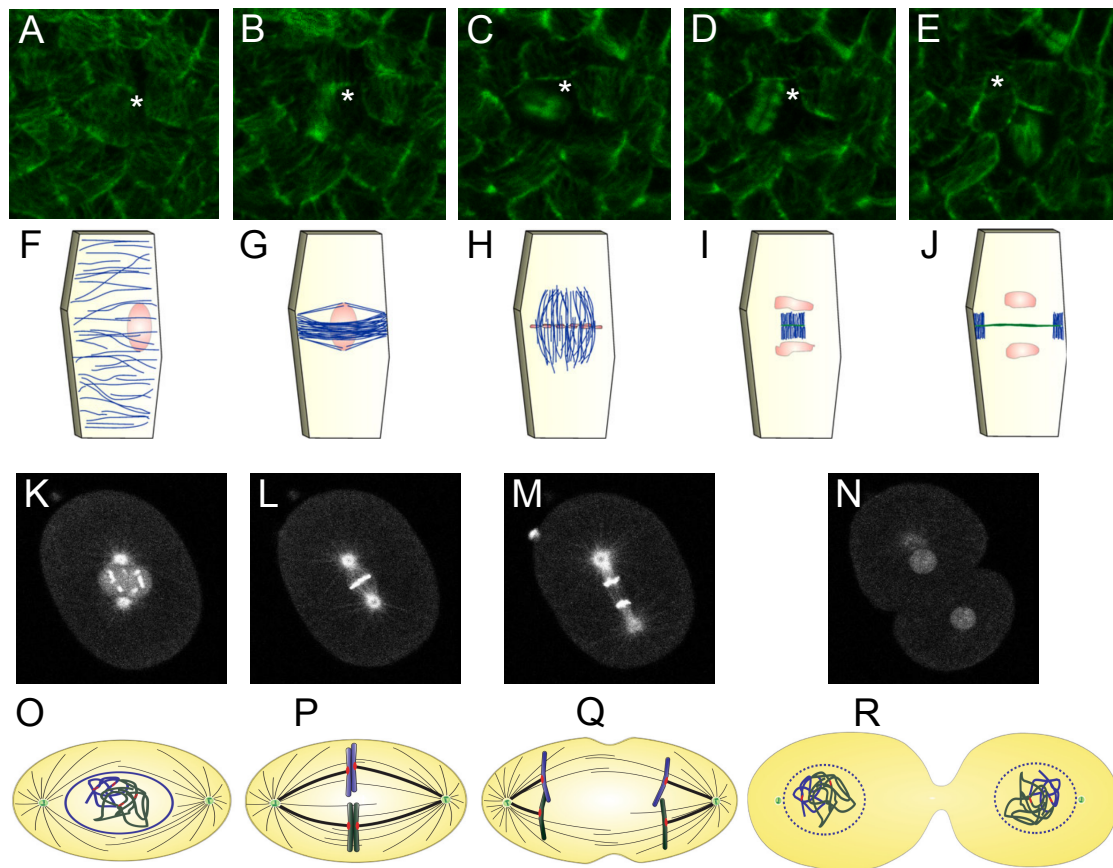


Figure 1.1: Cell division. (A-E) Close-up of confocal images of p35S::GFP-MBD (Microtubule Binding Domain) dissected shoot apical meristem. Images are taken every 2 h. White asterisk points at a dividing cell. (F-J) Schematic representation of plant cell division, adapted from [Zhu and Dixit 2011](#). Blue lines: microtubules. Pink structures: chromosomes condensed (F-G), aligned at metaphase plate (H) and separated between the two daughter cells (I-J). Green line: new cell wall. (A and F) Interphase. (B and G) Preprophase Band. (C and H) Spindle. (D and I) Phragmoplast. (E and J) New cell wall (E), and cell plate and late phragmoplast (J). (K-N) Snapshots from a film of the first division of a *Caenorhabditis elegans* embryo, tubulin::GFP and histone::GFP. Total duration of the first division: 2 min. Size of the embryo: 50*30 μm . Courtesy of Marie Delattre, LBMC, ENS de Lyon. (O-R) Schematic representation of animal cell division, adapted from [Silkworth and Cimini 2012](#). Blue and green thick structures: chromosomes. Red dots: kinetochores. Thin black cables: Microtubules. Green dots at spindle poles: centrosomes. (K) In *C. elegans* embryo, the phase preceding cell division differs from a traditional interphase (pictured in (O)): following gametes fusion, the two parental nuclei stay side by side. (L and P) Metaphase. Chromosomes are aligned at spindle equator. (M and Q) Anaphase. (N and R) Cytokinesis.

1.1.0.1 Mitosis

Mitosis is the series of events that leads to the separation of chromosomes and organelles between the future daughter cells into two identical pools. Mitosis is divided into five stages: prophase, prometaphase, metaphase, anaphase and telophase ([Alberts et al. 2014](#) and Fig. 1.1). Before M phase, each chromatid is duplicated and glued to one another by ring-shaped cohesins. In plants, cortical microtubules reorganise to form a ring surrounding the nucleus: the preprophase band (PPB) (Fig. 1.1A-B and F-G). During prophase,

replicated chromosomes condense and sister chromatids are resolved into distinct, separable units, under the action of condensins (Alberts et al. 2014 and Fig. 1.1O). Outside the nucleus, the spindle, a microtubule based structure assemble. In animals, spindle assembly is coordinated by two centrosomes (Fig. 1.1P). Each centrosome contains a pair of centrioles and several proteins, among which the *gamma*-tubulin ring complexes that nucleate microtubules and retain microtubule minus end. Centrosomes are absent in plants, and this is often associated with the presence of wider spindle poles (Fig. 1.1C and H). Phosphorylation of nuclear pore complexes and components of the nuclear lamina leads to disassembly of nuclear lamina and nuclear envelope breakdown (NEB). In plants, disassembly of the preprophase band occurs concomitantly to NEB. Chromosomes attach to spindle microtubules via their kinetochore, a multi layered protein structure built at the centromeric region of the chromatid on each side of the chromosome (Alberts et al. 2014). Three types of microtubules exist in animal spindle: astral microtubules, radiating from the poles to the plasma membrane, which are involved in spindle positioning, polar microtubules, which overlap at spindle equator and stabilise spindle architecture and control its length, and kinetochore microtubules, which pull and push on the chromosomes to align them at the equator of the spindle (Fig. 1.1L and P). In *Arabidopsis*, astral microtubules were reported only in suspension cells (Chan et al. 2005). At metaphase, each duplicated chromosome is attached by each side to a kinetochore microtubule from opposite cell poles (Fig. 1.1P). The molecular mechanism validating the correct attachment of chromosomes to kinetochore microtubule could be based on tension. Aurora-B kinase phosphorylation activity creates a low microtubule binding affinity at kinetochore site while chromosome is not attached or only attached on one side. When chromosome is attached on both sides, kinetochore is stretched and targets of Aurora-B phosphorylation are out of reach. Cleavage of cohesins release sister chromatids, which are pulled apart during anaphase by kinetochore microtubules (Fig. 1.1M and Q). The two set of daughter chromosomes are send to the opposite pole of the cell. During telophase a new nuclear envelope is formed around each set, isolating the two daughter nuclei (Fig. 1.1N and R).

1.1.0.2 Cytokinesis

Cytokinesis is the physical process of separation of the two daughter cells. Divisions are said to be symmetric when the two daughter cells have an equivalent volume and/or fate, and asymmetric when daughters have a different volume and/or fate (Rasmussen et al. 2011). In animals cells, a contractile ring of actin and myosin pinches the cell into two halves. Cleavage furrow forms at the equator of the spindle during anaphase (Fig. 1.1N and R). Displacement of spindle with a glass sphere melted at the end of a needle during anaphase provokes disparition of cleavage furrow and reformation around new equator, highlighting the role of spindle in positioning of cleavage furrow and thus contractile ring (Alberts et al. 2014; Rappaport 1961). In plants, mechanism of cytokinesis is completely different. The presence of a stiff polysaccharidic cell wall hinders constriction. Partition of the two daughter cells is instead performed by building a new cell wall between the two nuclei (Fig. 1.1E and J). Golgi vesicles containing polysaccharides, glycoproteins and enzymes are guided by a microtubule based structure called the phragmoplast (Fig. 1.1D and I). They fusion at the centre of the cell in a structure called the cell plate. Extension of the cell plate is centrifuge, e.g. cell plate extend from the centre of the cell to the periphery (Fig. 1.1J). Its correct attachment to mother cell wall requires notably the action of the protein TPLATE (Müller et al. 2009).

1.1.1 Temporal control

1.1.1.1 The cell cycle, a molecular clock

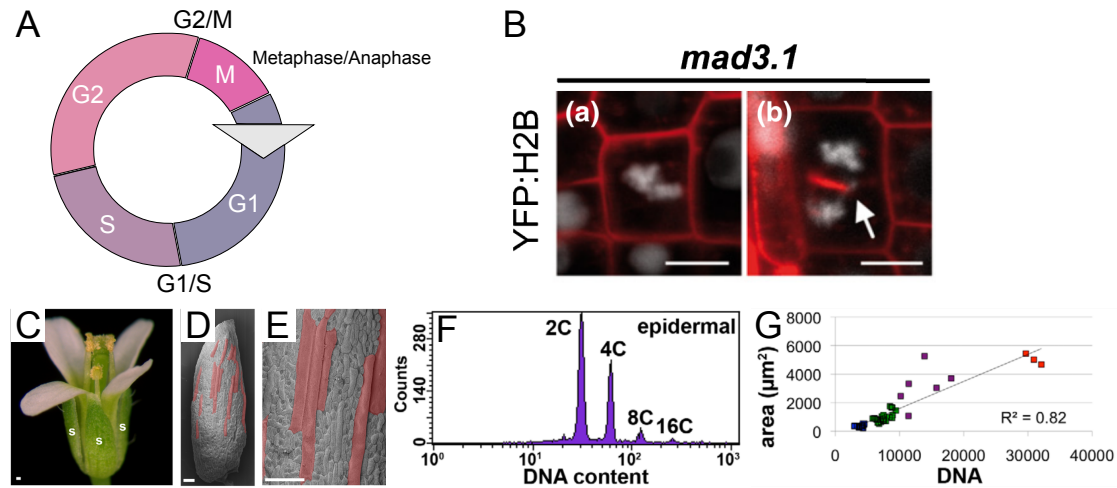


Figure 1.2: The cell cycle and its checkpoints. (A) Cell cycle and major checkpoints. (B) Example of defects at metaphase/anaphase transition in a meristematic root cell expressing H2B:YFP (white channel) and stained with FM4-64 (red channel) of the *Arabidopsis mad3.1* mutant, adapted from Paganelli et al. 2015. (a) At metaphase, some chromosomes are not well aligned. (b) At telophase, some chromosomes (white arrow) are still at cell equator, near the expanding cell plate. (C-G) Example of developmentally programmed skip of M phase in the giant cells of the sepals of *Arabidopsis*, adapted from Roeder et al. 2010. (C) *Arabidopsis* flower. s: sepals. (D-E) Scanning electron micrographs of a mature wild type sepal. Giant cells (false coloured red) are interspersed between smaller cells. (F) Flow cytometric analysis of the DNA contents of nuclei in the mature sepal epidermis (front and back) (G) Graph of DNA content (integrated density of DAPI fluorescence) versus cell area (μm^2) of mature sepal cells. The trend line of the data is displayed and $R^2 = 0.82$ ($n = 47$ pavement cells, normalized with fifty-nine guard cells which are known to be 2C). Ploidy of cells is indicated by color (red, 16C; magenta, 8C; green, 4C; and blue, 2C).

Division is preceded by a series of events in interphase: the duplication of the genome and organelles, and in most of the cases, growth. Interphase can be discretized in three phases: G1, S and G2 (Fig.1.2A). G1 is the first phase of the cell cycle and starts just after the previous round of division. S is the phase of replication of DNA, necessary to compensate for the split of chromatids in each daughter cells. G2 is a second short phase of growth. Progression through the cycle is dictated by the activity of cyclin-dependant kinases (CDKs), which are regulated by cyclins and other regulators. CDK are active only when bound to a cyclin. Concentration of CDKs is constant over time, whereas concentrations and activity of cyclins oscillated over time and determine the cell cycle stage (Alberts et al. 2014). These oscillations are at the base of cell cycle in all eukaryotes. However, there is subtle differences between species in term of proteins involved the cell cycle progression.

1.1.1.2 Progression through the cell cycle

Progression through the cell cycle orchestrates numerous events in the cell, and in particular the coordination of the molecular players of mitosis. In plants, several cell cycle proteins are localised on mitotic microtubule arrays. Whereas Cyclin-dependent kinases A;1 and B2;1 were found in PPB, spindle and phragmoplast of *Arabidopsis*, Cyclin A1;1 and B1;2 were found only on PPB and spindle (Duroc et al. 2011). Some were shown to interact with mitotic microtubule arrays or with proteins regulating dynamic of these arrays. Microinjection of an active Cyclin-dependent kinaseA;1/CyclinB in *Tradescantia* stamen hair cell caused rapid depolymerization of PPB, but not of interphase microtubule array, spindle or phragmoplast, and accelerated progression of mitosis by triggering chromosomes condensation and nuclear envelope breakdown (NEB) (Hush et al. 1996). The *Arabidopsis* MAP65-1 interacts with interphasic microtubules, with PPB, with midzone of the anaphase spindle and with the phragmoplast midzone during telophase, but not with metaphase spindle (Smertenko et al. 2006). Mutation of a potential cyclin-dependent kinase phosphorylation site restore binding of AtMAP65-1 with metaphase spindle. Phosphorylation of AtMAP65-1 by multiple kinases during prophase and metaphase inhibits its bundling activity. Expression of non-phosphorylatable AtMAP65-1 induces an accumulation of microtubules in the metaphase spindle midzone and a delay in the metaphase-anaphase transition.

We saw above that cyclin D and B homologues control the transition between G1 and S, and G2 and M, respectively (Fig. 1.2A). These transitions are conserved checkpoints. A third one is located at the transition between metaphase and anaphase and called the spindle assemble checkpoint (Fig. 1.2A). Cell progresses through the cycle only if checkpoint conditions are satisfied. Progression is regulated by intracellular and extracellular cues. Intracellular cues inform on the complete replication of DNA (before G2/S transition) or on the correct attachment of chromosomes on kinetochore microtubules at the transition between metaphase and anaphase ("spindle assembly checkpoint", see also §1.1.0.2). *Arabidopsis mad3.1* mutant is affected at metaphase/anaphase transition and present defects of chromosomes alignment on metaphase plate and of chromosomes lagging behind during anaphase (Paganelli et al. 2015 and Fig. 1.2B). In some cell types, checkpoints can be skipped by cells. For instance, giant cells of sepal skip the M phase and keep replicating their DNA, in a process called endoreduplication (Roeder et al. 2010). (Fig. 1.2C-G). Cytokinesis can also be disconnected in time from karyokinesis. In the *Drosophila* embryo, the first 13 round of nuclear division occur synchronously and without cytokinesis. Cellularisation occurs later, after migration of nuclei to the cortex (Alberts et al. 2014). Another example of syncytium is the plant endosperm (the tissue surrounding the seed). In this tissue, mitotic cells lack PPB (C. Lloyd and Chan 2006). Extracellular cues inform the cell on the opportunity to divide in the current environment. In animals, mitogens, such as the protein PDGF (platelet-derived growth factor), stimulate cell proliferation (Alberts et al. 2014), whereas antimitogen factor, such as the protein TGF β (transforming growth factor- β) block cell cycle in G1 (Alberts et al. 2014). In plants, an intermediate ratio of the phytohormones auxin and cytokinin promotes callus induction from differentiated cells in which cell cycle is arrested, while a high ratio of auxin-to-cytokinin or cytokinin-to-auxin induces root or shoot regeneration, respectively (Ikeuchi et al. 2013). Auxin induces the expression of two genes coding for the transcription factors LBD18 and LBD33. LBD18 and LBD33 form an heterodimer, which activates E2Fa (E2 PROMOTER BINDING FACTOR). E2Fa is a transcription factor, which in turn, dimerizes with

DIMERIZATION PARTNER (DP) and induces the expression of genes involved in DNA replication during S phase. Auxin also downregulates KIP-RELATED PROTEIN (KRP) genes, which encode Cdk inhibitors. Apart from these biochemical cues, light, as well as mechanical stress were shown to affect cell cycle. In protonemata of the fern *Adiantum capillus-veneris* L., divisions can be synchronized by blue light (Murata and Wada 1991). Compressive stress inhibits cell proliferation in tumor spheroids: cells are blocked in late G1 (Cheng et al. 2009; Montel et al. 2011; Montel et al. 2012). Compression was shown to provoke an overexpression of the $p27^{Kip1}$ cyclin-dependent kinase inhibitor, which is usually down-regulated to pass from G1 to S phase (Delarue et al. 2014). Compression of the spindle of single HeLa cells was shown to alter mitosis progression by either delaying (compression along spindle axis) or accelerating (compression perpendicular to spindle axis) the metaphase-anaphase transition (Itabashi et al. 2012). Compression is thought to act directly on mechanoperception of chromosomes attachment at spindle assembly checkpoint (see §1.1.0.2). In plants, experiments on the link between the cell cycle and mechanical stress are rare. Yeoman and Brown 1971 reports that both stretching and compression of explants accelerate division rate.

1.1.2 Spatial control

1.1.2.1 Molecular actors involved in cell division plane orientation

In plants, the division plane position is determined before mitosis, during late G2, with the formation of the PPB (Fig. 1.1B and G). Localisation of the PPB coincides with the position of the future division plane. Centrifugation of plant cells highlights the role of the nucleus in positioning the PPB and the role of the PPB in division plane orientation and maturation of the new cell wall. Centrifugation of protonemata of the fern *Adiantum capillus-veneris* L. before division caused a displacement of the nucleus and PPB formed around the new position of the nucleus (Murata and Wada 1991). Less than 10% of oblique (e.g. mispositioned) cell plates were observed. When nucleus was displaced after or during the formation of the PPB (at the apex), a second thinner and fainter PPB formed sometimes around the displaced nucleus, revealing the role of preprophase nucleus in the induction of PPB. In all centrifugation experiments, division occurred at the last location of the nucleus after centrifugation. When nucleus was displaced after or during the formation of the PPB, in 50% of the cases, new cell wall was oblique, highlighting the role of the PPB in the correct location of cell wall. Centrifugation during metaphase or anaphase of dividing *Tradescantia* stamen hair cells did not affect localisation and maturation of cell wall, whereas centrifugation during cytokinesis delayed cell plate formation (Mineyuki and Gunning 1990). When cell plate formed at a distinct location from the PPB, maturation of cell wall was altered, suggesting a role of PPB in the recruitment of maturation factors to the future division site (Mineyuki et al. 1991).

In *Arabidopsis*, the formation of the preprophase band is under the control of a complex of proteins: TONNEAU1, TONNEAU2 (also called FASS) and TRM (TON1 RECRUITING MOTIF). *tonneau* mutants lack preprophase band. In these mutants, cell division still occurs but division plane orientation is altered (J. Traas et al. 1995; Azimzadeh et al. 2008). The PPB is a transient structure, which disappears when the spindle is formed (Vos et al. 2004). Memory of the localisation of the PPB is kept by several proteins: some

remain located where the PPB formed and others are specifically absent from this region. The proteins Ran GTPase activating protein 1 (RanGAP1) and TANGLED were shown to colocalize with the PPB during preprophase and to maintain their location throughout mitosis (Walker et al. 2007). PPB of *tan* mutants are oriented as in WT, but phragmoplasts are shifted, as well as division planes. The double mutant *pok1-1;pok2-1* displays the same defects in phragmoplasts and division plane orientation (Müller et al. 2006; Walker et al. 2007). In this double mutant, TANGLED and RanGAP1 do not remain at division site after metaphase. POK1 and POK2 also localise at PPB and TANGLED interacts with the C-terminal domain of POK1. Maintenance but not recruitment of TANGLED to future division site requires POK1 (Lipka et al. 2014). POK1 thus appear as a reader of PPB position and TANGLED as the molecular link between phragmoplast and POK1 (Lipka et al. 2014). On the contrary, actin and KCA1 are depleted from PPB region (Lipka and Müller 2012; Rasmussen et al. 2013). KCA1 was reported to interact with CDKA;1 and with the microtubule severing protein KATANIN, but its role remains elusive (Lipka and Müller 2012; Rasmussen et al. 2013). Actin was shown to be involved in PPB narrowing and orientation of division plane (Mineyuki and Palevitz 1990; Kojo et al. 2013).

1.1.2.2 Identifying the centre of mass of the cell

The nucleus controls indirectly the position of the division plane, as it control localisation of the spindle (which forms around nucleus), and, in plants, localisation of PPB. Spindle, in animals, and PPB, in plants, control the orientation of the division plane. The nucleus is connected to the cytoskeleton by motor proteins (Tamura et al. 2013). The cytoskeleton, and in particular microtubules, stabilise the nucleus at the centre of mass of the cell prior to symmetric division. Stabilisation is achieved through the balance of forces between the different filaments. In vacuolated plant cells, nucleus is embedded in cytoplasmic strands, which contain actin and microtubules. Nucleus of vacuolated cells of *Datura stramonium* relocates toward centre of the cell before division (Flanders et al. 1990). Laser ablation of these cytoplasmic strands demonstrated that they are under tension (Goodbody et al. 1991 and Fig. 1.3A-B). Springs (modelling cytoplasmic strands) connected on one end to the edges of a rigid frame and on the other end by a central metallic element (modelling the nucleus) adopt the same configuration as cytoplasmic strands in a cell of the same shape (Flanders et al. 1990). In this analogy, springs are free to move along metallic edges of the frame. Position of the nucleus at cell centre of mass result from the balance of forces exerted by the different springs, which depend on cell shape. As demonstrated by modelling (Fig. 1.3C) and experiments on urchin egg cells (Fig. 1.3D-F), a modification of cell shape modifies the balance of forces and displace the nucleus toward the new centre of mass. Modification of the shape of urchin eggs induced a relocation of the nucleus toward the new centre of mass of the cell in less than 3 min (Minc and Piel 2012 and Fig. 1.3E). Relocalisation was blocked upon the addition of nocodazole, a drug inducing microtubules depolymerization, but not latrunculin B, a drug inducing actin depolymerization (Fig. 1.3F). Spindles of dividing urchin eggs blocked in metaphase also reoriented upon a change of shape in a microtubule but not actin dependent manner. Deformation of the nucleus gave an indirect evidence of the pulling and pushing forces exerted by microtubules.

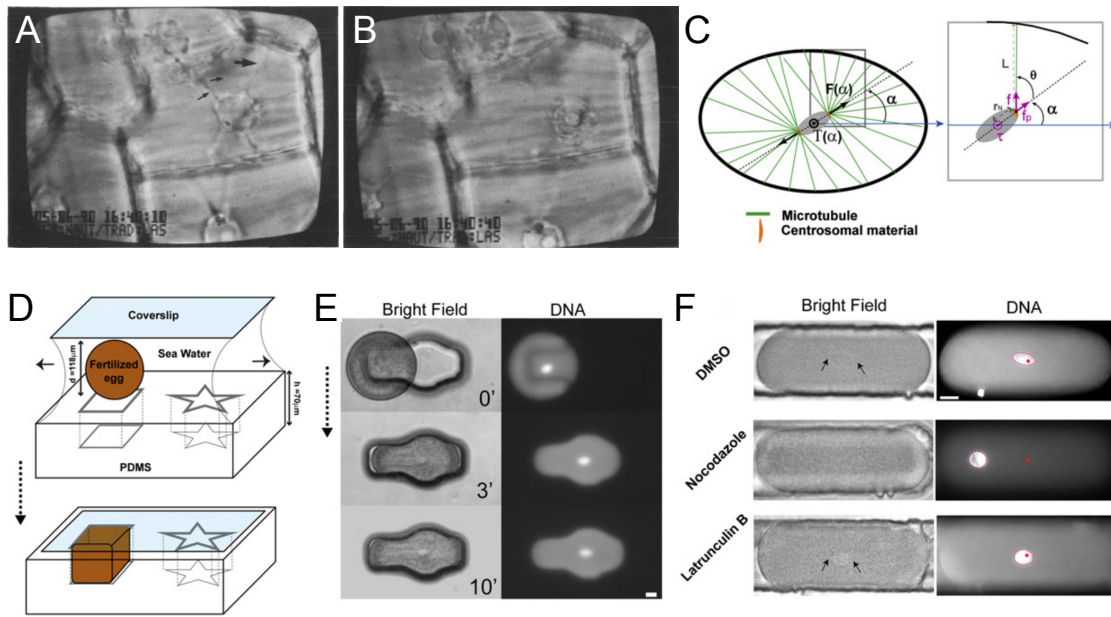


Figure 1.3: Positioning the nucleus. (A-B) Phase-contrast micrograph of *Nautilocalyx lynchii* epidermal peel after culturing on nutrient agar, adapted from Goodbody and C. W. Lloyd 1990. The nucleus is linked to plasma membrane by cytoplasmic strands populated by microtubules. (A) Some of these strands are severed with a laser (large black arrow). (B) Nucleus migrates towards the opposite, lower anticlinal wall. (C) Schematic 2D representation of the cellular organization used for modelling the balance of forces exerted by microtubules on the nucleus in urchin eggs. The nucleus (gray) is located at the centre of mass and oriented along an axis a . Microtubules (green) emanate from two centrosomes (orange) attached to each side of the nucleus and extend out to the cortex. The total force generated by the two MT asters along the α axis is $F(\alpha)$, and the total torque at the cell's centre is $T(\alpha)$. Inset: A microtubule in the aster has a length L and is nucleated at an angle θ from the axis α . It produces a pulling force f at its nuclear attachment and a torque τ at the nucleus centre. The projection of the force along the axis α is denoted f_p . (D-F) Modification of cell shape impacts nucleus position in urchin eggs, adapted from Minc et al. 2011. (D) Urchin eggs (diameter: 118 μm) are constrained in microfabricated PDMS wells of various shapes. (E) Dynamic alteration of interphase cell shape and imaging of nucleus position (stained with Hoechst). Time is indicated in min. (F) Alteration of interphase cell shape combined with cytoskeletal drug treatment: 1% DMSO (control), 20 μmol Nocodazole (microtubule depolymerizing drug), 20 μmol Latrunculin B (actin depolymerizing drug). Black arrows: asters adjacent to the nucleus. Red dot: cell center of mass. Purple dashed line: nucleus.

1.1.2.3 A probabilistic rule for division plane orientation

Since the end of the XIX^{th} century, the contribution of cell geometry on division plane positioning has been postulated empirically, both in animals and plants. Several rules were proposed at the same period. Hertwig's rule postulated that animal cells divide at cell centre of mass and perpendicular to longest axis (Hertwig 1884). Sachs's rule postulated that new division plane is perpendicular to parent wall and divide the cell evenly (Sachs 1878). Hofmeister's rule postulated that cell division planes are perpendicular to the direction of the fastest growth (Hofmeister 1863). Errera's rule originally postulated that "a cell wall, at the moment of its formation, tends to assume the form which a weightless liquid film would assume under the same conditions" (Errera 1888; Besson and Dumais

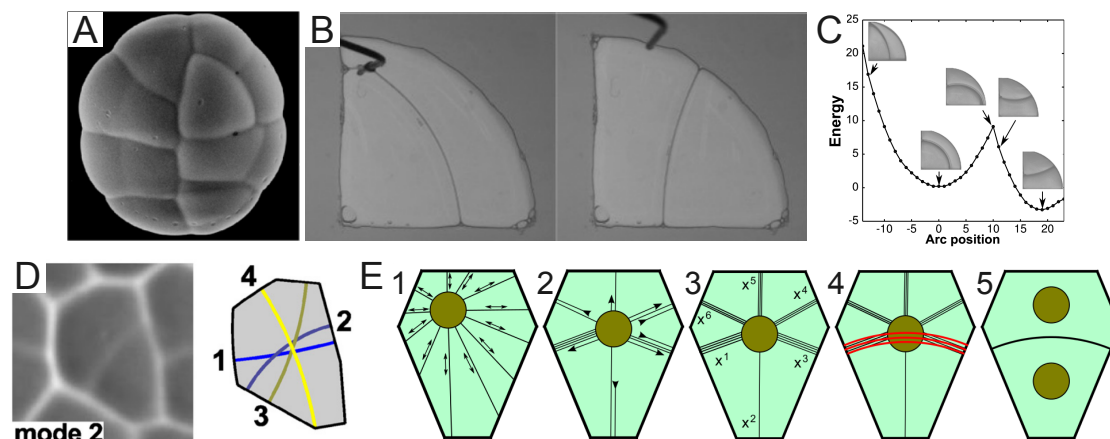


Figure 1.4: The Besson-Dumais rule, adapted from [Besson and Dumais 2011](#). (A) Two young glandular trichomes of *Dionaea muscipula*. The glands are made of four nearly identical quadrant cells that can divide according to three different planes: two mirror image anticlinal planes and one periclinal plane. (B) Equilibrium configurations of soap bubbles reproducing the observed periclinal and one of the two anticlinal divisions of the quadrant cells. (C) Experimental search of the configuration landscape for two soap bubbles trapped in a circular quadrant. The configurations corresponding to the observed division planes are local area minima, which are also energy minima in the case of soap bubbles. (D) Left: Replicas of recently divided cells in the leaf of the fern *Microsorium punctatum*. Cell divided along the second shortest plane. Right: The four shortest division planes predicted by the Besson-Dumais rule for this cell shape. (E) Mechanistic model for the selection of the division plane proposed by [Besson and Dumais 2011](#). 1. Before preprophase, microtubules radiate from the nucleus. 2. Microtubules reorganize into a finite number of configurations corresponding to the shortest distances between the nucleus and cell edges. 3. The equilibrium configuration favours short microtubules. 4. The PPB forms on the edges most heavily populated by microtubules. 5. The cell plate forms at the same position as the PPB.

2014). This latter rule was simplified as "the cell divide along the shortest path and divide the cell evenly" during the whole XX^{th} century. Derivations of Errera's and Sach's rule were successfully implemented in simulation of simple growing tissue, such as the meristematic region *Coleochatea*, which is a flat single cell thick layer ([Dupuy et al. 2010](#)). However, none of these rules perfectly explained divisions at the shoot apical meristem of *Arabidopsis thaliana*, but Errera's rule in its shortest path version was the closest ([Shapiro et al. 2015](#)). Moreover Errera's shortest path rule failed to explain why the quadrant cells of the trichomes of *Dionaea*, which, despite their identical shapes, can select different possible division planes (Fig. 1.4A). Recently, [Besson and Dumais 2011](#) went back to the exact definition of Errera's rule ([Besson and Dumais 2014](#)) and could reproduce the predicted planes positions with two soap bubbles confined in a quadrant shaped box (Fig. 1.4B). They showed that these planes were equilibrium configurations of soap bubbles interfaces and local length minima (Fig. 1.4C). They proposed a probabilistic version of Errera's rule in which several possible planes exist with different probabilities to be selected (Fig. 1.4D).

Based on the observations of [Flanders et al. 1990](#) (see §1.1.2.2), the molecular mechanism behind this rule was proposed to involve tension in microtubules guiding the relocation of nucleus at cell centre of mass prior to division and the selective stabilisation of microtubules spanning the shortest distance between the plasma membrane and the nucleus (Fig. 1.4E).

The higher dynamicity of microtubules during the formation of the PPB (Dhonukshe and Gadella 2003; Vos et al. 2004) was proposed to favor the exploration of a large number of division plane configurations.

Supracellular cues, such as auxin or mechanical stress may overcome this rule. While divisions of early *Arabidopsis* embryo stages are following Errera's rule, those giving rise to the 16-cell stage deviate from the rule and produce asymmetric cells (Yoshida et al. 2014). In the *bodenlos* mutant, affected in auxin signalling (BODENLOS is IAA12), default Errera's rule was restored, indicating a role of auxin in deviation from the geometrical rule. Microtubules align along maximal tensile stress in the meristem, suggesting that cell division plane could also follow this orientation (Hamant et al. 2008). But so far the relation between the principal direction of mechanical stress and the orientation of division remains unclear, as several contradicting results have been obtained (Louveaux and Hamant 2013) (reproduced below in §1.4). Bending explants of *Helianthus tuberosus* randomizes the orientation of division planes (Yeoman and Brown 1971). Compression of *Coleus* internodes and *Nicotiana tabacum* explants induce a preferential orientation of cell division planes perpendicular to the axis of compression (P. M. Lintilhac and T. B. Vesecky 1981; Philip M. Lintilhac and Thompson B. Vesecky 1984). And compression protoplasts or single cells from tobacco roots embedded in agarose induce a preferential orientation of cell division planes perpendicular to the axis of compression in three quarter of the tests and parallel to the axis of compression in the remaining quarter in one quarter (Lynch and Philip M. Lintilhac 1997).

1.1.2.4 The importance of cell division positioning and timing of division in development

Cell cycle was first studied in yeast (Nurse 2002). In this organism, progression through the cell cycle is coordinated with growth and division occurs at fixed cell size in constant growth conditions. This particular feature of yeast allowed discovery of genes, such as *wee1*, involved in the progression of the cell cycle. In multicellular organisms, and in particular in plants, increase or decrease in cell cycle rate can be compensated by a decrease or an increase of cell size (Inzé and De Veylder 2006). Moreover growth and cell proliferation are not always correlated. For instance, muscle and nerve cells, as well as some eggs grow without division (Alberts et al. 2014).

Randomized cell divisions can have important consequences on morphogenesis. In vertebrates, they are correlated with tumorigenesis and polycystic kidney disease (Castanon and González-Gaitán 2011). During embryo development of zebrafish, divisions are first oriented parallel to the animal-vegetal axis during gastrulation and then perpendicular during neurulation. During neurulation, cell divisions are coordinated: cells dividing in mirror across the midline of the neural rod. These mirror divisions are involved in lumen formation of the neural tube. In mutants displaying two midlines, mirror divisions still occur across both midlines and lead to the formation of two neural tubes (Tawk et al. 2007; Castanon and González-Gaitán 2011). In *Arabidopsis*, mispositioning of division planes in mutants such as *tangled* or *pok1-1;pok2-1*, have important consequences on global morphology of the plant. Double mutants *pok1-1;pok2-1* are dwarf, with thick stems, thick roots, thick roundish leaves and small siliques. In the root cell files are altered. Several polarized processes are regulated at plasma membrane, among which the direction of

auxin fluxes by PIN1 and disorganization of division plane orientation could perturb these fluxes. Development is also slower. However organs are positioned correctly on body plan and organ identity is not altered. Oriented asymmetric cell divisions are thought to be important for delimiting cell layers. In the *poltergeist/poltergeist-like Arabidopsis* double mutant loss of cell division asymmetry in the procambium and hypophysis of embryo accompanied by a loss of fate asymmetry and defects in specification of vasculature and root meristem (Song et al. 2008). In *Arabidopsis* embryo, asymmetric divisions at the transition between 8 and 16 cell stage parallel to the surface delimit the future epidermis. Transgenic *Arabidopsis* lines misexpressing BODENLOS protein and thus affected in transcriptional auxin response display switched planes, anticlinal to the surface. However, they do form an epidermis (Yoshida et al. 2014).

1.1.3 Case study: the shoot apical meristem, a place of divisions

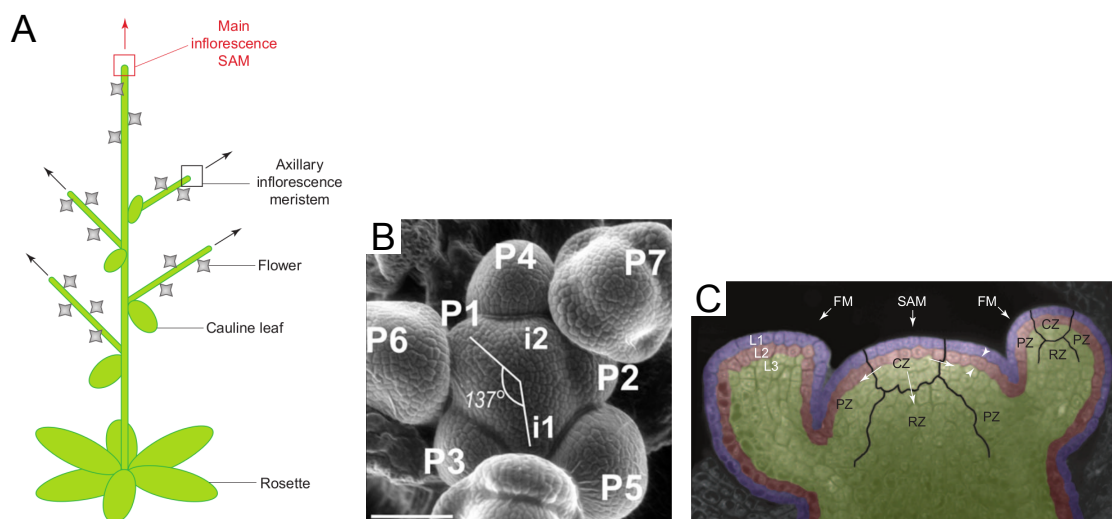


Figure 1.5: The shoot apical meristem of *Arabidopsis thaliana*. (A) The SAM is located at the tip of the stems and forms the leaves and flowers, adapted from Carles and Fletcher 2003. (B-C) The SAM has a stereotyped organisation. (B) Top view (scanning electron microscopy) of the SAM showing the regular spacing of primordia (P1 to P7) with a mean divergence angle of 137°, adapted from Besnard et al. 2011. (C) Orthogonal view of a confocal laser-scanning micrograph of the SAM, adapted from Carles and Fletcher 2003. False color highlight the meristem layers: the epidermis (L1) and the subepidermal layer (L2), forming the tunica, and the internal layers (L3), also called corpus. L1 and L2 are maintained by anticlinal divisions (white arrowheads). The black outlines represent the approximate boundaries between the different meristematic zones: peripheral zone (PZ), central zone (CZ) and rib zone beneath the central zone (RZ). The same organization is found in outgrowing flower primordia, albeit without a true L2 layer (FM: flower meristem).

In plants, divisions occur in specific places named meristems. Meristem come from the Greek word merizein ($\mu\epsilon\rho\iota\zeta\epsilon\iota\nu$), meaning "to divide". Primary meristems are located in the root and in the shoot of the plant. The root meristem provide the precursor cells for vasculature and surrounding tissues and the shoot apical meristem generates all the aerial organs (leaves and flowers) (Fig. 1.5A-B). In *Arabidopsis thaliana*, the shoot apical meristem (SAM) undergoes two phases: vegetative, during which the leaves of the rosette are produced, followed by the inflorescence phase, during which the flowers are produced.

Here we focus on the shoot apical meristem of *Arabidopsis* at the inflorescence stage and review a few studies on the cell cycle and division plane orientation at the SAM. Some were performed on fixed material (Laufs et al. 1998; Breuil-Broyer et al. 2004), while others were conducted on living meristems with either time-lapse confocal imaging or electron microscopy of epoxyresin replicates of living meristems (Reddy et al. 2004; Kwiatkowska 2004).

In the SAM, the M phase last less than 1 h (Reddy et al. 2004) but the total duration of cell cycle in the SAM is not homogeneous. Four regions can be distinguished on their division rate (Table 1.1 and Fig. 1.5C): the central zone, dividing slowly, the peripheral zone, where new primordia are initiated, which divide two to three times more rapidly than the central zone, the primordia, which division rate is similar to the peripheral zone until stage 2 and where a burst of divisions is observed at the transition between stage 2 and stage 3, and the boundary, where few divisions were observed. Several cell cycle genes, such as CyclinD2;1, CyclinD3;1, E2Fa and KRP2 and 3 were not detected in the boundaries, suggesting that the overall cell cycle has slowed down in this domain (Breuil-Broyer et al. 2004). CyclinD3;1 was shown to control the G1/S transition (Menges 2006). Cell cycle length is more homogeneous in the peripheral zone and primordia than in the central zone. Neighbouring cells can have very different cell cycle rates in the central zone (Laufs et al. 1998; Grandjean et al. 2004; Reddy et al. 2004), whereas synchronised divisions -within and accross cell layers- were observed in the peripheral zone and in primordia during the transition between stage 2 and stage 3 (Reddy et al. 2004). Cell cycle length is not constant within a lineage, as it can vary by a factor two between a cell and its immediate descendants (Reddy et al. 2004). Division rates in the SAM can be modified by local induction of cell cycle genes, suggesting that division rate is actively regulated in the SAM. Conversely, the increase or decrease in cell numbers can be buffered later on, as effects on adult organs are limited (J. Traas and Bohn-Courseau 2005).

Region	Division rate
Central zone	36 to 72 h
Peripheral zone	18 to 36 h
Boundary	rare
Primordia until stage 2	24 to 36 h
Primordia at stage 3	12 to 18 h

Table 1.1: Division rates in the SAM from (Laufs et al. 1998; Breuil-Broyer et al. 2004; Reddy et al. 2004; Kwiatkowska 2004). Primordia stages as defined in Reddy et al. 2004: P1 correspond to a visible bulge on the meristem flank ; P2 to its extension in the X-Y dimension and appearance of first sign of a groove between primordium and the meristem -e.g. the future boundary- ; P3: primordium begins to acquire height.

The orientation of division planes in the SAM are not random. Because of the presence of very small vacuoles and small cell size, nucleus occupies almost all the cell volume and, contrary to large vacuolated cells does not really relocate before mitosis. An orthogonal view of SAM reveals an organization into layers. The two most outer layers, referred as the tunica, or the L1 (epidermis) and L2, are clearly separated (Fig. 1.5C). In L1 and L2, divisions are mostly anticlinal (J. Traas and Bohn-Courseau 2005), maintaining the separation between layers. As a primordium emerges, divisions in the L2 can become periclinal and this can even be used as a landmark of organogenesis. Interestingly, ablation of L1 cells also provokes a local shift from anticlinal to periclinal in division plane orientation of dividing cells in the L2 (Reinhardt et al. 2003). The inner layers, referred as corpus, are

less well organised. In the L1, primordia outgrowth coincide locally with a preferential orientation of divisions parallel to the future boundary (Reddy et al. 2004). Not all the lineage originating from this division became part of the primordium.

1.2 The cytoskeleton

The word "cytoskeleton" was first used by a french scientist, Paul Wintrebert, in 1931, to describe the idea that cells have an internal organisation (Frixione 2000). Since the beginning of the XX^{th} century, it was clearer and clearer that cells could not be inorganised bag of enzymes. Centrifugation had been shown to disorganise the intracellular organisation of the cell only temporarily and the number and complexity of chemical reactions occurring in a cell implied a strict spatial and temporal compartmentalisation and dynamic organisation of the intracellular content (Frixione 2000). Thus, early on, the word "cytoskeleton" was used to reflect the idea of a physical structuration of the cell, without any reference to precise molecular structures. Fibrillar structures, such as sarcomeres and spindles, had been described since the XIX^{th} century, but the link with the conceptual idea of Paul Wintrebert was made only 20 years later, in the 1950's. At this time, development of electron microscopy had allowed to observe more clearly these fibrillar structures and to admit that they were not just artefact of preparation (Frixione 2000). Three families of small polymers of a diameter of a few nm were successively discovered: actin in 1943, microtubules in 1963 and intermediate filaments in 1976. They constitute the canonical components of the cytoskeleton. New components of the cytoskeleton have been identified in Prokaryotes in the past decades, some of them related to actin, microtubules, or intermediate filaments, such as mreB, ftsZ or crescentin respectively, and other unrelated such as bactofilins (Ingerson-Mahar and Gitai 2012). Here we will only provide an overview of the Eukaryotic cytoskeleton.

1.2.1 Historical and biochemical description of members of the cytoskeleton elements

1.2.1.1 Microtubules

Microtubules were discovered first in plants in 1963 (Ledbetter and Porter 1963). They are present in all Eukaryotes. Microtubules are cylindrical filaments of a diameter of 25 nm, constituted, most of the time, of 13 protofilaments (Chrétien et al. 1992; Alberts et al. 2014). Each protofilament is a regular association of two globular proteins : α and β tubulins. α and β tubulins are associated by pair with a non covalent link, forming a heterodimer: the microtubule subunit. The numerous non covalent links between microtubules subunits and between protofilaments confer to the filament a strong stability to thermal agitation and a high flexural rigidity (or bending stiffness), similar to those of plexiglas (Gittes et al. 1993). Flexural rigidity can be deduced by measuring the length, called persistence length, of a growing polymer before it starts to bend because of thermal fluctuations. The persistence length of microtubules is the highest of the 3 cytoskeleton components: it can reach several millimetres *in vitro* (Suresh 2007). However, *in vivo*, microtubule can bend at a scale of a few micrometres. MAP65-1, a microtubule binding

protein, involved in microtubule bundling, was shown *in vitro* to decrease microtubule persistence length by a factor of 4 (Portran et al. 2013b). Microtubules are almost inextensible and are expected to respond to forces either by bending or sliding along other microtubules (Gittes et al. 1993). Because of asymmetry of heterodimers of tubulin and ordered succession of these heterodimers in the protofilament, extremities of microtubules are structurally different: microtubules are polar. New heterodimers are added preferentially at the + end of the microtubule, where GTP molecules are exposed by β tubulins. *In vivo*, free heterodimer of $\alpha\beta$ tubulins are linked to GTP. One molecule of GTP is linked to the α tubulin and never hydrolysed because of the presence of β tubulin. The other GTP molecule is linked to the other side of the β tubulin and is exposed to cytoplasm. Incorporation of this heterodimer to a microtubule filament modifies the conformation of the heterodimer and accelerates GTP hydrolysis into GDP.

1.2.1.2 Actin

Actin was first discovered in 1943 in muscle extracts, in association with myosin. Like microtubules, actin is present in all Eukaryotes. Actin is a thin filament of 5 to 9 nm of diameter, constituted of two protofilaments coiled up together with a torsion period of 37 nm (Alberts et al. 2014). Actin filaments are more flexible than microtubules: their persistence length is only of a few dozens of μm . One protofilament is constituted of globular proteins : the actin monomers, which constitutes the actin subunits. Actin monomers are linked to ATP. The asymmetric structure of this globular protein and its ordered association in a protofilament creates a polar actin filament. New actin subunits are added preferentially at the + end of actin.

1.2.1.3 Intermediate filaments

Observation of intermediate filaments started also with the development of electron microscopy but they were identified as a distinct class of cytoskeletal components of intermediate size only at the end of the 1970's (Eriksson et al. 2009). Intermediate filaments exist only in metazoans (Eriksson et al. 2009; Alberts et al. 2014). In contrast to microtubules and actin, they are very diverse biochemically but share common structural features and the property of being insoluble under physiological conditions (Eriksson et al. 2009; Alberts et al. 2014). They have a diameter of around 10 nm and a rope-like structure, composed of many filaments. Each filaments is a complex assembly of monomers. Monomer structure is a conserved α -helical rod domain flanked by globular N and C terminal heads. Monomers assemble by two as a coiled-coil dimer, N terminal head along with N terminal head. Dimers are staggered along each other as tetramers, N terminal head with C terminal head, suppressing polarity of the filament. Tetramers are packed head to head in a protofilament. Eight protofilaments are twisted together in a filament. Intermediate filaments self assemble without any input of energy coming from nucleoside triphosphates such as ATP or GTP (Eriksson et al. 2009; Alberts et al. 2014) and incorporation of new subunits can occur at both ends of the apolar filament (Windoffer et al. 2011). Intermediate filaments are flexible (persistence length of less than 1 μm) and very resistant to traction forces. Four types of intermediate filaments were defined at the end of the 1970's, based on the structural features of the monomer (Eriksson et al. 2009):

acidic keratins (I), neutral-basic keratins (II), vimentins and desmins (III) and neurofilaments (IV) (Eriksson et al. 2009; Alberts et al. 2014; Peter and Stick 2015). Lamins were identified as a V^{th} type of intermediate filaments and the ancestors of this superfamily a decade later (Eriksson et al. 2009). In plants, only lamin-like analogues have been found (Ciska et al. 2013).

1.2.2 Regulation of cytoskeleton polymers

In the following we will review the mechanisms controlling cytoskeleton dynamics and organization, focusing on microtubules and including some comparisons with actin filaments.

1.2.2.1 Nucleation

Since the 1970's, *in vitro* studies revealed that actin and microtubules are very dynamic polymers. *In vitro*, polymerisation of purified actin or microtubules subunits is divided in 3 phases: a lag phase, where free subunits are dominant and seldom assemble into short polymers, a growth phase, where polymers elongate by addition of subunits, following a increase of temperature of the solution or addition of salt, and an equilibrium phase, characterised by a constant exchange of subunits between a pool of free subunits and the polymer (Alberts et al. 2014). Lag phase do not exist *in vivo* and disappears *in vitro* when fragments of stabilised polymers are added to the solution of free subunits. *In vivo*, nucleation is initiated by a small fragment of polymer stabilised by several proteins, such as the γ -tubulins (microtubules) and the Arp2/Arp3 complex (actin).

γ -tubulins associated with other proteins help stabilizing the minus end of microtubules in all Eukaryotes (Pastuglia and Bouchez 2007; Alberts et al. 2014). γ -tubulins were found to associate with γ -tubulins complex proteins (GCP) 2, 3, 4, 5 and 6, forming γ -tubulin ring complexes (γ -TURC) (Nakamura and Hashimoto 2009). These complexes are found near the nucleus, at centrosomes. Centrosome contain γ -TURC, other proteins and a pair of centrioles, which are small microtubule based structures (Alberts et al. 2014). In interphase, the centrosome organizes microtubules radially, trapping minus end near the nucleus. Centrioles are duplicated during S phase. During prophase, the centrosome splits into two and migrates at each pole of the nucleus, each with a pair of centrioles, to form the spindle. The *Arabidopsis* genome encodes putative orthologues for all GCPs (Pastuglia and Bouchez 2007), but only GCP2 and 3 were found in association with γ -tubulins by tandem affinity purification (Nakamura and Hashimoto 2009). γ -tubulins and GCPs associate with pre-existing microtubules and nucleate branched microtubules with an angle of 40° (Pastuglia and Bouchez 2007). Plants cells lack centrosome, but GCP2 was found to localise near nucleus, at cell edges and at cell cortex, suggesting existence of microtubule organization centers at each of these locations (Ambrose and Wasteney 2014). Plant microtubule networks are mostly cortical and organised in parallel or net-like arrays (Wightman and Turner 2007). GCP2 seem to be important for the angle of branching, as in *gcp2* mutants, angle of microtubule nucleation is less tightly controlled (Nakamura and Hashimoto 2009). Other proteins were shown to be involved in geometry of plant microtubule network, both in interphase and during mitosis, and share homologies with

centrosomal proteins, suggesting a conserved role in organisation of microtubule arrays. Two proteins, TONNEAU 1 and 2, were shown to be involved in PPB formation: *ton1* and *ton2* mutants lack PPB (J. Traas et al. 1995; Azimzadeh et al. 2008). TON2 was also shown to regulate ratio of branching to in-bundle microtubule nucleation during interphase (Kirik et al. 2012) and *ton1* mutant display highly disorganized interphasic microtubule arrays (Azimzadeh et al. 2008). Interestingly, TON1 was shown to interact with centrin, which is homologous to a human centrosomal protein, and is itself homologous to FOP, another human centrosomal protein (Azimzadeh et al. 2008; Spinner et al. 2013). TON1 was also shown to interact with TRM1 (TON1 RECRUITING MOTIF1) (Drevensek et al. 2012). TRM1 belongs to the TRM superfamily. TRM is a superfamily of proteins sharing common motifs, which are also found in the sequence of the CAP350 mammal protein, which is also located at centrosomes (Drevensek et al. 2012).

Three classes of nucleation factors are involved in the nucleation of actin: (i) the Arp2/Arp3 complex, (ii) formins and (iii) Spire, Cobl, Lmod and JMY (Chesarone and Goode 2009; Firat-Karalar and Welch 2011). Class (i) and (ii) are found in all Eukaryotes (Alberts et al. 2014), and so far class (iii) seem to have been reported only in animals. The Arp2/3 complex consist of seven subunits mimicking the beginning of an actin filament with a modified minus end. This modified end associates with already polymerized actin filaments at a 70° angle and integrates new actin subunits at plus end, creating branched actin networks. *Arabidopsis* mutants of these subunits show severe defects in the shape of pavements cells and trichomes, but no obvious changes in global plant morphology (S. Li et al. 2003). Formins associate dynamically with the growing plus end of the actin filament and thus do not prevent loss of actin subunits at the minus end. Formins are involved in the formation of actin bundles. Proteins of class (iii) gather and stabilise actin monomers into nucleation complexes.

1.2.2.2 Polymerization and depolymerization

The localisation and diversity of nucleation complexes and types of nucleation complexes create various types of network architectures, which are remodelled dynamically. One of the most spectacular remodelling mechanism is the use of toxins by plants, fungi and sponge to protect themselves from voracious animal predators: such molecules can control cytoskeleton network architecture by affecting the dynamics of polymerization/depolymerization (Fig. 1.6). For instance, by binding free tubulin, colchicine prevents the polymerization of new microtubules and, because of the adjustment of equilibrium between subunit pool and elongated polymers, provokes a massive depolymerization of microtubular arrays, and in particular of mitotic structures (PPB, spindle and phragmoplast) (Pickett-Heaps 1967). These drugs can destabilise or freeze whole cytoskeletal networks and have dramatic effects on numerous cells functions including mitosis. They are commonly used in research to explore the functions of cytoskeleton, and in medicine, notably in chemotherapy.

The cell itself controls its own networks architecture by using a very diverse range of proteins and strategies, very similar to those observed in the presence of cytoskeletal drugs. The diversity of proteins and their coordinated action insure a fine spatio-temporal tuning of network architecture, at local or whole cell scale (in the case of cell migration or mitosis, for instance).

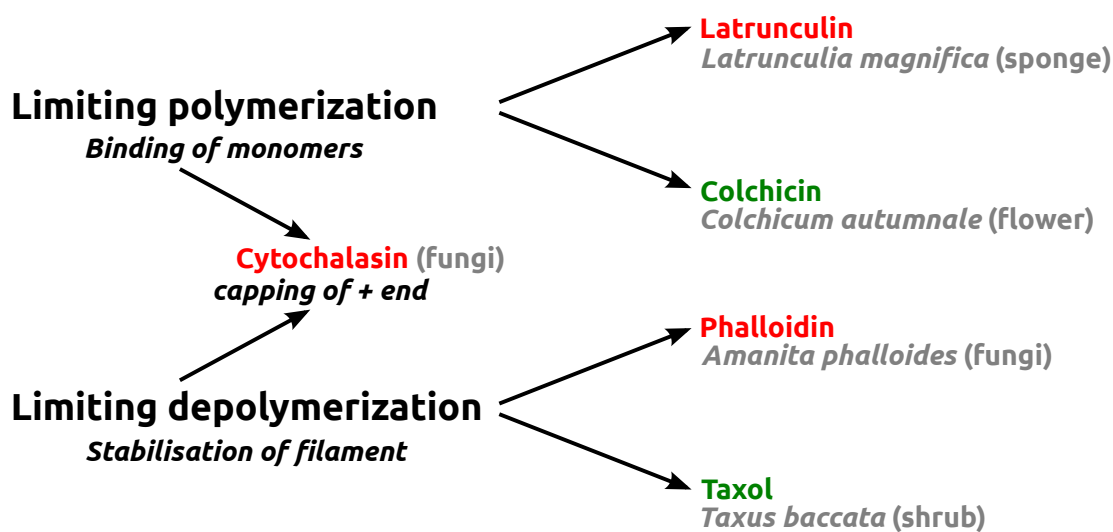


Figure 1.6: Examples of toxins produced by plants, fungi and sponge, which affect cytoskeletal dynamics, adapted from (Alberts et al. 2014). Colour code indicate the cytoskeletal component targeted by the drug: actin (red) or microtubules (green) and the specie producing this toxin (in grey)

1.2.2.3 Monomers sequestering and modulation of + and - ends

Polymers are constantly growing and shrinking, exchanging subunits with a cytoplasmic pool of free monomers. Sequestering monomers displace equilibrium between polymer and monomers and provoke depolymerization of existing polymers until a new equilibrium is found. Sequestering a pool of monomers also allow to rapidly mobilise a bigger quantity of monomers, without new synthesis, and to respond quickly to changing conditions. Sequestering can be achieved by binding physically to the monomer or by modifying the structure of the monomer. Stathmin or thymosin interact physically with microtubules or actin monomers, respectively (Fig. 1.7). The *Arabidopsis* protein PROPYRAMIDE-HYPERSENSITIVE 1 (PHS1) possesses a tubulin kinase domain and a phosphatase domain (Fujita et al. 2013). Phosphorylation of *alpha*-tubulin subunit by the kinase domain prevent their integration to an existing filament and thus provoke depolymerization of microtubules. Under normal physiological conditions, kinase activity is repressed by phosphatase domain. Hyper osmotic stress relieves this repression and provokes a transient depolymerization of microtubules. Conversely, other proteins interact with polymers end preventing or facilitating both loss and integration of monomers. Nucleation complexes, such as Arp2/3 (actin) and *gamma*-TURC (microtubules) bind minus end and prevent loss of subunits (Fig. 1.7). Capping proteins (actin) and +TIPs such as EB1 (microtubules), bind plus end and prevent both loss and incorporation of new subunits. Growing + ends can also be associated with elongation factors, which promote incorporation of new subunits or enhance + end dynamics. Formins and Ena/VASP facilitate + end elongation of actin filament (Chesarone and Goode 2009). MOR1, the *Arabidopsis* homologue of *Xenopus* MAP215, promotes rapid growth and shrinkage of microtubules (Kawamura and Wasteney 2008).

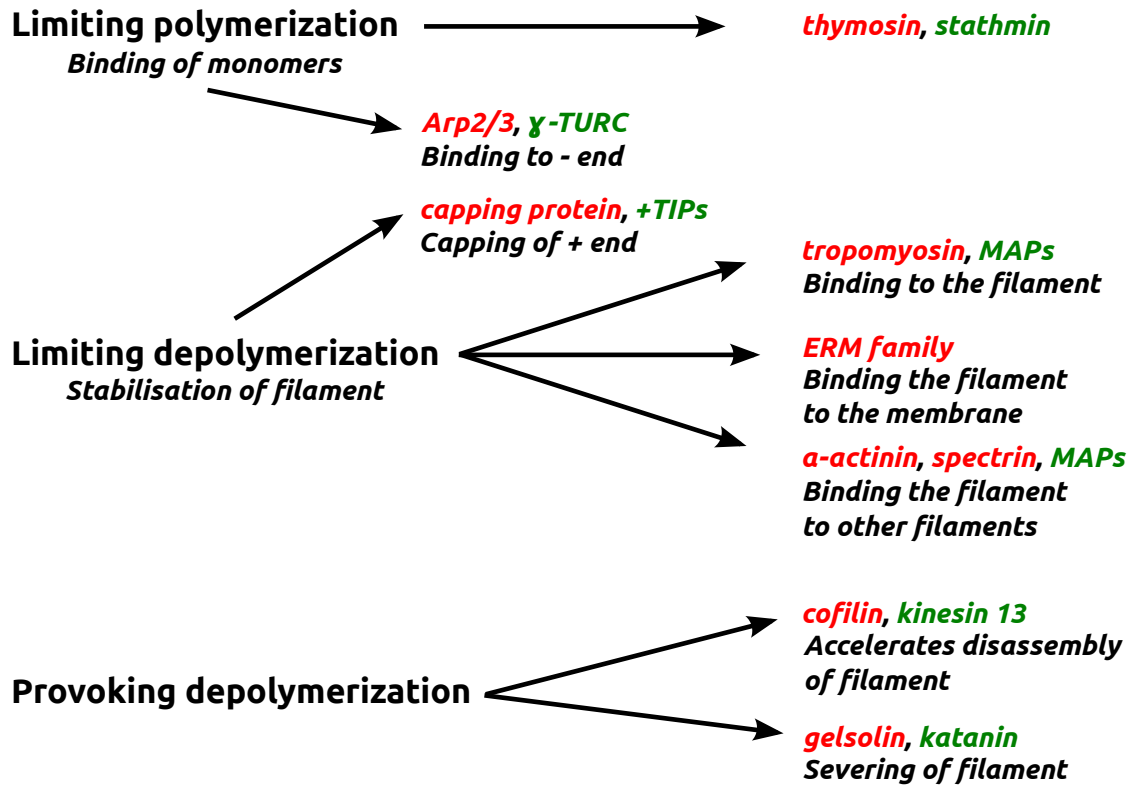


Figure 1.7: Examples of proteins modifying cytoskeleton dynamics, adapted from (Alberts et al. 2014). Colour code indicate the cytoskeletal network targeted by the drug: actin (red) or microtubules (green).

1.2.2.4 Severing

In addition to these mechanisms of stabilisation or destabilisation of polymers, some proteins can also provoke depolymerization, by breaking (e.g. severing) the filament. Severing is provoked by a steric destabilisation of the filament, involving (or not) hydrolysis of nucleotide triphosphate molecules.

Cofilin (Fig. 1.7) binds preferentially to ADP actin subunits, targeting the older parts of the filament, and destabilises actin filament by inducing a conformational change (Galkin et al. 2011; Blanchoin et al. 2014). Molecular motors, such as myosins, can provoke disassembly of a whole polymer network, such as actin, by sliding filaments in an antiparallel manner, which result in the contraction of the whole network (Blanchoin et al. 2014).

Katanin, as spastin and fidgetin belongs to the AAAATPase family (Roll-Mecak and McNally 2010). These three proteins require ATP hydrolysis to sever microtubules (Fig. 1.7). The *Arabidopsis* katanin plays an important role in the establishment and maintenance of microtubules arrays architecture. Severing of microtubules was first discovered in extract *Xenopus laevis* eggs arrested in metaphase of the second meiotic division in the early 1990's (Vale 1991). Incubation of this "mitotic" extract (*sic*) with taxol stabilized microtubules lead to shortening of these microtubules, whereas no shortening of microtubules could be observed in interphase extracts. Mitotic extract converted into interphase extract by addition of calcium and cycloheximide (cyclin degradation and blocking of new protein synthe-

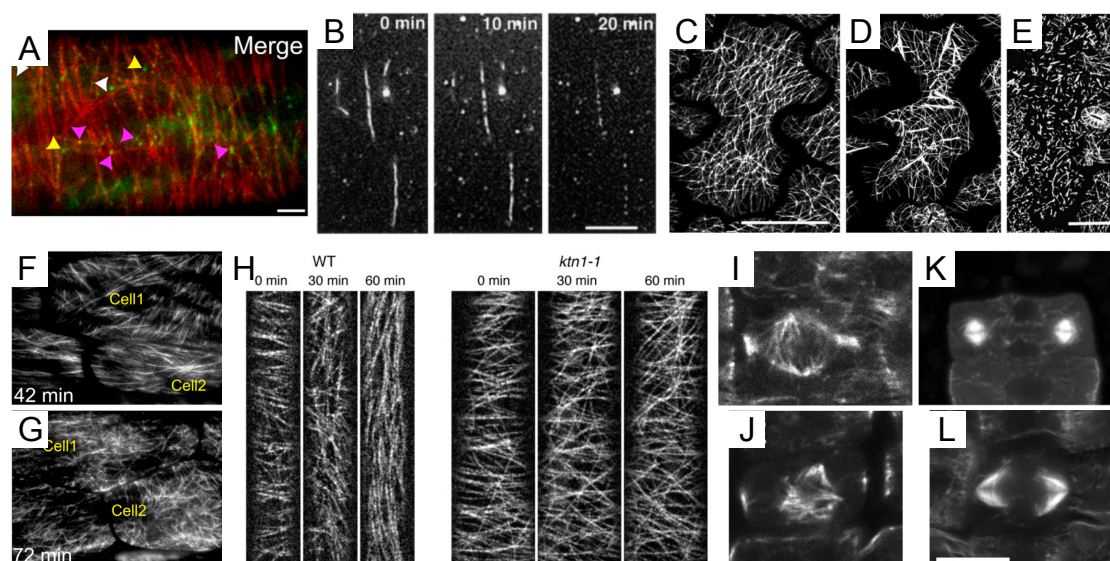


Figure 1.8: The katanin, a protein necessary to the establishment and maintenance of microtubule network architecture. (A) Confocal image showing preferential localisation of KATANIN-GFP at microtubules cross-overs in a wild-type *Arabidopsis* hypocotyl cell coexpressing RFP-TUB6 (Zhang et al. 2013). (B) *In vitro*, katanin severs microtubules (Stoppin-Mellet et al. 2002). (C-E) Inducible over-expression of katanin in *Arabidopsis* pavement cells. (C) Wild type. (D-E) After induction of katanin, microtubules gather into bundle (D) and then are severed (E) (Stoppin-Mellet et al. 2006). (F-G) Recovery after cold induced depolymerization of microtubules in (F) wild type and (G) *katanin* mutant. (H) Microtubule reorientation in WT and *katanin* (*ktn1-1*) mutant *Arabidopsis* etiolated hypocotyl cells under blue light stimulation (Lindeboom et al. 2013). (I-L) Role of katanin on mitotic arrays. (I-J) Spindles of (I) wild type and (J) *katanin* mutant. (K-L) Phragmoplasts of (K) wild type and (L) *katanin* mutant (Panteris et al. 2011).

sis) showed little severing activity. Conversely, addition of cyclin to interphase extract provoked an increase in severing activity. These experiments pointed out a cell cycle control of severing activity, correlated with major rearrangements of interphasic microtubule network into a spindle at the transition between G2 and M phase. The protein involved in this severing process was discovered two years later in urchin eggs extract and named katanin in reference to the Japanese word "kata" meaning "sword" (McNally and Vale 1993). This heterodimeric protein, composed of a regulatory subunit of 80kDa and a catalytic subunit of 60kDa requires ATP hydrolysis to sever microtubules (McNally and Vale 1993). Eight years later an *Arabidopsis thaliana* homologue with the gene of the animal catalytic subunit was discovered independently and almost at the same time by three different teams, in a screen for mutants with reduced cell elongation in the hypocotyl (Bichet et al. 2001), in a screen for mutants with reduced normal mechanical strength in the inflorescence stem (Burk et al. 2001), and from the bioinformatic screen of a cDNA gene bank with a research of homology similarities with animal katanin gene (McClinton et al. 2001). This gene was named *BOTERO1* (*BOT1*), *FAT ROOT* (*FTR*), *FRAGILE FIBERS* (*FRA2*) or *AtKSS*, underlying morphological and cellulose orientation defects of the mutant. In fact, this mutant is dwarf, has impaired microtubules and cellulose orientation, which affect cell expansion and mechanical resistance of the stem, and a few defects in division plane orientation only in some cell types, which could be side consequences of defects in cell expansion (Bichet et al. 2001; Burk et al. 2001; Burk and Zheng-Hua 2002). One

year later *erh3* and *lue* mutants were shown to be allelic to these previously described *katanin* mutants (Webb et al. 2002; Bouquin et al. 2003). Confocal imaging epidermal root cells from *Arabidopsis* transgenic lines expressing *KATANIN* fused to the Green Fluorescent Protein (GFP) showed that *KATANIN-GFP* colocalizes with microtubules and in particular with crossovers (Zhang et al. 2013 and Fig. 1.8A). Physical interaction of this *KATANIN* homologue, renamed AtKN1, with microtubules and its severing activity, requiring the hydrolysis of ATP, was then demonstrated *in vitro* by time-lapse imaging of purified taxol stabilised microtubules incubated with purified AtKN1 (Fig. 1.8B), co-precipitation of purified taxol stabilised microtubules with AtKN1 and ATPase assay on AtKN1 (Stoppin-Mellet et al. 2002). AtKN1 severing activity was confirmed *in vivo* by generating *Arabidopsis* inducible lines overexpressing AtKN1. Induction of AtKN1 overexpression in pavement cells result first in increased bundling and secondly in an increase of shorter microtubules (Stoppin-Mellet et al. 2006 and Fig. 1.8C-E).

Different type of microtubules network architecture exist in plants and the role of *KATANIN* in establishing and modulating these architecture has been studied intensively. Two main types of microtubules network architecture can be described: aligned networks, which can be found in hypocotyls, in elongation zone of the root and in petiole cells, and net-like networks, which are found in pavement cells and the division zone of the root (Wightman and Turner 2007). Severing events are more frequent in aligned networks than in net-like networks and occur preferentially at microtubules crossovers and nucleation sites (Wightman and Turner 2007; Zhang et al. 2013). At crossovers, *KATANIN* seems to selectively severs the last of the two microtubules arrived at crossover site (Zhang et al. 2013). The molecular mechanism behind this preference is not known, but it has been shown *in vitro* and by modeling that *KATANIN* targets preferentially defects in microtubules lattice (Davis et al. 2002; Díaz-Valencia et al. 2011). These defects can be for instance a change in the number of protofilaments, which can happen *in vivo* (Chrétien et al. 1992), a loss or misincorporation of tubulin, or any conformational change weakening the filament (Davis et al. 2002). When a microtubule crosses over another microtubules, it has to bend over it. This local change of conformation of the microtubule may look like a defect in the microtubule lattice and may attract the *KATANIN* (Zhang et al. 2013). This selective severing by the *KATANIN* protein has huge consequences on microtubules network architecture and their ability to respond to various stimuli. Severing by *KATANIN* is necessary to establish the architecture of the microtubule network, as demonstrated by the lower degree of coalignment of microtubule networks of *atkn1* hypocotyl cells after cold-induced depolymerization and recovery at room temperature (Zhang et al. 2013 and Fig. 1.8F-G) and microtubules networks in the *katanin* mutant are mostly net-like (Bichet et al. 2001; Burk et al. 2001; Burk and Zheng-Hua 2002). Severing by *KATANIN* is also necessary to reorganize microtubule networks in response to blue light (Lindeboom et al. 2013 and Fig. 1.8H) or mechanical stress perturbation (Uyttewaal et al. 2012; Sampathkumar et al. 2014). A few regulators of *KATANIN* are known. SPIRAL2 (SPR2), a microtubule-associated protein, has been shown to physically regulate access of katanin to crossover sites (Wightman et al. 2013). Auxin, through the ROP6-RIC1 signalling pathway, was shown to activate *KATANIN* in pavement cells of *A. thaliana* (Lin et al. 2013). Four homologues of p80 regulatory subunit were found in the *Arabidopsis* genome, but their regulatory activity in *Arabidopsis* has not been demonstrated yet.

1.2.2.5 Filament stabilisation, bundling and zippering

Other proteins stabilise filaments, either by binding to the filament, or by binding the filament to another filament or to another cell component (Fig. 1.7). Cross-linking of cytoskeletal components can occur either in branched networks, or in parallel or antiparallel networks. In the second case, this association is called bundling. *In vitro* studies showed that MAP65-1 has a greater affinity for antiparallel overlapping microtubules than for single microtubules or parallel overlapping microtubules, and is able to bundle only microtubules that form a shallow angle (below 40° to 60°) (Tulin et al. 2012). The incorporation of a microtubule at a shallow angle into a bundle is called zippering. Such antiparallel bundles are formed by polar microtubules at spindle equator. The type of bundling protein determines the space between polymers and allow the interaction with motor proteins. For instance, crosslink distances imposed by actin crosslinkers can vary by a factor 16 (from 10 nm for fimbrin to 160 nm filamin) (Blanchoin et al. 2014). Antiparallel actin bundles cross-linked with *alpha*-actinin are more spaced than parallel actin bundles cross-linked with fimbrin, allowing the interaction of actin with myosin. Myosins, along with kinesins and dyneins, are molecular motors. Myosins move along actin, whereas kinesins and dyneins move along microtubules. Molecular motors are involved in sliding of cytoskeletal components against each other, for instance in flagella (dyneins), in muscle sarcomeres (myosins), or, as suggested by *in vitro* studies, in sliding of spindle polar microtubules against each other (kinesins) (Portran et al. 2013a).

1.2.2.6 Cross-talk between cytoskeletal networks

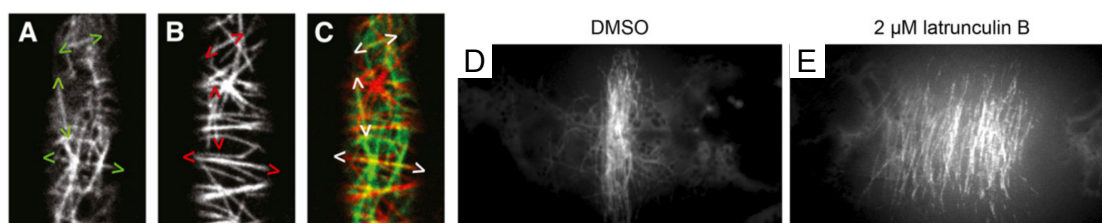


Figure 1.9: Examples of cross-talk between cytoskeletal networks. (A-C) Actin and microtubules are coaligned in *Arabidopsis* hypocotyl cells. (A) GFP:F-actin binding domain of fimbrin1 (GFP:FABD). (B) mCherry:*alpha*-tubulin 5 isoform (mCherry:TUA5). (C) merge of (A) and (B) (Sampathkumar et al. 2011). (D-E) Effects of actin depolymerising drug on the preprophase band in tobacco BY-2 cells stably expressing GFP-tubulin. (D) control. (E) Latrunculin B treated cell (Kojo et al. 2013).

SEM and live-imaging of cytoskeleton networks highlighted colocalisation of actin and microtubules (J. A. Traas et al. 1987; Y. Li et al. 2010; Sampathkumar et al. 2011 and Fig. 1.9A-C). Drug treatments, specific from one component, can impact another the other network (Fig. 1.9D-E). Drug-induced stabilisation of actin filaments provoked a disorganisation of microtubules array in *Arabidopsis* (Sampathkumar et al. 2011). Several candidate proteins homologous to yeast, nematode or animal proteins, which physically interact with both microtubules and actin, have been identified in *Arabidopsis* genome, among which TANGLED, CLASP, EB1 and formins (Petrášek and Schwarzerová 2009). The physical interaction of the CLASP, EB1 and *Arabidopsis* formin AFH14 with both microtubules and actin was demonstrated *in vitro* (Y. Li et al. 2010). *In vivo*, AFH14

decorates all mitotic structures: PPB, spindle and phragmoplast (Y. Li et al. 2010). Steric effects between networks can also be important and modify the dynamic of networks. For instance, microtubules are able to bear larger loads when embedded in a cytoskeletal matrix (Brangwynne et al. 2006).

1.2.3 Case study: the importance of cytoskeleton dynamics during plant mitosis

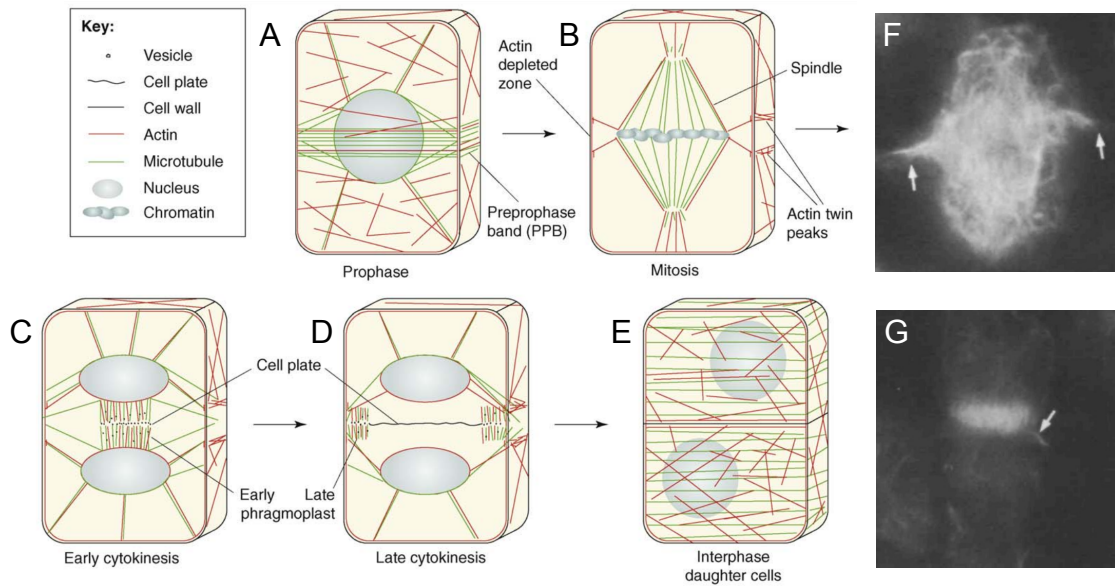


Figure 1.10: Cytoskeletal structures involved in mitosis. (A) Preprophase band. (B) Spindle. (C) Early Phragmoplast. (D) Late Phragmoplast. (E) Interphase daughter cells (Müller et al. 2009). (F-G) Staining of carrot suspension cells with rhodamine-lysine phalloidin reveals an actin cage around spindle (F), and the presence of actin within phragmoplast (G) (C. W. Lloyd and J. A. Traas 1988).

Mitosis is a phase during which several transitions between very different cytoskeletal networks occur. Interphase microtubule arrays reorganise drastically in late G2 to form the PPB (Fig. 1.1B and G and Fig. 1.10A). As described in §1.1.2.1 and in §1.2.2.1, PPB formation requires a complex of proteins, including TONNEAU1, TONNEAU2 (also called FASS) and TRM, which share similarities with animal centrosomal proteins. Preprophase band also contain actin filaments. Application of microtubules-depolymerizing drugs at the end of G2 block both microtubules and actin PPB formation. PPB can last several hours and narrows progressively around the future division site. Application of actin depolymerizing drugs on early PPB prevents its narrowing (Mineyuki and Palevitz 1990). Disappearance of PPB upon nuclear envelope breakdown is accompanied by a depletion in actin at the same location. This actin depleted zone (ADZ) remains during the rest of mitosis (Müller et al. 2009). The cortical actin pattern is thus characterized by depleted zone surrounded on each side by actin populated zones, and seems to be involved in the control of division plane orientation. Disorganisation, without total disruption of this pattern in BY-2 tobacco cells and *Arabidopsis* root cells by drugs such as TIBA and jasplakinolide provoked defects in spindle and cell plate orientation, but not on PPB (Kojo et al. 2013).

Spindle forms during prophase. Plant spindles are bipolar. They are constituted of kinetochore and polar microtubules and most of the time lack astral microtubules, which play an important role in connecting the spindle to the plasma membrane and controlling its position in animal cells (Kotak and Gönczy 2013). However plant spindles are surrounded by an actin cage, which is connected to the plasma membrane (Müller et al. 2009; Y. Li et al. 2010 and Fig. 1.10B and F). Application of actin depolymerizing drug provoke spindle rotation (C. W. Lloyd and J. A. Traas 1988). The whole spindle structure can also undergo rotation movements during mitosis in physiological conditions (Rasmussen et al. 2013). Kinetochore microtubules explore cellular space to catch chromosomes and to align them along metaphase plate, which is oriented along former PPB axis, and then drag chromosomes back to spindle poles.

At the end of telophase, a third cytoskeletal structure is formed: the phragmoplast. Phragmoplast consists in two cylinders of microtubules with antiparallel polarity that overlap with their plus ends at the previous location of PPB (Rasmussen et al. 2013). Phragmoplast guide Golgi vesicles containing polysaccharides and glycoproteins to the previous localisation of PPB. Fusion of these vesicles creates the cell plate. Cell plate expands centrifugally under the constant remodelling of the phragmoplast. Phragmoplast also contains actin and is linked to the cortex by actin strands (C. W. Lloyd and J. A. Traas 1988; Müller et al. 2009 and Fig. 1.10C, D and G). *Physcomitrella patens* dividing cells lack PPB, providing an interesting model to study the role of phragmoplast in positioning division plane. In *Physcomitrella patens*, Myosin VIII localises to the phragmoplast and myosin VIII null mutants have defects in division plane orientation, pointing at a role of myosin VIII and actin in phragmoplast guidance (Wu and Bezanilla 2014).

All these cytoskeletal arrays are dynamically regulated. We reviewed in §1.2.2.4 the importance of the microtubule severing protein KATANIN in interphase to establish organised microtubules arrays (Fig. 1.8F-G) and to allow quick reorganisation of microtubule networks in response to various cues, such as light (Fig. 1.8H) or mechanical stress. Arabidopsis *katanin* mutants also present defects in microtubules network architecture during mitosis. Dividing root cells of mutants exhibit poorly aligned microtubules in PPB, multipolar spindles (Fig. 1.8I-J) and deformed phragmoplasts (Fig. 1.8K-L), highlighting the role of KATANIN in the organisation of these arrays (Panteris et al. 2011).

1.3 Mechanical stress

In this section, we highlight the existence of mechanical stress within tissues, review different ways of quantifying, perturbing and predicting mechanical stress patterns. We focus mainly on plants and give some examples in animals.

1.3.1 Definitions

Mechanical stress, or stress σ is a force per unit area and is expressed in Newtons per metre squared N m^{-2} or in pascals Pa. $1 \text{ N m}^{-2} = 1 \text{ Pa}$. The word "mechanical" is used to make a distinction with other types of stress (chemical, heat...). Normal stress refers to a

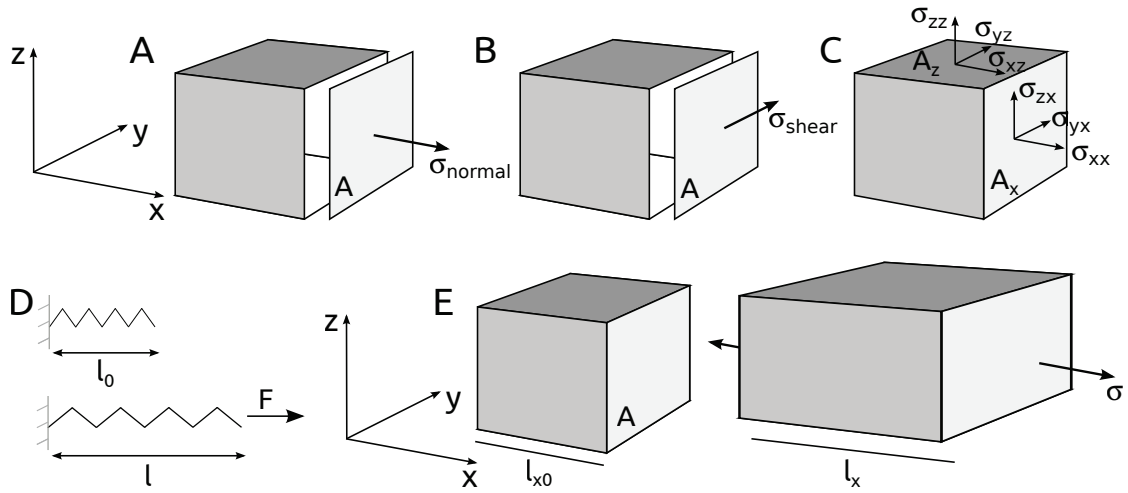


Figure 1.11: Definitions of Hooke's law, stress and strain. (A) Normal stress: σ_{normal} is perpendicular to the area A . (B) Shear stress: σ_{shear} is parallel to the area A . (C) Generalisation to 3D stress state. σ_{xx} : stress along x axis acting on the area A_x (perpendicular to x axis), σ_{yx} : stress along y axis acting on the area A_x (perpendicular to x axis) etc. (D) A force F is applied on a spring of original length l_0 and of spring constant k . Hooke's law for a spring: $F = -k(l - l_0)$. (E) A linear, elastic and isotropic bar is loaded uniaxially (here along x axis) by a stress σ (a force divided by the area A). Hooke's law along axis x : $\sigma = E\epsilon$, with E , the Young's modulus, and ϵ the normal strain (here $\epsilon = (l_x - l_{x0})/l_x$). In 3D, for a linear, elastic, isotropic material, normal and shear stress and normal and shear strains are also related through a 6x6 matrix, which coefficients are a combination of the three elastic moduli: the Young's modulus, the Poisson's ratio and the Shear modulus.

force normal and shear stress to a force parallel to the area on which the force is applied (Fig. 1.11A-B).

Strain ϵ is the amount of deformation per unit original length induced by the application of a stress. Strain is dimensionless. Normal strain refers to a deformation normal and shear strain to a deformation parallel to the area.

In the case of linearly elastic materials loaded uniaxially, Hooke's law defines the relationship between stress and strain as $\sigma = E\epsilon$, where E is the material Young's modulus (Fig. 1.11D-E). E also characterizes the stiffness of the material (for the strain ϵ , a bigger amount of stress σ is needed to deform a stiff material compared to a soft one). Young's modulus is expressed in Newtons per metre squared N m^{-2} or in pascals Pa. In 3D (Fig. 1.11C), for a linear, elastic, isotropic material, normal and shear stress and normal and shear strains are also related through a 6x6 matrix, which coefficients are a combination of the three elastic moduli: the Young's modulus, the Poisson's ratio and the Shear modulus.

Compression (respectively tension) is the application of balanced inward compressive (respectively outward tensile) stress on two opposite points of a material, provoking an decrease (respectively increase) in length of the material. Torsion is the application of shear stress, leads to an angular deformation.

1.3.2 Evidence of stress within tissues and their origin

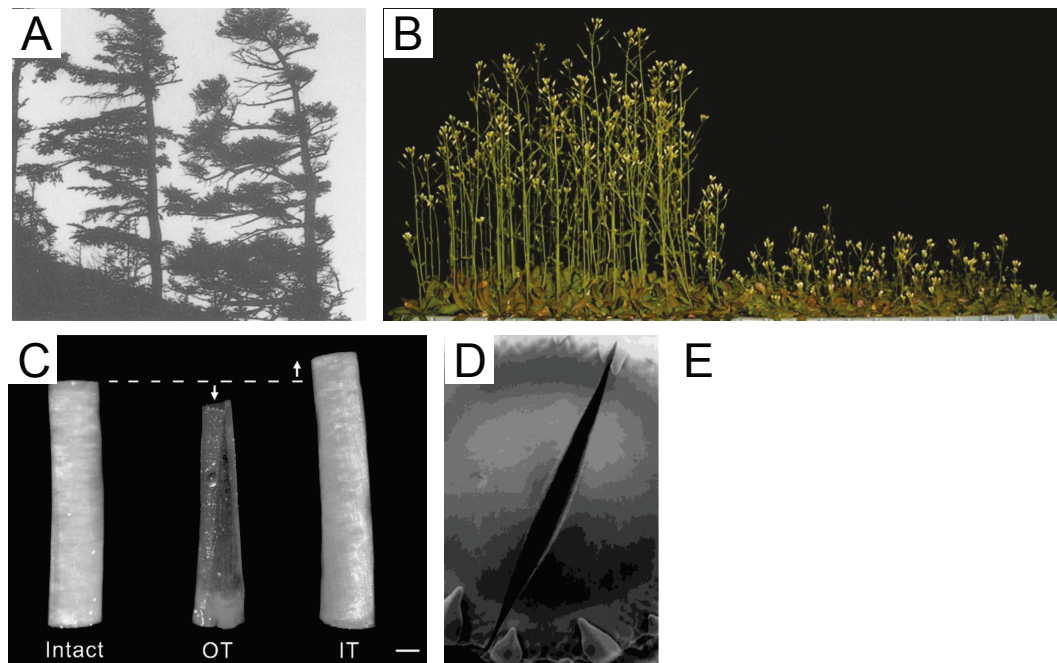


Figure 1.12: Evidence of forces within tissues and their origin. (A) Trees' morphology is sculpted by the force of wind (Jaffe and Forbes 1993). (B) *Arabidopsis thaliana* respond to repeated touch: control on the right, touched plants on the left (Braam 2004). (C) Peeling of sunflower hypocotyl segment. Peeled tissues are incubated in water. OT: outer tissues (e.g. epidermis) and IT: inner tissues. Scale bar=1 millimetre. (D) Scalpel cuts in sunflower capitulum (Dumais and Steele 2000). (E) Emergence of a growing root from a tree through asphalt. Courtesy of Olivier Hamant.

Whereas the effects of exogenous mechanical stress are easily visible, tissues also experience intrinsic mechanical stress. Responses to mechanical stimuli, such as touch or wind are well documented in plants (Jaffe and Forbes 1993; Braam 2004). Responses can be visible at very short timescale, as when the carnivorous plant *Drosera* closes its trap when an insect land on it, or when *Mimosa pudica* fold its leaves in response to touch (Braam 2004). In contrary, tree morphogenesis is sculpted by wind over several years (Jaffe and Forbes 1993 and Fig. 1.12A), and elongation of inflorescence of *Arabidopsis thaliana* is reduced by repetitive touch over several weeks (Braam 2004 and Fig. 1.12B). Although this is often ignored when looking at development from a biochemical point of view, mechanical stress is also present within growing organisms of all kingdoms. The presence of internal stress can be revealed by simple dissection. Peeling experiments on an excised hypocotyl segments of sunflower reveal an epidermis under tension -the peeled cortex shrinks when peeled off- and inner tissues in compression -the medulla expand when peeled off- (Kutschera and Niklas 2007 and Fig. 1.12C). Similarly, a cut in a sunflower capitulum stays wide open, revealing the presence of tensile stress in the cortex of the capitulum (Dumais and Steele 2000 and Fig. 1.12D). Mechanical stress are also present at subcellular scale. For instance, laser dissection of cytoplasmic strands in plant cells leads to their immediate shrinkage, revealing that they were under tension before their severing (Goodbody et al. 1991). In plants, one of the origin of mechanical stress within tissues is turgor pressure, the difference in osmotic pressure between the inside and the outside of the cell. Turgor

pressure is the motor of plant growth. Growth can be high enough to lift and/or crack stiff material such as asphalt (Fig. 1.12E).

1.3.3 Quantification of stress

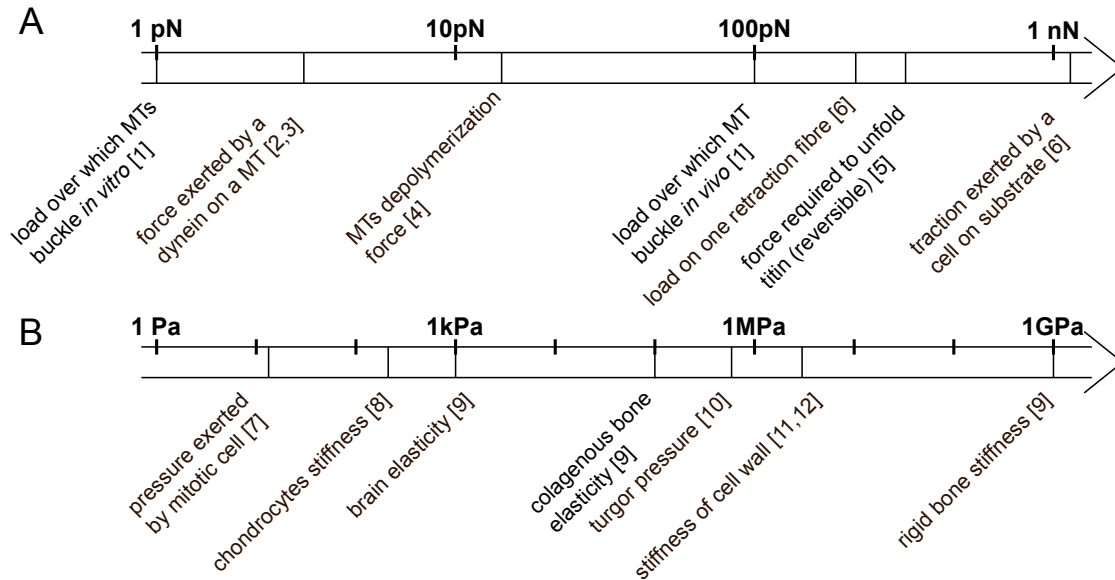


Figure 1.13: Range of forces, pressure and stiffness within tissues. (A) Range of forces in Newtons. [1] Brangwynne et al. 2006 [2] Toba et al. 2006 [3] Gennerich et al. 2007 [4] Grishchuk et al. 2005 [5] Rief et al. 1997 [6] Fink et al. 2011 (B) Range of pressure in Pascals. [7] Stewart et al. 2011 [8] Hochmuth 2000 [9] Engler et al. 2006 [10] Beauzamy et al. 2014 [11] Milani et al. 2011 [12] Sampathkumar et al. 2014.

If the existence of internal stress is relatively easy to demonstrate, its quantification is much harder. Stress cannot be measured directly, thus its quantification is done indirectly by measuring strains. In the case of linear elastic materials (or approximated so), an estimation of Young's modulus is sufficient to deduce stress from strains (from Hooke's law). Despite these simplifications, forces within living tissues are not easy to measure. Beyond the problems associated with the micrometric scale, intracellular forces are often low (on the order of pN between molecules, nN between animal cells and μ N between plant cells) and exert their effects over short distances (Fig. 1.13). Moreover, measuring tools can perturb the measure by inducing a mechanical modification of the tissues (for instance, an induced synthesis of cell wall components to reinforce cell walls, as in reaction to pathogens (Hardham et al. 2008) or even destroy the cell. Different types of forces can be measured: forces exerted by the cell on its environment, forces perceived by the cell and forces within the cell. Most of forces quantifications have been done on single animal cells or on isolated cells components *in vitro*.

1.3.3.1 Mechanical properties of living materials

Effects of mechanical stress on a tissue or a molecule depend on its mechanical properties. Mechanical properties of living tissues are complex. For instance, the plant cell wall is a

Proteinaceous filaments	Young's modulus
microtubules	1.2 GPa
actin	1.3 to 2.6 GPa
keratin (in wool)	4 GPa
other intermediate filaments	1 to 5 GPa

Table 1.2: Young's modulus of some proteinaceous filaments, from [Gittes et al. 1993](#) and [Suresh 2007](#).

composite material, composed of stiff cellulose microfibrils embedded in a gel-like structure of hemicellulose, pectins, enzymes and structural proteins ([Cosgrove 2005](#)). Its composition is variable between cell types, cell ages, tissues and species and allow both to resist turgor pressure and to let the cell elongate ([Milani et al. 2013](#)). Its thickness varies between a few hundreds of nm to a few μm ([Milani et al. 2013](#)). The cell wall is considered as visco-elastic. Under small variations of turgor pressure the cell wall behaves as an elastic solid: stress induced deformation is reversible and instantaneous ([Braybrook et al. 2012](#)). At higher stress, the cell wall behaves as a viscous fluid: stress induced deformation is time dependent and might be irreversible ([Braybrook et al. 2012](#)). Small deformations at small scales can thus be used to probe elastic behavior of the cell wall, and notably to extract the Young's modulus. The Atomic Force Microscope (AFM) is originally a tool to probe sample topography with a nanometric tip held by a flexible cantilever, but it can also be used to indent a sample at a known depth in order to extract the Young's modulus of the sample. AFM gives an apparent Young's modulus of the sample, under the hypothesis that material is locally isotropic, elastic and linear. The higher the Young's modulus of the sample is, the more the cantilever arm will be deflected for the same indentation depth. The AFM was recently adapted to measure Young's modulus of the plant cell wall ([Milani et al. 2011](#); [Sampathkumar et al. 2014](#)). Shallow indentations between 40 and a 100 nm with a tip of a few dozens of nm in diameter limits adhesion effects of cuticle, is insensitive to turgor pressure and remains in the range of elasticity of the sample ([Milani et al. 2013](#)). In these conditions, apparent Young's modulus characterizes cell wall stiffness of the outer cell wall of epidermis, which varies between 2 and 8 MPa, depending both on genetic domain and on local heterogeneities. Deeper indentations or bigger tips measure both cell wall stiffness and turgor pressure, if tissue is turgid, and merely cell wall stiffness if tissue is plasmolysed. AFM together with other indentations methods are reviewed in detail in [Milani et al. 2013](#). Mechanical properties of tissues can be related to their biological properties, as detailed below in §1.3.6.

Mechanical properties of isolated cell components can easily be probed *in vitro*, but their mechanical properties may be modulated by their association with other cell components *in vivo*. Cytoskeleton components, actin, microtubules and intermediate filaments are well mechanically characterized *in vitro* ([Suresh 2007](#)). They are characterized by their Young's modulus (see [Table 1.2](#)) but also their flexural rigidity. Flexural rigidity, also called bending stiffness, is deduced by measuring the persistence length of a growing polymer before it starts to bend because of thermal fluctuations. Actin has a persistence length of 15 μm and a bending stiffness of $7 \times 10^{-26} \text{ N m}^2$. Microtubules have a persistence length of 6 μm and a bending stiffness of $2.6 \times 10^{-23} \text{ N m}^2$. Intermediate filaments have a persistence length of 1 to 3 μm and a bending stiffness of 4 to $12 \times 10^{-27} \text{ N m}^2$. A few *in vitro* experiments suggest that bending stiffness can be modified by the interaction of cytoskeleton components with other proteins. For instance, association of actin with tropomyosin increase

persistence length of a few μm (Gittes et al. 1993), whereas association of microtubules with MAP65-1 decreases persistence length by a factor of 4 (Portran et al. 2013b). More generally, as microtubules are embedded in cytoplasm and other cytoskeleton components, they can bear loads that are a 100 time larger without buckling *in vivo* than *in vitro* when they are isolated (Brangwynne et al. 2006).

1.3.3.2 Intrinsic mechanical stress

As for mechanical properties, intrinsic mechanical stress can be quantified at cell/tissue and molecular scales. In plants, turgor pressure inflates cells, putting cell wall under tension. Cell wall stretches and cell increases in volume (e.g. grows). Turgor pressure can be measured with different destructive and non destructive tools (see Beauzamy et al. 2014 for a detailed review). Here we describe only three methods to measure turgor pressure. (i) At turgid state, turgor pressure is supposed to be equal to osmotic pressure which is related to the osmolarity of inner cell's content. Turgor pressure can be decreased by increasing osmolarity of external medium. When plasma membrane starts to detach from cell wall (plasmolysed state), osmolarity of external medium is equal to osmolarity of inner cell content and initial turgor pressure can be deduced, if the volume change between turgid and plasmolyzed state is considered to be negligible. This method also supposes that no osmoregulation occurs during the increase of osmolarity of external medium. (ii) Another way to measure turgor pressure is to insert a capillary filled with water in the cell. Pressure of cell content compresses the air bubble trapped between the cell content and water. Pressure can be deduced from the deformation of the air bubble. This method, known as pressure probe method, was first described by Paul Green (Beauzamy et al. 2014). It gives precise measurements but it is destructive and works well only on big cells. (iii) Turgor pressure can be deduced from indentations. However, it is hard to separate the contribution of cell wall stiffness from the contribution of turgor pressure with such methods. All these methods predict an internal pressure between 5 to 10×10^6 Pa (Beauzamy et al. 2014).

At molecular scale, depolymerization of microtubules generate forces of a few dozens of pN (Grishchuk et al. 2005). Molecular motors also exert forces when crawling on cytoskeleton. These forces contribute to the sliding of polar microtubules with one another and to the displacements of astral microtubules when positioning the spindle. Force exerted by dyneins crawling on microtubules are in the range of pN (Toba et al. 2006; Gennerich et al. 2007). Measurements of forces acting on the different components of the cell directly *in vivo* are not easy, due to the complexity of the system. *In vitro* experiments provide a simpler frame to test the importance of mechanical stress on small molecular systems, such as polymerizing actin, which polymerizing rate decreases when force of fluid flow exceed 0.2 pN (Courtemanche et al. 2013), or dyneins attached to the cortex, which exert pulling forces of a few pN on microtubules when centering asters of the spindle (Laan et al. 2012).

1.3.3.3 Range of forces exerted by the cell on its environment

Quantification of the range of forces exerted by the cell on its environment can be obtained by quantifying deformations of cell's environment, if its mechanical properties are known.

Adherent cultured animal cells exert traction forces when migrating on a substrate and when dividing, as they round up. Adhesive cells are anchored on the substrate by retraction fibres. Ablations of retraction fibres of HeLa cells reveal that each bear a tension of around 250 pN, exerting a total load of around 7 nN on the substrate (Fink et al. 2011). Thin sheets of silicone of a known stiffness observed by interference reflection microscopy wrinkle under traction forces of migrating cells (Harris et al. 1980). Quantification of wrinkles geometry allows to compute forces exerted by the cell, which is on the order of a few dozen of nN. This technique has the advantage to be non invasive. This method was later improved: adhesive cells are spread on PDMS (Poly(dimethylsiloxane) micropillars of a known Young's modulus (Du Roure et al. 2005). Position of top of each pillar is recorded across time and compared to its rest position to estimate the amount of deformation, and thus of force exerted by the adhesive cells on the substrate. When dividing, adhesive cells detach partially from the substrate and round up. As migrating forces, rounding force of dividing cells can be deduced from deformations of a silicon substrate of a known Young's modulus (Burton and Taylor 1997) Rounding force exerted by a dividing cell can also be measured with AFM. Cantilever is approached from prophase cell. When cell rounds up at metaphase, cantilever is displaced and rounding (pushing) force can be estimated (Stewart et al. 2011). The mitotic cell exert a force on the cantilever which is ten times higher, e.g. around 70 nN than the one exerted on the substrate by crawling cell, corresponding to a measured rounding pressure around $0.04 \text{ nN } \mu\text{m}^{-2}$. This rounding is generated by an osmotic pressure and is balanced by the actomyosin cortex, which limits cell expansion.

1.3.3.4 Range of mechanical stress perception

Quantifying the range of perception of cells gives an idea of their sensitivity to mechanical stress and if the response is proportional to intensity of stress. This also sheds light on biases, such as cell wall reinforcement, that repeated indentation or too high indentations measurements could induce. Quantified application of exogenous stress allows to identify range of forces to which the cell respond. Ablation of cell in plant tissue induce local circumferential reorientation of microtubules (Hamant et al. 2008; Sampathkumar et al. 2014). Raw modifications of the size of the ablation allow to distinguish two cases of high or low perturbation and underline a correlation with the response of microtubules (Sampathkumar et al. 2014). Quantitative relationship between mechanical loading of a bend stem was correlated with the level of expression of a mechanosensitive gene (Coutand et al. 2009). Culture of mesenchymal stem cells on substrates with an elastic modulus comprised between 1 kPa (softness of brain tissue) and 100 kPa (stiffness of collagenous bone tissue, way below stiffness of rigid mature bone: 10^6 kPa), induced different differentiation responses (Engler et al. 2006). The range of force exerted by fungi on plants lie within the range of 5 to 100 μN . This is higher than AFM local measurements of cell wall stiffness (Milani et al. 2013) but lower than AFM turgor pressure measurements.

1.3.4 Prediction/Deduction of stress patterns

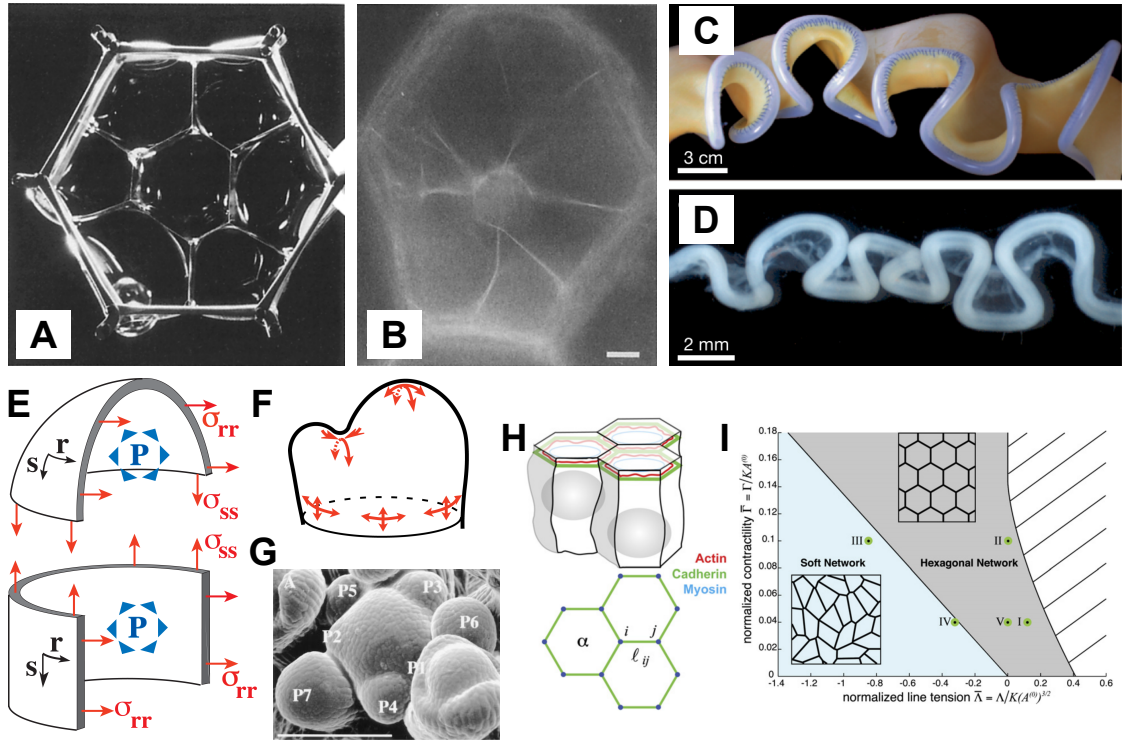


Figure 1.14: Prediction/Deduction of stress patterns. (A-B) Analogy between soap bubbles and epidermal cell of *Tradescantia* leaf (Flanders et al. 1990). Interfaces of soap bubbles mimic cytoplasmic strands of *Tradescantia* cell and show that surface tension is sufficient to explain positioning of nucleus. (C-D) Analogy between rubber bands and gut (Savin et al. 2011). (C) A thin rubber sheet mimicking the mesentery was stretched uniformly along its length and then stitched to a straight, unstretched rubber tube mimicking the gut. The system was then allowed to relax, free of any external forces and deformed into a structure very similar to the chick gut (D), demonstrating that differential growth of the two tissue (here mimicked by differential strain) is sufficient to make the gut loop. (E-G) Pressure vessel model and its application to the shoot apical meristem of *Arabidopsis thaliana*. (E) The SAM can be modeled as a thin vessel -the epidermis- of a radius R inflated by turgor pressure P . Each point has a coordinate in the orthonormal (r) and meridional (s) direction and is characterized by a stress tensor (σ_{ss} , σ_{rr} , σ_{rs}) (Hamant et al. 2008). (F) Stress pattern can be deduced from pressure vessel model and shape of the SAM. In the boundary region, stress is positive and tensile along the crease and negative and compressive in the perpendicular direction. (G) Scanning electron microscopy of a young inflorescence meristem (ecotype WS). P1 to P7: primordia. (Laufs et al. 1998) (H-J) Simulation of *Drosophila* epithelium (Farhadifar et al. 2007). (H) Cells of *Drosophila* epithelium have a similar height and a polygonal section. Epithelium can be simulated as a 2D vertex system, where cells are defined by their vertices i, j and edges of length l_{ij} . (I) Exploration of parameter space of the model. Normalized contractility reflects the influence of contractile forces compared to those from area elasticity. Similarly, line tension is normalized to area elastic tensions. When it is negative, cell boundaries tend to expand; when it is positive, they tend to shrink.

Because these measurements can involve specific set-up (e.g. AFM), and cannot always be conducted in parallel to live imaging, theoretical models and numerical simulations are very helpful to predict stress patterns in tissues, sometimes also building on these mechanical measurements.

1.3.4.1 Analogies with physical systems

Analogies with simpler physical systems offer precious tools to understand mechanics of tissues, scaling up and simplifying the problem. [Flanders et al. 1990](#) observed that the nucleus of vacuolated plant cells is embedded in cytoplasmic strands and gets centered before mitosis. When nucleus was at the centre of the cell, position of cytoplasmic strands in the cell could be reproduced qualitatively by packing soap bubbles packed in a metallic frame of the same shape as the cell (Fig. 1.14A-B). As soap bubbles, tend to minimize surface tension, their position result from the balance of forces between the different interfaces. With this analogy, [Flanders et al. 1990](#) proposed that cytoplasmic strands are under tension and, as soap bubbles interfaces, seek to minimize their length. The existence of tension within cytoplasmic strands was proved one year later by laser ablation [Goodbody et al. 1991](#). The parallel with a simpler physical system has also been used to analyse the balance of forces in the intestine of chick (Fig. 1.14C-D). The intestine tube of mammals has a looped shape structure and is associated on its whole length to another tissue, the mesentery. Surgical separation of the intestine from the mesentery results in a straight gut and a shrunk mesentery, revealing that the intestine was under compression before separation, while the mesentery was under tension ([Savin et al. 2011](#) and Fig. 1.14D). The difference in growth rates and elasticity between the mesentery (fast growing, stiffer) and the gut (slow growing, softer) creates mechanical stress, which is balanced by the apparition of loops all along the tube. To generate an analogue model of this organ, [Savin et al. 2011](#) associated two elastic materials with different stiffness properties and different initial tension loading, a rubber tube associated with a stretched latex sheet (Fig. 1.14C). Strikingly, this was sufficient reproduce qualitatively these loops. These helicoidal structures help the plant to hold on a support when searching for light. These structures are not simple springs, but laterally reinforced springs, as demonstrated by the comparison of the behaviour of real tendrils with different types of springs ([Gerbode et al. 2012](#)).

1.3.4.2 Numerical mechanical models

However analogies with simpler physical systems offer limited possibilities understand the complexity of living tissues, which can modify their mechanical properties and their geometry dynamically over time. Numerical mechanical models are used to integrate mechanical parameters (elasticity of membranes and cell walls, internal pressure, shape...) and to predict theoretical stress patterns, which can in turn be compared with experimental data. The simplest mechanical model defines the shoot apical meristem as a thin elastic shell under pressure and orients directions of stress only according to the shape of the meristem ([Boudaoud 2010](#) and Fig. 1.14E-G). The meristem can be modelled as a dome surrounded by smaller domes, the primordia. At the tip of the dome, stress is isotropic. On the flanks, stress is anisotropic. Analogy with a cylindrical vessel predicts that, on the flanks, circumferential stress is twice the axial stress. In the boundary between meristem and primordia, stress is also anisotropic. Other parts of the meristem are all under tension, but the boundary is particular. Because of its saddle shape, stress is expected to be positive along the crease (tension) and negative perpendicular to the crease (compression). This simple model is continuous and assumes that the epidermis of the shoot apical meristem behaves as a thin linear elastic isotropic shell, with an ho-

mogeneous stiffness. Other types of models take in account local stiffness heterogeneity and have a cellular resolution. Cell walls (or membrane portion) can be modelled in 2D with springs or in 3D with elastic sheets discretized with Finite Element Method. The wing disk epithelium of drosophila was modelled by a mass-spring 2D vertex model: cells shapes are approximated as polygons with straight elastic edges (springs) connected by vertices (mass) (Farhadifar et al. 2007 and Fig. 1.14H-I). The model integrates the different sources of stress existing in drosophila epithelium (cell elasticity, cell contractility and cell-cell interactions along edges) and compute equilibrium state of the network for which sum of forces at each vertex is null at each step of growth. This model is used to explore the influence of mechanics on tissue geometry and can be complexified by adding cell division. Stiffness of springs and sheets can be adjusted individually to modelize local heterogeneities and integrate mechanical feedbacks, such as cell wall reinforcement along principal stress directions (Hamant et al. 2008).

Stress patterns can also be modelled at cellular and subcellular scale. The model of Théry et al. 2007 on spindle positioning (see Fig. 1.3C) is based on the hypothesis that the stress pattern correlates with the position and density of retracting fibres on the substrate and that these forces act as levers on the astral microtubules to position the spindle. Final position of the spindle correspond to the equilibrium of these forces. Other models, such as those of Minc et al. 2011 on positioning of nucleus in urchin eggs, are based on the balance of internal tension within cytoskeleton, which is supposed to be proportional to the length of the microtubules. These numerical models echo analogies with soap bubbles used by Flanders et al. 1990 and Besson and Dumais 2011 to highlight the potential role of tension within cytoskeleton and tension balance in nucleus and PPB positioning in plant cells, and experimental laser ablation of cytoplasmic strands populated by cytoskeleton, also in plant cells, by Goodbody et al. 1991. In this example, experimental data, analogies with material science and numerical models give complementary informations and converge to the same conclusions.

1.3.5 Exploring the effects of mechanical stress on cells and tissues

The effects of mechanical stress on tissues and single cells have been widely explored in animal and plants. Mechanical stress was shown to have effects from tissues to cells and from molecular actors to genes. These effects can in turn induce new stress.

Various methods can be used to perturb the mechanical stress pattern in a tissue: ablation, compression, shear, stretching, touch and bending, or modifications of geometry or stiffness of cell's environment (Tab.1.3). These mechanical perturbations have different effects on cells and tissues. They can cause displacement of the nucleus (Goodbody et al. 1991; Minc et al. 2011) and other organelles (Braam 2004; Hardham et al. 2008). They can also perturb the dynamics (Courtemanche et al. 2013; Trushko et al. 2013), as well as the spatial organisation, of the cytoskeleton (Hardham et al. 2008; Hamant et al. 2008; Risca et al. 2012; Sampathkumar et al. 2014). In single animal cells, mechanical perturbation of cell shape by shearing or by modifying contact points of retraction fibers perturb spindle orientation and thus the position of division plane (Théry et al. 2007; P. Fernandez et al. 2011; Fink et al. 2011). Mechanical perturbations also impact cell cycle progression: compression of spheroids block cells in G1 (Montel et al. 2011; Delarue et al. 2014) and compression of single HeLa cells delay or accelerate the transition between metaphase and

Mechanical perturbations	Type	References
Ablation	cell components	(Goodbody et al. 1991; Fink et al. 2011)
	group of cells	(Goodbody et al. 1991; Hamant et al. 2008; Uyttewaal et al. 2012; Sampathkumar et al. 2014)
Shear stress	single cells	(Gao et al. 2007; P. Fernandez et al. 2011)
Compression	single cells	(Brangwynne et al. 2006; Zhou et al. 2006; Minc et al. 2011; Itabashi et al. 2012)
	whole tissues	(Hernandez and Green 1993; Farge 2003; Desprat et al. 2008; Hamant et al. 2008; Jacques et al. 2013; Kuhl 2014; Sampathkumar et al. 2014)
Stretching	single cells	(Fink et al. 2011)
Touch	whole plants	(Braam 2004)
Bending	explants and plants	(Yeoman and Brown 1971; Coutand et al. 2009)
Substrate stiffness	stiff- single cells	(Engler et al. 2006)
Substrate geometry	single cells	(Théry et al. 2007; Minc et al. 2011; Fink et al. 2011)

Table 1.3: Examples of exogenous mechanical perturbations.

anaphase, depending on the angle between axis of compression and axis of the spindle (Itabashi et al. 2012). For a more detailed review on mechanical stress and division, see Louveaux and Hamant 2013 (reproduced below in §1.4). Mechanical stress can also affect genes expression (Farge 2003; Braam 2004; Desprat et al. 2008), cell differentiation (Engler et al. 2006) and even global morphogenesis, through the control of growth (Zhou et al. 2006; Kuhl 2014), tissues reinforcement and even tissues and organs identity (Hernandez and Green 1993; Braam 2004). The molecular pathways involved in transduction of forces into biological processes are not fully known. There is evidence of physical links between the cytoskeleton and extracellular proteins. Components of extracellular matrix of animal cells, such as fibronectin, contain RGD motif (Arginin-Glycin-Asparagin). This motif is recognised by transmembrane proteins connected to actin cytoskeleton: the integrins (Schwartz 2009). Plant cells are embedded in a polysaccharidic cell wall. They lack integrins, but have other proteins sharing structural homologies with integrins. One of these proteins, NDR1, was shown to be involved in plasma membrane-cell wall adhesion (Knepper et al. 2011). Combination of shear stress with exogenous addition of RGD-peptide on plant protoplasts indicates that plants cells are able to recognize RGD-peptide and may use other RGD-binding proteins in mechanotransduction (Gao et al. 2007). Another plant specific example of physical link between the cytoskeleton and extracellular proteins is the interaction between microtubules and transmembrane cellulose synthase via a molecular linker named CSI1 (S. Li et al. 2012).

In turn, cells' response to stress may in turn induce new stress. For instance, in plants, turgor pressure inflates cells, putting cell wall under tension. Cell wall stretches and cell increase in volume (e.g. grows). Cells are glued by the cell wall. They may have different growth rates, because of different cell wall stiffness and/or because of differences

in turgor pressure. These differences in growth rate create local supracellular compressive and tensile stress.

1.3.6 Case study: mechanical stress within the shoot apical meristem of *Arabidopsis thaliana*

This PhD thesis used the shoot apical meristem (SAM) of the model plant *Arabidopsis thaliana* (see Fig. 1.5) to probe the contribution of mechanical stress to division plane orientation. Here we provide key elements about mechanical stress at the SAM. A review on mechanical stress and morphogenesis at the shoot apical meristem is added in Appendix §A, as direct contribution of M. Louveaux is limited to the paragraph concerning cell division at the SAM.

Existence of intrinsic stress at the SAM is highlighted by the gaps provoked by laser ablations on the epidermis of the SAM of *Arabidopsis thaliana* (Hamant et al. 2008). AFM measurements of cell wall stiffness at the SAM revealed heterogeneities which might be correlated with biological heterogeneities such as gene expression patterns. Cells at the centre of the SAM, where the CLAVATA3 gene is expressed, are stiffer than cells at the periphery (Milani et al. 2014). Tissue elasticity is greater in primordia and that it may be triggered by local demethylesterification of pectins (A. Peaucelle et al. 2011). Experiments of plasmolysis and swelling on the shoot apical meristem of tomato also highlighted heterogeneities in the elastic properties of these regions (Kierzkowski et al. 2012). Cells at the centre of the SAM are stretched at their maximum at smaller loads, explaining their greater stiffness and smaller growth rate *in vivo*. Note that in Kierzkowski et al. 2012, localisation of CLV3 was not compared to cell's properties and that central zone was defined only according to cell's growth rates. At the periphery, cells are not stretched at their maximum and thus keep enough elasticity to allow emergence of a new primordia in this region. Analogies with simpler systems also help understanding concepts such as "strain-stiffening" (Kierzkowski et al. 2012). Two elastic band of different Young's modulus are attached together and stretched. They bear the same load, but the softer elastic band deforms much more than the other one until it reaches its maximum size and stiffen. At this time, the other elastic band starts to deform. This analogy is useful to describe how differences in elastic properties of cell walls on the centre of the SAM versus the flanks can explain why cells are stiffer and have slower growth rate at the centre compared to the flanks. At a global scale, as described in §1.3.4.2, the SAM can be modelled as a thin elastic shell under pressure (Boudaoud 2010 and Fig. 1.14E-G). In this model, principal stress directions and isotropy of the stress can be deduced from the curvature of the SAM to predict a global mechanical stress pattern.

Organ emergence is thought to be preceded by wall softening. AFM measurements showed that tissue elasticity is greater in primordia and that it may be triggered by auxin-dependent local demethylesterification of pectins (A. Peaucelle et al. 2011; Braybrook and Alexis Peaucelle 2013). Auxin also plays an important role in organ emergence by affecting microtubule dynamics through ABP1 and KATANIN (Sassi et al. 2014). Microtubules guide cellulose synthases and thus regulate cell wall anisotropy. Computer simulations showed that combination of small decrease of cell wall stiffness with local loss of microtubules and cellulose anisotropy was sufficient to observe outgrowth of an organ (Sassi et al. 2014). Conversely, can mechanical stress channel organ emergence?

Organogenesis has been proposed to derive from mechanical buckling of tissue, induced by differential growth between tunica and corpus, or within tunica, in the meristem of sunflower (Dumais and Steele 2000). Cells grow slowly in the centre of the SAM and are spatially constrained on the flanks, forcing quick growing peripheral zone to buckle. Periodicity of buckling depend on mechanical properties of the tissue. Tomato and Arabidopsis meristem do not have the same shape and thus the buckling theory may not be translated from the sunflower capitulum to tomata or Arabidopsis meristems. Moreover, laser ablation of L1 of tomato meristem did not affect organ emergence within the next days, thus questioning the validity of the buckling theory (Reinhardt et al. 2003). However, mechanical stress was shown to affect both auxin transport and microtubules orientation. Application of exogenous mechanical stress on tomato shoot apex revealed that PIN1 auxin efflux carrier accumulated preferentially on the most strained membranes (Nakayama et al. 2012). Microtubules were shown to align along the crease of the boundary, along maximal tension predicted by the pressure shell model (Hamant et al. 2008). And local perturbation of mechanical stress pattern by ablation at the center of the SAM provoked a circumferential reorientation of microtubules, consistent with the new stress pattern (Hamant et al. 2008). However, out of the boundary, microtubule orientation neither correlated strictly with curvature nor with principal growth directions (Burian et al. 2013). Shape of the SAM is only an indirect output of mechanical stress, which arises primarily from local difference in growth rates.

1.4 The mechanics behind cell division

We reviewed above the main features of cell division, cytoskeleton and mechanical stress, with a particular focus on the shoot apical meristem. In this section, we present a review published in 2013 in Current Opinion in Plant Biology, which summarizes our current knowledge of interplay between mechanical stress and cell division.

Due to copyright restrictions, the article Louveaux and Hamant 2013 cannot be reproduced here. To read this article, please connect to doi:10.1016/j.pbi.2013.10.011 .

1.5 Aims of the PhD thesis

Cell division is a complex cellular process, controlled both temporally, by the cell cycle, and spatially, by the position of the division plane. Cell division involves both microtubules and actin, and a broad diversity of other proteins. In animal cells, division plane position is determined by the orientation of the spindle, which forms around the nucleus, just before nuclear envelope breakdown between the two centrosomes. The spindle is a microtubule based structure, which gather at its equator and then segregates chromosomes between the two daughter cells. In plant cells, division plane is controlled by another microtubule based structure, the preprophase band. The preprophase band forms at the end of G2, by a drastic reorganisation of cortical microtubules, and surrounds the nucleus. Preprophase band disappears concomitantly to nuclear envelope breakdown. Its position is memorized by several molecules, which ensure that phragmoplast, another microtubule

based structure guiding Golgi vesicles involved the formation of the new cell wall between the two daughter cells, takes the same localisation as the preprophase band.

However, we do not understand well how preprophase band is oriented at first. Its position is tightly controlled, as mutant impaired in either the formation of the preprophase band, or memory of its position and guidance of phragmoplast display disorganized cell patterns and have important morphological defects, such as dwarfism. Cell shape was proposed as a possible directional cue guiding the formation of the preprophase band. At the end of the *XIXth* century, Sachs, Hofmeister and Errera formulated three different rules based on cell geometry. Recently, the rule of Errera was re-examined and generalised into a probabilistic rule: the Besson-Dumais rule (Besson and Dumais 2011). The molecular mechanism supporting this rule was proposed to be based on length-dependent tension within microtubules during the formation of the preprophase band. Microtubules would seek to minimize tension and thus favor the shortest path between the nucleus and the plasma membrane. Cytoplasmic strands containing microtubules were shown to be under tension and to control nucleus position within the cell. This mechanism is cell based and suppose that microtubules are insensitive to other external mechanical stress. In this introduction, we highlighted the existence of mechanical stress in any supracellular context. Moreover single animal cells were shown to reorient their spindle in response to external mechanical stress (Fink et al. 2011). They can also be affected in mitosis progression (Itabashi et al. 2012) and even arrested in the G1 phase of the cell cycle by compressive stress (Montel et al. 2011; Delarue et al. 2014). In plants, the contribution of mechanical stress to division plane orientation is not clearly established (Louveaux and Hamant 2013) and nothing is known about the temporal control of division by mechanical stress. An hypothetical mechanical stress pattern can be deduced from the shape of the shoot apical meristem of *Arabidopsis thaliana*, based on the hypothesis that SAM behave like a pressure vessel (Boudaoud 2010). Hamant et al. 2008 showed that, at the SAM, microtubules align at supracellular level along maximal stress tension predicted by this mechanical stress pattern. Moreover, perturbation of this mechanical stress pattern by ablation or compression provoked a reorientation of microtubules along the maximal tension of the new stress pattern Hamant et al. 2008.

Several questions remain:

(i) Is the Besson-Dumais rule valid in a anisotropic tissue? (ii) Does mechanical stress contributes to division plane orientation in plant cells? (iii) To which range of mechanical stress plant cells are sensitive? (iv) Does mechanical stress affect cell cycle and/or mitosis progression in plant cells?

In the first chapter of this thesis, we address the question (i) at the epidermis of the shoot apical meristem of *Arabidopsis thaliana*. We show quantitatively, using a bootstrap-like approach, that Besson and Dumais geometrical rule is insufficient to explain divisions in this epithelia, and in particular in the boundary region. We then address the question (ii) and explore the contribution of mechanical stress with two strategies: modelling of a growing tissue with two possible division rules (geometrical or mechanical), which was closer to real tissues with mechanical division rule, and perturbation of mechanical stress pattern by laser ablation, which was sufficient to bias division plane orientation toward the new mechanical stress pattern.

In the second chapter, we propose a new compressive set-up to perturb mechanical stress pattern and quantitative image analysis tools adapted to the precision of this set-up, which could allow to answer question (iii).

In the last chapter, we present a R pipeline developed to explore cell division at the shoot apical meristem.

2 A mechanics-based rule accounts for the orientation of cell division in the boundary of the shoot apical meristem of *Arabidopsis thaliana*

Authors and contributions

M. Louveaux did all confocal image acquisition and laser ablations, computed Besson-Dumais rule predictions and performed bootstrap analysis on real and simulated observations of cell divisions. J.-D. Julien performed simulations. V. Mirabet wrote scripts to convert data to Matlab format. M. Louveaux, J.-D. Julien and V. Mirabet adapted Besson Matlab script to process large datasets. A. Boudaoud and O. Hamant supervised the work.

2.1 Abstract

Regulation of cell division plane orientation is a way for multicellular organisms to control the topology and geometry of their tissues, in particular in plant, where cells are glued to each other by stiff pectocellulosic cell walls. At the end of the *XIXth* century, cell geometry was proposed to play a key role in cell division plane orientation and several geometrical division rules were proposed by Hofmeister, Errera and Sachs. However none of these deterministic rules describes all the divisions at the shoot apical meristem (SAM) of *Arabidopsis thaliana*. Recently, the rule of Errera was re-examined and generalised into a probabilistic rule: the Besson-Dumais rule. The Besson-Dumais rule has been tested only on tissues with rather isotropic shapes or growth and the exact molecular mechanism controlling division plane orientation is still unknown. In the present paper, we tested the application of Besson-Dumais rule to the divisions at the SAM of *Arabidopsis thaliana*, which present both isotropic and anisotropic regions. We found that a non negligible proportion of cells do not choose the shortest plane at the epidermis of the SAM. The Besson-Dumais division rule partially accounted for observations but long plane were over-represented, in particular in the boundary region. We simulated growing tissues submitted to anisotropic stress and compared two division rules: geometrical or mechanical based. We found that the mechanical rule reproduced the enrichment of long planes observed in the boundary and thus better accounted for cell divisions in this region. We also simulated tissues submitted to isotropic stress. However, in these tissues, we could not found a perfect match between outputs of simulations with a mechanical rule and observed divisions in isotropic domains of the SAM.

2.2 Introduction

Regulation of cell division plane orientation is a way for multicellular organisms to control the topology (number of neighbours) and geometry (cell shapes and sizes) of their tissues, as highlighted by simulations of growing tissue under different division rules (see for instance [Sahlin and Jönsson 2010](#)). Whereas this process may be compensated by cell death and cell rearrangement in animal tissues, this is an essential mechanism in plants: plant cells are glued to each other by stiff pectocellulosic cell walls, which prevent cell movement, while cell death does not occur in young, rapidly dividing tissues.

At the end of the *XIXth* century, Hofmeister, Errera and Sachs proposed cell geometry as a spatial cue guiding cell division plane orientation, at least for symmetric cell divisions ([Hofmeister 1863](#); [Sachs 1878](#); [Errera 1888](#)). In particular, Léo Errera observed that cells behaved like soap bubbles when positioning their division plane, i.e. they tend to minimise the length of new interfaces between daughter cells. From this statement was derived the rule of Errera: "cells divide along the shortest path", which is a rough simplification of Errera's initial observation (for a full review, see [Besson and Dumais 2014](#)). The rules of Hofmeister, Errera (simplified version) and Sachs were recently tested at the shoot apical meristem (SAM) of *Arabidopsis thaliana* ([Shapiro et al. 2015](#)). None of these rules fully described all the divisions at the SAM, but Errera's rule was the one which described the highest percentage of divisions.

Errera's exact statement was recently reexamined and the deterministic "shortest path" rule was generalised in a probabilistic one by Sébastien Besson and Jacques Dumais ([Besson and Dumais 2011](#)). Here this rule will be referred as the Besson-Dumais rule. Like soap bubbles, cells do not always choose the shortest path, but one of the shortest. For a given cell geometry, several minima of energy exist and the probability to divide along one of these minima is related to the length of the interface. However, the Besson-Dumais rule has only been tested on tissues with rather isotropic shapes or growth, like the thallus of the green alga *Coleochaete orbicularis*, whereas most of the epithelia have a 3D shape and a non isotropic growth. Moreover, the molecular mechanism behind this rule remains speculative and limited to vacuolated cells: it was proposed to involve minimization of tension within cytoplasmic strands of vacuolated cells ([Besson and Dumais 2011](#)). Cytoplasmic strands are populated with microtubules, guide the relocation of nucleus at cell the centre of mass prior to division and coalesce into the phragmosome at the future division site. Such a mechanism would suggest that the reorganization of interphasic microtubules into the preprophase band (PPB) is primarily driven by cytoplasmic strands. The PPB circles the nucleus prior to division and marks the future division site. Its formation requires the presence of TONNEAU1 and TONNEAU2. PPB disappears concomitantly with nuclear breakdown but its former localisation is kept by the persistence of several molecular actors, such as TANGLED and POK, which are involved in phragmoplast guidance at division site. The *tonneau*, *tangled* and *pok* mutants exhibit defects in division plane orientation ([J. Traas et al. 1995](#); [Müller et al. 2006](#); [Walker et al. 2007](#)). Finally epithelial cells are exposed to different patterns of biochemical factors and mechanical stress. Microtubules are able to sense supracellular mechanical stress, as they were shown to align along maximal tensile stress direction in the boundary domain of the SAM of *Arabidopsis thaliana* ([Hamant et al. 2008](#)). And auxin signalling through the Aux/IAA factor BODENLOS was recently shown to bias Errera's rule towards longer divi-

sion planes in young embryos (Yoshida et al. 2014). How this heterogeneity and dynamics impact cell division plane orientation has not been characterized quantitatively yet.

In the present paper, we tested the application of Besson-Dumais rule to the divisions at the shoot apical meristem (SAM) of *Arabidopsis thaliana*, which present both mechanically isotropic and anisotropic regions. We found that a non negligible proportion of cells did not choose the shortest plane at the epidermis of the SAM. The Besson-Dumais division rule partially accounted for observations but long plane were over-represented, in particular in the boundary domain. We simulated growing tissues submitted to anisotropic stress and compared two division rules: geometrical or mechanical based. We found that the mechanical division rule reproduced the enrichment of long planes observed in the boundary and thus better accounted for cell divisions in this region. We also simulated tissues submitted to isotropic stress. However, in these tissues, we could not find a perfect match between outputs of simulations with a mechanical rule and observed divisions in isotropic domains of the SAM.

2.3 Results

2.3.1 A non negligible proportion of cells does not select the shortest plane at the epidermis of the SAM

We analysed cell division plane orientations at the epidermis of the shoot apical meristem of *Arabidopsis thaliana* with the plane classification used in the Besson-Dumais rule. We acquired confocal images of *LTi6B-GFP* (WS-4) dissected meristems every 12 h during 48 h (Fig. 2.1A). On each snapshot, 3D surface was reconstructed and segmented with MorphoGraphX to extract cell shapes (see Material and Methods and Fig. 2.1B). New cell walls were identified by a visual comparison between snapshots (from T=12 h to T=48 h). We hypothesized that cell shape did not change much immediately after division and thus that the recorded cell wall position between the two daughter cells corresponded to the position of the former PPB in the mother cell. The Besson-Dumais rule applies only to symmetrically dividing cells. Comparison of the areas of the two daughter cells, computed on the 3D surface, showed that 78 % of the cells within the SAM divided almost equally, i.e. the smallest daughter cell occupying between 40 % and 50 % of the sum of the two daughters areas (see Fig. 2.6B in §2.6 Supplemental Figures). The 22 % of asymmetrical dividing cells were located preferentially in the meristem region of the SAM (see Fig. 2.6C in §2.6 Supplemental Figures, and Fig. 2.2A for the definition of SAM regions). In the following, these asymmetrically dividing cells are removed from analysis, to be in line with the Besson and Dumais rule. The Besson and Dumais rule is defined only in 2D. Epidermis of the SAM has an almost constant thickness of around 5 μm and new cell walls in this layer are perpendicular, e.g. anticlinal, to the surface (Fig. 2.6A and Fig. S1 in Uyttewaal et al. 2012). Thus we could restrict our analysis to 3D surface of the SAM. Although SAM surface is curved (Fig. 2.1C and Fig. 2.6A), the surface of the pair of daughter cells is small enough compared to the variations of curvature to be locally flattened in 2D without too much shape deformations (see Material and Methods and Fig. 2.7).

We computed predictions of the Besson-Dumais rule using Sébastien Besson's Matlab

2 A mechanics-based rule accounts for the orientation of cell division in the boundary of the shoot apical meristem of *Arabidopsis thaliana*

script (see Material and Methods). This script is later referred as Besson script. For each cell, the Besson script seeks the shortest plane between each pair of edges that divide equally the mother's area (e.g., on our dataset, the fused daughter cells area). It happens that the Besson script do not find any solution satisfying the condition on area for a given pair of edges. All possible planes are ranked from the shortest to the longest. The probability P_i to divide along a given plane i depends on the length of the plane and takes the form (Besson and Dumais 2011):

$$P_i = \frac{e^{-\beta \ell_i / \rho}}{\sum_{j=1}^N e^{-\beta \ell_j / \rho}} \quad (2.1)$$

where ℓ_i is the length of plane i , ρ the mean cell diameter, β a constant and N the total number of theoretical possible planes of the cell.

The Besson script also compares theoretical predictions to observations and give the rank of the observed plane and its probability P_i to be chosen among other possibilities (Fig. 2.1F and Fig. 2.8). More precisely, the Besson script compares pair of edges connected to predicted cell walls to the pair of edges connected to the observed cell wall. In only 5 to 8% of the cases (depending on SAM), the Besson script did not find a match between observations and theoretical predictions (Fig. 2.1G). These observed planes are referred as NP for "not predicted" (by Besson script). By opposition, other planes are referred as predicted planes.

As cells in the SAM display different shapes and shape anisotropy and as the number of possible planes may vary from one cell to another, ranks are not sufficient to compare cells. As shown in Fig. 2.8A-B, the shortest plane (rank=1) in an elongated cell (Fig. 2.8A) has a higher probability P_1 to be observed than the shortest plane (rank=1 also) of a roundish cell (Fig. 2.8B). And the longest plane of the cell showed in Fig. 2.8C (rank=9) has a higher probability to be observed than the longest plane of the cell showed in Fig. 2.8D (rank=4).

In order to compare cells with one another, we compared all predicted planes of a given cell with the shortest predicted plane of this cell: we computed the pairwise probability p_{pw} between the shortest predicted plane of length ℓ_1 (e.g. Errera's predicted plane) and the observed plane of length ℓ_{obs} , with $\ell_1 \leq \ell_{obs}$ as the ratio between the probability P_{obs} of observed plane and the sum of the probabilities P_{obs} and P_1 (probability to observe the shortest plane):

$$p_{pw} = \frac{P_{obs}}{P_1 + P_{obs}} \quad (2.2)$$

Pairwise probability p_{pw} varies between 0 (long plane) and 0.5 (short plane). When observed plane is the shortest one (as for instance in Fig. 2.8A-B), pairwise probability is strictly equal to 0.5.

We defined 5 classes of pairwise probability: $= 0.5$; $[0.375; 0.5[$; $[0.250; 0.375[$; $[0.125; 0.250[$; $[0; 0.125[$ and added a 6th class, when no match between theoretical predictions and observations had been found. These classes are later referred as planes classes. The first class correspond to the choice of the shortest plane by the cell. Planes classes are not strictly equivalent to ranks, but they are independent of cell shape (Fig. 2.9).

Proportions of planes classes between meristems are similar but not identical (Fig. 2.1G). In each SAM, 65 to 77% of all planes, (corresponding to 68 to 81% of predicted planes), correspond to the shortest.

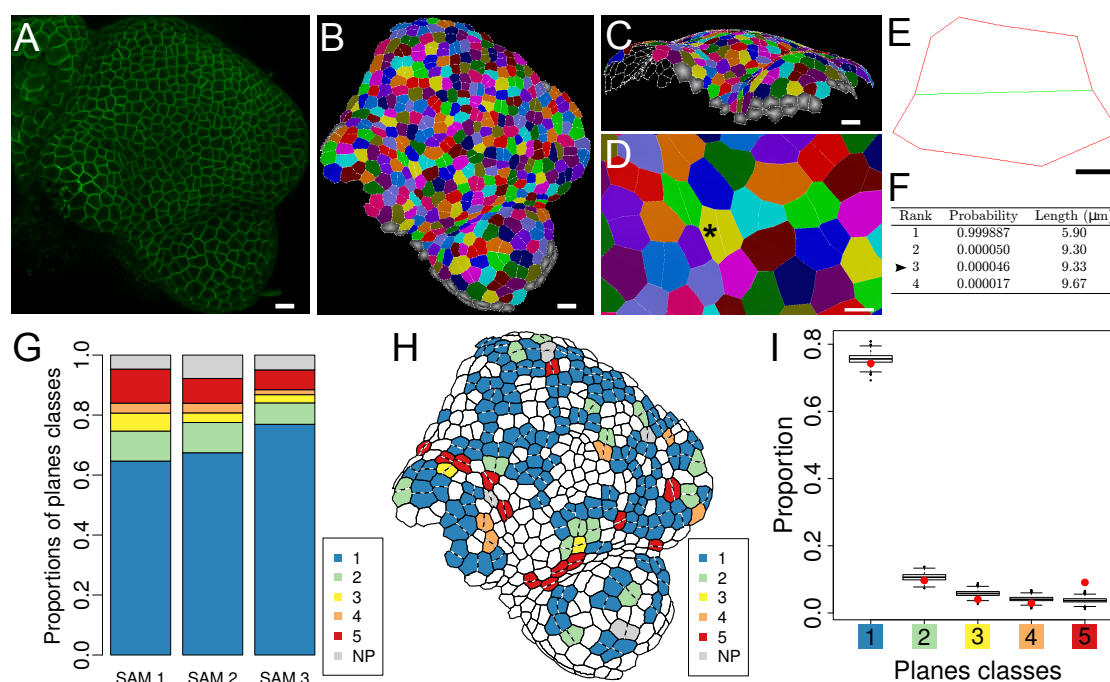


Figure 2.1: Division planes at the shoot apical meristem of *Arabidopsis thaliana*. (A) Confocal image of *LTI6B-GFP* (WS-4) dissected shoot apical meristem. Scale bar=10 µm. (B) Cellular segmentation of the shoot apical meristem with MorphoGraphX. Cells sharing the same colour are daughters from a division which occurred during the last 12 h. Scale bar=10 µm. (C) Segmentation is done on 3D surface. Scale bar=10 µm. (D) Close up of (B) in a young boundary region. The black asterisk points at a mother cell (e.g. two fused daughter cells) which is analysed with Besson script in panels (E) and (F). Scale bar=5 µm. (E) Flattened mother cell. Only the main vertices (i.e. at the junction between three cells) are kept. The new plane is coloured in green. Scale bar=2 µm. (F) Planes predicted by the Besson script for cell (E). The arrowhead indicates that the observed plane in cell (E) corresponds to predicted plane of rank three. $p_{pw} = 4 \times 10^{-11}$, e.g. this cell belongs the 5th plane class of pairwise probability. (G) Proportion of planes classes in each SAM (total number of symmetrically dividing cells in SAM1, 2 and 3 is respectively 150, 218 and 182). Classes 1 to 5 correspond to the ratio between the probability for a cell to choose the observed planes and the probability to choose the shortest plane, as predicted by the Besson script. Ratio varies from 0 to 0.5. Class 1 [=0.5] corresponds to the choice of the shortest plane and Class 5 [0;0.125[correspond to the choice of one of the longest planes. NP (not predicted) corresponds to an absence of match between theoretical predictions and observations. (H) Map displaying planes classes for the divisions which occurred in the 12 h following this snapshot. (I) Comparison of observed planes proportions within the different classes (red dots) with fluctuation range obtained by bootstrap among theoretical predictions given by the Besson script (boxplots). Planes which did not match prediction (NP class) were excluded from this analysis. Total number of symmetrically dividing cells: 517.

2.3.2 The Besson-Dumais division rule partially accounts for observations, but long planes are over-represented at the SAM

When compared to elongated cells of the hypocotyl, meristematic cell shapes are rather isotropic; this could explain the relatively high proportion of cell not dividing along the shortest plane in the shoot apical meristem. To test this hypothesis, we computed the range of fluctuation of the proportion of each planes class and compared to observed proportions. To compute the range of fluctuation of the proportion of each planes class, we used a bootstrap approach to produce theoretical set of planes corresponding to the observed tissue geometry. To compute a particular set of planes, for each dividing cell that had chosen a plane predicted by the Besson script, we sampled a new plane among the theoretical predictions given by the Besson script. The probability to sample this plane i was equal to the probability P_i described above. We then computed the pairwise probability p_{pw} between the shortest predicted plane of length ℓ_1 and the sampled plane s of length ℓ_s , with $\ell_1 \leq \ell_s$. We obtained a first set of simulated pairwise probabilities and computed the frequencies of each class, using the planes classes defined previously. We repeated this procedure a thousand time to generate a thousand sets of planes and the corresponding proportions. We plotted boxplots of proportions for each plane class and added our observed proportions (red dots) on the same graph (Fig. 2.1I). The boxplot (with its notches) represents a confidence interval at 95 %. For a given plane class, if observation dot is out of the boxplot, the probability to get this proportion of planes is lower than 5 %. Here, the probability to get observed proportions of planes classes 1 to 4 are above 5 %, whereas the probability to get observed proportion of class 5 is below 5 %. This result indicates that long planes are over-represented at the shoot apical meristem of *Arabidopsis thaliana* and that the Besson-Dumais rule only partially accounts for observed planes.

2.3.3 The boundary region is enriched in long planes

We spatialized results of the bootstrap analysis to evaluate the impact of tissue anisotropy on planes classes proportions. Three regions were defined manually: the meristem, which corresponds to the central zone and peripheral zone, the outgrowing primordia and the boundary, between primordia and meristem (Fig. 2.2A). Meristem and primordia have a rather isotropic shape and growth, compared to the boundary, which is creased and characterized by a lower growth rate when compared to surrounding tissues (Kwiatkowska and Dumais 2003). Cell localisation was identified on the timepoint preceding cell division. In the primordia, proportions of planes classes were found to be within the confidence interval, showing a good agreement between predictions of Besson-Dumais rule and observed planes (Fig. 2.2B-C). In the meristem, as in the whole tissue, the the probability to get the observed proportion of planes of class 5 was lower than 5 %. The proportion of long planes was higher than expected. This could be due to our restrictive definition of the boundary regions. In the boundary, the probability to get the observed proportion of planes of class 1, 4 and 5 was lower than 5 % (Fig. 2.2D). In this region, proportion of planes of class 1 was lower than expected and proportion of planes of class 4 and 5 higher.

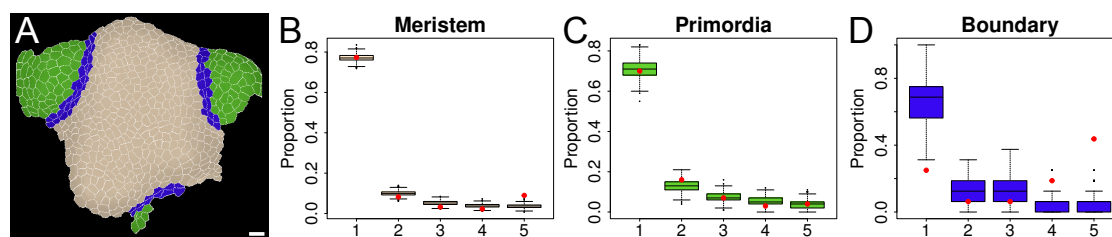


Figure 2.2: A domain-based comparison between observations at the SAM and predictions of the Besson-Dumais rule. (A) Example of expert manual definition of the boundary domain (blue), the meristem domain (beige) and the primordia domains (green). (B-D) Comparison of observed planes proportions (red dots) with fluctuation range obtained by bootstrap among theoretical predictions given by the Besson script (boxplots), displayed in function of regions: (B) Meristem, (C) Primordia and (D) Boundary. Planes that were not predicted by the Besson script (NP planes) were excluded from this analysis. Number of symmetrically dividing cells in these regions is respectively: 401, 100 and 16.

2.3.4 Simulation of a growing boundary suggests a contribution of mechanical stress to the bias in the division plane distribution

Boundaries have a very specific identity compared to other part of the SAM, both genetically and mechanically. In particular, the boundary domain is defined by the expression of specific transcription factors (Aida and Tasaka 2006; Rast and Simon 2008), hormonal levels (e.g. Heisler et al. 2005; Brunoud et al. 2012) and highly anisotropic tensile stress (Hamant et al. 2008). Dissecting the different factors contributing to the boundary identity and identifying the ones that are involved in this bias is thus complex. Simulations offer the possibility to simplify the system and test alternative and integrative hypotheses, notably by focusing on tissue geometry.

We used a vertex model that allowed to compute the mechanics and the geometry of the tissue at the cellular scale. The tissue is a two dimensional lattice of growing and dividing cells. Cells behave like rubber balloons, with a certain wall elasticity, under (turgor) pressure. They are packed together and thus cannot reach their optimal shape. Additional mechanical stress either emerges from differential growth (growth-derived stress) or is imposed as an anisotropic mechanical stress, mimicking shape-derived stress that are prescribed by the anisotropic curvature of the boundary (curvature-derived stress). In the growth-derived stress simulations, a ring of slow-growing cells surrounds a disc of fast-growing cells. Growth (e.g. displacement of vertices) is computed by minimizing the energy of the tissue, which is a balance between pressure and curvature and elasticity of cell walls resisting to this tension. Cells divide when reaching a certain size threshold. In all the simulations, the new division plane goes through the barycentre of the cell. Two division rules were tested: either the new division plane follows the direction of the short axis of the cell (the geometrical division rule) or it follows the direction of local maximal tensile stress (the mechanical division rule). These defined eight cases of study: growing tissue following either geometrical or mechanical division rule, undergoing either growth-derived or curvature derived stress, which is either isotropic (same growth on all the tissue and same force in x and y direction), and mimics meristem and primordia regions, or anisotropic (growth is three times higher in the central disc than in the surrounding ring or force is three times higher along x axis than along y axis), and mimics boundary regions.

2 A mechanics-based rule accounts for the orientation of cell division in the boundary of the shoot apical meristem of *Arabidopsis thaliana*

We computed cells' aspect ratio (ratio of short over long axis of the cell) in the different simulated tissues. Isotropic growth and curvature derived stress fields produced tissues with similar cell aspect ratio whatever the applied division rule. When tissue was submitted to anisotropic mechanical stress, the geometrical division rule produced tissues with rather isotropic cells' aspect ratio, whether the mechanical division rule produced tissues with more anisotropic cell's aspect ratio (Fig. 2.3A and B). In this last case, anisotropic cell shapes were mostly located at the interface between the fast and slow growing tissues in the differential growth simulations, and along maximal tensile stress in anisotropic curvature simulations. In comparison, at the SAM, mean cell aspect ratio is equal to 0.74. Boundary cells have a more anisotropic shape in average, with a mean aspect ratio of 0.58, compared to meristem and primordia cells (mean aspect ratio of 0.76, see Fig. 2.3E). Thus, the mechanical division rule produced tissues with an aspect ratio close (in average) to those of meristem and primordia when stress field was isotropic, and close (in average) to those of boundary regions when stress field was anisotropic (Fig. 2.3A and B compared to Fig. 2.3E). However, whereas mean aspect ratio do not differ much between dividing and non dividing cells (e.g. will or will not divide in the next 12 h) in the meristem and primordia, mean aspect ratio of boundary cells is higher (0.74) for dividing cells compared to non dividing cells (0.58) (Fig. 2.3E). Thus, aspect ratio do not differ much between dividing cells of the different regions.

We applied the Besson script on the output of simulated tissues to compute predictions of Besson-Dumais rule and match with observed division planes. We computed pairwise probabilities between observed plane and shorter predicted plane and subdivided this variable into the 6 classes defined previously in §2.3.1 (Fig. 2.3C-D). Tissues simulated with the geometrical rule, both in isotropic and anisotropic, growth- and curvature-derived stress, displayed a majority of short planes, as expected. The implemented geometrical division rule mimics Errera's simplified shortest path rule, but do not follow exactly the same conditions: division plane orient along short axis of the cell, with a straight cell walls going through the barycentre of the cell, but without condition on the equality of daughters area. This difference may explain the existence of planes in the class 2 to 5. Tissues simulated with the mechanical division rule displayed a higher proportion of long planes than tissues simulated with the geometrical rule, with a peak associated with the class 5, both in isotropic and anisotropic tissues, whatever the source of mechanical stress. Among tissues simulated with the mechanical division rule, those submitted to anisotropic stress displayed a higher proportion of long planes than those submitted to isotropic stress. And tissues submitted to anisotropic curvature-derived stress simulated with the mechanical division rule displayed a particularly high proportion of non predicted planes.

We spatialized proportion of planes classes in function of regions of the SAM (Fig. 2.3F). Proportion of planes classes in the meristem and primordia were very similar to proportion obtained in tissues simulated with the geometrical division rule. Proportion of planes classes in the meristem were also similar to tissues submitted to isotropic growth-derived stress and simulated with a mechanical division rule, which displayed a high proportion of planes of the class 1 and a small peak in the proportion of planes of the class 5 (Fig. 2.3C-D). The boundary had a high proportion of planes of the class 5 and of non predicted planes (NP), which was very similar to the proportion observed in tissues submitted to anisotropic curvature-derived stress simulated with a mechanical division rule (Fig. 2.3C-D).

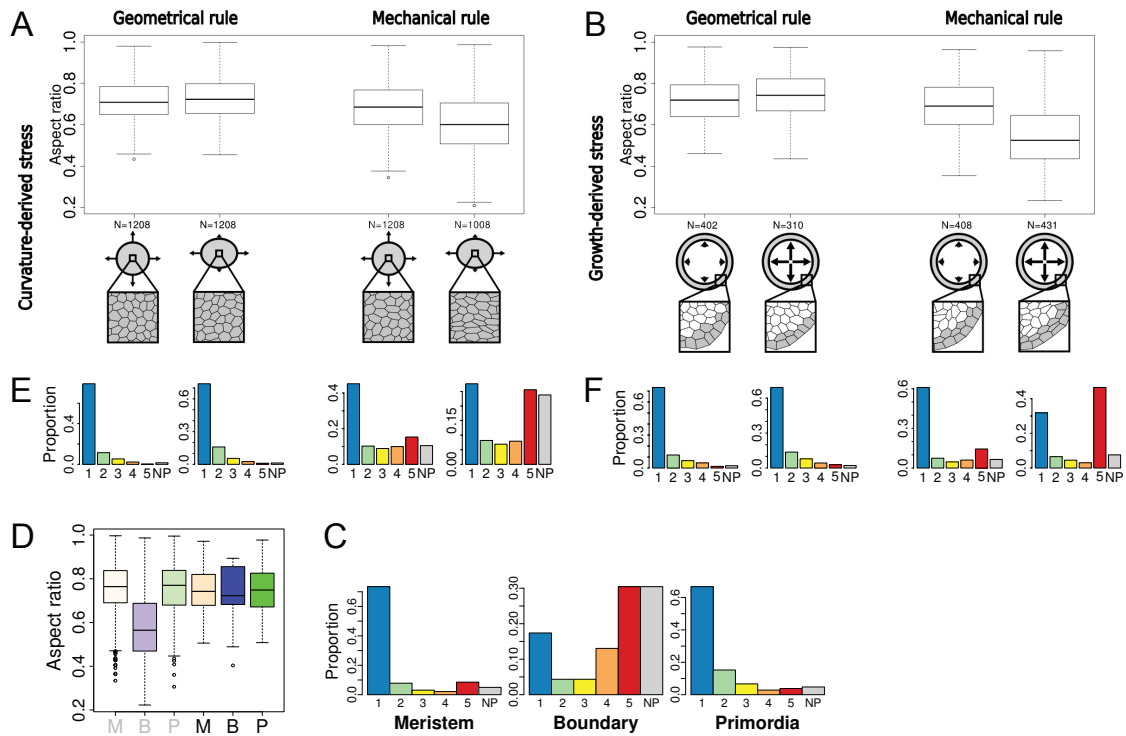


Figure 2.3: Modeling the contribution of mechanical stress to division plane orientation. (A-B) Aspect ratio of cells in simulated tissues, when mechanical stress is derived from curvature (A) or growth (B). Tissues divide according to either geometrical or mechanical division rule. Mechanical stress field is either isotropic (on the left) or anisotropic (on the right). (C-D) Computation of planes classes proportion given by the Besson-Dumais rule on simulated tissues, when mechanical stress is derived from curvature (C) or growth (D). Classes 1 to 5 correspond to the ratio between the probability for a cell to choose the observed planes and the probability to choose the shortest plane, as predicted by the Besson script. Ratio vary from 0 to 0.5. Class 1 [=0.5] corresponds to the choice of the shortest plane and Class 5 [0;0.125[correspond to the choice of one of the longest planes. NP corresponds to an absence of match between theoretical predictions and observations. Tissues divide according to either geometrical or mechanical division rule. Mechanical stress field is either isotropic (on the left) or anisotropic (on the right). The order is the same order as above in (A-B). Number of dividing cells in each simulation from left to right: 393, 402, 372, 391, 194, 139, 215 and 198. (E) Observed aspect ratio of non dividing cells (grey) and symmetrically dividing cells (black) in the different regions of the SAM. M: meristem, B: boundary, P: primordia. Number of cells from left (non dividing meristem cells) to right (dividing primordia cells) is respectively 3220, 527, 1082, 422, 23 and 105. (F) Computation of proportion of planes classes given by the Besson-Dumais rule (see definition in (C)) on the different regions of the SAM. Number of symmetrically dividing cells in meristem, boundary and primordia is respectively: 422, 23 and 105

2.3.5 Mechanical perturbations influence division plane orientation

Our analysis so far showed that Besson-Dumais did not predict well all division plane orientations at the SAM, and in particular in the boundary region. Simulations of growing tissues revealed that, when submitted to curvature derived anisotropic stress and following a mechanical division rule, simulated tissues mimicked both more anisotropic cell aspect ratio and the high proportion of long planes observed in boundary regions of the SAM. An

2 A mechanics-based rule accounts for the orientation of cell division in the boundary of the shoot apical meristem of *Arabidopsis thaliana*

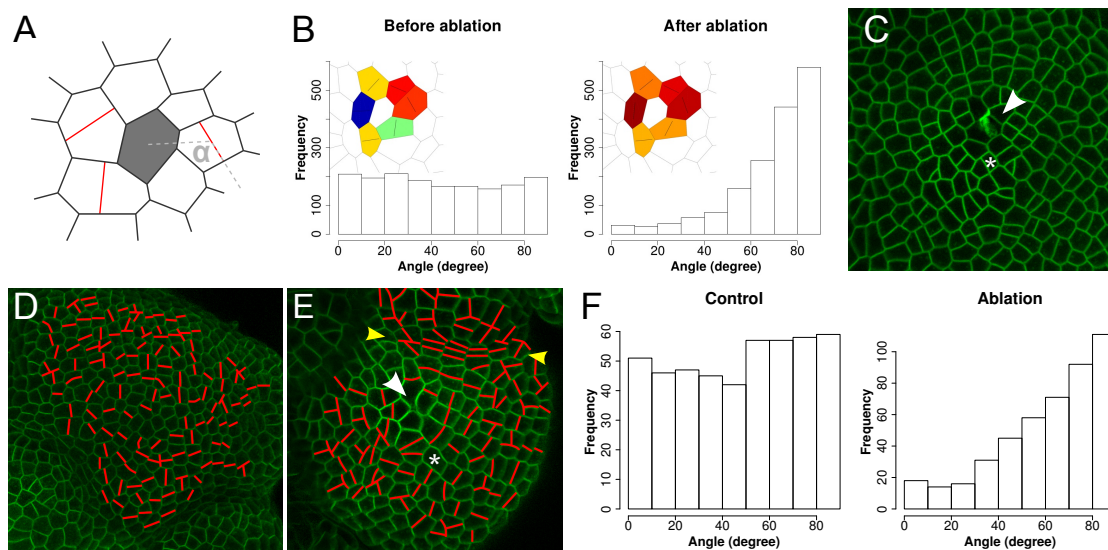


Figure 2.4: Effects of mechanical perturbation on division plane orientation. (A) Angle α between principal stress axis (simulated tissues) or new cell wall (real tissues) and radius of the ablation is measured in each cell neighbouring the ablation site. (B) Angle α before and after ablation on simulated tissues. Close-up on a simulated tissue shows direction of maximal tension within the cells (black bar). Cells are coloured according to the value of angle α , from blue (0°) to red (90°). (C) Confocal image of *LTi6B-GFP* (WS-4) dissected SAM 30 min after pulsed UV laser ablation. White arrowhead points at ablation site. White asterisk: same cell as in (E). (D-E) New cell walls formed within 48 h (red lines) on (D) control and (E) ablated *LTi6B-GFP* (WS-4) dissected SAM. White arrowhead points at ablation site. Yellow arrowheads: boundary. White asterisk: same cell as in (C). (F) Distribution of the angle α in neighbouring cells of 30 ablated meristems. Control: 30 cells of the same meristem are taken as "ablation site" and α is computed in neighbouring cells.

anisotropic modification of the mechanical stress pattern should thus also affect the pattern of cell division plane orientation. We tested this hypothesis using single cell ablation.

FEM simulation of L1 layer under tension predicts that an ablation in the epidermis induces circumferential maximal tensile stress directions in the cells adjacent to the ablated zone (Hamant et al. 2008). We first ensured that our model was consistent with these previously published results: on different tissues undergoing homogeneous growth and isotropic external stress, a cell was removed from the template and the stress pattern before and after the ablation was analysed (Fig. 2.4A). As expected, the stress pattern, which was random before ablation, became locally circumferential after the ablation (Fig. 2.4B).

We next performed ablations on real meristems with a pulsed UV laser (Fig. 2.4C) and computed the orientation of division planes in the neighbouring cells 48 h after ablation (Fig. 2.4D-E). New cell walls formed after the ablation oriented circumferentially around, following the predicted tensile stress pattern (Fig. 2.4F).

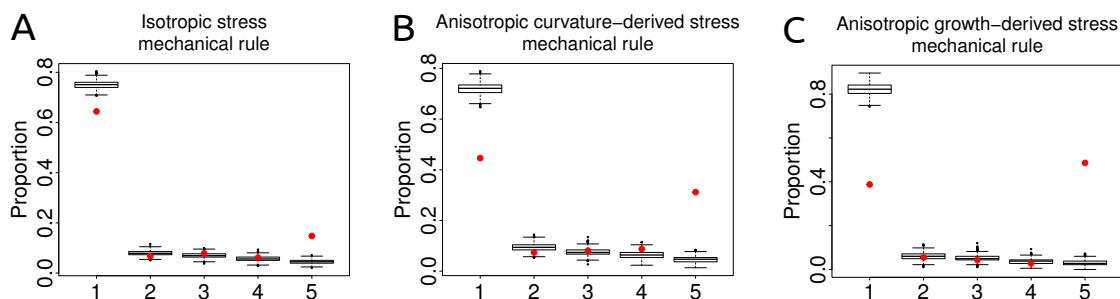


Figure 2.5: Comparison between simulated tissues and predictions of the Besson-Dumais rule (A) Isotropic mechanical stress pattern (either curvature or growth-derived). Number of cells=587. (B-C) Anisotropic mechanical stress pattern derived from (B) curvature (number of cells=391), or (C) growth (number of cells=198).

2.3.6 Towards a mechanics-based division rule?

We applied the same bootstrap approach described in §2.3.2 on tissues simulated with the mechanical division rule to see how far this rule was from Besson-Dumais rule predictions in isotropic cases and to confirm depletion in planes of class 1 and enrichment of planes of class 5 in anisotropic, as observed in the boundary region of the SAM (Fig. 2.5). We found that output of isotropic simulations (Fig. 2.5A) are closer to Besson-Dumais predictions than output of anisotropic simulations (Fig. 2.5B-C). However, in all cases, we observed a depletion in planes of class 1 and an enrichment of planes of class 5, with a probability lower than 5% to get these two proportions. Proportions of other planes classes were within the confidence interval.

NB: In Fig. 2.3C-D we did not filter mother cells according to the symmetry of divisions (as done in Fig. 2.6B), and we did not exclude either the most anisotropic cell shapes (whereas in the boundary, the most anisotropic cells do not divide, see Fig. 2.3E). New analysis are currently ongoing to assess if this could explain the discrepancy between Besson-Dumais predictions and the proportion of planes classes of tissues simulated with the mechanical division rule. Meanwhile, we propose to compare outputs of simulations also to observations on all the divisions at the SAM, even the most asymmetrical (see Fig. 2.10). We can see that the addition of the most asymmetrically dividing cells do not change much the results, except for shortest and longest plane classes: the proportion of shortest plane is slightly decreased, whereas the proportion of longest planes is slightly increased. In any cases, proportion of planes classes from simulations of growing tissue in an isotropic stress field with a mechanical division rule appear more biased (in planes classes 1 and 5) than proportion of planes classes in the meristem and primordia.

2.4 Discussion

Cell division is a defining feature of the shoot meristem, both etymologically (meresis means cell division) and histologically (the meristem organization in layers and zones relates to cell division planes and rates respectively). The shoot apical meristem is therefore a place of choice to investigate how cell division is regulated. Since the end of the *XIXth*

2 A mechanics-based rule accounts for the orientation of cell division in the boundary of the shoot apical meristem of *Arabidopsis thaliana*

century, geometrical division rules were proposed to explain positioning of new division planes in plants. However none of these rules accounted for all the divisions at the shoot apical meristem (SAM) of *Arabidopsis thaliana* (Shapiro et al. 2015). Recently, one of these rules, the rule of Errera, was re-examined and generalised into a probabilistic rule: the Besson-Dumais rule.

We investigated whether the Besson-Dumais rule can be extended to the different regions of the SAM of *Arabidopsis thaliana* and most particularly to the boundary region. We found that around one quarter of the cells did not choose the shortest plane at the epidermis of the shoot apex. Throughout a bootstrap-like approach we showed that the Besson-Dumais division rule partially accounted for observations, but that long plane were over-represented. A spatialisation of our analysis revealed that the boundary was enriched in long planes. Boundary have a very specific identity compared to other part of the SAM, both genetically and mechanically. We chose a simulation-based approach to simplify the system and tested two alternative division rules hypothesis, either based on geometry or on mechanics, in isotropic or anisotropic mechanical stress field, mimicking either meristem and primordia regions, or boundary regions. We classified planes with the Besson script in order to compare outputs of the simulations with observations made at the SAM. Simulations of a growing tissue following mechanical division rule and submitted to anisotropic stress field displayed a high proportion of long planes, very similar to what had been observed in the boundary. Simulations of a growing tissue following mechanical division rule and submitted to isotropic growth-derived stress field (but not curvature-derived stress field) displayed planes classes proportions similar to those of the meristem region, but not to the primordia. However, the geometrical rule better accounted for planes classes proportions in the primordia. Simulations predicted a local circumferential mechanical stress pattern (e.g. anisotropic) in response to an ablation in a tissue undergoing homogeneous growth and isotropic external stress, consistent with previous simulations of mechanical stress (Hamant et al. 2008). We performed UV pulsed laser ablations on the meristem region and observed that new cell walls formed after the ablation were oriented circumferentially around. We performed bootstrap-like approach on the predictions of Besson-Dumais rule on the output of simulations of growing tissue following a mechanical division rule. We found that even if output of isotropic simulations are closer to Besson-Dumais predictions than output of anisotropic simulations, they do not mimic exactly predictions of Besson-Dumais rule. Thus we propose that Besson-Dumais rule is valid in isotropic regions of the SAM, such as the meristem and the primordia, and that anisotropic mechanical stress fields, such as the one in the boundary region or the one provoked by the ablation, may overcome this rule.

Here we pointed at a possible interference between anisotropic mechanical stress field and division plane orientation. Biochemical signals, such as auxin, may as well only interfere with a local geometrical division plane rule, for instance by constraining localisation of microtubules. The identification of the synergies and antagonisms between these molecular and mechanical cues will certainly be a fruitful area of research in the future.

2.5 Material and Methods

2.5.1 Plant material and growth conditions

The *LTi6B-GFP* (WS-4) was already described in [Marc et al. 1998](#). Plants were sown on soil, kept at 4 °C during 48 h, then grown in short day conditions (8 h light at 19 °C ; 16 h night at 17 °C) during 4 weeks and transferred 2 to 3 weeks in long days conditions (16 h day at 21 °C ; 8 h night at 19 °C) prior to dissection. Meristems were cut from the stem, dissected the day before imaging and stuck in "Arabidopsis apex culture medium" (2.2 g l⁻¹ Duchefa Biochemie MS basal salt mixture without vitamins, 1% sucrose, 0.8% agarose, pH 5.8), as described in ([Hamant et al. 2014](#)). Medium was supplemented with vitamins (1000X stock solution: 5 g Myo-inositol Sigma, 0.05 g Nicotinic acid Sigma, 0.05 g Pyridoxine hydrochloride Sigma, 0.5 g Thiamine hydrochloride Sigma and 0.1 g Glycine Sigma in 50mL water) and 200 nmol N6-Benzyladenine. Dissected meristems were kept in a phytotron in long days conditions (Sanyo, 16 h day at 20 °C ; 8 h night at 20 °C, synchronised with growth culture chambers).

2.5.2 Imaging

1024x1024 pixels stacks of dissected meristems, with Z slices every 0.5 µm, were acquired every 12 h during 48 h on a Zeiss LSM 700 upright confocal microscope, with a 40x water-dipping lens. Stacks from the kinetics were processed with a C++ script using Level Set Method ([Landrein et al.](#), submitted) to detect the 3D surface of the meristem at high resolution. Meshes of these surfaces were then created with MorphoGraphX ([Kierzkowski et al. 2012](#); [Barbier de Reuille et al. 2015](#)). Surface geometry of processed stack was extracted with a marching cube algorithm. Initial mesh had a 5 µm resolution. Mesh was smoothed and subdivided until its resolution went below membrane signal thickness (around 0.5 µm). Fluorescence signal (1 to 3 µm below the surface) was projected on this mesh. Semi-automatic segmentation was performed using watershed method, allowing delineation of cells.

For each cell, lineage and localisation (referred as "primordia", "boundary" and "meristem", e.g. central zone + peripheral zone) were recorded manually for each 12h-snapshots. A boundary is defined as a curved region between an outgrowing primordia and the meristem. Very young boundaries and primordia are gathered with the "meristem" region. Maps of area and curvature (with a radius of 20 µm) for each snapshot, and growth rates and growth directions between each pair of contiguous snapshots, were computed with MorphoGraphX. Each snapshot was exported as a .vtk text file, recording vertices coordinates and associations of vertices to cells. Lineage, localisation of cells, growth, curvature and area raw data were saved as separate text files. .vtk and other MorphoGraphX output text files were processed with R ([R Core Team 2015](#)) to extract various cells indicators (orientation and length of long and short axis, area, growth rate, local direction and intensity of curvature). For each of the snapshots between T12h and T48h, fused daughters cells that came from a division between previous and current snapshot were projected in 2D using a principal component analysis on vertices. Vertices are more spread in x and y, meaning that third dimension always correspond to z. Third dimension explain only a few percent of dispersion of vertices (between 0 and 2.5 %, with a mean at 0.15 %, see [Fig. 2.7C](#)), indicating that local flattening does not deform too much mother cell shape. We kept only the two first dimensions and ordered these vertices clockwise or anti-clockwise.

2 A mechanics-based rule accounts for the orientation of cell division in the boundary of the shoot apical meristem of *Arabidopsis thaliana*

We adapted the input required by Matlab® (The MathWorks, Inc. 2013) script, written by Sébastien Besson. Predictions given by the rule of Besson and Dumais were obtained with the Matlab® (The MathWorks, Inc. 2013) script written by Sébastien Besson. This script seeks the shortest plane between each pair of edges dividing the cell into two equal areas and rank these planes according to their length. It then compares observed plane with theoretical predictions and gives the rank of the plane and the probability to observe this plane. Principal Component Analysis were performed with the R package FactoMineR (Lê et al. 2008).

2.5.3 Ablations

UV laser ablations were performed on an inverted Leica DMI4000 microscope, equipped with a confocal spinning disk head (Yokogawa CSU22), with a 20x dry lens. Stacks from the ablations were processed with MerryProj (Barbier de Reuille et al. 2005) to obtain a top view 2D projection of the meristems. New cell walls within the two first rank of neighbours around the ablation were identified manually using layers and paths tool of the GNU Image Manipulation Program (The GIMP team 2012). Angles between the new plane and the radius of the ablation zone were measured with Fiji angle tool (Schindelin et al. 2012). A non ablated meristem was used as a control. On this meristem, 30 cells were taken as "centre of non ablated zone" to compare with the 30 ablations.

2.5.4 Model

We modelled two possible mechanisms driving the positioning of the new wall during a cell division: the new wall can be positioned either to minimize its length or in the direction of highest tension. Then we compared the development of tissues following one or the other mechanism.

We employed a vertex model that allows to compute the mechanics and the geometry of the tissue at the same scale. The model is 2D but 3D information can be incorporated as an external stress.

2.5.4.1 Mechanics

The cells form a flat polygonal tiling, each polygon being a cell. The mechanics of a single cell C is driven by its anisotropic deformation $M_C - M_C^{(0)}$ where M_C is the actual shape of the cell and $M_C^{(0)}$ its equilibrium state. The shape tensor is computed as the covariance matrix:

$$M_C = \frac{1}{N_C} \begin{pmatrix} \sum_{i=1}^{N_C} (x_i - x_C)^2 & \sum_{i=1}^{N_C} (x_i - x_C)(y_i - y_C) \\ \sum_{i=1}^{N_C} (x_i - x_C)(y_i - y_C) & \sum_{i=1}^{N_C} (y_i - y_C)^2 \end{pmatrix}$$

where (x_i, y_i) are the coordinates of the cell's vertices, (x_C, y_C) the barycenter of the

vertices and N_C the number of vertices. Thus we are able to measure the anisotropy of the cells.

The positions of the vertices is given by the minimization of the mechanical energy of the tissue. Taking into account the elasticity and the turgor pressure, we can define the energy of a single cell:

$$E_C = -pA_C + \frac{\alpha}{2}A_C \frac{\|M_C - M_C^0\|_F^2}{\text{tr}^2(M_C^0)}$$

with p the pressure and α the shear modulus of the periclinal wall. The stress tensor of the periclinal wall is then given by the functional derivative of its energy density with respect to its strain:

$$S_C = \frac{\partial \left(\alpha \frac{\|M_C - M_C^0\|_F^2}{\text{tr}^2(M_C^0)} \right)}{\partial \left(\frac{M_C - M_C^0}{\text{tr}(M_C^0)} \right)} = \alpha \frac{M_C - M_C^0}{\text{tr}(M_C^0)}$$

where I is the identity matrix.

In a folded boundary, stress is predicted to be anisotropic. Therefore, to take into account the curvature of a real tissue, an external stress is introduced in the energy of the whole tissue:

$$E_T = \sum_C E_C - A_T \frac{M_T - M_T^0}{\text{tr}(M_T^0)} : S_T$$

where A_T is the area of the tissue, M_T its shape, M_T^0 its reference shape and S_T the external stress. The reference shape of the tissue is computed by minimizing the energy without the external term.

As new divisions in the epidermis of the shoot apical meristem are anticlinal (see Fig. 2.6A), we hypothesized that mechanical stress within periclinal cell walls controls the orientation of new anticlinal cell wall. Thus we simulated only mechanics of periclinal cell walls.

2.5.4.2 Tissue growth

Because of the turgor pressure and the cellular interactions, the cells' shapes are different from their targets when the mechanical energy is minimal. To model the growth as the evolution of the equilibrium state of the cell, the target matrix evolves proportionally to its difference with the actual shape.

$$\frac{dM_C^0}{dt} = a_C (M_C - M_C^0) \text{ for } C \text{ in } 1..N_C$$

where a_C is the growth rate of the cell.

2 A mechanics-based rule accounts for the orientation of cell division in the boundary of the shoot apical meristem of *Arabidopsis thaliana*

We employed an incremental approach to growth: after minimizing the mechanical energy, the targets evolve according to the differential equation system.

2.5.4.3 Cellular division

During cell growth, if the area of a cell is higher than the division threshold, the cell is divided according to one of the two following rules

For the geometrical hypothesis, we mimicked the simplified "shortest path" version of Errera's rule (Errera 1888) by choosing the division direction \vec{n} as the one which minimizes the shape of the cell:

$$\vec{n}, \quad \vec{n}^t M_C \vec{n} = \min \left\{ \vec{u}^t M_C \vec{u} \right\}_{\|\vec{u}\|=1}$$

For the mechanical hypothesis, the division direction \vec{n} is the one which maximizes the stress:

$$\vec{n}, \quad \vec{n}^t S_C \vec{n} = \max \left\{ \vec{u}^t S_C \vec{u} \right\}_{\|\vec{u}\|=1}$$

The cell is divided by a straight line going through its center, which is defined as the barycenter of its vertices.

2.5.4.4 Properties of the daughter cells

After division, the growth rate of the daughter cells is equated with the growth rate of the mother cell:

$$a_D = a_M$$

The targets of the daughter cells are chosen in order to keep the stress constant over the division:

$$\frac{M_D - M_D^0}{\text{tr}(M_D^0)} = \frac{M_M - M_M^0}{\text{tr}(M_M^0)}$$

where D stands for a daughter cell and M for the mother cell. One can show that this relation is equivalent to the following definition for the daughter's target:

$$M_D^0 = M_D + \frac{\text{tr}(M_D)}{\text{tr}(M_M)} (M_M^0 - M_M)$$

As the two neighbouring cells in the direction of the division get a new vertex, their shape matrix is slightly modified. Therefore, their targets are also adapted to keep the mechanical stress constant. The relation is identical:

$$M_{C'}^0 = M_{C'} + \frac{\text{tr}(M_{C'})}{\text{tr}(M_C)} (M_C^0 - M_C)$$

where C and C' stands for the neighbouring cell before and after the division.

2.5.4.5 Implementation

Model was implemented in a C program. The energy was minimized thanks to the BFGS algorithm, implemented in the NLOpt library. The differential equation system was solved thanks to the GNU Scientific Library. Simulation parameters were $p = 0.01$ for the turgor pressure, $\alpha = 2$ for the shear modulus, $S_{T,xx} = 0.03$ and $S_{T,yy} \in \{0.01, 0.03\}$ for the curvature-derived stress, and $a_C \in \{0.3, 1\}$ for the growth rate. Initially the energy was minimized every $\Delta t = 10^{-2}$, but this time step was reduced proportionally to the number of cells in order to keep a constant temporal resolution on the divisions. Mechanical parameters were set to lead to a strain corresponding to a few percent, as it is observed in real tissues. The external stress was estimated to vary between 1 and 10 times the pressure stress, thus we set the parameters so that the external stress contribution is 75% of the total stress. The tissues are initially 100 cells large and grow up to 250 or 300 cells depending on the simulation. Noise in the initial conditions and in the growth rates allows us to perform each kind of simulation several times. The noise in the initial conditions was tuned so that no vertex cross a cell wall. The noise in the growth rates was a white noise of amplitude 10 percent that was reset at each time step.

2.6 Supplemental Figures

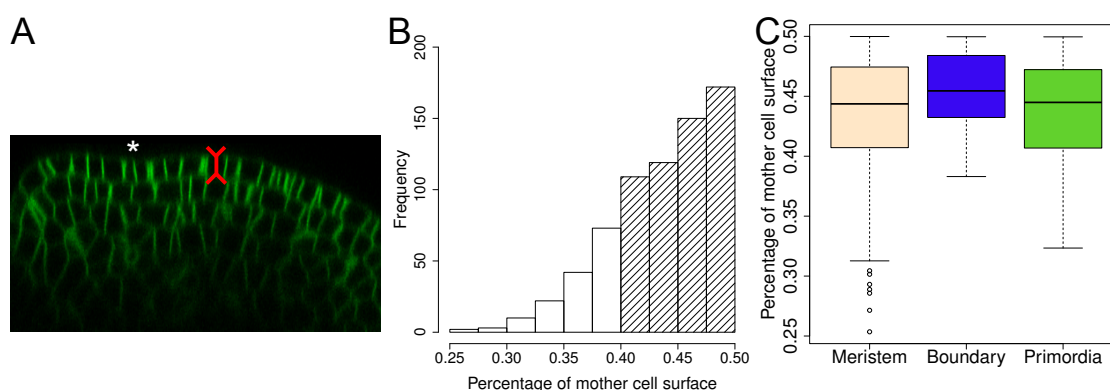


Figure 2.6: Besson script can be applied on 3D surface of the SAM. (A) Orthogonal view of a *LTi6B-GFP* (WS4) dissected meristem. L1 has a constant thickness and divisions are anticlinal to the surface. White asterisk: crease of a forming boundary. (B) Distribution of the surface ratio occupied by the smallest of the two daughter cells. $N=702$ cell divisions. Striped bars: 78% of cells divided almost symmetrically. (C) Distribution of the surface ratio occupied by the smallest of the two daughter cells in the different regions of the SAM. Number of division in the Meristem, Boundary and Primordia region is 544, 26 and 132, respectively.

2 A mechanics-based rule accounts for the orientation of cell division in the boundary of the shoot apical meristem of *Arabidopsis thaliana*

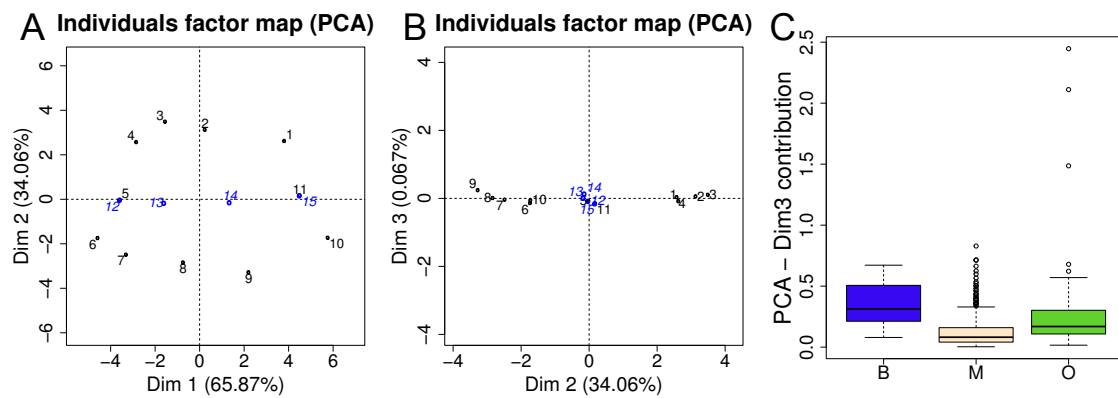


Figure 2.7: 2D projection of two daughter cells. (A-B) Example of individual factor map of a projected daughters. Cell is the same as in Fig. 2.1D (black asterisk) and E. Vertices of new cell wall are coloured in blue. (A) Plane of dimension one and two. (B) Plane of dimension two and three. (C) Contribution of third dimension in percent in the different regions of the SAM.

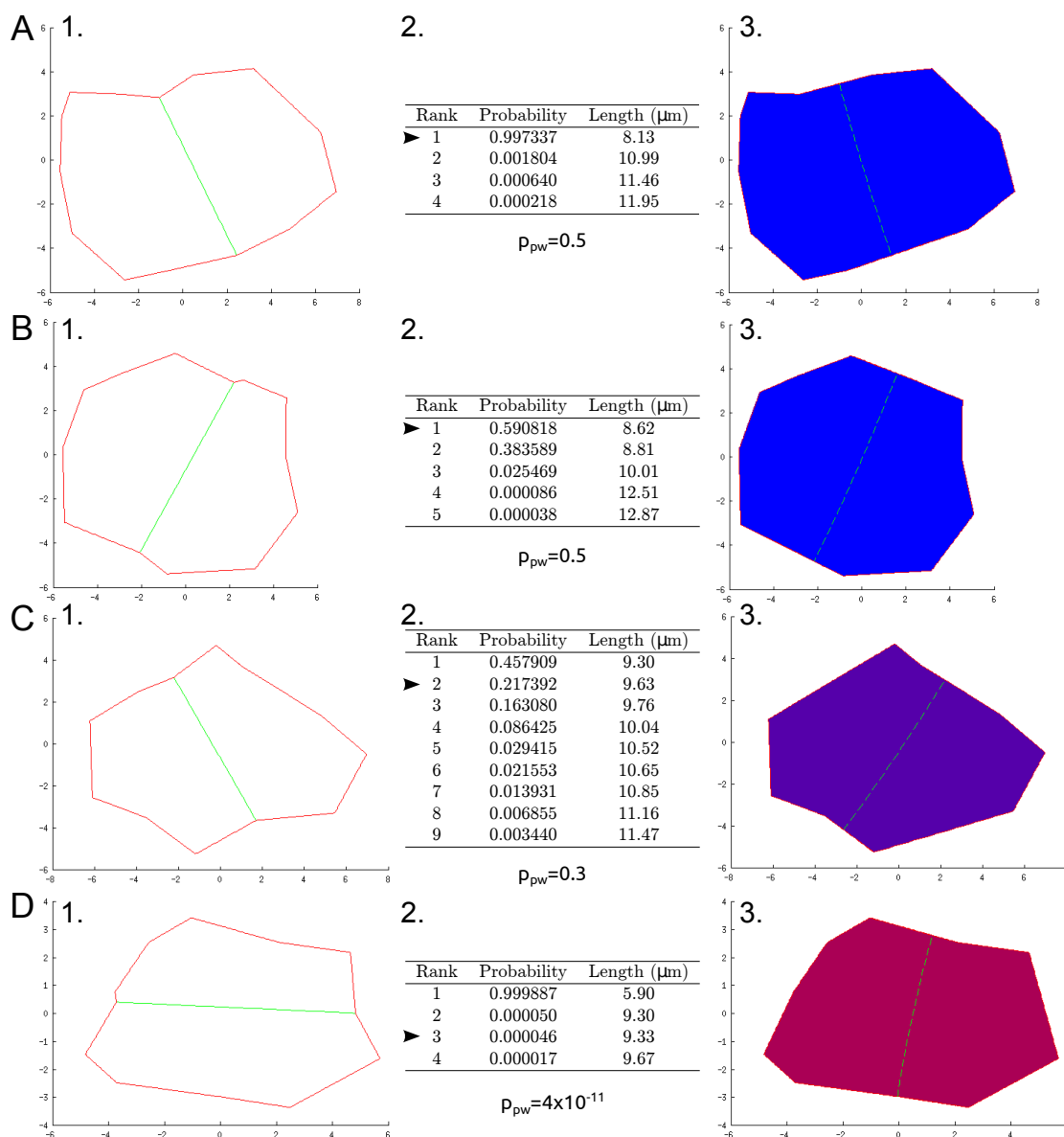


Figure 2.8: Examples of computations of the Besson script. (A-D) Different cell shapes, theoretical predictions of the Besson script and their choice of plane. 1. Flattened divided cells. Only main vertices (between the junction of three cells) are kept. New plane are displayed in green. Division occurred in the last 12 h. 2. The Besson script computes theoretical predictions and gives match between chosen plane and predictions (arrowhead). 3. The Besson script colours cells according to the rank of theoretical plane matching with the chosen division plane. Blue = shortest plane, purple = second shortest plane, magenta = third shortest plane. Green dashed line indicate position of the shortest theoretical plane. 1. and 3.: X and Y axis are in μm .

2 A mechanics-based rule accounts for the orientation of cell division in the boundary of the shoot apical meristem of *Arabidopsis thaliana*

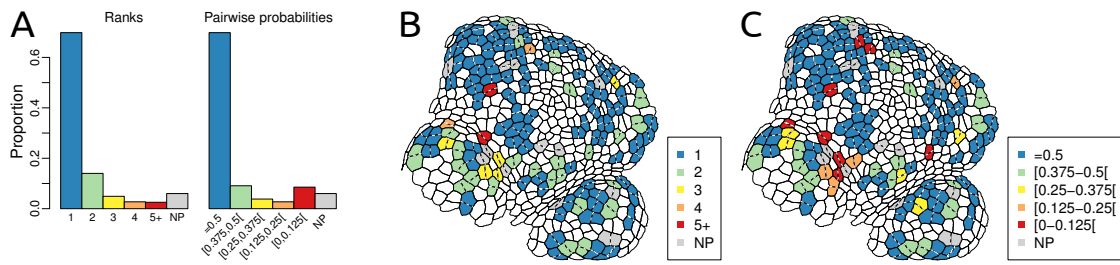


Figure 2.9: Comparison between ranks and pairwise probabilities. (A) Proportions of plane ranks and classes of pairwise probabilities (ratio between probability of observed plane and the sum of this probability and the probability of shortest plane). (B) Example of map of planes choices in function of ranks. (C) Example of map (same snapshot as in (B)) of planes choices in function of pairwise probabilities classes.

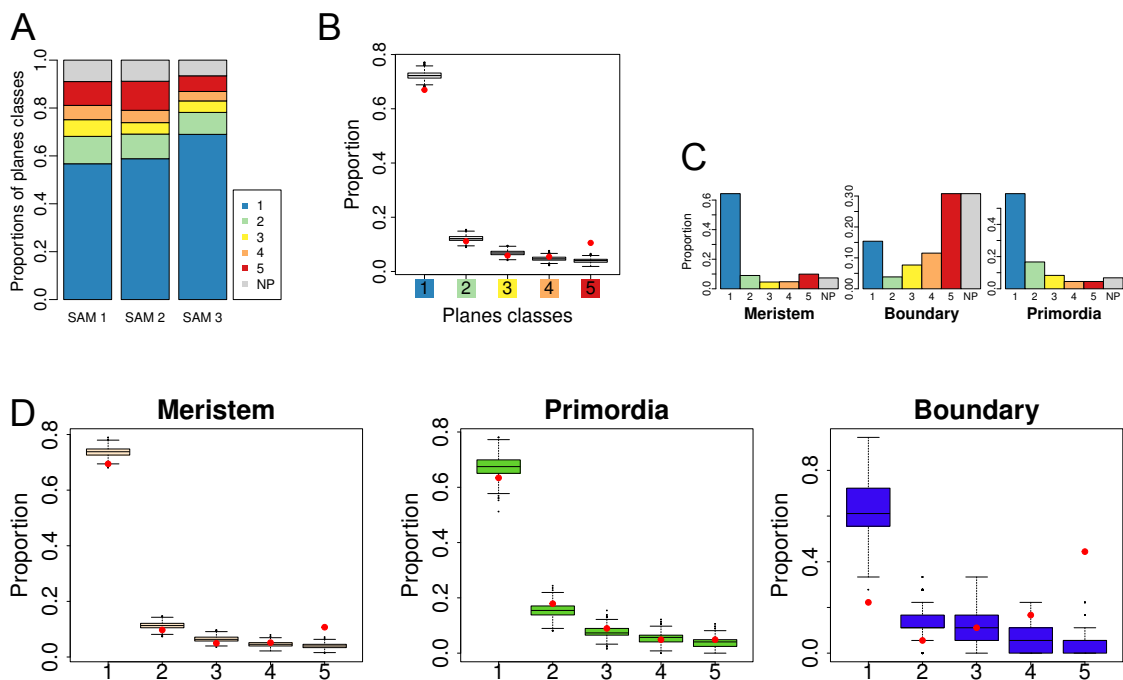


Figure 2.10: Predictions of Besson-Dumais and bootstrap tests on all dividing cells (including the most asymmetric divisions). (A) Proportion of plane categories in each SAM (total number of dividing cells in SAM1, 2 and 3 is respectively 201, 272 and 229). Classes 1 to 5 correspond to the ratio between the probability for a cell to choose the observed planes and the probability to choose the shortest plane, as predicted by the Besson script. Ratio vary from 0 to 0.5. Class 1 $[\leq 0.5]$ correspond to the choice of the shortest plane and Class 5 $[0;0.125[$ correspond to the choice of the longest plane. NP corresponds to an absence of match between theoretical predictions and observations. (B) Comparison of observed planes proportions within the different classes (red dots) with fluctuation range obtained by bootstrap-like approach among theoretical predictions given by the Besson script (boxplots). Planes which did not match prediction (NP class) were excluded from this analysis. Total number of dividing cell: 645. (C) Proportion of plane categories in function of cell localisation. (D) Comparison of observed planes proportions within the different classes (red dots) with fluctuation range obtained by bootstrap-like approach among theoretical predictions given by the Besson script (boxplots) in function of regions. Planes which did not match prediction (NP class) were excluded from this analysis. Total number of dividing cell in meristem, primordia and boundary is respectively: 504, 123 and 18.

3 Mechanical compression leads to microtubule bundling in *Arabidopsis*: a quantitative approach

Authors and contributions

M. Louveaux did all confocal image acquisition, compressions with the indenter, image processing, analysis of indenter curves, design of indices and writing of R script to analyze indenter curves; S. Rochette wrote R script to compute indices; L. Beauzamy provided training on the indenter. A. Boudaoud and O. Hamant supervised the work.

3.1 Preamble

In chapter 2, we showed quantitatively, using a bootstrap-like approach, that Besson and Dumais geometrical rule was insufficient to explain divisions at the shoot apical meristem of *Arabidopsis thaliana*, and in particular in the boundary region. We proposed a new division rule based on another directionnal cue, which can act both at cellular and supracellular scale: the mechanical stress. We explored the contribution of mechanical stress with two strategies: modeling of a growing tissue with two possible division rules (geometrical or mechanical), which was closer to real tissues with mechanical division rule, and perturbation of mechanical stress pattern of the SAM by laser ablation, which was sufficient to bias division plane orientation toward the new mechanical stress pattern. At the center of the SAM, mechanical stress pattern is predicted to be isotropic. Laser ablation is predicted to create locally a circumferential stress pattern. We observed that new planes were positionned circumferentially around the ablation.

However, perturbation of mechanical stress pattern by laser ablation presented several limitations. In *LTi6B-GFP* meristems, ablation was followed by elongation of neighbours (Fig. 3.1) and thus, we could not conclude if the observed bias in division plane orientation was a direct or indirect consequence, e.g. mediated by cell elongation, of the perturbation of mechanical stress pattern.

During the PhD thesis, we performed other mechanical perturbation tests and obtained several preliminary results which were consistent with a mechanical bias of division plane orientation and pointed at the limitations of our micromechanical tools.

We performed single or double UV laser ablation on *clv3 GFP-MBD* and *GFP-MBD* meristems and acquired confocal stacks at 30 min and at 24 h after ablation to explore consequences of ablation on preprophase band (PPB) (Fig. 3.2). Resolution of spinning disk, on which the laser ablation system is installed, was not sufficient to target ablation

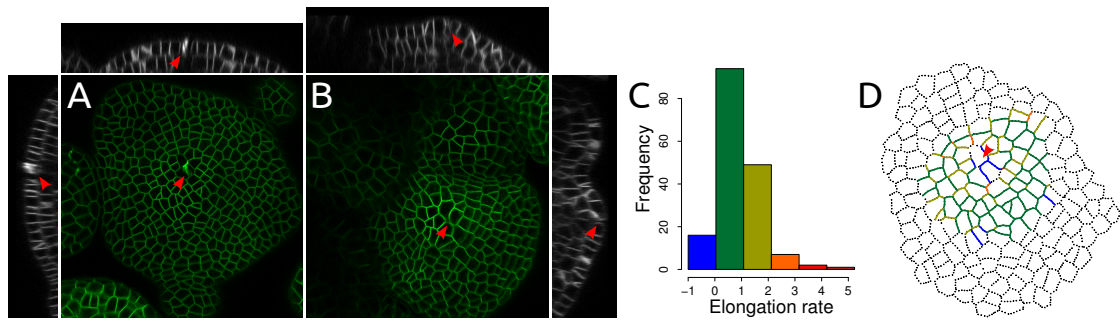


Figure 3.1: Cell wall elongation following an ablation. (A-B) Confocal images of p35S::LTi6B-GFP dissected meristem projected from top in 2D with MerryProj (Barbier de Reuille et al. 2005) surrounded by orthogonal views of the stack obtained with Fiji (Schindelin et al. 2012). (A) 30 min and (B) 48 h after the ablation. Red arrowhead: ablation site. (C) Elongation rate is equal to $(l_B - l_A)/l_A$ with l_A : cell wall length at 30 min and l_B cell wall length at T48 h after ablation. (D) Map of cell wall elongations projected on confocal image of the tissue taken 30 min after ablation. Red arrowhead: ablation site.

laser near a preprophase cell and we could only count on luck. We observed a few perturbations of preprophase band located near ablation sites. 14 PPB were observed at 30 min on *clv3 GFP-MBD* meristems, 5 close to the ablation (first or second rank of cells neighbouring the ablation site) and 9 at further distance. All these preprophase cells completed cytokinesis within the next 24 h. All the cells far from the ablation positioned new cell wall in the same orientation as PPB. Among the 5 cells close to an ablation site, 3 positioned new cell wall in the same orientation as PPB, 1 had deviated slightly (Fig. 3.2A-B) and 1 had divided perpendicularly to previous PPB (Fig. 3.2C-D). In the last case, the cell was located between two ablation sites. And in both cases, cell shape did not change much, which . Among the 9 PPB observed on *GFP-MBD* meristems, 6 were close to an ablation site and 3 far from ablation site. All these preprophase cells completed cytokinesis within the next 24 h and all positioned new cell wall parallel to previous position of PPB.

We also performed compression with an homemade set-up: NPA treated meristem was put on Arabidopsis medium and held with plastic blades. A coverslip was put on top of the meristem and glued to the blades. This set-up was too simple to control applied load and growing plants either crashed on coverslip or bent on the coverslip.

The aim of this chapter is to propose a new controlled compressive set-up to perturb the mechanical stress pattern of the SAM, as well as quantitative image analysis tools adapted to the precision of this set-up. This set-up, based on the indenter technique, offers many advantages: compression is almost non invasive, compression can be applied over several hours and stopped at any time, load is controlled and recorded at all time, and scale of compression is determined precisely by the size of the tip. Moreover, the indenter has a x10 (dry) objective allowing to localise the meristem on the stage and to position the tip. Confocal images of the sample can be acquired before and after compression on a nearby confocal microscope. No image can be taken during compression.

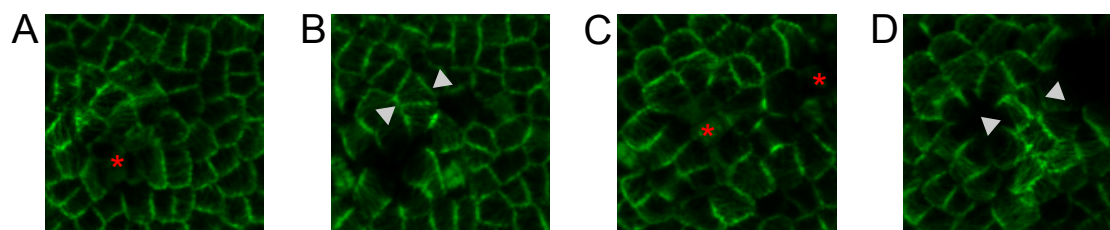


Figure 3.2: Preliminary results on abnormal positioning of division plane close to an ablation site. (A-D) 2D projections of confocal stacks of *clv3 GFP-MBD* meristems projected from top in 2D with MerryProj (Barbier de Reuille et al. 2005). Red stars indicate ablation sites 30 min after ablation. (A-B) Single ablation site. (A) 30 min after ablation. (B) 24 h after ablation. A new cell wall, deviating slightly from preprophase band orientation at 30 min (indicated with grey arrowheads) has formed at 24 h. (C-D) Double ablation site. (C) 30 min after ablation. (D) 24 h after ablation. Two new cell wall are visible at 24 h after ablation. One cell wall is perpendicular to preprophase band orientation observed at T30 min after ablation (indicated with grey arrowheads).

3.2 Abstract

Exogenous mechanical perturbations on living tissues are commonly used to investigate how cells react to mechanical stress, but applied stress is not always quantitatively correlated with biological response. Here we used a microindenter to apply a controlled compression on living plant tissues. We tested two microtubule marker lines, *GFP-MBD* and *TUA-GFP*, and two mutants impaired in microtubule dynamics, *bot1-7 GFP-MBD* and *spr2-2 GFP-MBD* and we first observed qualitatively microtubule response in these different lines. We observed that compressive stress induces reversible apparent bundling in the *GFP-MBD* line and depolymerisation of microtubules in the *TUA-GFP* line. These observations were consistent with previous published results. Compressive stress also induced apparent bundling in the *spr2-2* mutant, but not in the *bot1-7* mutant. Our observations of the *bot1-7* mutant are consistent with previous published results. So far the response of *spr2-2 GFP-MBD* to compression had never been explored. Then we explored different tools to quantify objectively cytoskeleton response to mechanical perturbations and to provide adapted tools to this new controlled compressive set-up. With these tools, we were able to separate *bot1-7 GFP-MBD* from the other lines.

3.3 Introduction

Exogenous mechanical perturbations on living tissues are commonly used to investigate how cells react to mechanical stress, but applied stress is not always quantitatively correlated with biological response. Several set-ups exist to apply mechanical stress, either on whole organs or only on part of the organ or isolated cells. Exogenous mechanical perturbations in animals can be exerted at much shorter time scales than in plant cells. Farge 2003 applied a compression during a few minutes on *Drosophila* embryo with a cover-slip, which position is precisely controlled in z, and records qualitatively the expression of Twist gene. Itabashi et al. 2012 applied single mechanical impulses on the order of several tens of milliseconds, with a precisely controlled amplitude, over metaphasic HeLa cells and

3 Mechanical compression leads to microtubule bundling in *Arabidopsis*: a quantitative approach

recorded changes in centromeres distance before and after impulse. Yeoman and Brown 1971 inserted ends of a cylindrical explant of *Helianthus tuberosus* into ends of a U-shaped tube, imposing a semicircular conformation on the tissue. They explored the qualitative effects of mechanical stress (compressive on the inner face and tensile on the outer face) on division rates and division plane orientation over several days. Coutand et al. 2009 bent stem of a young poplar around a plastic tube and quantified diameter growth and level of expression of the mechanosensitive transcription factor gene PtaZFP2 relatively to strain over several days.

Effects of exogenous mechanical stress on microtubules in plants are well documented. Effects occur within a few hours, a relatively short time scale compared to divisions or organ growth. Microtubules are able to reorient along maximal stress direction in response to an ablation or a compression (Hamant et al. 2008). Compression was shown to induce a better supracellular coalignment of microtubules (Jacques et al. 2013; Sampathkumar et al. 2014). However, none of these experimental protocols allowed to link quantitatively microtubule response to applied stress. Mechanism behind the reorganisation of microtubule network in response to mechanical stress requires microtubule self-organization processes. In particular *katanin* mutants reorganise their microtubules network in response to ablation and compression much more slowly than the wild type (Uyttewaal et al. 2012; Sampathkumar et al. 2014). Conversely, ablations increase the microtubule severing rate in neighbouring cells (Sampathkumar et al. 2014). This shows that microtubule severing by the KATANIN protein promotes the microtubule response to mechanical stress.

Here we adapted a microindenter-based system to apply quantified loads on living plant tissues. This system compensates growth over time by adjusting the position of the compressive tip, thus maintaining the load constant over time. We applied this system on shoot apical meristems of *Arabidopsis thaliana* and tested two microtubule marker lines, *GFP-MBD* and *TUA-GFP*, and two mutants, *bot1-7* (e.g. *katanin*) and *spiral2*, both crossed with *GFP-MBD*. We tested the effect of a compression of a few hours on the coalignment of microtubules and its reversibility after compression arrest. Then we explored different tools to quantify objectively cytoskeleton response to mechanical perturbations and to provide adapted tools to this new controlled compressive set-up.

3.4 Results

3.4.1 Applying controlled compression on living plant tissues with a microindenter

Indenter are used in material science and industry to check mechanical properties of lifeless objects. While atomic force microscopy is adapted for nanoscale deformations, micro-indenters allows to probe bigger domains of the tissue of a few μm to $100\ \mu\text{m}$, depending on the choice of tip. Here we adapted this technology to the indentation of living material: the shoot apical meristem of *Arabidopsis thaliana* (Fig. 3.3A and B). Shoot apices were cut from the plant and young floral buds were dissected out to give access to the shoot apical meristem at the centre of the apex. These apices were kept alive in agarose medium supplemented with sugar and vitamins (see Material and Method). Meristems were im-

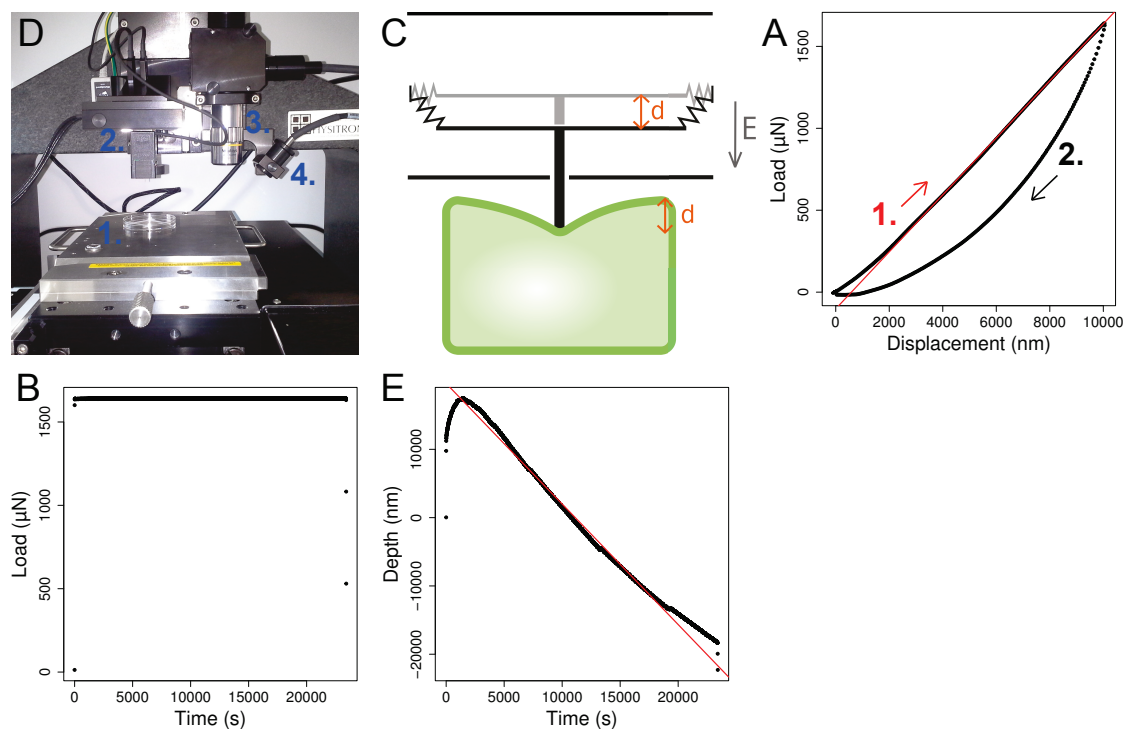


Figure 3.3: Indentation protocol. (A) The indenter. 1. Motorized stage. 2. Tip and transducer. 3. x10 (dry) objective. 4. Bright light. (B) Schema of the transducer (black) indenting a biological object (green). Transducer is a three-plate capacitor. The central plate is attached to springs and can move between the two other fixed plates. When a voltage current E is applied on fixed plate, central plate is displaced over a distance d . A feedback loop is implemented in the system to compensate growth or shrinkage of the meristem over time. (C) Load~Displacement curve. A first indentation at known displacement (here $d=10\mu\text{m}$) is performed on the sample over a few seconds. The fitted part of the curve (red line) is the tip approach (1.) and is linear. The slope is the apparent stiffness of the sample. The other part of the curve (2.) corresponds to the retraction of the tip. Its non linearity highlights the visco-elastic behaviour of the sample. (D) Load~Time curve. A constant load is applied to the sample over 6 h 30 min, e.g. 23 400 s. Load value is chosen according to the maximum load in (C). (E) Tip depth~Time curve. Position of the tip along z axis over time. A linear fit (red line) was applied between 4000 and 20 000 s to compute speed displacement of the tip, which is linked to growth of the apex.

mersed in pure water during the whole experiment to avoid dehydration. To indent, a flat tip of a $100\mu\text{m}$ in diameter was used.

Indentations can be performed over variable time scale (from a few seconds to a few hours) and indenter can be configured to apply either a fixed load or indent at a fixed depth. As meristems may vary in shape and stiffness, they were indented first at a known depth during a few seconds (Fig. 3.3C). This first indentation ramp gave an estimation of the load needed to indent a given depth. Then, load was applied continuously during 6 h 30 min (Fig. 3.3D). Living plant tissues are continuously growing. If tip is static, the growing meristem presses on the tip and increases progressively the total compressive force exerted on the tissue. Growth can also deviates from the vertical axis. In such cases, the apex escapes compression by growing preferentially on one side of the device and is thus exposed to a smaller load. Here we took advantage of the indenter features and maintained a constant known load on the sample, by adjusting the position of the tip in function of

3 Mechanical compression leads to microtubule bundling in Arabidopsis: a quantitative approach

load measured at the tip. At any time during compression, current applied load and tip position are precisely known (Fig. 3.3D-E).

The mechanical stress pattern of the indented region of the meristem before indentation is predicted to be isotropic at the top and anisotropic circumferentially on the flanks. The indentation is expected to lower stress intensity at the center of the indented region and to increase stress intensity at the periphery. Thus mechanical stress pattern of the compressed meristem is still isotropic at the center and becomes gradually more anisotropic and circumferential toward the periphery. This pattern (isotropy at the center and anisotropy on the flanks) is not qualitatively different from the non indented situation.

3.4.2 Compressive stress induces reversible apparent bundling in the *GFP-MBD* microtubule marker line and depolymerisation of microtubules in the *TUA-GFP* microtubule marker line

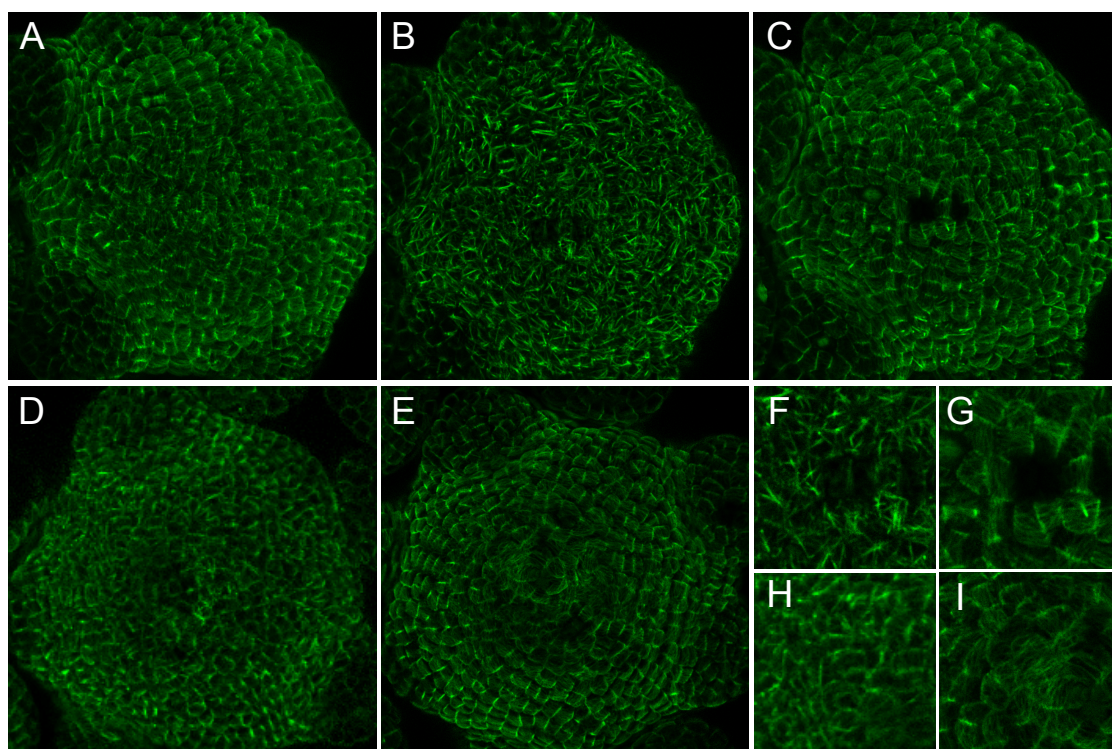


Figure 3.4: Effect of compressions on *GFP-MBD* at a load value corresponding to different initial displacements. (A-E) Confocal image of *GFP-MBD* meristems projected in 2D. (A-C) Load value corresponds to an initial displacement of 10 μm . (A) Before compression. (B) A few minutes after release of compression. (C) 16 h after release of compression. (D) Load value corresponds to an initial displacement of 5 μm . Image is taken a few minutes after the release of compression. (E) Load value corresponds to an initial displacement 2 μm . Image is taken a few minutes after the release of compression. (F-I) Close ups of B (F), C (G), D (H), and E (I). (F-G) is centered on an ablation.

To analyze the microtubule response to mechanical compression, we acquired confocal images of the meristems before (Fig. 3.4 A) and after (Fig. 3.4 B) compression. A 6 h 30 min compression on *p35S::GFP-MBD* (WS-4) lines induced apparent microtubule bundling.

This response was visible when imaging the meristem as early as 15 min after indentation (Fig. 3.4 B and F). This response was also reversible: microtubule network at 16 h after the end of compression looked very similar to microtubule network before compression (Fig. 3.4 C and G). Our results confirmed previous observations of bundling on leaves and cotyledons, after compression with a coverslip (Jacques et al. 2013; Sampathkumar et al. 2014). However, the degree of apparent bundling varied among meristems from very aligned network to very thick bundles (as the ones shown in Fig. 3.4 B and F).

To check whether dose-response could be induced with the indenter, we also tested different indentation depths. Indentations at 5 μm , followed by continuous compression at corresponding load, had a visible effect on cortical microtubules (Fig. 3.4 D and H), whereas indentations at 2 μm had no visible impact (Fig. 3.4 E and I). These preliminary tests guided choice of indentation depth. In the following experiments, an indentation depth of 10 μm was chosen to be sure to induce a maximal response.

It is worth noting that compression induced ablation of one or a few cells in several cases (Fig. 3.4 F and G). Microtubules reoriented circumferentially around the ablation during the following night and this local circumferential pattern (on the first row of cells neighbouring the ablation) could still be observed 16 h after the end of compression, whereas in other part of the meristem microtubules had recovered from compression (Fig. 3.4 C and G). No correlation with asperity on the tip, which could locally increase load on a few cells, could be established.

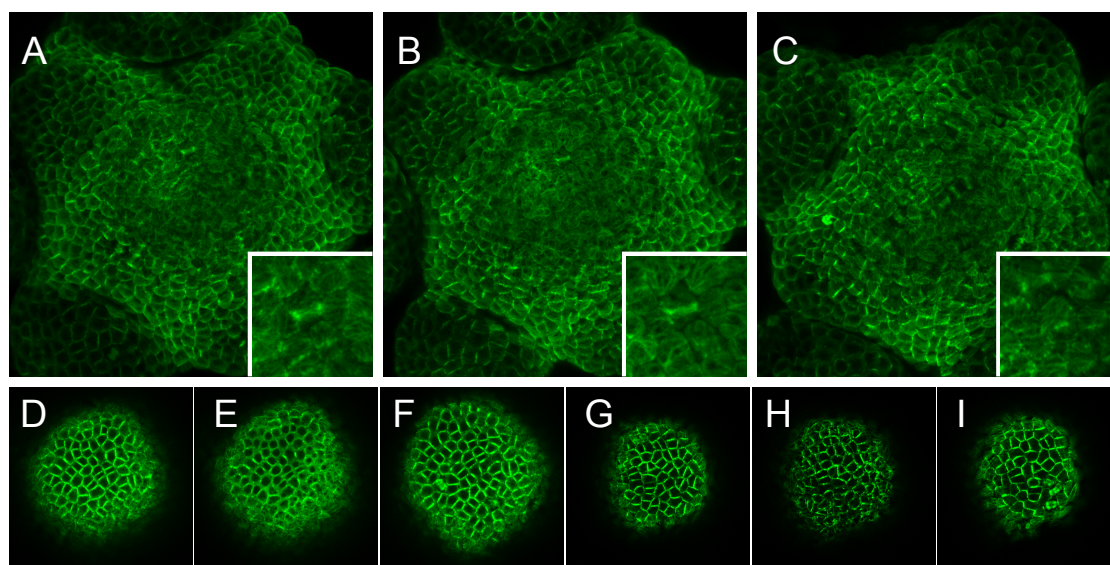


Figure 3.5: Effects of compression on *TUA-GFP* compared to *GFP-MBD*. (A-E) Confocal images of *TUA-GFP* meristems projected in 2D from the top, (A) before, (B) just after and (C) 16 h after release of compression. Bottom right corner of (A-C): close ups on a preprophase band (A-B) and the corresponding new cell wall (C). (D-I) Close-ups on one slice of the confocal stack, at the equator of epidermal cells of a *TUA-GFP* meristem (D-F) and *GFP-MBD* meristem (G-I), before (D and G), just after (E and H) and 16 h after release of compression (F and I).

Interestingly, the microtubule response in the *TUA-GFP* line was different from the *GFP-MBD* line. Microtubular network seemed less intermingled, but no apparent bundling could be observed (Fig. 3.5A-B). Views of cells' equator revealed a cytoplasmic localisation of GFP signal, suggesting a depolymerisation of microtubules in response to the com-

3 Mechanical compression leads to microtubule bundling in Arabidopsis: a quantitative approach

pression (Fig. 3.5D-F). Such relocalisation was not observed in *GFP-MBD* (Fig. 3.5G-I). A depolymerization of microtubules in the *TUA-GFP* would be consistent with previous published results on the effects of a local compression exerted with a needle on cotyledon epidermal cells (Hardham et al. 2008). Both modification of network geometry and cytoplasmic relocalisation of GFP signal were reversible: microtubule network at 16 h after the end of compression looked very similar to microtubule network before compression (Fig. 3.4C).

Close-ups of Fig. 3.5 A to C, are centered on a cell displaying a PPB at T0 before compression (Fig. 3.5 A), which is still present after compression (Fig. 3.5 B) and which is replaced by a new cell with the same orientation at 16 h after compression (Fig. 3.5 C). This image is representative of the longer persistence of PPB observed in compressed meristems compared to control: in half of the *TUA-GFP* compressed meristems and three quarter of the *GFP-MBD* PPB was still visible just after release of compression, whereas this was the case in only of a third of *TUA-GFP* and *GFP-MBD* control meristems. To give more details, in the compressed meristems of the *TUA-GFP* line, among a total of 11 cells showing a PPB before compression, 1 cell had collapsed, 5 were still showing PPB just after compression and completed mitosis and cytokinesis in the next 16 h, 2 had completed mitosis and cytokinesis during compression, and 3 displayed no more PPB but at the end 2 of them still completed mitosis and cytokinesis in the next 16 h. Division plane orientation was not affected by compression. In the *TUA-GFP* control (non compressed) meristems, among the 13 cells displaying a PPB at T0 (before the compression experiment), 5 were still showing PPB just after compression and had completed mitosis and cytokinesis in the next 16 h and 8 had completed mitosis and cytokinesis on the snapshot taken just after release of compression time. In the *GFP-MBD*, most of the confocal images were taken only before and just after compression and thus we lack information at 16 h after release of compression. In the compressed meristems, among the 16 cells displaying a PPB before compression on indented meristems, 1 cell divided during compression, PPB was not visible anymore in 3 cells and PPB was still there in 12 cells. In the control meristems, among the 16 cells displaying a PPB at T0, a PPB was still visible after compression time in 6 cells and the 10 other cells had completed mitosis and cytokinesis during compression time. It is worth noting that compressions did not affect division plane orientation, as new cell walls observed after the end of compression oriented in the same direction as PPB observed before the compression.

To sum up, in both microtubule marker lines (*GFP-MBD* and *TUA-GFP*), preprophase band seemed to persist a longer time in compressed cells compared to control cells. PPB persisted with the same orientation after compression and, when cytokinesis was recorded, division plane oriented along the same axis as the PPB. Compressive stress on top of the meristem seems then to induce a delay in mitosis progression, but not to perturb division plane orientation.

3.4.3 The *spr2-2* mutant has a lower apparent stiffness and lower growth speed compared to wild type microtubule marker lines and *bot1-7* mutant

Previous experiments showed that in the *bot1-7 GFP-MBD* mutant, microtubules were more disorganised than control microtubule marker line *GFP-MBD* and responded less to

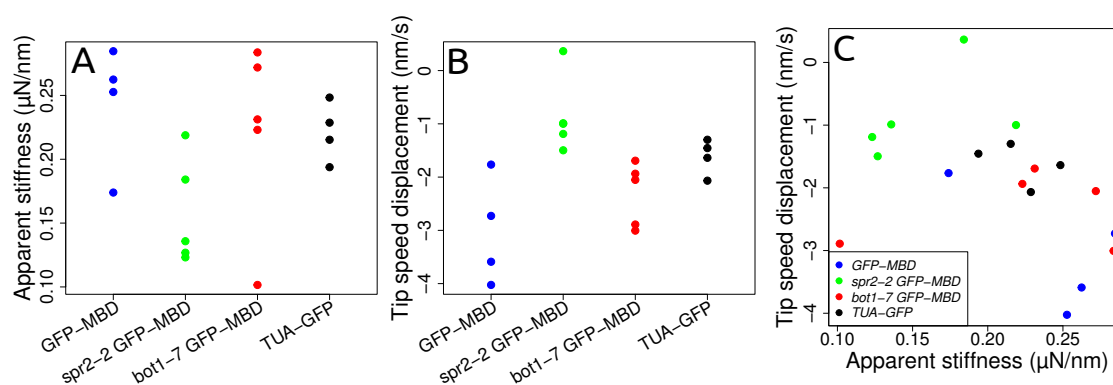


Figure 3.6: Apparent stiffness of meristems and tip displacement speed. (A) Apparent stiffness (slope of part 1. of Load~Displacement curve at $d=10\ \mu\text{m}$, see Fig. 3.3C). (B) Displacement speed of indenter tip during the compression (slope computed from Tip Depth~Time curve, see Fig. 3.3E). (C) Displacement speed of indenter tip during the compression in function of apparent stiffness.

top compression over 6-7 hours and to ablation (Uyttewaal et al. 2012; Sampathkumar et al. 2014). We included the *bot1-7* mutant to test whether our compression protocol revealed the same reduced response. As SPIRAL2, also called TORTIFOLIA (Buschmann et al. 2004), was shown to act antagonistically on KATANIN (Wightman et al. 2013), we also included the *spr2-2* mutant crossed with *GFP-MBD* in the analysis.

We extracted apparent stiffness and speed displacement of indenter from indenter curves, for both mutants and of both microtubule marker lines. Apparent stiffness was obtained by fitting linearly the approach curve presented in Fig. 3.3C. Apparent stiffness is the global stiffness of the meristem, resulting from both turgor pressure and cell wall stiffness. We found an apparent stiffness of 0.10 to 0.30 $\mu\text{N nm}^{-1}$. As expected, the apparent stiffness varied among the different genotypes. The *spr2-2 GFP-MBD* mutant seemed to be softer than the three others (Fig. 3.6A). Speed displacement was obtained by fitting linearly the displacement time curve between 4000 and 20 000 s. We found a displacement speed of the tip of a few nano metre per second (Fig. 3.3E). In most of the cases, we observed that the tip was pushed backward (negative slope), consistent with the growth of the apex toward the tip (Fig. 3.6B). Displacement was not perfectly linear in most of the cases and speed displacement was often slower on the 3 last hours of the indentation test, suggesting either that the compression may impact growth or that the growth medium cannot fully replace the context of an intact stem, leading to reduced growth. For one *spr2-2 GFP-MBD*, we observed that the tip was continuously going down (e.g. slope was positive, see Fig. 3.6B). This response might reflect an incorrect fixation of the stem in agarose. All the *spr2-2 GFP-MBD* apices showed slower tip speed (Fig. 3.6B). Displacement speed of the tip was not correlated to apparent stiffness (Fig. 3.6C).

3.4.4 Compressive stress induces apparent bundling in the *spr2-2* mutant but not in the *bot1-7* mutant

Compressions during 6 h 30 min were performed on *bot1-7 GFP-MBD* and *spr2-2 GFP-MBD*. As expected and contrary to the *GFP-MBD* control line (Fig. 3.7 A and D), no

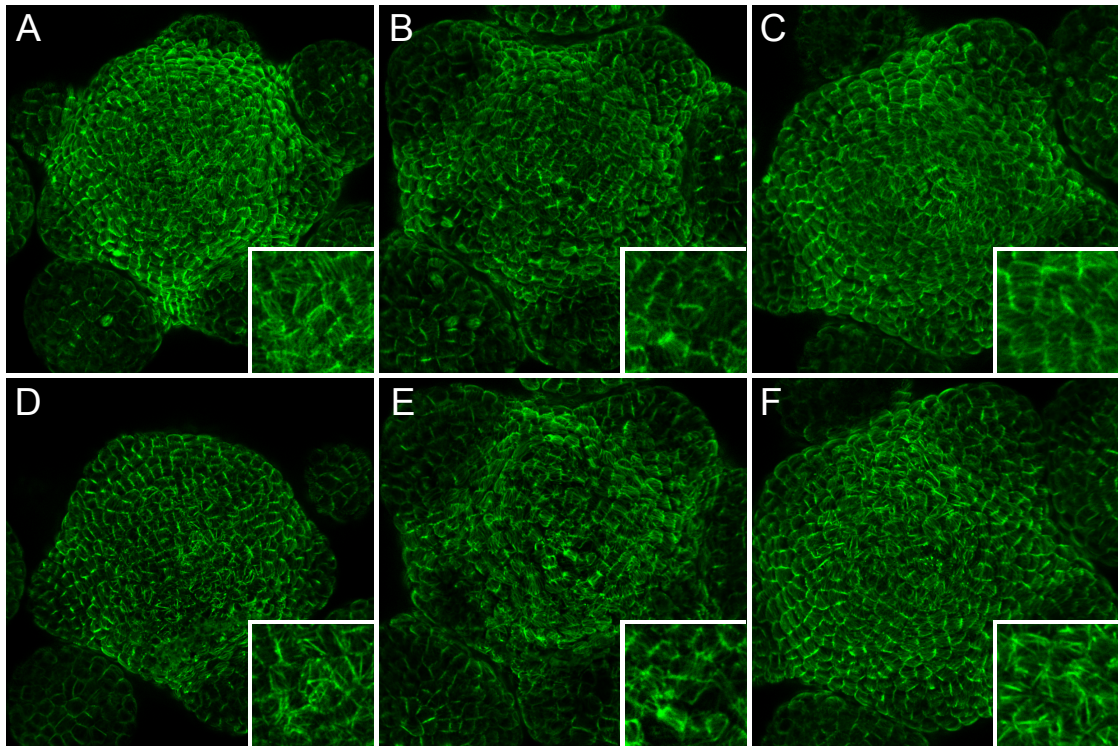


Figure 3.7: Effects of compression on *spr2-2 GFP-MBD* and *bot1-7 GFP-MBD*. Confocal images of dissected meristems projected in 2D from top and corresponding close-ups taken (A-C) before compression and (D-F) just after release from 6 h 30 min of compression. (A and D) *GFP-MBD* microtubule marker line (control). (B and E) *bot1-7 GFP-MBD*. (C and F) *spr2-2 GFP-MBD* dissected meristem.

bundling was observed in *bot1-7 GFP-MBD* (Fig. 3.7 B and E), and microtubule networks seemed only slightly less intermingled. A few ablation sites could be observed, but microtubules did not show well circumferential reorientation, contrary to the *GFP-MBD* control line.

Strong apparent bundling, stronger than in the *GFP-MBD* control line, was observed on half of the *spr2-2 GFP-MBD* meristems just after compression (Fig. 3.7 C and F). Other compressed meristems only showed less intermingled microtubule networks just after compression. In two over the three meristems for which an image had been taken 16 h after release of compression, apparent bundling could still be observed in some cells at this time. For one of these meristems, an ablation was visible and microtubules had reoriented circumferentially at 16 h after release of compression (data not shown).

3.4.5 Quantifying the microtubule response to mechanical perturbations

To go beyond our qualitative assessments, we used previous and new quantitative tools to estimate responses in the different lines. The approach was partially automatised with the perspective to ease statistical analysis of big samples. Here, we analysed 13 *GFP-MBD* (4 indented and 9 control meristems), 7 *spr2-2 GFP-MBD* (4 indented and 3 control meristems), 6 *bot1-7 GFP-MBD* (3 indented and 3 control plants) and 2 *TUA-*

GFP (1 indented and 1 control meristem). On each meristem, on the snapshots taken before and just after compression, 80 cells were segmented manually with Fiji Polygon tool (Schindelin et al. 2012). The Fiji plugin FibrilTool (Boudaoud et al. 2014) was used to measure compute microtubule array anisotropy and mean orientation per cell. Polygon segmentation was then imported in R software with the RImageJROI package (Sterratt and Vihtakari 2015).

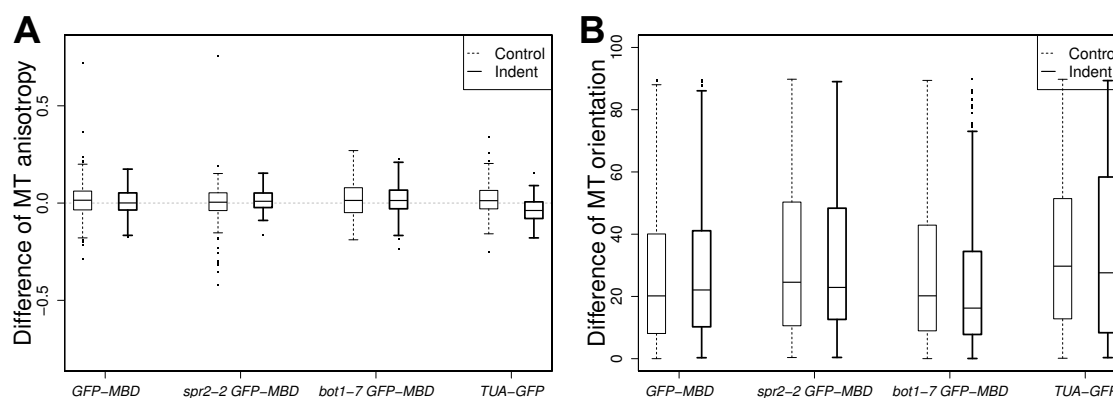


Figure 3.8: FibrilTool measures of difference of microtubules anisotropy and orientation. (A) Variation of microtubule anisotropy during compression. Microtubule anisotropy characterizes the degree of alignment of microtubules in the cells. (B) Reorientation of microtubules during compression. A mean direction of microtubules with the x axis is computed and compared to those of the previous snapshot. Difference is computed in degrees modulo 90.

Response to mechanical perturbation on *Arabidopsis* meristems is known to induce a better alignment of microtubules within the cell (*e.g.* an increase in microtubules anisotropy) under compression and to induce the formation of supracellular microtubules alignments in the direction of maximal tensile stress (Hamant et al. 2008; Sampathkumar et al. 2014; Jacques et al. 2013). The difference of anisotropy between the two snapshots (before and after compression) was computed separately for control and indented meristems of each line. Results showed absence of variation of microtubule anisotropy between the two snapshots (Fig. 3.8A). Reorientation of microtubules was also computed and revealed no differences between indented and control meristems (Fig. 3.8B). In all cases, cells showed little microtubules reorientation, with a median around 20 degree. These quantifications seemed consistent with our qualitative observations: we observed bundling, but never in a preferential direction. Therefore both direction and anisotropy at the entire cell scale are not dramatically changed.

To quantify the increase in apparent bundling, we combined image analysis and geostatistics approaches to compute different indices. Indices of fluorescence intensity within each cells can be used to characterise effect of compression on microtubule network. The distribution of fluorescent intensity of pixels composing each cell of a meristem was described with different indices as presented on Fig. 3.9A: (*i*) coefficient of variation (CV) of the pixel colour distribution (ratio of standard deviation over mean) is a measure of dispersion of the distribution, (*ii*) skewness is a measure of symmetry of the distribution, and (*iii*) kurtosis is a measure of peakedness of the distribution. Non parametric tests (Wilcoxon) were used to test for significant differences between the distribution of indices, which are not Gaussian. The two sample Wilcoxon test allowed to highlight or not the effect of compression on each line (Table 3.1 in §3.7). In parallel, we computed two different ways

3 Mechanical compression leads to microtubule bundling in Arabidopsis: a quantitative approach

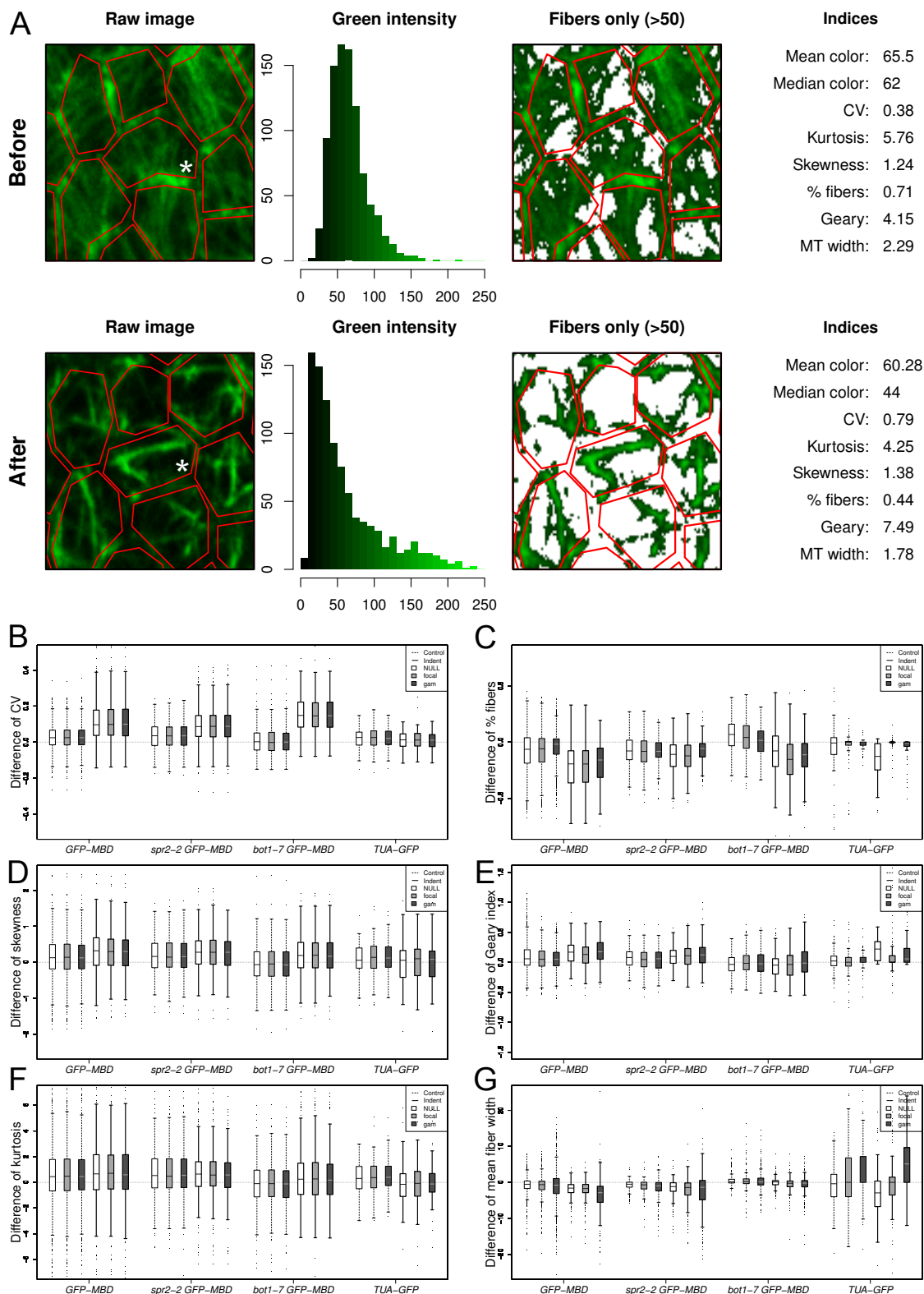


Figure 3.9: Characterization of microtubule networks. (A) Example of analysis performed on a *GFP-MBD* compressed cell (white asterisk). Several informations were extracted from green channel of confocal images ("raw image") before and after indentation: distribution of fluorescence intensity in each cell (delineated with the red polygons) and its characteristic parameters (coefficient of variation (standard deviation over mean), kurtosis, skewness). A threshold (here, 50) was applied on the distribution to extract microtubules. The percentage of microtubules per cell, width of bundles ("distance ind") and complexity of microtubular network (Geary ind) and their with ("distance ind") were also computed. (B, D and F) Indices relative to green fluorescence intensity. (C, E and G) Indices relative to microtubule network. Indices were computed on raw images ("NULL") and on images corrected for fluorescence intensity ("focal and "gam") (see Material and Method)

to normalize fluorescence intensity ("focal" and "GAM"), as distribution of fluorescence intensity could be biased by image acquisition protocol. Indeed, gain and laser were not exactly the same between the two snapshots and between meristems, though cell walls were deliberately over exposed but not microtubules. Both normalization methods aimed at ensuring that each part of the meristem would have an equal fluorescence exposure, relatively to nearby cell walls. Comparison between normalized and raw data revealed that distribution of fluorescence intensity was unbiased by our image acquisition protocol (Fig. 3.9B-G). We describe below only the results of Wilcoxon tests on raw data (NULL normalization).

Cell coefficients of variation (CV, Fig. 3.9B and Table 3.1 in §3.7) increased significantly in the indented region, when compared to the control in *GFP-MBD*, *bot1-7 GFP-MBD* and *spr2-2 GFP-MBD* (p-value < 0.05), but not in *TUA-GFP* (p-value = 0.16), confirming the visual impression that fluorescence is more contrasted after indentation.

Skewness (Fig. 3.9D and Table 3.1 in §3.7) increased significantly in *GFP-MBD*, *bot1-7 GFP-MBD* and *spr2-2 GFP-MBD* (p-value < 0.05), but not in *TUA-GFP* (p-value = 0.20), consistent with the longer tail of distributions toward high grayscale values after indentation.

Kurtosis values were high (Fig. 3.9F and Table 3.1 in §3.7), indicating that distributions were more peaked than a Gaussian distribution, but changes in Kurtosis was only significant for *bot1-7 GFP-MBD* (p-value < 0.05).

To analyze further the microtubule response to compression, microtubules were skeletonized in each cell by applying a threshold on grayscale intensities of images. Some preliminary tests on our 2D projected confocal images showed that a threshold equal to 50 over 255 gave the best compromise between a good filtering of microtubules and large spreading of resulting indices, useful to discriminate the different cell configurations (See example on Fig. 3.9A). Our qualitative observations indicated that compression induced less complex (less intermingled) and more aggregated ("bundled") microtubules (see for instance Fig. 3.9A -After-).

To verify this observation on microtubules network and quantify the changes, three indices were computed: (i) the percentage of microtubules fiber per cell, (ii) the complexity of the network and (iii) the width of microtubule network. The word fiber is used to design and distinguish aggregated microtubules from isolated microtubules. As for the indices on the fluorescence distributions, indices on microtubule network were also calculated with different exposition normalisations.

(i) Percentage of microtubules fiber was computed as the ratio of the number of pixels above threshold over total number of pixels in each cell between the two snapshots (before and after) for indented and control meristems. Percentage of microtubules decreased significantly for all genotypes, even if the difference was smaller for *spr2-2 GFP-MBD* (p-value < 0.05, Fig. 3.9C and Table 3.1 in §3.7).

(ii) The complexity of the network was approached through the Geary index, which is a measure of local spatial autocorrelation. The Geary index was computed on a 0/1 grid, representing a not-microtubule/microtubule value for each pixel of a cell and averaged over

3 Mechanical compression leads to microtubule bundling in Arabidopsis: a quantitative approach

each cell. An increase in Geary index reflects a decrease in complexity of the network, e.g. network is less intermingled (see example on Fig. 3.9A). Geary index significantly increased in all genotypes (p-value < 0.05) excepted in *bot1-7 GFP-MBD* (p-value =0.19, Fig. 3.9E and Table 3.1 in §3.7). Results of Wilcoxon tests are consistent with our qualitative observations: microtubules networks of compressed meristems seem less intermingled for all genotypes excepted *bot1-7 GFP-MBD*.

(iii) Width of microtubule network is complementary to Geary index and also characterizes the complexity of a microtubular network. This index was calculated as the distance of a microtubule pixel to the nearest non-microtubule pixel. In our case, small width indicates that microtubules are isolated and large width that the network is intermingled (Fig. 3.9A). Width significantly decreased in all genotypes (p-value < 0.05, Fig. 3.9G and Table 3.1 in §3.7), but results were more contrasted in *TUA-GFP* depending on normalisation method applied.

Interestingly, in the control (not compressed) *bot1-7 GFP-MBD* lines the different indices showed opposite results compared to other lines. CV and kurtosis were centered on zero indicating no evolution of both parameters accross the duration of the compression experiments, skewness and Geary were lower than in other lines and the differences of percentage of microtubule fibers and mean fiber width were higher. These differences could reflect the difference of microtubule architecture (more intermingled) observed in the *bot1-7 GFP-MBD* line. However, as revealed by indices computed on compressed meristems, response of *bot1-7 GFP-MBD* is similar to the response of other lines, except for the Geary index (Fig. 3.9E and Table 3.1 in §3.7). These quantitative results contradict the qualitative impression that *bot1-7 GFP-MBD* do not respond to compression and suggest that *bot1-7 GFP-MBD* might respond as well, but that its response might be partially hidden by its particular microtubule network architecture.

3.5 Discussion

In this chapter, we used an indenter to apply a quantified and constant mechanical compression on a living tissue over several hours. We coupled this system with confocal imaging and observed an apparent bundling response to compression in the *GFP-MBD* marker line, but not in *TUA-GFP* line, which instead showed a depolymerization response. Our qualitative observations on *GFP-MBD* confirmed previous results obtained on cotyledons (Sampathkumar et al. 2014). Depolymerization of microtubules in the *TUA-GFP* had been previously observed in response to a local compression exerted with a needle on cotyledon epidermal cells (Hardham et al. 2008). The discrepancies between the *GFP-MBD* and *TUA-GFP* lines might reflect differences in microtubule stability in these different contexts: the *GFP-MBD* is known to stabilize microtubules, whereas the *TUA-GFP* line tends to have a greater microtubule turnover. The stabilisation effect of *MBD* might amplify or even be responsible for apparent bundling.

Apparent bundling was previously shown to be provoked by an increase in severing activity of the protein katanin (Sampathkumar et al. 2014). We extended our compression tests to two mutants, *bot1-7* and *spr2-2*, both crossed with *GFP-MBD*. *bot1-7* is a katanin mutant. SPIRAL2 (*SPR2*) is known to prevent severing by a steric competition with the

KATANIN protein at crossover sites (Wightman et al. 2013). *bot1-7 GFP-MBD* has a more disorganised microtubule network, which responds less to mechanical perturbations (Bichet et al. 2001; Burk et al. 2001; Burk and Zheng-Hua 2002; Uyttewaal et al. 2012; Sampathkumar et al. 2014). So far, effects of mechanical stress on microtubules in the *spr2-2* mutant had never been explored. Here the number of meristems was too small to conclude on a correlation between mechanical properties or growth, and genotype, but we observed that *spr2-2 GFP-MBD* seemed softer and had a slower growth, when compared to the others.

To go beyond these qualitative assessment, we used several quantitative tools to estimate responses of the different lines to compression. Variation of microtubule anisotropy and reorientation of microtubules over time, computed with an ImageJ/Fiji macro called FibrilTool (Boudaoud et al. 2014), did not seem to be affected by the compression. Bundling was much more pronounced in our images than in other studies where FibrilTool was used (Uyttewaal et al. 2012; Sampathkumar et al. 2014), which might perturb measures of FibrilTool macro.

We extracted fluorescence distribution of pixels of each cells and computed characteristic features: coefficient of variation, kurtosis and skewness. After compression, fluorescence distributions were more spread, with a longer tail on higher grayscale fluorescence values. Normalisation of fluorescence intensity over meristems did not change a lot our results. This supports the chosen image acquisition protocol, in which only cell walls (but not microtubules) were over exposed and the image segmentation protocol, in which only cells located at the top of meristem were delineated (those are more equally lighted and less subjected to alterations by 2D projection). To go further on the analysis of fluorescence, we selected a threshold and binarized confocal image to extract microtubules and computed three indices: (i) the percentage of microtubules per cell, (ii) the complexity of the network and (iii) the width of microtubule network. On the control meristems, all indices separated *bot1-7 GFP-MBD* from the others. This result is consistent with previous description of microtubular network of the mutant, which display a more intermingled architecture (Bichet et al. 2001; Burk et al. 2001; Burk and Zheng-Hua 2002). However results on the compressed meristems partially contradicted the absence of reorganization of microtubule network in response to mechanical perturbations (Uyttewaal et al. 2012; Sampathkumar et al. 2014).

The protocol proposed and its coupling with confocal live-imaging offers interesting perspectives to test quantitatively the response of actin and gene expression to a quantified and constant mechanical compression. Biological response cannot be monitored during application of compressive stress and switching from machines directly impose a minimum of 15 min between the end of compression and observation under the confocal. Actual limitations of the indenter software limit duration of compression to a few hours, but these technical limitations could be circumvented, and such system could also help probing effects of compressive stress on cell division.

3.6 Material and Method

3.6.1 Plants material and growth conditions

The Microtubule Binding Domain marker line GFP-MBD (WS-4) was first described in [Marc et al. 1998](#). The *TUA-GFP* line was first described in [Ueda et al. 1999](#). The *bot1-7xGFP-MBD* line was first described in [Uyttewaal et al. 2012](#). *spr2-2* mutant (in Col0) was ordered from NASC (NASC ID: N6549) and crossed with GFP-MBD (WS-4).

Seeds were sown on soil, kept at 4 °C during 48 h, then grown in short day conditions (8 h light at 19 °C ; 16 h night at 17 °C) during 4 weeks and at last transferred 2 to 3 weeks in long days conditions (16 h day at 21 °C ; 8 h night at 19 °C) prior to dissection.

Meristems were cut from the stem, dissected the day before indentation and stuck in "Arabidopsis apex culture medium" (2.2 g/l Duchefa Biochemie—MS basal salt mixture without vitamins, 1 % sucrose ; adjust pH to 5.8 with KOH and add 1.6 % agarose) supplemented with vitamins and BAP. If necessary, meristems were stabilised by extra drops of ACM without vitamins and BAP. Dissected meristems were kept in a phytotron in long days conditions (Sanyo, 16 h day at 21 °C ; 8 h night at 19 °C, synchronised with growth culture chambers).

3.6.2 Imaging

Plants were imaged prior to indentation, 15 min indentation and 18 h after indentation. 1024x1024 pixels images with slices every 1 µm were acquired on a LSM 700 upright confocal microscope (Zeiss), with a water-dipping 40x lens. At each indentation experiment, a minimum of three plants (two control and one indented) were dissected and put in ACM medium.

3.6.3 Indentation

30x10mm Petri dish is fixed on the stage with adhesive gum and optically centered. A quick approach of the tip in the air is performed to position the surface of the meristem. Then the meristem is drown in pure water.

The force (in µN) needed to indent the meristem at 10 µm depth is deduced from a first indentation ramp (5 s from 0 to 10 µm ; 5 s from 10 µm to 0). This force value is used as the setpoint of the second indentation ramp (5 s from 0 to setpoint ; 6 h 30 min at setpoint ; 15 s from setpoint to 0). Extended stage is on to compensate growth or shrinkage of the meristem (rest position at 250 µm).

All indenter curves were exported as text files and analyzed in R software.

3.6.4 Image analysis

All confocal stacks were projected in 2D with MerryProj (Barbier de Reuille et al. 2005). On each stack, starting from the top of the stack, 80 cells were delimited as ROI with ImageJ Polygon tool. Dividing cells were identified manually and suppressed from next analysis steps, as their microtubule network is not comparable to interphase network. This represented less than 4 cells in average on each image (between 0 and 9 cells maximum).

FibrilTool macro (Boudaoud et al. 2014) was used to compute direction and quality of orientation of microtubules on 2D projection within each ROI. Reorientation of microtubules during the two snapshots was computed as the difference of angle with the x axis, which did not rotate between snapshots.

Polygon segmentation was then imported in R software thanks to the RImageJROI package (Sterratt and Vihtakari 2015).

Image fluorescence intensity could be linked to changes in image acquisition. Although, a great attention has been taken to assure similar fluorescence exposition conditions among snapshots, differences could remain, possibly intensified by the 2D projection. Two different ways of normalisation have been tested, allowing comparison of results with the "NULL" normalisation, which is simply the raw image. Both methods used walls fluorescence intensities as reference of maximum fluorescence, following the seminal idea that contrast should normally have been fixed so that all walls should be over-exposed in each slice. For each pixel, if no nearby cell wall reach maximal intensity (green=255), then it is probably under-exposed and its green intensity should be increased. (i) The method named "focal" is a local normalisation. For each pixel, the value of green intensity in surrounding pixels in a radius of 70 pixels (big enough to include 1.5 to 2 cells on average) is computed. If the maximum (255) was not reached, the pixel intensity was multiplied by $255 / \max$ of the neighbours. This assured an intensity still included in the 0-255 interval for each pixel. (ii) The method named "gam" is a global smoothed normalisation based on cell walls. The aim is to fit a statistical model linking green intensity to the coordinates of cell wall pixels only: $intensity = f(x, y)$. As for "focal", this model predicts for each pixel, the mean intensity of surrounding cell walls but smoothed over the entire meristem, thus avoiding too local effects, in contrast to "focal". As green intensity cannot be used directly to detect cell walls in a context of possible under-exposition, we needed to detect variations of intensities to detect cell walls. In spatial science, the topographic position index (tpi) allows to detect hollows and bumps on altimetric maps. Here, we used a modified tpi to detect major bumps of green intensities with an appropriately chosen radius (here, 3, which is the half of an average cell wall width). Bumps is defined as pixel for which $intensity \geq 1.2 \times \text{average of 3-radius neighbours}$. This method could be applied here as cell walls were generally well identified against microtubules. The model then applied is a generalized additive model (GAM) defined with a tensor having a low smoothing parameter corresponding to configuration of our meristems: $intensity = tensor(x, y, k = 5)$. As for "focal", predictions of the model for each pixel were rescaled from 0 to 255 to estimate the smoothed local maximum for each pixel of the meristem. If the maximum (255) is not attained in the prediction, the pixel intensity is multiplied by $255 / \text{prediction of the model}$. Gam was fitted with library "mgcv" in the R-software (Wood 2011; R Core Team 2015).

3 Mechanical compression leads to microtubule bundling in Arabidopsis: a quantitative approach

The distribution of fluorescent intensity of pixels and the microtubule network composing each cell of a meristem were described with different indices calculated with the R-software (R Core Team 2015). Skewness and kurtosis of distributions were computed with the R package moments (Komsta and Novomestky 2015). The Geary spatial autocorrelation index and the width index (e.g. distance to the nearest non-microtubule pixel) were computed with the R package raster (Hijmans 2015). Geary index was computed on an equally weighted 3x3 neighbourhood (default R library raster settings).

3.7 Supplemental Figures

CV	GFP-MBD	<i>spr2-2</i> GFP-MBD	<i>bot1-7</i> GFP-MBD	TUA-GFP
NULL	7.083132e-33	3.17881e-14	1.459396e-44	0.16349330
focal	1.978985e-32	8.90389e-14	5.156242e-45	0.36592830
gam	1.368895e-32	4.84739e-14	4.788727e-44	0.16782200
Skewness				
NULL	6.305612e-05	0.01395385	1.574326e-06	0.20559291
focal	1.647689e-04	0.01906753	1.854049e-06	0.23352814
gam	7.752087e-05	0.04024234	1.711803e-06	0.09633574
Kurtosis				
NULL	0.097406410	0.88756370	0.018752490	0.05201791
focal	0.146872990	0.91846720	0.036047160	0.08745534
gam	0.138218360	0.54433520	0.028909520	0.02220118
Percentage of fibers				
NULL	8.966103e-22	0.00045129	1.981383e-15	6.69682e-06
focal	1.701260e-22	0.01094615	1.498439e-23	1.85753e-01
gam	2.572623e-31	0.42062100	1.492758e-15	5.51658e-02
Geary				
NULL	6.814353e-09	2.10935e-01	0.193841760	6.03526e-08
focal	2.714735e-05	5.78762e-04	0.050436170	2.29855e-01
gam	4.977375e-20	1.39195e-05	0.332363740	3.65963e-05
Mean fiber width				
NULL	8.666810e-17	2.17469e-05	1.911068e-03	0.01909140
focal	2.557572e-14	4.18810e-05	1.039310e-06	0.26627974
gam	1.151311e-16	1.81051e-01	2.786456e-04	0.01317896

Table 3.1: Wilcoxon tests. The Wilcoxon test was used to compare the effect of compression (versus no compression) on meristems for each indice (Coefficient of Variation, Skewness, Kurtosis, Percentage of fibers, Geary, Mean fiber width), each genotype (GFP-MBD, *spr2-2* GFP-MBD, *bot1-7* GFP-MBD and TUA-GFP) and each normalization procedure (NULL, focalLA, gamLA). We considered the response of compressed meristems to be significantly different from control (non compressed) meristems when Wilcoxon test p-value was inferior to 0.05

4 A pipeline for the quantitative analysis of epithelia from cell to tissue scale

Authors and contributions

M. Louveaux did all confocal images acquisition and all image processing. S. Rochette provided R training and wrote .vtk reading script. Other parts of R script were written by M. Louveaux. A. Boudaoud and O. Hamant supervised the work.

4.1 Preamble

In chapter 2 and 3, we improved already existing analysis pipelines and developed new ones to face different challenges: (i) to integrate different sources of information, such as outputs on division planes probabilities from Besson script (written on Matlab) and outputs on cell geometry from 3D surface reconstruction and segmentation (performed on MorphoGraphX), (ii) to synthesise information, for instance by the visualizing output of the Besson script on 3D surface, and to create new indices, such as the proportions of each class of planes probabilities, (iii) to ensure reproducibility of analysis and (iv) to give weight to our results by increasing the number of observations.

The aim of the present chapter is to detail the possibilities offered by the tools developed during the PhD and which could apply to any 3D surface epithelia processed with MorphoGraphX. The potential applications are proposed in the case of the cell division at the shoot apical meristem of *Arabidopsis thaliana*.

4.2 Abstract

Microscopy now offers the possibility to record complex morphogenetic processes and produce big and complex spatio-temporal datasets within a few hours. Numerous tools allow image processing and/or analysis of epithelia structure from microscopical outputs. Each is written in a different language, designed for a specific question and cannot deal with a high number of image acquisition at the same time. In the present paper, we developed a pipeline based on the statistics and data analysis oriented R-software to (i) fill the gaps between the different existing tools and allow a transverse integration of the outputs of these tools and (ii) to compute new variables and synthesise information in a semi-automatic way allowing for rapid computation of high number of microscopy images. Our pipeline may apply to any epithelia processed with the visualisation and analysis of 3D confocal images MorphoGraphX software and can easily be adapted to any 3D cell mesh

structure. The ability of our R pipeline to merge information of multiple spatio-temporal meshes opens multiple possibilities for the study of epithelia features or cell-tissue relations. Here we present this pipeline in the context of the shoot apical meristem of *Arabidopsis thaliana* and propose scientific perspectives about the study of cell division.

4.3 Introduction

Morphogenesis is a complex process during which multiple geometric, molecular and mechanical changes occur at subcellular, tissue and organ scale, across variable time scales. Confocal microscopy now offers the possibility to record complex morphogenetic processes such as growth of *Drosophila* wing imaginal disk (see for instance [Aegerter-Wilmsen et al. 2012](#)) or the polarization of auxin transport at the shoot apical meristem of *Arabidopsis thaliana* (see for instance [Nakayama et al. 2012](#)). Within a few hours of acquisition, large and complex spatio-temporal datasets can be produced. Human eye cannot capture and synthesize all this information at once. Moreover, a qualitative and global visual analysis would be biased, as the brain is in essence subjective. Information has to be quantified, synthetised and represented simply in an objective way. In the case of epithelia, several cells' features can be used as descriptive indices: area, growth rate, growth direction, local curvature, number of neighbours, angle at vertices, ... These measurements are by essence objective because of their precise geometrical definition. Together these features define cells' profile. They can be compared (*i.e.* angle between growth direction and main curvature axis) or combined (*i.e.* local growth heterogeneity compares growth rate of a cell to growth rate of its neighbours) to create new features of interest. Biological features such as gene expression patterns, hormone gradients and orientation and anisotropy of cytoskeletal components can also be recorded.

Different tools exist to extract characteristics of epithelia, either from single or multiangle confocal microscopy images or from multiangle electron microscopy images. Confocal images are 3D stacks, which can be projected in 2D with softwares such as Fiji ([Schindelin et al. 2012](#)) or MerryProj ([Barbier de Reuille et al. 2005](#)). Confocal images and multi-angle electron microscopy images can also be reconstructed in 3D by different means: (i) Multi-angle scanning electron microscopy images of replicas of plant tissues have been computed into Matlab to calculate growth and curvature on shoot apical meristem ([Dumais and Kwiatkowska 2002](#)). This method has notably been used to correlate microtubule behaviour with tissue shape. In this case, a confocal stack was acquired just before making the replica ([Burian et al. 2013](#)). (ii) Multi-angle confocal stacks can be processed with MARS-ALT for 3D volume reconstruction, cell segmentation and automated lineage tracking ([R. Fernandez et al. 2010](#)). (iii) Both multiple and single angle confocal stacks can be processed with MorphoGraphX for 3D surface and volume reconstruction and cell segmentation ([Barbier de Reuille et al. 2015](#)). Other softwares perform post processing of projected or reconstructed images (either data analysis or modeling based on real tissue output): for instance, FibrilTool is an ImageJ/Fiji plugin and a MorphoGraphX process, which computes orientation and anisotropy of microtubules on 2D projected stacks (in ImageJ/Fiji) and on 3D reconstructed surface (in MorphoGraphX) ([Boudaoud et al. 2014](#); [Barbier de Reuille et al. 2015](#)), and Besson Matlab script computes predictions of Besson-Dumais rule ([Besson and Dumais 2011](#)). Contrary to 3D analysis, 2D analysis allows manual quantification of cells and tissue features, such as the number of neighbours per

cell on the epithelia of the *Drosophila* wing disk (e.g. Gibson et al. 2011). However most of epithelia are not flat and results issued from top view images of a hilly surface may be biased.

All these tools have interesting features but each is written in a different language, designed for a specific question and cannot deal with a high number of image acquisition at the same time. The aim of the present paper is to present a pipeline developed on the R-software, which merges the outputs of multiple spatio-temporal meshes of epithelia in an automatic way, in order to analyse efficiently the combination of a big amount of data. Regarding the multiplicity of existing tools and programming languages, the development of our pipeline is also an opportunity to propose R-scripts allowing integration of these different tools (Fig. 4.1). The R-software was chosen for its flexibility to read multiple input formats but also for its initial aim as a statistical software, which allows to propose a set of maps and figures to describe cell and epithelia quantitative features.

The choice of the 3D reconstruction and segmentation software MorphographX is discussed first. Then, the steps of the pipeline are detailed from image processing to the development of new variables exploration. The complete set of operations and softwares used in the pipeline is presented on figure 4.1. The pipeline could be used with any set of confocal images of an epithelia processed with MorphoGraphX. Here we illustrated each step with our own dataset on the shoot apical meristem (SAM) of *Arabidopsis thaliana*. For all examples presented, results rely on images of 3 *LTi6B-GFP* (WS-4) dissected meristems acquired every 12 h during 48 h at a single angle with a confocal laser scanning microscope. This number of samples might be too limited for robust conclusions but is sufficient to present the possibilities of our pipeline and to draw future research perspectives. As an important variety of variables may be explored with such a combined set of 3D mesh data, we focused the illustrative examples around the question of cell division at cell and tissue scale.

4.4 The choice of 3D surface

In this section we discuss the choice of 3D surface, relatively to our research questions. For our case study, one aim was to compute the predictions of Besson-Dumais rule at the SAM of *Arabidopsis thaliana* (Besson and Dumais 2011). For each cell, the Matlab script written by Sébastien Besson, later referred as "Besson script" (Fig. 4.1), computes all plane possibilities and indicates if the cell selected the shortest plane or another one. The Besson script offers a graphic interface to draw manually the position of each vertices and edges of a 2D tissue. Confocal stacks of the shoot apical meristem were projected in 2D with MerryProj (Barbier de Reuille et al. 2005, Fig. 4.1) and a few images were processed manually or using the semi-automatic segmentation tool Merrysim. The first results obtained on 2D top-projection of *p35S::LTi6B-GFP* shoot apical meristems were encouraging: we could see that length of chosen plane computed by Besson script was variable, but that a majority of cells had selected the shortest division plane. We were also struck by a spatial bias: a preferential enrichment of long planes in the boundary region. This region has a saddle shape which evolves over time. As 2D projection could strongly bias length of plane in this region, we could not be sure that the observed spatial bias was linked to the real plane length. At the shoot apical meristem of *Arabidopsis thaliana*, the

4 A pipeline for the quantitative analysis of epithelia from cell to tissue scale

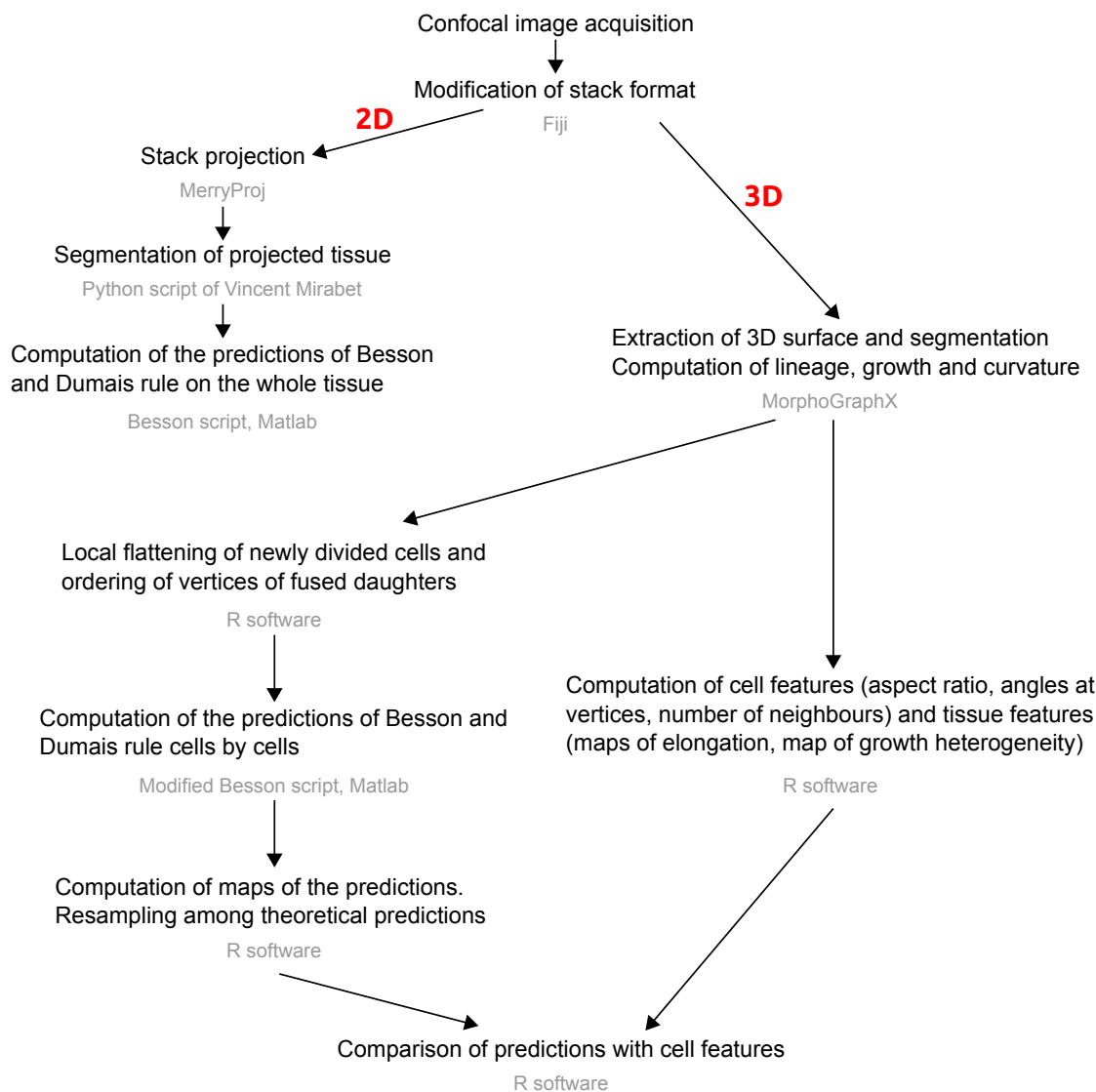


Figure 4.1: Analysis pipelines in 2D and surface 3D.

epidermis layer has a constant thickness and divisions are anticlinal (see previous chapter), ensuring that plane length and symmetry of daughters area at surface is consistent with plane area and equality of volumes in 3D. Thus, for our case study, we chose to extract cell shape directly from 3D surface and to project cell vertices locally in 2D to limit as much as possible the bias induced by the projection. As presented in the introduction, different tools exist to extract 3D characteristics of biological tissues: the Matlab scripts of Kwiatkowska and Dumais for scanning electron microscopy images of replicas (Dumais and Kwiatkowska 2002), MARS-ALT (R. Fernandez et al. 2010) or MorphographX (Barbier de Reuille et al. 2015). The two first methods require the acquisition of images at multiple (2 or 3) angles. Multiple angle acquisition is time consuming, and, in the case of confocal imaging, increases the time of image acquisition, which is not without damage for the meristem. The lightness and the quickness of the image process allowed by MorphographX to reconstruct 3D surface oriented our choice. The different topological features of the 3D mesh and other useful cell characteristics were also easily extractable from MorphographX outputs files with R.

4.5 Detailed description of the pipeline

4.5.1 Reconstruction of 3D surface and segmentation with MorphoGraphX

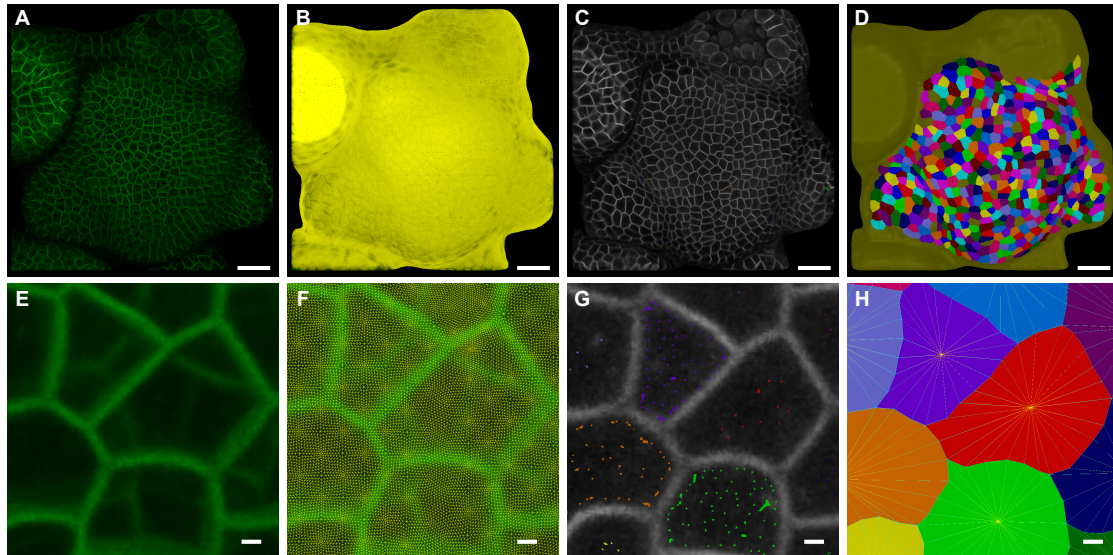


Figure 4.2: Extraction of 3D surface and cell segmentation with MorphoGraphX. (A-D) Global view of the tissue. Scale=10 μm (E-H) Close-up on a few cells. Scale=1 μm . (A) and (E) Confocal image of *LTi6B-GFP* (WS-4) dissected shoot apical meristem imported in MorphoGraphX. Plasma membranes of L2 layer are visible by transparency on (E). (B) and (F) Smoothed and subdivided mesh. (F) Mesh resolution is below membrane signal thickness. (C) and (G) *LTi6B-GFP* membrane fluorescent signal is projected on mesh. Colored seeds, visible on (G), are added manually to label each cell and to allow initiation of segmentation with a watershed algorithm. (D) and (H) Cellular segmentation of the shoot apical meristem with MorphoGraphX. Mesh is decimated (e.g. simplified) and adapted to cells' morphologies, as shown on (H): only one vertex at the center and a few on the edges. Here cell walls must be longer than 1 μm to receive an extra vertex (or more) in their middle.

The 3D pipeline (4.1) starts with the acquisition of confocal images in a proprietary format, its saving under the .tif format with Fiji (Schindelin et al. 2012) and its importation in MorphoGraphX (Fig. 4.2A and E). Methodology for 3D surface reconstruction in MorphoGraphX is extensively described in Kierzkowski et al. 2012 and Barbier de Reuille et al. 2015. Here, mesh was smoothed and subdivided until its resolution went below membrane signal thickness (around 0.5 μm , Fig. 4.2B and F). Fluorescence signal of membrane marker *LTi6B-GFP*, taken between 1 to 3 μm below the surface, was projected on this mesh, and cells were identified manually with coloured seeds (Fig. 4.2C and G). Other fluorescent signals can also be projected on the mesh. Semi-automatic segmentation was performed using watershed method, allowing delineation of cells (Fig. 4.2D and H). Lineage between two snapshots was recorded by superimposing two snapshots and identifying manually corresponding cells.

MorphoGraphX provides tools to compute area, Gaussian curvature and main curvature axis on a single snapshot, and growth rates and principal growth directions between two snapshots, when a lineage has been previously defined. It also allows to define manually regions of interest. Outputs of these computations can be displayed in MorphoGraphX

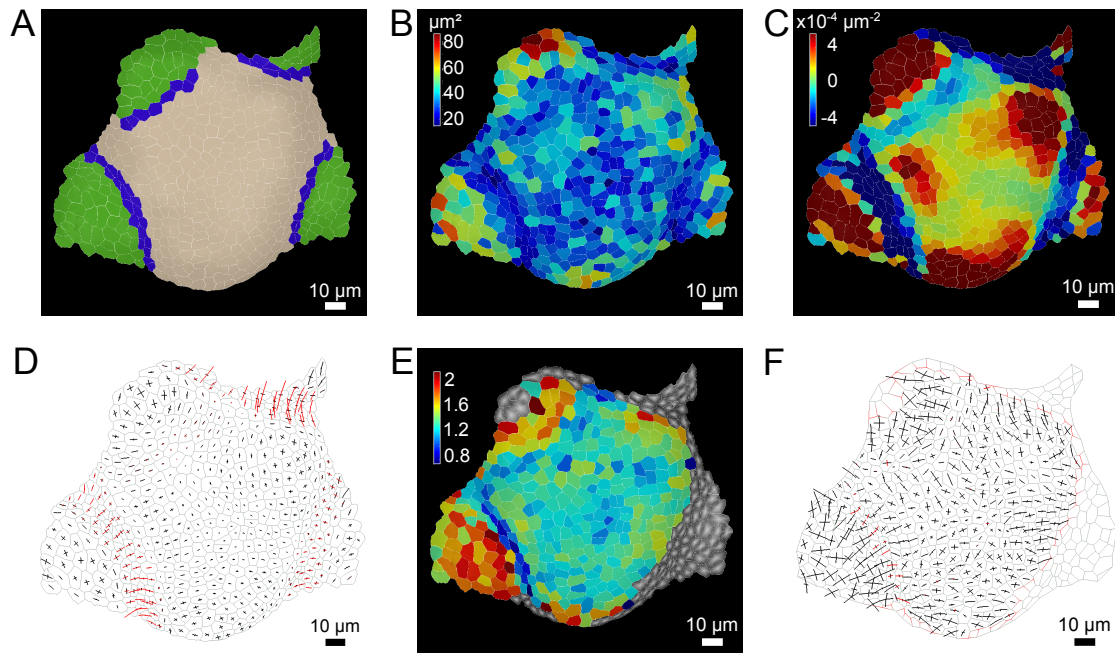


Figure 4.3: Examples of maps generated by MorphoGraphX. (A) Map of regions. Regions are defined manually: main meristem (beige), primordia (green) and boundary region (blue). (B) Map of cell surface area. (C-D) Maps of curvature. Curvature is computed locally in each cell, on an area of $20\mu\text{m}$ in diameter. (C) Map of Gaussian curvature (product of principal curvatures). (D) Map of principal curvatures. Red lines indicate a negative curvature and black lines indicate a positive curvature. (E) Map of growth rates between two snapshots. Here growth rate are projected on the oldest of the two snapshots. (F) Map of growth directions between two snapshots. Red lines indicate cell shrinkage and black lines, cell expansion.

as maps or exported as text files. For our case study, we defined manually three regions based on a visual appreciation of curvature and an expert knowledge of the SAM: the meristem, forming a dome at the center of the SAM, the outgrowing primordia surrounding the meristem, and the boundary region, which is the crease between primordia and main meristem (Fig. 4.3A). Then, we computed maps of area, main curvature axis and Gaussian curvature, growth rates and principal growth directions, to compare with our definition of regions. Such maps are relevant for any epithelia and already provide a lot of information per se. Here we see that variables are spatialised enough to distinguish, by eye, different regions on the SAM, which are more or less the ones we defined by hand. Map of cell surface areas showed that, on the particular snapshots of figure 4.3B, cell areas can vary by a factor 4, ranging from 20 to $80\mu\text{m}^2$, but the biggest cells are located in the primordia and the smallest are preferentially in the boundary region. Map of Gaussian curvature clearly showed a strong spatialisation of curvature at the shoot apical meristem: negative in the boundaries (*i.e.* curved inward), positive in the primordia (*i.e.* curved outward) and close to zero on the meristem domain (*i.e.* almost flat, Fig. 4.3C). Gaussian curvature is the product of the two main orthogonal curvatures. Map of main curvatures showed that the boundary had a saddle shape, with a positive curvature along the crease and negative curvature perpendicular to the crease (Fig. 4.3D). In the boundary region, curvature is thus anisotropic. In the primordia and main meristem, curvature is mostly isotropic. While comparing two snapshots of the same meristem, map of growth rates (Fig. 4.3E) indicated that, during 12 h, cells in outgrowing primordia grew more than other cells. Cells in boundary grew less than others or even apparently shrink, when curvature is

high, even if this surface shrinkage is not necessarily traducing a volume shrinkage. Map of growth direction (Fig. 4.3F) indicated that growth was more isotropic in young outgrowing primordia.

4.5.2 From MorphoGraphX to R: integration of several snapshots and computation of new variables

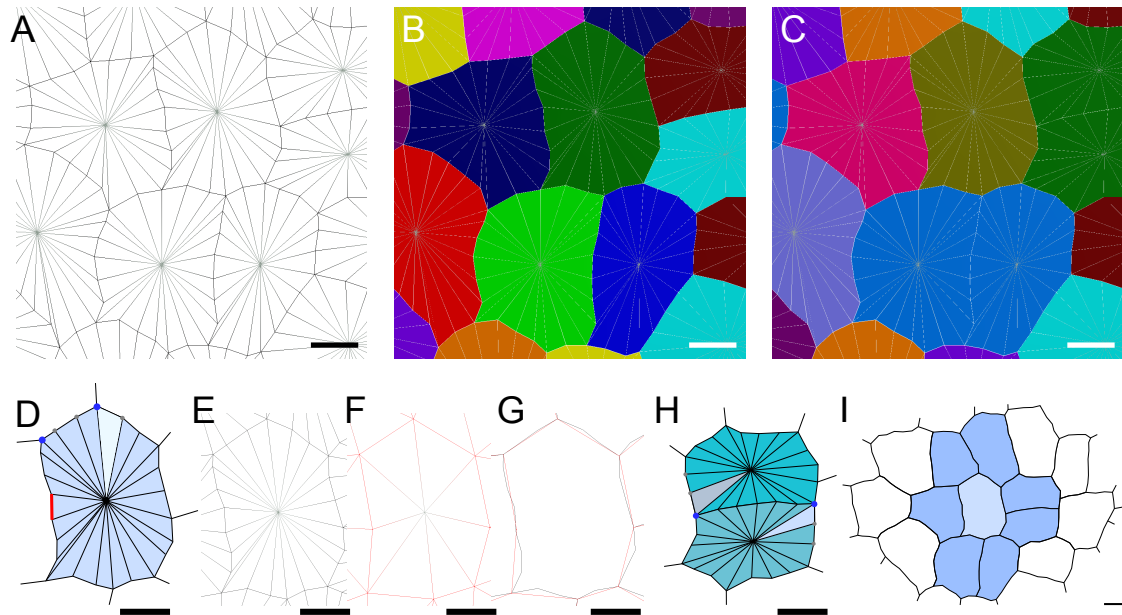


Figure 4.4: Cellular Mesh. (A) Example of cellular mesh (min wall length=1 μm). (B) Cells are identified by colored labels. (C) Cells can also be labeled according to lineage. Daughter cells share the same label. (D-G) Close-up on one cell of the mesh. (D) Definition of edge (red line), vertex (blue: main vertex at the intersection of three cells, black: central vertex and grey: secondary vertex between two cells) and triangle (pale blue). (E) Default resolution of mesh (min wall length=1 μm , e.g. vertex are added in the middle of an edge). (F) Decimated mesh (min wall length=3 μm). (G) Comparison of default (E) and decimated mesh (F). (H) Ordering vertices of two daughter cells. New wall is between the two blue vertices. (I) Definition of neighbourhood. Neighbour cells (blue) share a common wall with the central cell (grey).

MorphoGraphX can load only two snapshots at the same time and thus displays a maximum two maps in parallel, which is limiting for studies on higher number of snapshots in a longer temporal range. Moreover, informations from the different maps cannot be compared directly in MorphoGraphX. However MorphoGraphX allows the exportation of text files containing information on the mesh structure (Fig. 4.1D and H) and on the different cell features computed directly in MorphoGraphX, such as cells' area, growth rates etc. (Fig. 4.3). We gathered these outputs into R-software (Fig. 4.1) in order to compute new complementary variables and to provide new data visualisation possibilities. Mesh structure is a triangle mesh defined as follows: (i) Mesh is fitted to cells morphologies (Fig. 4.4A). Each cell is defined by two labels maximum: the label in current snapshot (called "label" in Barbier de Reuille et al. 2015, Fig. 4.4B) and the lineage label (called "parent" in Barbier de Reuille et al. 2015, Fig. 4.4C), if a previous snapshot exists. The lineage label gives the correspondance with the parent cell in previous snapshot. (ii) Cells are defined by a set of triangles. Each triangle has a unique label and is delineated by

three vertices, one being at the centre of the cell -the central vertex- and the two others on a cell edge (Fig. 4.4D). We define two types of edges vertices: main vertices are located at the intersection of three cells and secondary vertices are located between two cells. On the mesh computed with MorphoGraphX default parameters, secondary vertices are added to a wall only if its length is superior to 1 μm . The minimum size of cell wall can be adjusted by the user. An increase of this size decimates (e.g. simplifies) the mesh (Fig. 4.4E-G). (iii) Each vertex is defined by its own label, a set of x-y-z coordinates, the labels of triangles and labels of cells it belongs to.

Many features can be computed from mesh information only. For our case study, (i) We explored computed cell wall elongation to assess the effects of an ablation (see Fig. 3.1 in chapter 3), (ii) We extracted main and secondary vertices of fused daughter cells (Fig. 4.4H) and projected them in 2D thanks to a Principal Component Analysis performed on the 3D coordinates of vertices and for which we kept only the two first dimensions (see Fig. 2.7 in chapter 2). Coordinates of 2D projected vertices of fused daughter cells were then ordered, identified either as mother vertices or as new cell wall vertices and injected in Besson script. (iii) We also computed the number of neighbours (Fig. 4.5). Neighbours of a given cell share a wall with this cell (Fig. 4.4I). Connectivity between cells can easily be reconstructed by looking at cell labels associated with main and secondary vertices. The number of neighbours also defines the number of sides of a cell. The number of sides of neighbours was shown to influence the orientation of division plane in *Drosophila* epithelia (Gibson et al. 2011). This definition of neighbourhood can also be used to compute local features such as growth heterogeneity (as defined in Uyttewaal et al. 2012), circular variance of main curvature direction or main growth direction.

4.5.3 Combining and synthesizing information

The main aim of this pipeline is to gather and merge observations of multiple epithelia to be able to show results on quantified variables with a significant statistical weight. The use of R for combining information allowed the computation of different statistics on the variables collected and the production of graphical representations of merged observations. As we saw above, maps of MorphoGraphX highlighted differences between our manually defined regions on the SAM (Fig. 4.5A). Here, to give an example of application of the pipeline, we combined information from 15 snapshots (3 SAM, 5 snapshot per SAM, one snapshot taken every 12 h) and presented the contribution of four variables to the region identity: number of neighbours, cells' area, cells' growth rate and cells' growth anisotropy. Each variable was plotted in function of the region. We observed that whereas the number of neighbours was not different between regions of the shoot apical meristem (Fig. 4.5B), cells' area (Fig. 4.5C), cells' growth rate (Fig. 4.5D) and cells' growth anisotropy (Fig. 4.5E) were different in average between regions. Boundaries seemed to be characterised by smaller cells, more anisotropic shapes, slower growth rates and more anisotropic growth.

When the number of variables is large, multivariate analysis tools, such as Principal Component Analysis are useful to explore the data and isolate the variables explaining the greatest part of the variability. Here to give an example, we performed a PCA on 8 quantitative variables: cell area, cell growth rate, cell aspect ratio, growth anisotropy, sign of Gaussian curvature, curvature anisotropy (ratio of main curvatures), absolute value of Gaussian curvature, number of neighbours and we added one illustrative qualitative

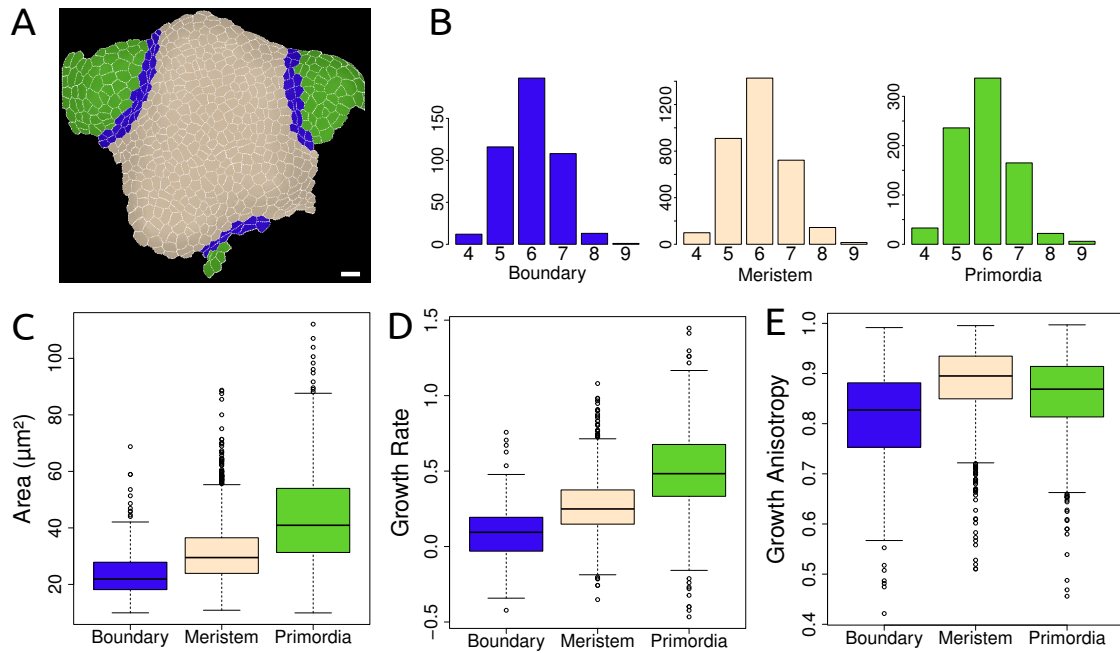


Figure 4.5: Description of regions. (A) Example of manual definition of regions. Blue: boundary. Beige: Meristem. Green: Primordia. (B) Number of neighbours. (C) Area (in μm^2). (D) Growth rate. (E) Growth anisotropy.

variable: the localisation of cells at the SAM. The first and second dimensions explained only 50% of the variability of our data, which is low. Variables were not very well projected, but curvature anisotropy and sign of Gaussian curvature appeared to be the ones contributing the most to the first dimension (Fig. 4.6). On the individual factor map, the individuals were coloured according to their region of origin and we could see that boundary individuals partially detached from meristem and primordia individuals along the first dimension, which is not very surprising as our manual definition of regions is based mainly on the visual appreciation of curvature.

4.6 Application: New perspectives for the study of cell division at the shoot apical meristem

Looking at individual meristem maps does not always allow the expert eye to distinguish patterns. In particular, when the number of events is relatively small. The combination of results from many epithelia gives a new vision of the biological phenomenon considered and produces more trustable results. Here we took advantage of the combination of information of multiple observations into figures of objective variables offered by our pipeline to address two questions about cell division: (i) How is the division regulated spatially and temporally at the boundary? (ii) What are the cell shapes characteristics correlating the fact to divide or not in the short term?

4 A pipeline for the quantitative analysis of epithelia from cell to tissue scale

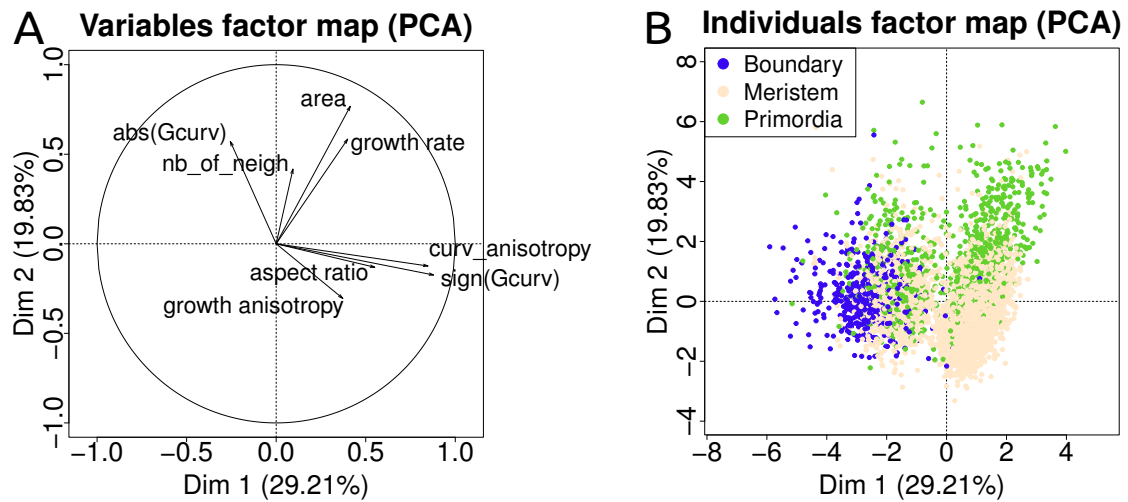


Figure 4.6: PCA on all SAM cells. 8 quantitative variables: cell area, cell growth rate, cell aspect ratio, growth anisotropy, sign of Gaussian curvature, curvature anisotropy (ratio of main curvatures), absolute value of Gaussian curvature, number of neighbours and 1 illustrative qualitative variable: localisation of cells. (A) Variable factor map, plane 1-2. (B) Individual factor map, plane 1-2. Individuals are colored according to their localisation.

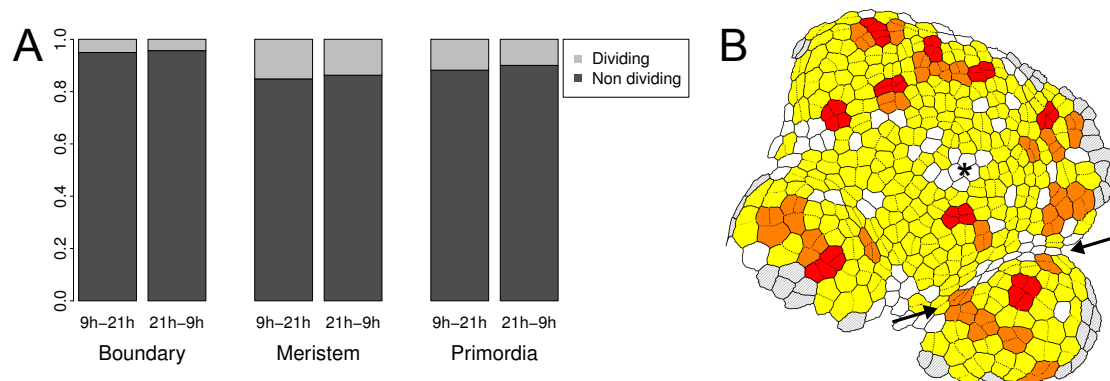


Figure 4.7: Mitotic index. (A) Mitotic index in function of region and type of interval: day (9am to 9pm) or night (9pm to 9am). (B) Heatmap of clonal origin. Cells sharing the same mother (one row of division) or grandmother (two rows of division) have the same color and are separated by dashed cell walls. Color code gives the number of descendant within the patch. White=1 (no division occurred). Yellow=2 descendants. Orange=3 descendants. Red=4 descendants. Dashed cells: missing lineage information. Black asterisk: group of non dividing cells at the center of the SAM. Black arrows: this boundary is already curved at T0.

4.6.1 Spatio-temporal regulation of the division at the SAM

We took advantage of our pipeline to combine results across time and we performed a spatial and temporal exploration of our 48h kinetic data. Here, as described above we defined manually three regions based on a visual appreciation of curvature and an expert knowledge of the SAM: the meristem, forming a dome at the centre of the SAM, the outgrowing primordia surrounding the meristem, and the boundary region, which is the crease between primordia and main meristem (Fig. 4.3A). We focused our interest on the division activity in the boundary region.

We observed a few divisions in the boundary regions: mitotic index was inferior to 10%, (Fig. 4.7A). Boundary mitotic index was lower than meristem and primordia mitotic index (Fig. 4.7A). Mitotic index was previously reported to be very low in the boundary region (Breuil-Broyer et al. 2004; Reddy et al. 2004). No striking difference of mitotic index between day and night intervals was observed (Fig. 4.7A). Contradictory informations have been published on a possible circadian control of mitotic index. Whereas Reddy et al. 2004 did not observe "any striking diurnal variations in time-lapse experiments", Shapiro et al. 2015 reported that the quantity of division occurred "in waves" over time, the period of these waves being around 10 to 12 h. In these two cases, plants were grown under continuous light, while in our study, plants were grown in long day conditions (see Material and Methods).

We computed a heatmap of clonal origin (e.g. of common ancestry) to get a more precise spatial distribution of divisions and highlight regions that were dividing the most and the least (Fig 4.7B). We could observe that divisions were well spread over the whole meristem and that cells at T0 gave only a few descendants at T48h (between 0, when no division had occurred, and 4 at most). On the presented snapshot, we observed a zone of a few cells at the centre of the SAM, where no division had occurred during the 48 h of image acquisition (black star on Fig. 4.7B). This observation is consistent with previous study which found a cell cycle rate of 36 to 72 h in the central zone of the SAM (Reddy et al. 2004). On the contrary, there were hotspots of division (2 rows of division) in outgrowing primordia but also in younger primordia and even in young boundaries. Localisation of these hotspots are consistent with cell cycle rates of 18 to 36 h in the peripheral zone and in primordia until stage 2 calculated by Reddy et al. 2004. One boundary exhibited no divisions at all in our 48 h time frame (black arrows on Fig. 4.7B). This boundary was starting to fold on the first timepoint of the kinetics, and was folded 12 h later (e.g. second timepoint of the kinetics). This result is consistent with the low mitotic index observed in boundaries by Breuil-Broyer et al. 2004 and Reddy et al. 2004. This also raise the question the existence of a folding threshold that would stop the divisions.

4.6.2 Cell shapes characteristics correlating with the absence of division in the short term

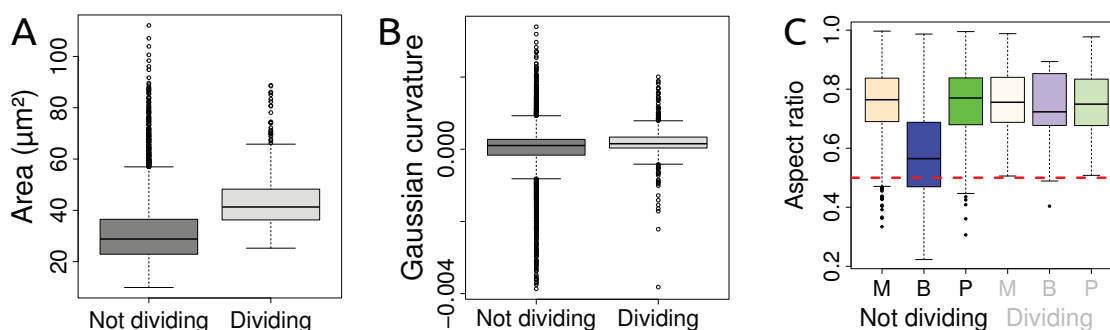


Figure 4.8: Characteristics of dividing cells. Not dividing: cells which will not divide in the next 12 h. Dividing: cells which will divide within the next 12 h. (A) Cells areas (μm^2). (B) Local Gaussian curvature (in a radius of $20\ \mu\text{m}$ around the cell). (C) Aspect ratio per regions.

We saw above that boundaries were characterized by smaller cells, negative Gaussian

curvature and smaller aspect ratio (Fig. 4.5). We also saw that mitotic index was lower in the boundary region (Fig. 4.7). However, smaller cells and small aspect ratio were also found in the other regions of the SAM. Here we address the question of the permissive range of these variables toward the possibility to divide or not, independently of the region. Here dividing (resp. not dividing) cells refers to cells that will (resp. will not) divide in the following 12 h. We compare this division status with cell area, Gaussian curvature and aspect ratio on current snapshot. In the SAM, dividing cells tended to have bigger surface area than non dividing cells (resp. median around $40 \mu\text{m}^2$ compared to $30 \mu\text{m}^2$, Fig. 4.8A). The interesting point is that the range of cell areas was smaller for dividing cell, suggesting that being too small ($<25 \mu\text{m}^2$) or too big ($>90 \mu\text{m}^2$) may interfere with the possibility to divide (Fig. 4.8A). Similarly, although the median of the Gaussian curvature was very similar between dividing and non dividing cells, the range associated with cell division seemed narrower, suggesting that a high curvature (inward or outward) could prevent cell division. Regarding aspect ratio (ratio of short over long axis of a cell), dividing cells were on average very similar to non dividing cells, except that very anisotropic cells (aspect ratio lower than 0.5, meaning that length of short axis represent less than 50% of long axis) did not divide (Fig. 4.8C). These very anisotropic cells were mainly located in the boundary region, but interestingly, the few very anisotropic cells of the meristem and primordia did not divide either, suggesting that low aspect ratio is limiting for cell division independently of the region (Fig. 4.8C). The combination of different meristems observations allowed to highlight correlations between extreme values of area, Gaussian curvature and aspect ratio and the fact to not divide in the short term (e.g. within the following 12 h). In a single meristem observation, even through time, these non-frequent values could have been treated as outliers, noise or natural variability. Here a larger sample size would be needed to definitely confirm these initial findings.

4.7 Discussion

This paper proposes a pipeline combining different tools to analyse 3D surface of an epithelia thanks to the R software. So far, MorphoGraphX has been used in surface 3D on the shoot apical meristem of *Arabidopsis thaliana* (Shapiro et al. 2015) and of tomato (Kierzkowski et al. 2012; Nakayama et al. 2012), and on *Drosophila* (Barbier de Reuille et al. 2015), and in whole 3D on Arabidopsis embryo (Bassel et al. 2014; Yoshida et al. 2014). Its use and thus, use of described R pipeline might be extended to any cohesive epithelium processed only in surface 3D. The pipeline combines outputs text files of several whole kinetics from MorphoGraphX. It can display graphically cellular mesh of the epithelia and compute new variables such as the number of neighbours. We chose to implement our pipeline on R because R is free, open-source and is a statistical software, which offers many packages to analyse datasets. Here we presented simple boxplots, maps and an example of multivariate analysis, the principal component analysis, but R offers more complex tools, notably, to analyse spatial correlations.

We did not integrate the tools developed on cytoskeleton (see Chapter 3) but they could be integrated in the pipeline to analyse the locally (e.g. at cell scale) projected fluorescent signal of microtubules or actin. MorphoGraphX allows to select the depth at which the fluorescent signal is projected and, for instance, for cortical microtubules, we can keep only the few first micrometres below the surface to get a clearer signal than on 2D projection.

Note that FibrilTool has already been implemented in MorphoGraphX (Boudaoud et al. 2014; Barbier de Reuille et al. 2015)

Finally, as revealed by the two examples seeded in this paper, and in particular the last one, the combination of information from multiple observations into figures of objective variables may lead to unintended vision. This reinforces the idea that human eye cannot capture and synthesize all this information at once. This pipeline and the different scripts developed open a Pandora box in which new perspectives of research are numerous. In a growing context where scientific results are questioned, using quantitative tools into automatized procedure helps to increase number of observations and to give statistical weight to scientific results.

4.8 Material and Methods

4.8.1 Plant material and growth conditions

The *LTi6B-GFP* (WS-4) was already described in Marc et al. 1998. Plants were sown on soil, kept at 4 °C during 48 h, then grown in short day conditions (8 h light at 19 °C ; 16 h night at 17 °C) during 4 weeks and transferred 2 to 3 weeks in long days conditions (16 h day at 21 °C ; 8 h night at 19 °C) prior to dissection. Meristems were cut from the stem, dissected the day before imaging and stuck in "Arabidopsis apex culture medium" (2.2 g l⁻¹ Duchefa Biochemie MS basal salt mixture without vitamins, 1% sucrose, 0.8% agarose, pH 5.8), as described in Hamant et al. 2014. Medium was supplemented with vitamins (1000X stock solution: 5 g Myo-inositol Sigma, 0.05 g Nicotinic acid Sigma, 0.05 g Pyridoxine hydrochloride Sigma, 0.5 g Thiamine hydrochloride Sigma and 0.1 g Glycine Sigma in 50mL water) and 200 nmol N6-Benzyladenine. Dissected meristems were kept in a phytotron in long days conditions (Sanyo, 16 h day at 20 °C ; 8 h night at 20 °C, synchronised with growth culture chambers).

4.8.2 Imaging

1024x1024 pixels stacks of dissected meristems, with Z slices every 0.5 µm, were acquired every 12 h during 48 h on a Zeiss LSM 700 upright confocal microscope, with a 40x water-dipping lens. Stacks from the kinetics were processed with a C++ script using Level Set Method (Landrein et al., submitted) to detect the 3D surface of the meristem at high resolution. Meshes of these surfaces were then created with MorphoGraphX (Kierzkowski et al. 2012; Barbier de Reuille et al. 2015). Surface geometry of processed stack was extracted with a marching cube algorithm. Initial mesh had a 5 µm resolution. Mesh was smoothed and subdivided until its resolution went below membrane signal thickness (around 0.5 µm). Fluorescence signal (1 to 3 µm below the surface) was projected on this mesh. Semi-automatic segmentation was performed using watershed method, allowing delineation of cells.

4.8.3 R pipeline

.vtk files exported from MorphoGraphX are composed of a series of matrices gathering all the informations coming from the mesh: four matrices describe the vertices of the cells ("Points") and four matrices describe the triangles formed by these vertices and one vertex at the centre of the cell ("Cells"). Only four of them are used afterwards: matrix of x, y, z coordinates of vertices, vector of labels of the vertices (equal to -1 if the vertex is on an edge and equal to the label of the cell if at the centre), matrix of triangles and matrix of labels of these triangles.

We can combine these informations to create new variables. A cell is defined by a group of triangles (see Fig. 4.4D and H). Starting from any of these triangles and choosing one vertex as starter point, one can easily order vertices of the cell. This step was parallelized with the R snow library (Tierney et al. 2013). Cell shape was projected in 2D by performing a principal component analysis on coordinates of cell vertices R package FactoMineR (Lê et al. 2008) and keeping only the two first dimensions (see also Fig. 2.7). Vertices can also be ordered on fused daughter cells (see Fig. 4.4H).

Cell shape tensor is computed as the covariance matrix:

$$M_C = \frac{1}{N_C} \begin{pmatrix} \sum_{i=1}^{N_C} (x_i - x_C)^2 & \sum_{i=1}^{N_C} (x_i - x_C)(y_i - y_C) \\ \sum_{i=1}^{N_C} (x_i - x_C)(y_i - y_C) & \sum_{i=1}^{N_C} (y_i - y_C)^2 \end{pmatrix}$$

Angles at main vertices (see Fig. 4.4D) are computed using a scalar product between the two vectors starting from this main vertex and joining one of the two next main vertex.

Each vertex can now be defined by the labels of cells it connects (3 labels if it a corner, 2 if on an edge and 1 if at the centre of a cell). When lineage has been computed, main vertex lineage can also be defined by comparing the set of three labels between two snapshots. Match between main vertices of different snapshots are useful to compute cell wall elongation, as well as cell deformation and thus project growth directions or curvature directions from one snapshot on another, using the method described in Goodall and Green 1986. Neighbours of a cell are identified by looking at the labels of the vertices of the cell which differ from cell's label. Number of sides of a cell is equal to the number of neighbours. Number of sides of cells located at the border of the mesh are ill defined, as part of their neighbours have been suppressed during image processing. A specific label is added to indicate that connectivity of these cells is partially missing and allow to suppress these cells from analysis (as done in neighbours barplots, see Fig. 4.5B).

3D visualisation is achieved with the RGL package (Adler and Murdoch 2014).

5 General discussion

5.1 Anisotropic mechanical stress fields contribute to the orientation of division plane at the epidermis of the SAM

This PhD thesis addressed the question of the contribution of mechanical stress to the orientation of division plane at the epidermis of the shoot apical meristem (SAM) of *Arabidopsis thaliana*. During the PhD, we explored the effects of different internal (regions of the SAM) and external (ablations and compressions) mechanical stress fields on cell division plane orientation. Analysis were performed with a quantitative approach: we developed an integrated pipeline to track cell division in the different regions of the SAM and quantitative tools to measure response of cytoskeleton to compression.

The effects of mechanical stress on cell division plane orientation are not very well known and cell geometry is currently proposed as the default directional cue in symmetric divisions, both in plants and animals. In animals, mechanical stress is known to influence division plane orientation in single cells (Fink et al. 2011) but its effects on whole tissues is less well characterized. In plants, contribution of mechanical stress to the orientation of division planes has been probed in different tissues but results are contradictory (Louveaux and Hamant 2013). Indeed, since the end of the XIXth century, cell geometry had been hypothesized as the main default factor influencing cell division plane positioning in both plants and animal cells. Several rules were proposed at the same period. Hertwig's rule postulated that animal cells divide at cell center of mass and perpendicular to longest axis (Hertwig 1884). Sachs's rule postulated that new division plane is perpendicular to parent wall and divide the cell evenly (Sachs 1878). Hofmeister's rule postulated that cell division planes are perpendicular to the direction of the fastest growth (Hofmeister 1863). Errera's rule originally postulated that "a cell wall, at the moment of its formation, tends to assume the form which a weightless liquid film would assume under the same conditions" (Errera 1888; Besson and Dumais 2014). This latter rule was simplified as "the cell divide along the shortest path and divide the cell evenly" during the whole XXth century. None of these rules perfectly explains divisions at the shoot apical meristem of *Arabidopsis thaliana*, but Errera's rule in its shortest path version is the closest (Shapiro et al. 2015). However, Errera's shortest path rule fails to explain why the quadrant cells of the trichomes of *Dionaea*, despite their identical shapes, can select different possible division planes. In 2011, Besson and Dumais went back to the exact definition of Errera's rule (Besson and Dumais 2014) and could reproduce the predicted planes positions with two soap bubbles confined in a quadrant shaped box. They showed that these planes were equilibrium configurations of soap bubbles interfaces and local length minima. They proposed a probabilistic version of Errera's rule in which several possible planes exist with different probabilities to be selected.

In the present work, we explored the limits of the Besson and Dumais division rule and pointed out the specificity of anisotropic tissues, where the orientation given by mechanical stress seemed to overcome the orientation given by cell geometry. The Besson-Dumais rule had been tested only in rather isotropic tissues, such as the central zone of the *Zinnia* capitulum or the thallus of the green alga *Coleochaete orbicularis*. However, most of the epithelia have a 3D shape and a non isotropic growth. We took advantage of the shoot apical meristem of the model plant *Arabidopsis thaliana*, which is a place of divisions and which has different regions with different growth dynamics and shapes, to explore the application of Besson-Dumais rule in a more general epithelial context. We showed that if Besson-Dumais rule accounts well for divisions in the meristem and primordia regions, it does not account for divisions in the boundary region, which has a saddle shape and a lower growth rate than surrounding regions. Our hypothesis was that, as none of geometrical rule account for all the divisions, directional cues other than cell geometry might be involved in the control of division plane orientation. We explored specifically mechanical stress, as this cue is non specific of a given epithelia (contrary to biochemical signals) and can be derived from shape or differential growth. To test for this hypothesis, we compared *in silico* two division rules: one based on cell geometry, a simplification of Besson-Dumais rule, and the other based on supracellular mechanical stress. Growing tissues simulated with mechanical division rule and submitted to an anisotropic supracellular stress field gave outputs which were not consistent with Besson-Dumais predictions, as observed in the boundary region of the SAM, but tissues submitted to an isotropic stress field also gave non consistent outputs. To sum up, mechanical rule better accounts for division plane orientation in the (anisotropic) boundary region, whereas Besson-Dumais rule better accounts for division plane orientation in the (isotropic) meristem and primordia regions. To comfort our observations suggesting that anisotropic mechanical stress fields gives a directional cue which overcome cell geometry, we produced local anisotropic perturbation of mechanical stress pattern with laser ablation. We performed single cell ablation on the meristem region of the SAM and quantified division planes orientation around the ablation. We observed that new planes oriented circumferentially around the ablation, which is consistent with the stress pattern predicted by our simulations and with previous published simulations (Hamant et al. 2008), and which is also consistent with the reorientation of microtubules around ablation (Hamant et al. 2008) and with division plane orientation observed around punctured cells in *Tradescantia* leaf cells (Goodbody and C. W. Lloyd 1990).

However laser ablation induced local elongation of cells neighbouring the ablation site along the radial axis. Moreover laser ablation wounds the tissue and do not allow to quantify the mechanical stress pattern produced. As we hypothesized that effect of mechanical stress was apparently in competition with the form of the cell for the choice of the division plane in an anisotropic mechanical stress field, this mechanical perturbation tools was not sufficient to disentangle and quantify both effects. We developed a new non invasive method using an indenter to apply controlled (compressive) forces on the SAM. We also developed image analysis tools to analyse quantitatively microtubule response to this mechanical perturbation. Our results confirmed previous published observations obtained on microtubule response in two microtubule marker lines, *TUA-GFP* and *GFP-MBD*, and on the *katanin* (*bot1-7*) mutant. We could notably observe that the response of the two microtubule marker lines upon compression was different: in *TUA-GFP*, microtubules depolymerized, whereas in *GFP-MBD*, microtubules were stabilised into bundles. The *katanin* mutant responded less to compression and had a more intermingled microtubule

5.2 Towards an experimental demonstration of the contribution of mechanical stress on division plane orientation

network even in control meristems. We also brought new observations of the *spr2-2* mutant under compression: its response could not be distinguished from the response of the control line. Both *katanin* and *spr2-2* were crossed with the *GFP-MBD* microtubule marker line, thus their response to mechanical stress perturbation might be different when crossed with the *TUA-GFP* microtubule marker line. However, the current system did not allow to modify drastically the pattern of isotropy and anisotropy on the SAM. Interestingly, we also observed that such system had an effect on the duration of the PPB phase, but not on the orientation of division plane.

The different results of this PhD thesis relied on a will to multiply the number of observations, which required to develop an integrative analytical pipeline. This (R-software based) pipeline was developed to allow for the study of cell divisions of any epithelia. It integrates the outputs of several scripts, in particular the 3D surface reconstruction and segmentation of the SAM made in MorphoGraphX and the outputs of the Besson script for division plane prediction. Its strength relies on the possibility to merge observations of multiple epithelia (e.g. multiple snapshots from a kinetic, but also multiple individuals with different or identical genotypes), to combine data to create new variables and maps, and to perform quantitative and statistical analysis of datasets. We used this pipeline throughout this thesis, but it also opened new perspectives of research requiring quantitative objective tools and numerous combined data. For instance, we could observe with a few variables (aspect ratio, Gaussian curvature and area) that the range of conditions allowing cell division seemed to be limited. Cells outside a specific range that were not dividing were not numerous in each snapshot, but the combination of data from different meristems allowed by this pipeline highlighted their presence. In a single meristem observation, even through time, these non-frequent values could have been treated as outliers, noise or natural variability.

5.2 Towards an experimental demonstration of the contribution of mechanical stress on division plane orientation

Our observations in the boundary region of the meristem and our results of ablation and compression experiments supported the effect of an anisotropic mechanical stress field on division plane orientation. To be able to confirm this effect and to go further, both the tools we used and the experiments we performed would need to be developed.

With the pulsed UV laser ablation of single cell, we observed a modification in division plane orientation in the cells neighbouring the ablation site at the SAM of *p35::LTI6B-GFP* meristems: new planes oriented circumferentially around ablation site, along the new predicted maximal tensile stress direction. Although we attributed this reorientation directly to the mechanical stress field imposed by the ablation, this could be due (i) to a wounding signal induced by the ablation or (ii) to the radial cell elongation following the ablation: (i) We cannot completely rule out that wounding signals could affect division plane orientation. However, arguments are accumulating in favor of the mechanical effect of ablation: it has been previously shown in the SAM of *Arabidopsis thaliana* that microtubules reorient circumferentially around an ablation (Hamant et al. 2008) and that this response is impaired in the *katanin* (*bot1-7*) mutant (Uyttewaal et al. 2012). KATANIN severs microtubules and was shown to be necessary and sufficient to the establishment

and to maintenance or reorganisation of *Arabidopsis* microtubule network architecture in response to light (Lindeboom et al. 2013), cold (Zhang et al. 2013) or mechanics (Uyttewaal et al. 2012). Microtubules also reoriented in response to non wounding mechanical perturbations such as lateral compressions and their orientation at the SAM was shown to follow supracellular mechanical stress patterns, at least in regions where mechanical stress was clearly anisotropic (Hamant et al. 2008; Burian et al. 2013). (ii) Ablation provoked a radial elongation of neighbouring cells. In this case, without a precise temporal kinetics, we cannot exclude that cell elongation appeared first and that observed bias in division planes orientation was only a consequence. However, in parallel to our work, we also performed preliminary ablation experiments on *clv3 GFP* dissected meristems, in which cell elongation was limited. In the only two cases where a PPB was observed near the ablation site, we could observe a defect of division plane orientation: position of the new cell wall deviated from PPB position and was more aligned with the predicted circumferential pattern than the PPB was. Whereas the angle varied by a dozen of degree in the first case (single ablation), it was close to 90° in the second case (cell located between two ablation sites). Unfortunately, for technical reasons, we could not obtain a higher number of observations, but these preliminary results reinforced the idea of the effect of an anisotropic mechanical stress.

To further explore the effects of ablation on preprophase band (PPB), and thus on division plane orientation, we would need a more precise laser system that could target precisely the region of interest. With a laser ablation system directly coupled to an upright confocal laser-scanning microscope having a sufficient resolution to see microtubules, we could select precisely both the size and location of the ablation site. Selecting an ablation site near a cell in which a PPB has already started to form, would help to confirm the preliminary results obtained on *clv3 GFP* dissected meristems. If the reorientation is confirmed in the isotropic region of the meristem after an ablation, this would be interesting to observe what happens in the case of an anisotropic region, like the boundary. Indeed, the supracellular alignment of microtubules along the crease may be in contradiction with a targeted stress provoked by an ablation. Another set of questions could raise around the timing of mechanosensitivity of the dividing cell to mechanical perturbation, that could also be explored with a precise laser ablation system. As we could confirm that ablation induces the reorientation of a preformed PPB, we could also probe the effect of an ablation on a neighbouring spindle or phragmoplast.

Compression is another method to test for the effect of mechanical stress on division, which is non-invasive compared to ablation. In the PhD, we did not test the effect of lateral compression on division plane orientation because the experimental set-up available in the team was reported to stop cell division (Olivier Hamant, pers. comm.). However, our observations of divisions in the boundary region of the SAM, where compression is important, suggest that cells should support such experiments, provided that a more precise set-up could be implemented. In the original experiment, NPA-treated meristem were hold between two plastic blades and compression was adjusted by displacing manually the blades (see Fig.4C-D in Hamant et al. 2008). We can make the hypothesis that compressive stress applied with this system was high because tissue deformation was large. However, at the SAM, divisions can occur under compressive stress: we observed divisions in the boundaries, at stages where the crease was already visible. Whether the source of stress is growth or whether it is curvature, in this context, we expect cells to experience a compressive stress perpendicular to the crease of the boundary. Thus we can hypothesize

that divisions should still be observed in the lateral compressive experiment if we were able to reduce the amount of applied compressive stress. Such hypothesis raises the question of the interplay between mechanical stress and the cell cycle, which is discussed in more details below. As microtubules were shown to reorient along maximal stress tension under this lateral compression (Hamant et al. 2008), we would expect division planes to orient in the same direction under smaller compressive stress permissive to cell division.

The compression method with the indenter was developed to be able to control the amount of mechanical stress applied in order to produce more reproducible results. The approach is brand new and needs adjustments but it promises good perspectives. The current set-up did not affect division plane orientation, as new cell walls observed after the end of compression oriented in the same direction as PPB observed before the compression. We propose an explanation to the absence of effect on plane orientation and propose modifications of this set-up. The mechanical stress pattern of the indented region of the meristem before indentation is isotropic at the top and anisotropic circumferentially on the flanks. The compression on the top of the SAM is expected to lower stress intensity at the centre of the indented region and increase stress intensity at the periphery. Mechanical stress pattern is still isotropic at the centre and becomes gradually more anisotropic and circumferential toward the periphery, which is not qualitatively different from the non indented situation. Indeed, the directional mechanical stress pattern is not qualitatively affected, which could explain why division plane orientation did not seem affected. To affect the direction of mechanical stress pattern without modifying too much the set-up, the idea would be to modify the shape of the tip. The actual shape is a flat end of 100 μm in diameter. The other tips proposed by Hysitron (indenter manufacturer) have a pointed end at their centre and thus are not very well adapted, because the applied load will be much higher at this contact point. The long axis of a cylindrical tip of a curvature radius smaller than curvature of the SAM would be ideal to create a directional crease. After this adjustment, one can imagine experiments with different forces applied onto the SAM to see if there is a gradual responses of the orientation of the planes along the new directional mechanical stress pattern. Beside the direct exploration of the effects of mechanical stress on division plane orientation, the indenter could be used to probe the effects of mechanical stress on cytoskeletal components (both actin and microtubules), which are widely involved in cell division and on gene expression, for instance, cell cycle genes. As the amount of applied mechanical stress is controlled and can be applied over a few minutes to a few hours (or more if we can modify the indenter software), we could probe the effects of different levels of mechanical stress across different durations.

Beside the application of exogenous mechanical stress, mechanical stress pattern could also be perturbed genetically. We could develop inducible lines expressing cell wall modifying enzymes, such as expansins or pectin methylesterase (PME), under the promoter of a gene which is expressed specifically in one domain of the SAM, such as pLEAFY in the primordia. Expansins are supposed to remodel and loosen the cell wall by disrupting bonds between glycans and cellulose microfibrils (Cosgrove 2000). The impact of PME on cell wall is still debated and could depend on the interaction with other cell wall components: depending on studies, it was shown either to increase or decrease cell wall stiffness (A. Peaucelle et al. 2011). By modifying cell wall stiffness locally, we expect to modify growth rates in one domain of the SAM. This should impact differential growth as well as curvature, and thus modify mechanical stress pattern.

5.3 Contribution of mechanical stress to cell cycle

The contribution of mechanical stress to cell cycle may require more attention, since spatial and temporal control of cell division are linked and since several of our side observations suggested (i) a slow-down and (ii) even a possible stop of the cell cycle controlled by mechanical stress intensity.

(i) Compression on the top of the SAM performed with the indenter seemed to be correlated with delays in mitosis progression: among the cells displaying a PPB before the beginning of the compression experiment, a higher proportion of compressed cells was still displaying a PPB just after the end of compression compared to control cells, and in some of the compressed cells, PPB had even disappeared without completion of mitosis. Even if the timing of PPB appearance during G2 phase and its lasting period is known to vary between species and cell types (Duroc et al. 2011) and is probably variable even among cells of the same cell type and species, here PPB seemed to persist during a longer period in compressed cells, as if cells were blocked at this stage of the cell cycle. The formation of the PPB is linked to the cell cycle: PPB forms in cycling cells at the end of G2 phase and several cell cycle proteins, such as CDKA, were shown to localize at PPB, and even could be involved in its disassembly and in the concomitant nuclear envelope breakdown (NEB) (Duroc et al. 2011). However, the cell can enter M phase in the absence of PPB, either in mutants, such as *TONNEAU*, in cell types in which karyokinesis is temporally disconnected from cytokinesis, such as cells of the endosperm, or in suspension cells (Duroc et al. 2011; Chan et al. 2005). It would be interesting to know what is the difference between the compressed cells that divided and the ones that are still displaying a PPB. For instance, to probe if this is a question of age of the PPB, we could evaluate the maturation stage of the PPB by measuring its width and/or the presence of some proteins, such as CDKA, which seem to associate preferentially with mature (e.g. narrow) PPB (Duroc et al. 2011). The apparent delay in PPB phase provoked by compression can also be compared to mechanical perturbation of mitosis progression in single animal cells: compression of single HeLa cells along spindle axis delayed the transition between metaphase and anaphase, whereas compression perpendicular to spindle axis accelerated the transition (Itabashi et al. 2012). PPB disappearance was only observed in compressed cells. These cells seem to be back in early G2 interphase, but they could also have skipped M phase, endoreduplicated and be in G1 phase of a new cell cycle. In our experiments, we cannot conclude but these observations raise several questions: could we observe PPB disappearance in a control meristem? Why do we observe PPB disappearance in some cells only and not in all compressed cells? Is there a PPB maturation checkpoint or a nuclear envelope breakdown checkpoint before which the cell only explore possible division plane configurations and after which the PPB is stabilised and cell is committed to complete M phase whatever the environmental cues? Is PPB disappearance really observed in the same proportions between the two microtubules marker lines (as interphase microtubules do not respond similarly to compression)?

(ii) Lateral compressions of NPA treated meristems were reported to stop divisions (Olivier Hamant, pers. comm.). This observation echoes several works on animal cells. Compressive exogenous stress applied on animal cells spheroids was shown to decrease cell proliferation (Montel et al. 2011). Decrease in cell proliferation is inversely correlated to the amount of stress applied (the higher the load, the less dividing cells are observed

in spheroids) (Montel et al. 2012). Cells are arrested in late G1 and inhibition of proliferation is reversible upon stress relief (Delarue et al. 2014). As stated above, at the SAM, divisions can occur under internal compressive stress as we observed divisions in the boundaries, at stages where the crease was already visible. Moreover, when the crease of the boundary was already pronounced on the first snapshot of our kinetics, no divisions were observed on following snapshots. The localisation of cycling cells as well as the gene expression pattern of some cell cycle genes has been explored in Breuil-Broyer et al. 2004. SAM were cut from the stem and cultured *in vitro* in a medium supplemented with BrdU during 12 to 15 h, a time interval long enough to catch most of the cycling cells. 5-bromo-2H-deoxyuridine (BrdU) is a non-radioactive thymidine analogue which incorporate into DNA during S phase. No BrdU could be observed in the boundaries. Then, mRNA *in situ* hybridization was performed to correlate BrdU patterns with cell cycle genes. The D-type cyclin CycD3;1, a marker of G1/S transition was absent from the boundary regions. In Breuil-Broyer et al. 2004, no indication was given on the shape of the boundaries and the absence of CycD3;1 does not prove that cells are arrested in G1, but these observations raise several questions: Can we correlate the boundary curvature with a decrease, leading to an arrest of cell division? Are the cells arrested in G1 as in compressed spheroids? Does lateral compression experiments mimics cell cycle arrest at the boundary? Is this arrest reversible? To answer these questions, we could record divisions in function of the curvature of the boundary and look for a threshold curvature in wild type and mutants impaired in the formation of boundaries. We could also work with transgenic lines expressing, as described above, cell wall modifying enzymes under the promoter of a gene which is expressed specifically in one domain of the SAM to impair SAM stress pattern and modify the shape of the boundary. A more promising experience would be to use the dual-color *Arabidopsis* marker line published by Yin et al. 2014 to visualize the different phases of the cell cycle. Until this paper, only lines expressing G2/M specific markers, such as Cyclin B1, were available. This new line marks both S to G2 and G2 to M cell cycle stages with two different fluorescent markers (respectively, Red Fluorescent Protein and Green Fluorescent Protein). The G1 phase is marked by the absence of fluorescence. If cells are arrested in G1 when boundary gets too curvy, we would expect cells to express successively RFP and GFP in young (not too curved) boundaries and then to stop expressing fluorescent markers in older (more curved) boundaries. We would expect to observe also a decrease of fluorescence in the cells of NPA treated meristem submitted to a lateral compression. If cell cycle arrest is dependent on mechanical stress level, we would expect that, when the shape of the boundary is impaired (e.g. the boundary is flatter), or with more precise set-up of lateral compression allowing to apply smaller loads, cells are still cycling. If cell cycle arrest is reversible, cell should recover from a release of lateral compression and cycle again. Otherwise, we can make the hypothesis that cells are not arrested at one phase of the cell cycle, but that they exited the cell cycle.

5.4 About the complex interplay between cytoskeleton and mechanical stress

In parallel to the experimental demonstration of the effect of mechanical stress on cell division plane orientation and cell cycle, there is a need to explore further the molecular mechanisms behind these processes. Literature on plane orientation is quite abundant and some molecular mechanisms have already been proposed. In the following, we will (i)

review different molecular actors involved in the formation of the preprophase band (PPB), (ii) discuss the hypothesis of a cortical microtubule network solely guided by cytoplasmic microtubules, and (iii) propose a more bilateral link between cortical and cytoplasmic microtubules. Concerning cell cycle, literature is less abundant and we can only draw a parallel with the few observations made in animals

The molecular control of division plane orientation is different between animal and plant cells and here, as lot of molecular actors are already known, we will focus only on plant cells. The molecular actors involved the late steps of division plane positioning in plants are well known but we lack knowledge on the first steps. At the end of G2 phase, cortical microtubules reorganise to form a circular cortical band around the nucleus called the preprophase band (PPB). PPB orientation correlates with the orientation of cell wall at the end of the division. A few molecular actors involved in memorization of PPB orientation are known. However, we lack knowledge on how PPB is positioned first and here we propose to discuss how mechanical stress could be involved in this early step, with a focus on microtubules.

(i) Despite the great number of molecular actors involved in PPB formation, none has been proven to instruct PPB orientation and further research need to be conducted on the localisation of these actors during G2, before and after the apparition of the PPB. TON1 and TON2 localise at PPB, but they also localise on microtubules during interphase. Moreover, they were shown to be involved in the organisation of microtubule networks in interphase. TON1 was shown to interact with centrin, which is homologous to a human centrosomal protein, and is itself homologous to FOP, another human centrosomal protein (Azimzadeh et al. 2008; Spinner et al. 2013). TON1 was also shown to interact with TRM1 (TON1 RECRUITING MOTIF1) (Drevensek et al. 2012). TRM1 belongs to the TRM superfamily. Proteins of the TRM superfamily share common motifs, which are also found in the sequence of the CAP350 mammal protein, which is also located at centrosomes (Drevensek et al. 2012). The homolog of TON2 in *C. elegans*, RSA-1, also localises to the centrosome (Duroc et al. 2011). Centrosomes are a proteinaceous structure containing γ -TURC, other proteins and a pair of centrioles, which are small microtubule based structures (Alberts et al. 2014). In interphase, a unique centrosome organize microtubules radially, trapping minus end near the nucleus. Centrioles are duplicated during S phase and, during prophase, centrosome splits into two and migrates at each pole of the nucleus, each with a pair of centrioles. The two daughter centrosomes organize microtubules at spindle poles and thus, as equator of the spindle determine cleavage site in animal cells, are involved in division plane position. We lack information on the localisation of TON1 and TON2 when PPB starts to form and thus, we don't know if these proteins, which are spread along microtubules in interphase, relocalise prior to PPB formation and constrain its formation at a certain location or if these proteins only enhance the formation of the PPB without instructing its localisation. Apart from TON1 and TON2, other proteins are involved in microtubules dynamics during PPB formation. PPB are likely to be formed from remodelling of interphase microtubule network, as PPB still form in cells where proteins synthesis (and in particular tubulin synthesis) is blocked (Duroc et al. 2011). Microtubules are more dynamic and less stable during the formation of PPB (Dhonukshe and Gadella 2003; Vos et al. 2004). The severing protein KATANIN was shown to be involved in PPB organisation and could also be involved in PPB disassembly: in the *katanin* mutant PPB are populated with microtubules with various orientation and persist until prometaphase (Panteris et al. 2011). EB1, CLASP or MOR1 were also

proposed to regulate microtubule dynamics during PPB formation, but their role is less clear (Dhonukshe and Gadella 2003; Vos et al. 2004; Duroc et al. 2011). Microtubule dynamic instability within the PPB seems to be lower than outside the PPB. Vos et al. 2004 describes microtubules selective stabilisation at PPB site as a "search-and-capture" mechanism (microtubules explore dynamically cellular space until they get trapped in the forming PPB). Proteins of the MAP65 family, such as MAP65-1 could be involved in stabilisation of microtubules at PPB (Duroc et al. 2011). MAP65-1 was shown to colocalise with PPB (Chang et al. 2005), to bundle microtubules, to increase rescue events (aborted depolymerization of microtubules) and to decrease frequency of microtubules catastrophe (sudden microtubule depolymerization) (Stoppin-Mellet et al. 2013). However, MAP65-1 also colocalises with interphase microtubules and phragmoplast (Chang et al. 2005). Here also, we don't know if stabilising factors, that can be found also in interphase, relocalise prior to PPB formation and constrain its formation at a certain location or if these proteins only enhance formation of PPB without instructing its localisation.

(ii) Besson-Dumais rule makes the hypothesis that PPB positioning is mainly driven by microtubules linking the nucleus to the cortex and not by cortical microtubules. Equations of the Besson-Dumais rules are derived from two experimental observations: microtubules are highly dynamic during PPB formation and PPB formation can occur without *de novo* synthesis of tubulin. As microtubules are dynamics, many configurations will be explored and distribution of microtubules connecting the nucleus to the cortex will tend to be uniform, but, as the pool of tubulin is limited, the edges that are the closer from the nucleus will be connected by more microtubules (the closest edges flanking the shortest axis). Non probable configurations may be favoured by lower dynamic instability and the inability to find a shortest configuration. However, a lower dynamic instability cannot explain alone the orientation of PPB observed in the boundary region of the shoot apical meristem of *Arabidopsis thaliana*, which correlates with the supracellular alignment of interphasic cortical microtubules (Hamant et al. 2008). In this region, we showed that Besson-Dumais rule failed to explain division plane orientation and that a mechanical division rule was more likely to account for observed orientations.

In both vacuolated and non vacuolated cells, microtubules connect the nucleus to the cell cortex during PPB formation. In vacuolated cells, these microtubules are embedded in tensed cytoplasmic strands, whereas in non vacuolated cells (perinuclear) microtubules surround the nucleus and radiate in the cytoplasm toward the cell cortex. Tension within cytoplasmic strands of vacuolated cells could reinforce the fact to favour short path between the nucleus and cell edges. Nothing is known about tension in perinuclear microtubules of non vacuolated cells. Cytoplasmic strands are a characteristic feature of vacuolated cells: in this cell, vacuole occupies the major part of the cell volume and cytoplasm is confined in small strands linking the nucleus to the cell cortex. These strands are populated with microtubules and actin. Laser ablation of one of these strands was shown to provoke the relocation of the nucleus suggesting that these strands are under tension (Goodbody et al. 1991). In vacuolated cells, division is preceded by a relocation of the nucleus at the cell center of mass. Cytoplasmic strands then coalesce into a plane named the phragmosome, which contains the nucleus at its centre and marks the future site of division. Nucleus relocation prior to mitosis was proposed to be due to an equilibrium of tensile forces applied by each cytoplasmic strand on the nucleus Flanders et al. 1990; Goodbody et al. 1991. The tension within cytoplasmic strands is supposed to be proportional to the length of the strands. Flanders et al. 1990 modelled this process with two different set-ups: springs

(modelling cytoplasmic strands) connected on one end to the edges of a rigid frame and on the other end by a central metallic element (modelling the nucleus), and soap bubbles packed in a rigid frame (one soap bubble at the centre model the position of the nucleus and the interfaces between soap bubbles, experiencing tension surface, model the cytoplasmic strands). In these set-ups, both springs and soap bubbles interfaces are free to move along the rigid frame and tend to minimize tension, e.g. their length (Flanders et al. 1990; Goodbody et al. 1991; Clive W. Lloyd 1991). Formation and positioning of the phragmosome was proposed to follow the same tension minimisation rules: strands ultimately coalesce along one of the shortest path. It is worth noting that springs and soap bubbles analogy assume that all cytoplasmic strands have identical mechanical properties (e.g. all springs are the same, with the same stiffness constant). Indeed, microtubules bending stiffness was shown to be much smaller *in vitro*, where microtubules are isolated, than *in vivo*, where microtubules are embedded with other cytoskeletal components (Brangwynne et al. 2006). As composition of each cytoplasmic strands in microtubules and actin may vary and as other proteins involved in cytoskeletal dynamic may be associated with these strands (for instance proteins stabilising cytoskeletal bundles), properties of each strands are likely to differ. In non vacuolated cells, such as SAM cells, the nucleus is already centered in interphase and occupies the major part of the cell. During PPB formation, perinuclear microtubules can be observed surrounding the nucleus and radiating in the cytoplasm toward cell cortex. Perinuclear microtubules have been described in root tip cells of *Arabidopsis* (Spinner et al. 2013), as well as in non-vacuolated *Pisum* meristem cells (Bakhuizen et al. 1985). In our confocal images, perinuclear microtubules were visible when PPB was forming, but we could not be sure that they were not present in interphase, since the resolution of our images was limited. Perinuclear microtubules could be nucleated close to nucleus surface, as fluorescently tagged γ tubulin-complex protein 2 (GCP2), which participate to microtubule nucleation complexes, were found near nucleus of *Arabidopsis* root hairs (Ambrose and Wasteneys 2014).

(iii) On the basis of our observations, we propose to look at the PPB as the emerging consequence of a physical interplay between cortical and cytoplasmic microtubules (e.g. microtubules within cytoplasmic strands or perinuclear microtubules). In both vacuolated and non vacuolated cells, the physical interaction between cortical microtubules and cytoplasmic microtubules can be supposed from the close vicinity of the two networks, but has not been fully explored experimentally. In regions where nucleus was close to plasma membrane, electron microscopy images of root cells of the male fern *Dryopteris filix-mas* suggested that these microtubules could bend when reaching the cortex and be intermingled with PPB microtubules (Burgess 1970). Based on these observations, but without further experimental proofs, microtubules populating cytoplasmic strands were also proposed to bend and interact with PPB microtubules (Bakhuizen et al. 1985). Several microscopical observations attested of the close vicinity of the two microtubules networks at the cortex (Flanders et al. 1990). However, bending of perinuclear microtubules, as well as the physical interaction between cytoplasmic and cortical microtubules and the molecular actors involved in this interaction has not been re-examined since. As Besson-Dumais rule explains PPB positioning by the positioning of cytoplasmic microtubules in function of cell geometry, it supposes implicitly that both cytoplasmic and cortical microtubule networks are interacting and that cytoplasmic microtubules govern the reorganisation of cortical microtubules into the PPB. The same hypothesis was made by Flanders et al. 1990 and supported by experimental observations. Flanders et al. 1990 said that "the cortical band and transvacuolar strands form a continuum such that formation

of a tight PPB and formation of the planar, transvacuolar phragmosome are one and the same process: as the band condenses, the nucleus-radiating microtubular strands gather in the phragmosomal plane." Later on, [Flanders et al. 1990](#) added that "According to our observations on elongated cells, the "bunching up" of the cortical PPB and the realignment of the radial MT strands into the phragmosome, occur concomitantly. Further work is needed to decide whether narrowing of the band draws the radiating, nucleus-associated MTs into the phragmosome or whether it is realignment of the radiating MTs that helps tighten the PPB. However, several observations already indicate that positioning of the PPB can be more readily understood in terms of the underlying MTs that radiate from the nucleus than by bunching up of the PPB." This affirmation is supported by the observation of X shaped phragmosomes and associated PPB: during preprophase, microtubules condense preferentially along one of the limbs or between the tips of the X, forming a double PPB. PPB position thus directly reflects the junction of strands with the cortex. We agree with the idea of a physical interaction between cytoplasmic and cortical microtubules. However, our observations suggest that cortical microtubules can impose PPB positioning, as they conserve their interphasic alignment in the boundary region of the SAM when condensing into the PPB. We propose that PPB would be stabilised both by the interaction of cortical microtubules with bundling proteins such as MAP65 and by the interaction with cortical microtubules. In turn, perinuclear microtubules would also be constrained and stabilised progressively by the narrowing PPB. Such mechanism could add robustness to division plane choice and allow the cell to make a trade off between the polarity given by the cell geometry and other polarized external cues, such as mechanical stress. Interestingly, in the *ton1* and *ton2* mutants, which both lack PPB, perinuclear microtubules are still present around the nucleus and this microtubule network seems even more dense than in the wild type ([Spinner et al. 2013](#)). We propose that the TON-NEAU proteins, necessary to the formation of the PPB, could either be involved only in cortical microtubule network geometry (and their absence would impair so dramatically microtubule network that it would be unable to condense and form a PPB) or be the direct molecular linkers between perinuclear and cytoplasmic microtubules (thus, in the *ton* mutants, division plane positioning would rely only on cell geometry and be more noisy).

Concerning the potential effect of mechanical stress on cell cycle, the lack of studies in animals and in plants, authorize only cautious hypothesis on the mechanotransduction pathway. Since the first discoveries of Paul Nurse in yeast ([Nurse 2002](#)), a lot of molecular actors involved in the cell cycle were discovered in different organisms. Progression through the cell cycle is dictated by the interaction of cyclin-dependent kinases (Cdks) with cyclins. Concentration of Cdks is constant over time, whereas concentrations and activity of cyclins oscillate over time and determine the cell cycle stage ([Alberts et al. 2014](#)). These oscillations are at the basis of cell cycle in all eukaryotes. In animals, exogenous stress was shown to induce an overexpression of the $p27^{Kip1}$ protein, which is usually down-regulated to pass from G1 to S phase ([Delarue et al. 2014](#)). Plant homologs of the $p27^{Kip1}$ protein are known, but their expression has not been checked in response to application of mechanical stress. The transition between G1 and S phase (also called restriction point) is controlled by the phosphorylation state of the Retinoblastoma protein pRb. pRb is phosphorylated by cyclin-dependent kinases (cyclin E and cyclin D1). Phosphorylation of pRb can be inhibited by cyclin-dependent kinases inhibitors such as $p27^{Kip1}$. In compressed spheroids, the $p27^{Kip1}$ protein is overexpressed, but levels of cyclin D1 and E are not affected. The molecular pathway involved in overexpression of

$p27^{Kip1}$ is only hypothetical. Transcription of $p27^{Kip1}$ may be induced by a molecular cascade activated by an increase of intracellular calcium concentration. Calcium influx could be provoked by the opening of calcium mechano-sensitive channels at plasma membrane (strained by the compression). Tensile stress was also shown to arrest single cells in G1 and to be accompanied by an overexpression of the $p27^{Kip1}$ protein. Tension was applied by restricting cell shape and size of single cells, which were cultured on small squared microfabricated pattern coated with adhesive proteins. In plants, the Kip-related proteins (KRPs) share a small conserved domain with the mammal Kip family and seven genes encode the KRPs in *Arabidopsis* (Scofield et al. 2014). KRPs bind to cyclin-dependent kinases and to cyclin/cyclin-dependent kinase complexes and inhibit kinase activity (De Veylder et al. 2001; Nakai et al. 2006). KRP2 overexpression was shown to increase cell cycle duration without affecting the timing of cell differentiation (De Veylder et al. 2001). However, mRNA in situ hybridisation at the SAM revealed an absence of KRP2 and 3 in the boundaries (Breuil-Broyer et al. 2004). Further studies need to be conducted on the expression of cell cycle genes upon the application of exogenous mechanical stress.

5.5 Conclusion

Mechanical stress impacts division plane positioning and timing of division. Our different experiments contributed to observe these phenomena in boundary regions of the shoot apical meristem, but also under external mechanical stress like ablation or compression. Further experiments would be needed to better quantify the conditions and the potential gradual response of the meristem, but trying to identify the molecular mechanisms underlying these processes will remain the biggest challenge. Besides, it is worth noting that both spatial and temporal division choices have an important impact on tissue morphology and may notably create mechanical feedbacks. Indeed, in simulations of growing 2D tissues with different division rules based on the combination of two criteria: the position of division centre (random or at cell centre of mass) and the direction of division (random, along shortest path, perpendicular to the direction of previous cell division or perpendicular to cell elongation), Sahlin and Jönsson 2010 created very different tissue topologies and geometries. Similarly, our simulations tested two division rules (shortest path or following maximal tension) in isotropic or anisotropic stress fields. Whereas both division rules produced similar distribution of cell aspect ratio in an isotropic field, mechanical rule produced more anisotropic cell shapes in an anisotropic mechanical stress field. Hence, we note that the local integration of supracellular cues can conduct to a regionalisation of tissue topology and could give more possibilities for the tissue to achieve complex morphogenetic processes. The re-exploration of now well established knowledge about cell division throughout its sensitivity to and its consequences on mechanical stress in a morphogenetic context offers new exciting perspectives of research.

Bibliography

- Adler, D. and Murdoch, D. (2014). *rgl: 3D visualization device system (OpenGL)*.
- Aegerter-Wilmsen, T., Heimlicher, M. B., Smith, A. C., Reuille, P. B. de, Smith, R. S., Aegerter, C. M., and Basler, K. (2012). “Integrating force-sensing and signaling pathways in a model for the regulation of wing imaginal disc size”. *Development* 139.17, pp. 3221–3231.
- Aida, Mitsuhiro and Tasaka, Masao (2006). “Genetic control of shoot organ boundaries”. *Current Opinion in Plant Biology* 9.1, pp. 72–77.
- Alberts, B., Johnson, A., Lewis, J., Morgan, D., Raff, M., Roberts, K., and Walter, P. (2014). *Molecular Biology of the Cell*. 6th. Garland Science.
- Ambrose, C. and Wasteneys, G. O. (2014). “Microtubule Initiation from the Nuclear Surface Controls Cortical Microtubule Growth Polarity and Orientation in *Arabidopsis thaliana*”. en. *Plant and Cell Physiology* 55.9, pp. 1636–1645.
- Azimzadeh, J., Nacry, P., Christodoulidou, A., Drevensek, S., Camilleri, C., Amiour, N., Parcy, F., Pastuglia, M., and Bouchez, D. (2008). “*Arabidopsis* TONNEAU1 proteins are essential for preprophase band formation and interact with centrin”. *The Plant Cell Online* 20.8, pp. 2146–2159.
- Bakhuizen, R., Van Spronsen, P. C., Sluiman-den Hertog, F. A. J., Venverloo, C. J., and Goosen-de Roo, L. (1985). “Nuclear envelope radiating microtubules in plant cells during interphase mitosis transition”. *Protoplasma* 128.1, pp. 43–51.
- Barbier de Reuille, P., Bohn-Courseau, I., Godin, C., and Traas, J. (2005). “A protocol to analyse cellular dynamics during plant development”. *The Plant Journal* 44.6, pp. 1045–1053.
- Barbier de Reuille, P., Routier-Kierzkowska, A.-L., Kierzkowski, D., Bassel, G. W., Schüpbach, T., Tauriello, G., Bajpai, N., Strauss, S., Weber, A., Kiss, A., Burian, A., Hofhuis, H., Sapala, A., Lipowczan, M., Heimlicher, M. B., Robinson, S., Bayer, E. M., Basler, K., Koumoutsakos, P., Roeder, A. H. K., Aegerter-Wilmsen, T., Nakayama, N., Tsiantis, M., Hay, A., Kwiatkowska, D., Xenarios, I., Kuhlemeier, C., and Smith, R. S. (2015). “MorphoGraphX: A platform for quantifying morphogenesis in 4D”. *eLife* 4.
- Bassel, G. W., Stamm, P., Mosca, G., Barbier de Reuille, P., Gibbs, D. J., Winter, R., Janka, A., Holdsworth, M. J., and Smith, R. S. (2014). “Mechanical constraints imposed by 3D cellular geometry and arrangement modulate growth patterns in the *Arabidopsis* embryo”. en. *Proceedings of the National Academy of Sciences* 111.23, pp. 8685–8690.
- Beauzamy, L., Nakayama, N., and Boudaoud, A. (2014). “Flowers under pressure: ins and outs of turgor regulation in development”. en. *Annals of Botany* 114.7, pp. 1517–1533.
- Besnard, F., Vernoux, T., and Hamant, O. (2011). “Organogenesis from stem cells in planta: multiple feedback loops integrating molecular and mechanical signals”. *Cellular and Molecular Life Sciences* 68.17, pp. 2885–2906.

- Besson, S. and Dumais, J. (2011). “Universal rule for the symmetric division of plant cells”. *PNAS* 108.15, pp. 6294–6299.
- (2014). “Stochasticity in the symmetric division of plant cells: when the exceptions are the rule”. *Frontiers in Plant Science* 5.
- Bichet, A., Desnos, T., Turner, S., Grandjean, O., and Höfte, H. (2001). “BOTERO1 is required for normal orientation of cortical microtubules and anisotropic cell expansion in Arabidopsis”. *The Plant Journal* 25.2, pp. 137–148.
- Blanchoin, L., Boujemaâ-Paterski, R., Sykes, C., and Plastino, J. (2014). “Actin Dynamics, Architecture, and Mechanics in Cell Motility”. en. *Physiological Reviews* 94.1, pp. 235–263.
- Boudaoud, A. (2010). “An introduction to the mechanics of morphogenesis for plant biologists”. *Trends in plant science* 15.6, pp. 353–360.
- Boudaoud, A., Burian, A., Borowska-Wykręć, D., Uyttewaal, M., Wrzalik, R., Kwiatkowska, D., and Hamant, O. (2014). “FibrilTool, an ImageJ plug-in to quantify fibrillar structures in raw microscopy images”. *Nature Protocols* 9.2, pp. 457–463.
- Bouquin, T., Mattsson, O., Naested, H., Foster, R., and Mundy, J. (2003). “The Arabidopsis *luel* mutant defines a katanin p60 ortholog involved in hormonal control of microtubule orientation during cell growth”. *Journal of Cell Science* 116.5, pp. 791–801.
- Braam, J. (2004). “In touch: plant responses to mechanical stimuli”. *New Phytologist* 165.2, pp. 373–389.
- Brangwynne, C. P., MacKintosh, F. C., Kumar, S., Geisse, N. A., Talbot, J., Mahadevan, L., Parker, K. K., Ingber, D. E., and Weitz, D. A. (2006). “Microtubules can bear enhanced compressive loads in living cells because of lateral reinforcement”. *The Journal of cell biology* 173.5, pp. 733–741.
- Braybrook, Siobhan A., Hofte, Herman, and Peaucelle, Alexis (2012). “Probing the mechanical contributions of the pectin matrix: Insights for cell growth”. en. *Plant Signaling & Behavior* 7.8, pp. 1037–1041.
- Braybrook, Siobhan A. and Peaucelle, Alexis (2013). “Mechano-Chemical Aspects of Organ Formation in Arabidopsis thaliana: The Relationship between Auxin and Pectin”. en. *PLoS ONE* 8.3. Ed. by Markus Grebe.
- Breuil-Broyer, S., Morel, P., De Almeida-Engler, J., Coustham, V., Negrutiu, I., and Trehin, C. (2004). “High-resolution boundary analysis during Arabidopsis thaliana flower development”. *The Plant Journal* 38.1, pp. 182–192.
- Brunoud, G., Wells, D. M., Oliva, M., Larrieu, A., Mirabet, V., Burrow, A. H., Beeckman, T., Kepinski, S., Traas, J., Bennett, M. J., and Vernoux, Teva (2012). “A novel sensor to map auxin response and distribution at high spatio-temporal resolution”. *Nature* 482.7383, pp. 103–106.
- Burgess, J. (1970). “Interactions between microtubules and the nuclear envelope during mitosis in a fern”. *Protoplasma* 71.1-2, pp. 77–89.
- Burian, A., Ludynia, M., Uyttewaal, M., Traas, J., Boudaoud, A., Hamant, O., and Kwiatkowska, D. (2013). “A correlative microscopy approach relates microtubule behavior, local organ geometry, and cell growth at the Arabidopsis shoot apical meristem”. *Journal of Experimental Botany*.
- Burk, D. H., Liu, B., Zhong, R., Morrison, W. H., and Ye, Z.-H. (2001). “A Katanin-like protein regulates normal cell wall Biosynthesis and cell elongation”. *The Plant Cell* 13.4, pp. 807–827.

- Burk, D. H. and Zheng-Hua, Ye** (2002). “Alteration of Oriented Deposition of Cellulose Microfibrils by Mutation of a Katanin-Like Microtubule-Severing Protein”. *The Plant Cell* 14.9, pp. 2145–2160.
- Burton, Kévin and Taylor, D. Lansing** (1997). “Traction forces of cytokinesis measured with optically modified elastic substrata”. *Nature* 385, pp. 450–454.
- Buschmann, H., Fabri, C. O., Hauptmann, M., Hutzler, P., Laux, T., Lloyd, C. W., and Schäffner, A. R.** (2004). “Helical growth of the Arabidopsis mutant *torifolia1* reveals a plant-specific microtubule-associated protein”. *Current Biology* 14.16, pp. 1515–1521.
- Carles, C. C. and Fletcher, J. C.** (2003). “Shoot apical meristem maintenance: the art of a dynamic balance”. *Trends in plant science* 8.8, pp. 394–401.
- Castanon, I. and González-Gaitán, M.** (2011). “Oriented cell division in vertebrate embryogenesis”. *Current opinion in cell biology*.
- Chan, J., Calder, G., Fox, S., and Lloyd, C.** (2005). “Localization of the microtubule end binding protein EBI reveals alternative pathways of spindle development in Arabidopsis suspension cells”. *The Plant Cell* 17.6, pp. 1737–1748.
- Chang, H.-Y., Smertenko, A. P., Igarashi, H., Dixon, D. P., and Hussey, P. J.** (2005). “Dynamic interaction of NtMAP65-1a with microtubules in vivo”. en. *Journal of Cell Science* 118.14, pp. 3195–3201.
- Cheng, G., Tse, J., Jain, R. K., and Munn, L. L.** (2009). “Micro-Environmental Mechanical Stress Controls Tumor Spheroid Size and Morphology by Suppressing Proliferation and Inducing Apoptosis in Cancer Cells”. *PLoS ONE* 4.2. Ed. by M. V. Blagosklonny.
- Chesarone, M. A. and Goode, B. L.** (2009). “Actin nucleation and elongation factors: mechanisms and interplay”. en. *Current Opinion in Cell Biology* 21.1, pp. 28–37.
- Chrétien, D., Metoz, F., Verde, F., Karsenti, E., and Wade, R. H.** (1992). “Lattice defects in microtubules: protofilament numbers vary within individual microtubules”. *The Journal of cell biology* 117.5, pp. 1031–1040.
- Ciska, M., Masuda, K., and Moreno Diaz de la Espina, S.** (2013). “Lamin-like analogues in plants: the characterization of NMCP1 in *Allium cepa*”. en. *Journal of Experimental Botany* 64.6, pp. 1553–1564.
- Cosgrove, D. J.** (2000). “Loosening of plant cell walls by expansins”. *Nature* 407.6802, pp. 321–326.
- (2005). “Growth of the plant cell wall”. *Nature Reviews Molecular Cell Biology* 6.11, pp. 850–861.
- Courtemanche, N., Lee, J. Y., Pollard, T. D., and Greene, E. C.** (2013). “Tension modulates actin filament polymerization mediated by formin and profilin”. *Proceedings of the National Academy of Sciences* 110.24, pp. 9752–9757.
- Coutand, C., Martin, L., Leblanc-Fournier, N., Decourteix, M., Julien, J. L., and Moulia, B.** (2009). “Strain mechanosensing quantitatively controls diameter growth and PtaZFP2 gene expression in poplar”. *Plant physiology* 151.1, pp. 223–232.
- Davis, L. J., Odde, D. J., Block, S. M., and Gross, S. P.** (2002). “The importance of lattice defects in katanin-mediated microtubule severing in vitro”. *Biophysical journal* 82.6, pp. 2916–2927.
- De Veylder, L., Beeckman, T., Beemster, G. T. S., Krols, L., Terras, F., Landrieu, I., Van Der Schueren, E., Maes, S., Naudts, M., and Inzé, D.** (2001). “Functional analysis of cyclin-dependent kinase inhibitors of Arabidopsis”. *The Plant Cell* 13.7, pp. 1653–1668.

- Delarue, M., Montel, F., Vignjevic, D., Prost, J., Joanny, J.-F., and Cappello, G. (2014). “Compressive Stress Inhibits Proliferation in Tumor Spheroids through a Volume Limitation”. en. *Biophysical Journal* 107.8, pp. 1821–1828.
- Desprat, N., Supatto, W., Pouille, P. A., Beaurepaire, E., and Farge, E. (2008). “Tissue Deformation Modulates Twist Expression to Determine Anterior Midgut Differentiation in *Drosophila* Embryos”. *Developmental cell* 15.3, pp. 470–477.
- Dhonukshe, P. and Gadella, T. W. J. (2003). “Alteration of microtubule dynamic instability during preprophase band formation revealed by yellow fluorescent protein–CLIP170 microtubule plus-end labeling”. *The Plant Cell Online* 15.3, pp. 597–611.
- Díaz-Valencia, J. D., Morelli, M. M., Bailey, M., Zhang, D., Sharp, D. J., and Ross, J. L. (2011). “*Drosophila* Katanin-60 Depolymerizes and Severs at Microtubule Defects”. en. *Biophysical Journal* 100.10, pp. 2440–2449.
- Doorn, W. G. van and Woltering, E. J. (2005). “Many ways to exit? Cell death categories in plants”. en. *Trends in Plant Science* 10.3, pp. 117–122.
- Drevensek, S., Goussot, M., Duroc, Y., Christodoulidou, A., Steyaert, S., Schaefer, E., Duvernois, E., Grandjean, O., Vantard, M., Bouchez, D., and Pastuglia, M. (2012). “The Arabidopsis TRM1-TON1 Interaction Reveals a Recruitment Network Common to Plant Cortical Microtubule Arrays and Eukaryotic Centrosomes”. *The Plant Cell* 24.1, pp. 178–191.
- Du Roure, O., Saez, A., Buguin, A., Austin, R. H., Chavrier, P., Silberzan, P., and Ladoux, B. (2005). “Force mapping in epithelial cell migration”. *PNAS* 102.7, pp. 2390–2395.
- Dumais, J. and Kwiatkowska, D. (2002). “Analysis of surface growth in shoot apices”. *The Plant Journal* 31.2, pp. 229–241.
- Dumais, J. and Steele, C. R. (2000). “New evidence for the role of mechanical forces in the shoot apical meristem”. *Journal of plant growth regulation* 19.1, pp. 7–18.
- Dupuy, L., Mackenzie, J., and Haseloff, J. (2010). “Coordination of plant cell division and expansion in a simple morphogenetic system”. *Proceedings of the National Academy of Sciences* 107.6, pp. 2711–2716.
- Duroc, Y., Bouchez, D., and Pastuglia, M. (2011). “The preprophase band and division site determination in land plants”. *The Plant Cytoskeleton*. New York: Springer, pp. 145–185.
- Engler, A. J., Sen, S., Sweeney, H. L., and Discher, D. E. (2006). “Matrix Elasticity Directs Stem Cell Lineage Specification”. *Cell* 126.4, pp. 677–689.
- Eriksson, J. E., Dechat, T., Grin, B., Helfand, B., Mendez, M., Pallari, H.-M., and Goldman, R. D. (2009). “Introducing intermediate filaments: from discovery to disease”. en. *Journal of Clinical Investigation* 119.7, pp. 1763–1771.
- Errera, L. (1888). “Über Zellformen und Seifenblasen”. *Botanisches Centralblatt* 34, pp. 395–398.
- Farge, E. (2003). “Mechanical Induction of Twist in the *Drosophila* Foregut/Stomodaeal Primordium”. *Current biology* 13.16, pp. 1365–1377.
- Farhadifar, R., Röper, J.-C., Aigouy, B., Eaton, S., and Jülicher, F. (2007). “The Influence of Cell Mechanics, Cell-Cell Interactions, and Proliferation on Epithelial Packing”. *Current Biology* 17.24, pp. 2095–2104.
- Fernandez, P., Maier, M., Lindauer, M., Kuffer, C., Storchova, Z., and Bausch, A. R. (2011). “Mitotic Spindle Orients Perpendicular to the Forces Imposed by Dynamic Shear”. *PLoS one* 6.12, e28965.

- Fernandez, R., Das, P., Mirabet, V., Moscardi, E., Traas, J., Verdeil, J.-L., Malandain, G., and Godin, C. (2010). "Imaging plant growth in 4D: robust tissue reconstruction and lineaging at cell resolution". *Nature Methods* 7.7, pp. 547–553.
- Fink, J., Carpi, N., Betz, T., Bétard, A., Chebah, M., Azioune, A., Bornens, M., Sykes, C., Fetler, L., Cuvelier, D., and Piel, M. (2011). "External forces control mitotic spindle positioning". *Nature Cell Biology* 13, pp. 771–778.
- Firat-Karalar, E. N. and Welch, M. D (2011). "New mechanisms and functions of actin nucleation". en. *Current Opinion in Cell Biology* 23.1, pp. 4–13.
- Flanders, D. J., Rawlins, D. J., Shaw, P. J., and Lloyd, C. W. (1990). "Nucleus-associated Microtubules Help Determine The Division Plane of Plant Epidermal Cells: Avoidance of Four-way Junctions and the Role of Cell Geometry." *The Journal of Cell Biology* 110.4, pp. 1111–1122.
- Frixione, E. (2000). "Recurring views on the structure and function of the cytoskeleton: a 300-year epic". *Cell motility and the cytoskeleton* 46.2, pp. 73–94.
- Fujita, S., Pytela, J., Hotta, T., Kato, T., Hamada, T., Akamatsu, R., Ishida, Y., Kutsuna, N., Hasezawa, S., Nomura, Y., Nakagami, H., and Hashimoto, T. (2013). "An Atypical Tubulin Kinase Mediates Stress-Induced Microtubule Depolymerization in Arabidopsis". en. *Current Biology* 23.20, pp. 1969–1978.
- Galkin, V. E., Orlova, A., Kudryashov, D. S., Solodukhin, A., Reisler, E., Schröder, G. F., and Egelman, E. H. (2011). "Remodeling of actin filaments by ADF/cofilin proteins". *Proceedings of the National Academy of Sciences* 108.51, pp. 20568–20572.
- Gao, H., Gong, Y. W., and Yuan, Y. J. (2007). "RGD-Dependent Mechanotransduction of Suspension Cultured Taxus Cell in Response to Shear Stress". *Biotechnology progress* 23.3, pp. 673–679.
- Gennerich, A., Carter, A. P., Reck-Peterson, S. L., and Vale, R. D. (2007). "Force-Induced Bidirectional Stepping of Cytoplasmic Dynein". *Cell* 131.5, pp. 952–965.
- Gerbode, S. J., Puzey, J. R., McCormick, A. G., and Mahadevan, L. (2012). "How the Cucumber Tendril Coils and Overwinds". en. *Science* 337.6098, pp. 1087–1091.
- Gibson, W. T., Veldhuis, James H., Rubinstein, Boris, Cartwright, Heather N., Perrimon, Norbert, Brodland, G. Wayne, Nagpal, Radhika, and Gibson, Matthew C. (2011). "Control of the Mitotic Cleavage Plane by Local Epithelial Topology". *Cell* 144, pp. 427–438.
- Gittes, F., Mickey, B., Nettleton, J., and Howard, J. (1993). "Flexural rigidity of microtubules and actin filaments measured from thermal fluctuations in shape." *The Journal of cell biology* 120.4, pp. 923–934.
- Goodall, C.R. and Green, P. B. (1986). "Quantitative analysis of surface growth". *Botanical Gazette* 147.1, pp. 1–15.
- Goodbody, K. C. and Lloyd, C. W. (1990). "Actin filaments line up across Tradescantia epidermal cells, anticipating wound-induced division planes". *Protoplasma* 157.1, pp. 92–101.
- Goodbody, K. C., Venverloo, C. J., and Lloyd, C. W. (1991). "Laser microsurgery demonstrates that cytoplasmic strands anchoring the nucleus across the vacuole of premitotic plant cells are under tension. Implications for division plane alignment". *Development* 113, pp. 931–939.

- Grandjean, O., Vernoux, T., Laufs, P., Belcram, K., Mizukami, Y., and Traas, J. (2004). “In vivo analysis of cell division, cell growth, and differentiation at the shoot apical meristem in Arabidopsis”. *The Plant Cell Online* 16.1, pp. 74–87.
- Grishchuk, E. L., Molodtsov, M. I., Ataulakhanov, F. I., and McIntosh, J. R. (2005). “Force production by disassembling microtubules”. *Nature* 438.7066, pp. 384–388.
- Hamant, O., Das, P., and Burian, A. (2014). “Time-Lapse Imaging of Developing Meristems Using Confocal Laser Scanning Microscope”. *Plant Cell Morphogenesis*. Ed. by V. Žárský and F. Cvrčková. Vol. 1080. Totowa, NJ: Humana Press, pp. 111–119.
- Hamant, O., Heisler, M. G., Jönsson, H., Krupinski, P., Uyttewaal, M., Bokov, P., Corson, F., Sahlín, P., Boudaoud, A., Meyerowitz, E. M., Couder, Y., and Traas, J. (2008). “Developmental Patterning by Mechanical Signals in Arabidopsis”. *Science* 322.5908, pp. 1650–1655.
- Hardham, A. R., Takemoto, D., and White, R. G. (2008). “Rapid and dynamic subcellular reorganization following mechanical stimulation of Arabidopsis epidermal cells mimics responses to fungal and oomycete attack”. *BMC Plant Biology* 8.1, p. 63.
- Harris, Albert K., Wild, Patricia, and Stopak, David (1980). “Silicone Rubber Substrata: A New Wrinkle in the Study of Cell Locomotion”. *Science* 208.4440, pp. 177–179.
- Heisler, M. G., Ohno, C., Das, P., Sieber, P., Reddy, G. V., Long, J. A., and Meyerowitz, E. M. (2005). “Patterns of Auxin Transport and Gene Expression during Primordium Development Revealed by Live Imaging of the Arabidopsis Inflorescence Meristem”. en. *Current Biology* 15.21, pp. 1899–1911.
- Hernandez, L. F. and Green, P. B. (1993). “Transductions for the Expression of Structural Pattern: Analysis in Sunflower.” *The Plant Cell Online* 5.12, pp. 1725–1738.
- Hertwig, O. (1884). “The problem of fertilization and of isotropy of the egg, a theory of heredity.” *Jena. Z. Naturwiss.* 18, pp. 21–23.
- Hijmans, R. J. (2015). *raster: Geographic Data Analysis and Modeling*.
- Hochmuth, R. M. (2000). “Micropipette aspiration of living cells”. *Journal of biomechanics* 33.1, pp. 15–22.
- Hofmeister, W. (1863). “Zusatze und berichtigungen zu den 1851 veröffentlichen untersuchungen der entwicklung höherer kryptogamen.” *Jahrbucher für Wissenschaft und Botanik* 3, pp. 259–293.
- Hush, J., Wu, L., John, P. C. L., HEPLER, L. H., and HEPLER, P. K. (1996). “Plant mitosis promoting factor disassembles the microtubule preprophase band and accelerates prophase progression in Tradescantia”. *Cell biology international* 20.4, pp. 275–287.
- Ikeuchi, M., Sugimoto, K., and Iwase, A. (2013). “Plant Callus: Mechanisms of Induction and Repression”. en. *The Plant Cell* 25.9, pp. 3159–3173.
- Ingerson-Mahar, M. and Gitai, Z. (2012). “A growing family: the expanding universe of the bacterial cytoskeleton”. en. *FEMS Microbiology Reviews* 36.1, pp. 256–267.
- Inzé, D. and De Veylder, L. (2006). “Cell Cycle Regulation in Plant Development”. en. *Annual Review of Genetics* 40.1, pp. 77–105.
- Itabashi, T., Terada, Y., Kuwana, K., Kan, T., Shimoyama, I., and Ishiwata, S. (2012). “Mechanical impulses can control metaphase progression in a mammalian cell”. *PNAS* 109.19, pp. 7320–7325.
- Jacques, E., Verbelen, J.-P., and Vissenberg, K. (2013). “Mechanical stress in Arabidopsis leaves orients microtubules in a ‘continuous’ supracellular pattern”. *BMC plant biology* 13.1, p. 163.

- Jaffe, M. J. and Forbes, S.** (1993). “Thigmomorphogenesis: the effect of mechanical perturbation on plants”. *Plant Growth Regulation* 12.3, pp. 313–324.
- Kawamura, E. and Wasteneys, G. O.** (2008). “MOR1, the Arabidopsis thaliana homologue of Xenopus MAP215, promotes rapid growth and shrinkage, and suppresses the pausing of microtubules in vivo”. *Journal of Cell Science* 121.24, pp. 4114–4123.
- Kierzkowski, D., Nakayama, N., Routier-Kierzkowska, A. L., Weber, A., Bayer, E., Schorderet, M., Reinhardt, D., Kuhlemeier, C., and Smith, R. S.** (2012). “Elastic domains regulate growth and organogenesis in the plant shoot apical meristem”. *Science* 335.6072, p. 1096.
- Kirik, A., Ehrhardt, D. W., and Kirik, V.** (2012). “TONNEAU2/FASS regulates the geometry of microtubule nucleation and cortical array organization in interphase Arabidopsis cells”. *The Plant Cell Online* 24.3, pp. 1158–1170.
- Knepper, C., Savory, E. A., and Day, B.** (2011). “Arabidopsis NDR1 Is an Integrin-Like Protein with a Role in Fluid Loss and Plasma Membrane-Cell Wall Adhesion”. en. *Plant Physiology* 156.1, pp. 286–300.
- Kojo, K. H., Higaki, T., Kutsuna, N., Yoshida, Y., Yasuhara, H., and Hasezawa, S.** (2013). “Roles of Cortical Actin Microfilament Patterning in Division Plane Orientation in Plants”. *Plant and Cell Physiology*.
- Komsta, L. and Novomestky, F.** (2015). *moments: Moments, cumulants, skewness, kurtosis and related tests*.
- Kotak, S. and Gönczy, P.** (2013). “Mechanisms of spindle positioning: cortical force generators in the limelight”. en. *Current Opinion in Cell Biology* 25.6, pp. 741–748.
- Kuhl, E.** (2014). “Growing matter: A review of growth in living systems”. *Journal of the mechanical behavior of biomedical materials* 29, pp. 529–543.
- Kutschera, U. and Niklas, K. J.** (2007). “The epidermal-growth-control theory of stem elongation: An old and a new perspective”. *Journal of Plant Physiology* 164.11, pp. 1395–1409.
- Kwiatkowska, D.** (2004). “Surface growth at the reproductive shoot apex of Arabidopsis thaliana pin-formed 1 and wild type”. *Journal of experimental botany* 55.399, pp. 1021–1032.
- Kwiatkowska, D. and Dumais, J.** (2003). “Growth and morphogenesis at the vegetative shoot apex of Anagallis arvensis L.” *Journal of experimental botany* 54.387, pp. 1585–1595.
- Laan, L., Pavin, N., Husson, J., Romet-Lemonne, G., Duijn, M. van, López, M. P., Vale, R. D., Jülicher, F., Reck-Peterson, S. L., and Dogterom, M.** (2012). “Cortical Dynein Controls Microtubule Dynamics to Generate Pulling Forces that Position Microtubule Asters”. en. *Cell* 148.3, pp. 502–514.
- Laufs, Patrick, Jonak, Claudia, and Traas, Jan** (1998). “Cells and domains: Two views of the shoot meristem in Arabidopsis”. *Plant Physiol. Biochem.* 36.1-2, pp. 33–45.
- Lê, S., Josse, J., and Husson, F.** (2008). “FactoMineR: an R package for multivariate analysis”. *Journal of statistical software* 25.1, pp. 1–18.
- Ledbetter, M. C. and Porter, K. R.** (1963). “A microtubule” in plant cell fine structure”. *The Journal of cell biology* 19.1, pp. 239–250.
- Li, S., Blanchoin, L., Yang, Z., and Lord, E. M.** (2003). “The Putative Arabidopsis Arp2/3 Complex Controls Leaf Cell Morphogenesis”. en. *Plant Physiology* 132.4, pp. 2034–2044.
- Li, S., Lei, L., Somerville, C. R., and Gu, Y.** (2012). “Cellulose synthase interactive protein 1 (CSI1) links microtubules and cellulose synthase complexes”. en. *Proceedings of the National Academy of Sciences* 109.1, pp. 185–190.

- Li, Y., Shen, Y., Cai, C., Zhong, C., Zhu, L., Yuan, M., and Ren, H. (2010). “The Type II Arabidopsis Formin14 Interacts with Microtubules and Microfilaments to Regulate Cell Division”. *The Plant Cell* 22.8, pp. 2710–2726.
- Lin, D., Cao, L., Zhou, Z., Zhu, L., Ehrhardt, D., Yang, Z., and Fu, Y. (2013). “Rho GTPase Signaling Activates Microtubule Severing to Promote Microtubule Ordering in Arabidopsis”. en. *Current Biology* 23.4, pp. 290–297.
- Lindeboom, J. J., Nakamura, M., Hibbel, A., Shundyak, K., Gutierrez, R., Ketelaar, T., Emons, A. M. C., Mulder, B. M., Kirik, V., and Ehrhardt, D. W. (2013). “A Mechanism for Reorientation of Cortical Microtubule Arrays Driven by Microtubule Severing”. en. *Science* 342.6163.
- Lintilhac, P. M. and Vesecky, T. B. (1981). “Mechanical stress and cell wall orientation in plants. II. The application of controlled directional stress to growing plants; with a discussion on the nature of the wound reaction”. *American Journal of Botany* 68.9, pp. 1222–1230.
- Lintilhac, Philip M. and Vesecky, Thompson B. (1984). “Stress-induced alignment of division plane in plant tissues grown in vitro”. *Nature* 307, pp. 363–364.
- Lipka, E., Gadeyne, A., Stockle, D., Zimmermann, S., De Jaeger, G., Ehrhardt, D. W., Kirik, V., Van Damme, D., and Muller, S. (2014). “The Phragmoplast-Orienting Kinesin-12 Class Proteins Translate the Positional Information of the Preprophase Band to Establish the Cortical Division Zone in Arabidopsis thaliana”. en. *The Plant Cell* 26.6, pp. 2617–2632.
- Lipka, E. and Müller, S. (2012). “Potential roles for Kinesins at the cortical division site”. *Frontiers in Plant Science* 3.
- Lloyd, C. W. and Traas, J. A. (1988). “The role of F-actin in determining the division plane of carrot suspension cells. Drug studies”. *Development* 102.1, pp. 211–221.
- Lloyd, C. and Chan, J. (2006). “Not so divided: the common basis of plant and animal cell division”. *Nature Reviews Molecular Cell Biology* 7, pp. 147–152.
- Lloyd, Clive W. (1991). “How does the cytoskeleton read the laws of geometry in aligning the division plane of plant cells ?” *Development* 113, pp. 55–65.
- Louveaux, M. and Hamant, O. (2013). “The mechanics behind cell division”. *Current Opinion in Plant Biology* 16.6, pp. 774–779.
- Lynch, Timothy M. and Lintilhac, Philip M. (1997). “Mechanical Signals in Plant Development: A New Method for Single Cell Studies”. *Developmental biology* 181.2, pp. 246–256.
- Marc, J., Granger, C. L., Brincat, J., Fisher, D. D., Kao, T., McCubbin, A. G., and Cyr, R. J. (1998). “A GFP–MAP4 reporter gene for visualizing cortical microtubule rearrangements in living epidermal cells”. *The Plant Cell* 10.11, pp. 1927–1939.
- McClinton, R. S., Chandler, J. S., and Callis, J. (2001). “cDNA isolation, characterization, and protein intracellular localization of a katanin-like p60 subunit from Arabidopsis thaliana”. *Protoplasma* 216.3-4, pp. 181–190.
- McNally, F. J. and Vale, R. D. (1993). “Identification of Katanin, an ATPase that severs and disassembles stable microtubules”. *Cell* 75, pp. 419–429.
- Menges, M. (2006). “The D-Type Cyclin CYCD3;1 Is Limiting for the G1-to-S-Phase Transition in Arabidopsis”. en. *The Plant Cell* 18.4, pp. 893–906.
- Milani, P., Braybrook, S. A., and Boudaoud, A. (2013). “Shrinking the hammer: micromechanical approaches to morphogenesis”. en. *Journal of Experimental Botany* 64.15, pp. 4651–4662.
- Milani, P., Gholamirad, M., Traas, J., Arnéodo, A., Boudaoud, A., Argoul, F., and Hamant, O. (2011). “In vivo analysis of local wall stiffness at the shoot

- apical meristem in Arabidopsis using atomic force microscopy: Measuring wall stiffness in meristems with AFM". en. *The Plant Journal* 67.6, pp. 1116–1123.
- Milani, P., Mirabet, V., Cellier, C., Rozier, F., Hamant, O., Das, P., and Boudaoud, A.** (2014). "Matching Patterns of Gene Expression to Mechanical Stiffness at Cell Resolution through Quantitative Tandem Epifluorescence and Nanoindentation". en. *Plant Physiology* 165.4, pp. 1399–1408.
- Minc, N., Burgess, D., and Chang, F.** (2011). "Influence of cell geometry on division-plane positioning". *Cell* 144.3, pp. 414–426.
- Minc, N. and Piel, M.** (2012). "Predicting division plane position and orientation". *Trends in Cell Biology* 22.4, pp. 193–200.
- Mineyuki, Y. and Gunning, B. E. S.** (1990). "A role for preprophase bands of microtubules in maturation of new cell walls, and a general proposal on the function of preprophase band sites in cell division in higher plants". *Journal of Cell Science* 97, pp. 527–537.
- Mineyuki, Y., Murata, T., and Wada, M.** (1991). "Experimental obliteration of the preprophase band alters the site of cell division, cell plate orientation and phragmoplast expansion in *Adiantum protonemata*". *Journal of Cell Science* 100.3, pp. 551–557.
- Mineyuki, Y. and Palevitz, B. A.** (1990). "Relationship between preprophase band organization, F-actin and the division site in *Allium*". *Journal of Cell Science* 97, pp. 283–295.
- Montel, F., Delarue, M., Elgeti, J., Malaquin, L., Basan, M., Risler, T., Cabane, B., Vignjevic, D., Prost, J., Cappello, G., and Joanny, J.-F.** (2011). "Stress Clamp Experiments on Multicellular Tumor Spheroids". *Physical Review Letters* 107.18.
- Montel, F., Delarue, M., Elgeti, J., Vignjevic, D., Cappello, G., and Prost, J.** (2012). "Isotropic stress reduces cell proliferation in tumor spheroids". *New Journal of Physics* 14.5, p. 055008.
- Müller, S., Han, S., and Smith, L. G.** (2006). "Two Kinesins Are Involved in the Spatial Control of Cytokinesis in *Arabidopsis thaliana*". *Current biology* 16.9, pp. 888–894.
- Müller, S., Wright, A. J., and Smith, L. G.** (2009). "Division plane control in plants: new players in the band". *Trends in cell biology* 19.4, pp. 180–188.
- Murata, T. and Wada, M.** (1991). "Effects of centrifugation on preprophase-band formation in *Adiantum protonemata*". *Planta* 183.3, pp. 391–398.
- Nakai, T., Kato, K., Shinmyo, A., and Sekine, M.** (2006). "Arabidopsis KRPs have distinct inhibitory activity toward cyclin D2-associated kinases, including plant-specific B-type cyclin-dependent kinase". en. *FEBS Letters* 580.1, pp. 336–340.
- Nakamura, M. and Hashimoto, T.** (2009). "A mutation in the Arabidopsis gamma-tubulin-containing complex causes helical growth and abnormal microtubule branching". en. *Journal of Cell Science* 122.13, pp. 2208–2217.
- Nakayama, N., Smith, R. S., Mandel, T., Robinson, S., Kimura, S., Boudaoud, A., and Kuhlemeier, C.** (2012). "Mechanical Regulation of Auxin-Mediated Growth". en. *Current Biology* 22.16, pp. 1468–1476.
- Nurse, P. M.** (2002). "Nobel Lecture: Cyclin dependent kinases and cell cycle control". *Chembiochem* 3.7, pp. 596–603.
- Paganelli, L., Caillaud, M.-C., Quentin, M., Damiani, I., Govetto, B., Lecomte, P., Karpov, P. A., Abad, P., Chabouté, M.-E., and Favery, B.** (2015). "Three BUB1 and BUBR1/MAD3-related spindle assembly checkpoint proteins are required for accurate mitosis in Arabidopsis". en. *New Phytologist* 205.1, pp. 202–215.

- Panteris, E., Adamakis, I.-D. S., Voulgari, G., and Papadopoulou, G. (2011). “A role for katanin in plant cell division: microtubule organization in dividing root cells of *fra2* and *lue1* *Arabidopsis thaliana* mutants”. *Cytoskeleton* 68.7, pp. 401–413.
- Pastuglia, Martine and Bouchez, David (2007). “Molecular encounters at microtubule ends in the plant cell cortex”. *Current Opinion in Plant Biology* 10, pp. 557–563.
- Peaucelle, A., Braybrook, S. A., Le Guillou, L., Bron, E., Kuhlemeier, C., and Höfte, H. (2011). “Pectin-Induced Changes in Cell Wall Mechanics Underlie Organ Initiation in *Arabidopsis*”. *Current Biology*.
- Peter, A. and Stick, R. (2015). “Evolutionary aspects in intermediate filament proteins”. en. *Current Opinion in Cell Biology* 32, pp. 48–55.
- Petrášek, J. and Schwarzerová, K. (2009). “Actin and microtubule cytoskeleton interactions”. en. *Current Opinion in Plant Biology* 12.6, pp. 728–734.
- Pickett-Heaps, J. D. (1967). “The Effects of Colchicine on the Ultrastructure of Dividing Plant Cells, Xylem Wall Differentiation and Distribution of Cytoplasmic Microtubules”. *Developmental biology* 15.206-236.
- Portran, D., Gaillard, J., Vantard, M., and They, M. (2013a). “Quantification of MAP and molecular motor activities on geometrically controlled microtubule networks”. *Cytoskeleton* 70.1, pp. 12–23.
- Portran, D., Zoccoler, M., Gaillard, J., Stoppin-Mellet, V., Neumann, E., Arnal, I., Martiel, J. L., and Vantard, M. (2013b). “MAP65/Ase1 promote microtubule flexibility”. *Molecular biology of the cell* 24.12, pp. 1964–1973.
- R Core Team (2015). *R: A Language and Environment for Statistical Computing*. Vienna, Austria.
- Rappaport, R. (1961). “Experiments concerning the cleavage stimulus in sand dollar eggs”. *Journal of Experimental Zoology* 148.1, pp. 81–89.
- Rasmussen, C. G., Humphries, J. A., and Smith, L. G. (2011). “Determination of Symmetric and Asymmetric Division Planes in Plant Cells”. *Annual Review of Plant Biology* 62.1, pp. 387–409.
- Rasmussen, C. G., Wright, A. J., and Müller, S. (2013). “The role of the cytoskeleton and associated proteins in determination of the plant cell division plane”. *The Plant Journal* 75.2, pp. 258–269.
- Rast, M. I. and Simon, R. (2008). “The meristem-to-organ boundary: more than an extremity of anything”. *Current opinion in Genetics & Development* 18.4, pp. 287–294.
- Reddy, G. V., Heisler, M. G., Ehrhardt, D. W., and Meyerowitz, E. M. (2004). “Real-time lineage analysis reveals oriented cell divisions associated with morphogenesis at the shoot apex of *Arabidopsis thaliana*”. *Development* 131.17, pp. 4225–4237.
- Reinhardt, D., Frenz, M., Mandel, T., and Kuhlemeier, C. (2003). “Microsurgical and laser ablation analysis of interactions between the zones and layers of the tomato shoot apical meristem”. en. *Development* 130.17, pp. 4073–4083.
- Rief, M., Gautel, M., Oesterhelt, F., Fernandez, J. M., and Gaub, H. E. (1997). “Reversible unfolding of individual titin immunoglobulin domains by AFM”. *Science* 276.5315, pp. 1109–1112.
- Risca, V. I., Wang, E. B., Chaudhuri, O., Chia, J. J., Geissler, P. L., and Fletcher, D. A. (2012). “Actin filament curvature biases branching direction”. *Proceedings of the National Academy of Sciences* 109.8, pp. 2913–2918.
- Robinson, S., Burian, A., Couturier, E., Landrein, B., Louveaux, M., Neumann, E. D., Peaucelle, A., Weber, A., and Nakayama, N. (2013). “Mechanical

- control of morphogenesis at the shoot apex”. *Journal of Experimental Botany* 64.15, pp. 4729–4744.
- Roeder, A. H. K., Chickarmane, V., Cunha, A., Obara, B., Manjunath, B. S., and Meyerowitz, E. M.** (2010). “Variability in the Control of Cell Division Underlies Sepal Epidermal Patterning in *Arabidopsis thaliana*”. en. *PLoS Biology* 8.5. Ed. by E. Coen.
- Roll-Mecak, A. and McNally, F. J.** (2010). “Microtubule-severing enzymes”. en. *Current Opinion in Cell Biology* 22.1, pp. 96–103.
- Sachs, J.** (1878). “Über die Anordnung der Zellen in jungsten Pflanzentheilen.” *Arbeiten des Botanisches Institut Würzburg* 2, pp. 46–104.
- Sahlin, P. and Jönsson, H.** (2010). “A Modeling Study on How Cell Division Affects Properties of Epithelial Tissues Under Isotropic Growth”. en. *PLoS ONE* 5.7. Ed. by N. Monk, e11750.
- Sampathkumar, A., Krupinski, P., Wightman, R., Milani, P., Berquand, A., Boudaoud, A., Hamant, O., Jönsson, H., and Meyerowitz, E. M.** (2014). “Sub-cellular and supracellular mechanical stress prescribes cytoskeleton behavior in *Arabidopsis* cotyledon pavement cells”. *Elife* 3, e01967.
- Sampathkumar, A., Lindeboom, J. J., Debolt, S., Gutierrez, R., Ehrhardt, D. W., Ketelaar, T., and Persson, S.** (2011). “Live cell imaging reveals structural associations between the actin and microtubule cytoskeleton in *Arabidopsis*”. *The Plant Cell* 23.6, pp. 2302–2313.
- Sassi, M., Ali, O., Boudon, F., Cloarec, G., Abad, U., Cellier, C., Chen, X., Gilles, B., Milani, P., Friml, J., Vernoux, T., Godin, C., Hamant, O., and Traas, J.** (2014). “An Auxin-Mediated Shift toward Growth Isotropy Promotes Organ Formation at the Shoot Meristem in *Arabidopsis*”. en. *Current Biology* 24.19, pp. 2335–2342.
- Savin, T., Kurpios, N. A., Shyer, A. E., Florescu, P., Liang, H., Mahadevan, L., and Tabin, C. J.** (2011). “On the growth and form of the gut”. *Nature* 476.7358, pp. 57–62.
- Schindelin, J., Arganda-Carreras, I., Frise, E., Kaynig, V., Longair, M., Pietzsch, T., Preibisch, S., Rueden, C., Saalfeld, S., Schmid, Benjamin, Tinevez, J.-Y., White, D. J., Hartenstein, V., Eliceiri, K., Tomancak, P., and Cardona, A.** (2012). “Fiji: an open-source platform for biological-image analysis”. *Nature Methods* 9.7, pp. 676–682.
- Schwartz, M. A.** (2009). “The force is with us”. *Science* 332, pp. 588–589.
- Scofield, S., Jones, A., and Murray, J. A. H.** (2014). “The plant cell cycle in context”. en. *Journal of Experimental Botany* 65.10, pp. 2557–2562.
- Shapiro, B. E., Tobin, C., Mjolsness, E., and Meyerowitz, E. M.** (2015). “Analysis of cell division patterns in the *Arabidopsis* shoot apical meristem”. en. *Proceedings of the National Academy of Sciences* 112.15, pp. 4815–4820.
- Silkworth, W. T. and Cimini, D.** (2012). “Transient defects of mitotic spindle geometry and chromosome segregation errors”. *Cell Div* 7.1, pp. 19–19.
- Smertenko, A. P., Chang, H. Y., Sonobe, S., Fenyk, S. I., Weingartner, M., Bögre, L., and Hussey, P. J.** (2006). “Control of the AtMAP65-1 interaction with microtubules through the cell cycle”. *Journal of Cell Science* 119.15, pp. 3227–3237.
- Song, S.-K., Hofhuis, H., Lee, M. M., and Clark, S. E.** (2008). “Key Divisions in the Early *Arabidopsis* Embryo Require POL and PLL1 Phosphatases to Establish the Root Stem Cell Organizer and Vascular Axis”. en. *Developmental Cell* 15.1, pp. 98–109.

- Spinner, L., Gadeyne, A., Belcram, K., Goussot, M., Moison, M., Duroc, Y., Eeckhout, D., De Winne, N., Schaefer, E., Van De Slijke, E., Persiau, G., Witters, E., Gevaert, K., De Jaeger, G., Bouchez, D., Van Damme, D., and Pastuglia, M. (2013). “A protein phosphatase 2A complex spatially controls plant cell division”. *Nature Communications* 4, p. 1863.
- Sterratt, D. C. and Vihtakari, M. (2015). *RImageJROI: Read 'ImageJ' Region of Interest (ROI) Files*.
- Stewart, M. P., Helenius, J., Toyoda, Y., Ramanathan, S. P., Muller, D. J., and Hyman, A. A. (2011). “Hydrostatic pressure and the actomyosin cortex drive mitotic cell rounding”. *Nature* 469.7329, pp. 226–230.
- Stoppin-Mellet, V., Fache, V., Portran, D., Martiel, J-L., and Vantard, M. (2013). “MAP65 Coordinate Microtubule Growth during Bundle Formation”. *PLoS ONE* 8.2. Ed. by T. Toda.
- Stoppin-Mellet, V., Gaillard, J., and Vantard, M. (2002). “Functional evidence for in vitro microtubule severing by the plant katanin homologue”. *Biochem. J* 365, pp. 337–342.
- (2006). “Katanin’s severing activity favors bundling of cortical microtubules in plants”. *The Plant Journal* 46.6, pp. 1009–1017.
- Suresh, S. (2007). “Biomechanics and biophysics of cancer cells”. *Acta Materialia* 55.12, pp. 3989–4014.
- Tamura, K., Iwabuchi, K., Fukao, Y., Kondo, M., Okamoto, K., Ueda, H., Nishimura, M., and Hara-Nishimura, I. (2013). “Myosin XI-i Links the Nuclear Membrane to the Cytoskeleton to Control Nuclear Movement and Shape in Arabidopsis”. en. *Current Biology* 23.18, pp. 1776–1781.
- Tawk, M., Araya, C., Lyons, D. A., Reugels, A. M., Girdler, G. C., Bayley, P. R., Hyde, D. R., Tada, M., and Clarke, J. D. W. (2007). “A mirror-symmetric cell division that orchestrates neuroepithelial morphogenesis”. *Nature* 446.7137, pp. 797–800.
- The GIMP team (2012). *GNU Image Manipulation Program*.
- The MathWorks, Inc. (2013). *Matlab*. Natick, Massachusetts.
- Théry, M., Jiménez-Dalmaroni, A., Racine, V., Bornens, M., and Jülicher, F. (2007). “Experimental and theoretical study of mitotic spindle orientation”. *Nature* 447.7143, pp. 493–496.
- Tierney, L., Rossini, A. J., Li, N., and Sevcikova, H. (2013). *snow: Simple Network of Workstations*.
- Toba, S., Watanabe, T. M., Yamaguchi-Okimoto, L., Toyoshima, Y. Y., and Higuchi, H. (2006). “Overlapping hand-over-hand mechanism of single molecular motility of cytoplasmic dynein”. *Proceedings of the National Academy of Sciences* 103.15, pp. 5741–5745.
- Traas, J. A., Doonan, J. H., Rawlins, D. J., Shaw, P. J., Watts, J., and Lloyd, C. W. (1987). “An actin network is present in the cytoplasm throughout the cell cycle of carrot cells and associates with the dividing nucleus.” *The Journal of cell biology* 105.1, pp. 387–395.
- Traas, J., Bellini, C., Nacry, P., Kronenberger, Jocelyne, Bouchez, D., and Caboche, M. (1995). “Normal differentiation patterns in plants lacking microtubular preprophase bands”. *Nature* 375.6533, pp. 676–677.
- Traas, J. and Bohn-Courseau, I. (2005). “Cell proliferation patterns at the shoot apical meristem”. en. *Current Opinion in Plant Biology* 8.6, pp. 587–592.

- Trushko, A., Schäffer, E., and Howard, J.** (2013). “The growth speed of microtubules with XMAP215-coated beads coupled to their ends is increased by tensile force”. en. *Proceedings of the National Academy of Sciences* 110.36, pp. 14670–14675.
- Tulin, A., McClerklin, S., Huang, Y., and Dixit, R.** (2012). “Single-Molecule Analysis of the Microtubule Cross-Linking Protein MAP65-1 Reveals a Molecular Mechanism for Contact-Angle-Dependent Microtubule Bundling”. en. *Biophysical Journal* 102.4, pp. 802–809.
- Ueda, K., Matsuyama, T., and Hashimoto, T.** (1999). “Visualization of microtubules in living cells of transgenic *Arabidopsis thaliana*”. *Protoplasma* 206.1-3, pp. 201–206.
- Uyttewaal, M., Burian, A., Alim, K., Landrein, B., Borowska-Wykret, D., Dedieu, A., Peaucelle, A., Ludynia, M., Traas, J., Boudaoud, A., Kwiatkowska, D., and Hamant, O.** (2012). “Mechanical Stress Acts via Katanin to Amplify Differences in Growth Rate between Adjacent Cells in *Arabidopsis*”. *Cell* 149.2, pp. 439–451.
- Vale, R. D.** (1991). “Severing of stable microtubules by a mitotically activated protein in *Xenopus* egg extracts”. *Cell* 64, pp. 827–839.
- Vos, J. W., Dogterom, M., and Emons, A. M. C.** (2004). “Microtubules become more dynamic but not shorter during preprophase band formation: A possible “search-and-capture” mechanism for microtubule translocation”. *Cell motility and the cytoskeleton* 57.4, pp. 246–258.
- Walker, K. L., Müller, S., Moss, D., Ehrhardt, D. W., and Smith, L. G.** (2007). “*Arabidopsis* TANGLED Identifies the Division Plane throughout Mitosis and Cytokinesis”. *Current Biology* 17.21, pp. 1827–1836.
- Webb, M., Jouannic, S., Foreman, J., Linstead, P., and Dolan, L.** (2002). “Cell specification in the *Arabidopsis* root epidermis requires the activity of ECTOPIC ROOT HAIR 3—a katanin-p60 protein”. *Development* 129.1, pp. 123–131.
- Wightman, R., Chomicki, G., Kumar, M., Carr, P., and Turner, S. R.** (2013). “SPIRAL2 Determines Plant Microtubule Organization by Modulating Microtubule Severing”. en. *Current Biology* 23.19, pp. 1902–1907.
- Wightman, R. and Turner, S. R.** (2007). “Severing at sites of microtubule crossover contributes to microtubule alignment in cortical arrays: Microtubule dynamics”. en. *The Plant Journal* 52.4, pp. 742–751.
- Windoffer, R., Beil, M., Magin, T. M., and Leube, R. E.** (2011). “Cytoskeleton in motion: the dynamics of keratin intermediate filaments in epithelia”. en. *The Journal of Cell Biology* 194.5, pp. 669–678.
- Wood, S. N.** (2011). “Fast stable restricted maximum likelihood and marginal likelihood estimation of semiparametric generalized linear models”. *Journal of the Royal Statistical Society* 73.1, pp. 3–36.
- Wu, S.-Z. and Bezanilla, M.** (2014). “Myosin VIII associates with microtubule ends and together with actin plays a role in guiding plant cell division”. *Elife* 3, e03498.
- Yeoman, M. M. and Brown, R.** (1971). “Effects of mechanical stress on the plane of cell division in developing callus cultures”. *Annals of Botany* 35.5, pp. 1102–1112.
- Yin, K., Ueda, M., Takagi, H., Kajihara, T., Sugamata Aki, S., Nobusawa, T., Umeda-Hara, C., and Umeda, M.** (2014). “A dual-color marker system for in vivo visualization of cell cycle progression in *Arabidopsis*”. en. *The Plant Journal* 80.3, pp. 541–552.
- Yoshida, S., Barbier de Reuille, P., Lane, B., Bassel, G. W., Prusinkiewicz, P., Smith, R. S., and Weijers, D.** (2014). “Genetic Control of Plant Development by Overriding a Geometric Division Rule”. en. *Developmental Cell* 29.1, pp. 75–87.

- Zhang, Q., Fishel, E., Bertroche, T., and Dixit, R.** (2013). “Microtubule Severing at Crossover Sites by Katanin Generates Ordered Cortical Microtubule Arrays in Arabidopsis”. en. *Current Biology* 23.21, pp. 2191–2195.
- Zhou, J., Wang, B., Zhu, L., Li, Y., and Wang, Y.** (2006). “A system for studying the effect of mechanical stress on the elongation behavior of immobilized plant cells”. *Colloids and Surfaces B: Biointerfaces* 49.2, pp. 165–174.
- Zhu, C. and Dixit, R.** (2011). “Functions of the Arabidopsis kinesin superfamily of microtubule-based motor proteins”. *Protoplasma*, pp. 1–13.

A Appendix Chapter

Due to copyright restrictions, the article [Robinson et al. 2013](#) cannot be reproduced here.
To read this article, please connect to [doi:10.1093/jxb/ert199](https://doi.org/10.1093/jxb/ert199) .